UNIVERSIDADE DE LISBOA
FACULDADE DE CIÊNCIAS
DEPARTAMENTO DE QUÍMICA E BIOQUÍMICA

A STUDY ON THE MODE OF ACTION OF CLINICALLY RELEVANT ANTIMICROBIAL PEPTIDES

Manuel Nuno Melo

DOUTORAMENTO EM BIOQUÍMICA
(Especialidade de Biofísica Molecular)

Tese orientada pelos Profs. Doutores

Miguel Augusto Rico Botas Castanho
e
Ana Isabel Abrantes Coutinho

2010

ESTUDO DO MECANISMO DE ACÇÃO DE PÉPTIDOS MICROBICIDAS RIBOSSOMAIS DE INTERESSE CLÍNICO

A STUDY ON THE MODE OF ACTION OF CLINICALLY RELEVANT ANTIMICROBIAL PEPTIDES

Este livro foi impresso sobre papel reciclado pela Cadaval Gráfica.
A composição tipográfica foi feita em LaTeX 2ε utilizando adaptações dos tipos de letra Goudy Bookletter 1911 e Petita, criados por Barry Schwartz e Manfred Klein, respectivamente.

This book was printed on recycled paper by Cadaval Gráfica.
Typesetting was performed in LaTeX 2ε using the customized fonts Goudy Bookletter 1911 and Petita, originally created by Barry Schwartz and Manfred Klein, respectively.

Sobrecapa desenhada por / Book jacket design by
Alexandra Montalvão

Acknowledgements

Throughout my PhD I became deeply indebted to many people for the practical, theoretical, and motivational contributions they made to my work. Rather than just stating that they are "fortunately too many to name individually" I made it a point to explicitly include their contributions in the text. This not only blends naturally with the description of the work but also gives proper credit to each contributor. Ultimately, this book is a tribute to these friends.

There are, however, some people I want to specifically acknowledge here. They are:

Miguel Castanho, who has been a great supervisor, a close collaborator, and a good friend. He gave me liberty to plan my own work but also guidance and support when I needed, in more ways than I can describe in this book;

Marta Ribeiro and Henri Franquelim, for having brought a young, cheerful mood to the group, making it a very fun place to work in;

my mother, Maria Manuela Melo, for reviewing the written English of several manuscripts, which frequently only got to her hands on the night before submission;

my brother, Tiago Melo, for the printing of this book, and my cousin, Alexandra Montalvão, for the book jacket design;

and Ana Coutinho, for having accepted, on a very short notice, to be my internal supervisor at the Faculty of Sciences.

I thank the people at the Department of Chemistry and Biochemistry of the Faculty of Sciences, and the people at the Institute of Molecular Medicine — both at the University of Lisbon — for always having made me feel at home. I also thank my friends at the Federal University of Rio de Janeiro for the six unforgettable months I spent there, and those at the

University of Karlsruhe and the Karlsruhe Research Center for warmly welcoming me into their group during my short winter stay.

I thank the Portuguese government — embodied in the Foundation for Science and Technology — for having sponsored my PhD work for the past four years under the grant SFRH/BD/24778/2005, and the Portuguese National Conference of Rectors for supporting my stay in Karlsruhe.

Lastly, I thank the Portuguese Biochemical Society, the Portuguese Biophysical Society, the European Peptide Society, the European Biophysical Societies' Association, the Federation of European Biochemical Societies, and the International Union of Biochemistry and Molecular Biology for having sponsored my participation in several scientific meetings and young scientists' fora around the world, at once enriching my scientific and cultural (and gastronomic!) backgrounds.

Resumo

Este trabalho centra-se no estudo do mecanismo de acção dos péptidos microbicidas (AMPs) omiganan (ILRWPWWPWRRK–NH_2) e BP100 (KKLFKKILKYL–NH_2). Estes péptidos catiónicos foram desenhados com base na sequência de AMPs naturais, nomeadamente da indolicidina — dos neutrófilos de bovino — no caso do omiganan e da cecropina e melitina — da traça e do veneno de abelha, respectivamente — no caso do BP100. Foram empregadas principalmente técnicas de espectroscopia óptica em conjunto com sistemas modelo de membranas (vesículas fosfolipídicas); estes foram preparados para mimetizar tanto membranas celulares bacterianas — de natureza aniónica — como de mamíferos — essencialmente zwitteriónicas. Na constituição destes modelos foram utilizados principalmente fosfolípidos com o par de cadeias acilo palmitoíl e oleoíl, ligados a uma fosfatidilcolina ou a um fosfatidilglicerol (formando fosfolípidos zwitteriónicos ou aniónicos, respectivamente). O grau de afinidade dos péptidos para os modelos de membrana foi interpretado de acordo com um formalismo de partição de Nernst, onde bicamadas fosfolipídicas num meio aquoso são vistas como uma fase líquida imiscível para a qual a partição de um soluto é regida pela constante de partição K_p (a razão das concentrações locais de soluto nas fases lipídica e aquosa, respectivamente). A partição foi seguida experimentalmente por alterações na emissão dos resíduos fluorescentes de cada péptido ao longo de titulações com vesículas. Ambos os péptidos se particionaram para os modelos bacterianos com valores de K_p com uma magnitude de 10^4, uma ordem de grandeza superior à da partição para modelos de mamíferos. Esta observação explica em parte a selectividade dos péptidos para bactérias e a sua baixa taxa de hemólise. A afinidade do péptido omiganan para um mo-

delo de parede bacteriana (extractos de parede celular de *Staphylococcus aureus*) foi também testada, desta vez por quantificação no sobrenadante após separação por centrifugação. Observou-se uma afinidade elevada do omiganan para os extractos de parede celular — equivalente a um valor de K_p na ordem de 10^3 — mas inferior à demonstrada para os modelos de membrana celular bacteriana.

Observaram-se, para os dois péptidos, desvios ao comportamento de partição esperado sempre que se atingiram altas concentrações locais de péptido nos modelos de membranas aniónicos. Foi desenvolvido um método para melhor caracterizar estes desvios, baseado numa titulação de lípido com péptido na presença do *quencher* de fase aquosa acrilamida, tendo-se determinado que correspondem a uma saturação das bicamadas fosfolipídicas: a partir desse ponto de saturação as moléculas de péptido adicionadas deixam de poder ligar-se à membrana e escapar ao efeito de *quenching* da acrilamida. Conjugando a ocorrência de saturação da membrana com o formalismo de partição pôde ser estabelecida uma relação entre as concentrações globais de péptido e lípido nos pontos de saturação. A partir desta relação pôde descrever-se quantitativamente o fenómeno da saturação, nomeadamente a razão péptido-lípido (P:L) neste limite. Os valores elevados obtidos para a razão P:L são consistentes com a ocorrência de saturação; tendo em conta a proporção de fosfolípidos aniónicos e zwitteriónicos pôde prever-se a neutralização da carga superficial das vesículas ao ser atingido este limite. Postulando-se uma alteração conformacional na saturação com impacto na fluorescência dos péptidos foi ainda desenvolvido um modelo que explica os desvios no comportamento de partição. A aplicação deste modelo permite determinar a partir de um único ajuste a uma curva de partição os valores de K_p e da razão P:L na saturação.

Detectou-se na saturação, por metodologias de *quenching* diferencial (onde *quenchers* de fluorescência a diferentes profundidades na membrana são utilizados para inferir a posição do fluoróforo), uma internalização em profundidade do péptido omiganan. Com o péptido BP100 foi observado na saturação um aumento de acção permeabilizadora (usando vesículas marcadas com fosfolípidos fluorescentes); foi ainda detectada neste limite

a indução da agregação de vesículas e a neutralização da sua carga superficial por metodologias de dispersão de luz, confirmando as previsões anteriores; por dicroísmo circular observou-se ainda que estes fenómenos são acompanhados de uma alteração da estrutura secundária do péptido na membrana, de uma conformação essencialmente de hélice α antes da saturação para uma outra com um conteúdo aparentemente elevado de voltas β. Esta observação valida em parte os pressupostos do método explicativo dos desvios no comportamento de partição.

A observação de vários comportamentos potencialmente disruptivos ao ser atingida a saturação levou a que fosse proposta a hipótese da correlação deste limite biofísico com a ocorrência de morte bacteriana. A plausibilidade desta relação foi testada pela construção de um modelo matemático que prevê a quantidade de um AMP genérico que se ligará à membrana bacteriana sob condições fisiológicas. Este modelo aplica o formalismo de partição descrito acima à quantidade de membrana disponível para a ligação do péptido numa situação como a encontrada nos testes microbiológicos de actividade microbicida. Resultou da aplicação deste modelo que, embora apenas uma fracção muito pequena do péptido total se ligue às membranas bacterianas, a concentração local deste pode atingir os valores necessários para a ocorrência de saturação. Esta conclusão verifica-se especialmente para as concentrações globais micromolares de péptido às quais os AMPs tipicamente se tornam activos contra bactérias. Isto sugere que a saturação, mais do que possível, pode ser necessária para a actividade destes péptidos. As conclusões da aplicação deste modelo foram validadas usando dados publicados para as afinidades e actividades de vários AMPs. O modelo foi ainda modificado para, ao invés de prever a quantidade de péptido que se acumula na membrana, passar a permitir a previsão da concentração de péptido necessária para alcançar na membrana uma concentração que cause a morte bacteriana; ou seja, uma previsão da potência de um AMP. A aplicação deste método requer apenas o conhecimento do valor de K_p para a membrana bacteriana e a razão péptido-lipido correspondente à saturação ou a outro limite que espolete a actividade microbicida do péptido. São apresentadas várias metodologias para obter estimativas biofísicas destes parâmetros,

nomeadamente a partir da relação péptido-lípido na saturação ou a partir do modelo integrado para ajustar os dados de fluorescência na saturação.

Conduziram-se também experiências *in vivo* com *Escherichia coli* para testar a correlação entre a ocorrência de saturação da ligação do péptido BP100 a bactérias e a perda de viabilidade destas. Tentou-se adaptar o método de separação de fases por centrifugação, utilizado anteriormente na medição da afinidade do omiganan para extractos de parede bacteriana, para quantificar a quantidade de péptido ligado a bactérias. A aplicação da metodologia não foi bem sucedida devido principalmente a um elevado grau de contaminação fluorescente do sobrenadante por proteínas bacterianas, não tendo sido possível obter dados conclusivos. No entanto, utilizando técnicas de dispersão de luz foi possível observar a ocorrência da morte das bactérias e a neutralização do respectivo potencial ζ a partir da mesma concentração de BP100, o que sugere que os dois fenómenos podem estar relacionados entre si e, indirectamente, com a saturação.

Aperfeiçoaram-se ainda várias metodologias relacionadas com o estudo da interacção péptido membrana. Foi desenvolvido um método para a determinação de constantes de partição onde se infere a fracção de péptido na membrana a partir dos valores do potencial ζ de vesículas aniónicas a várias concentrações de péptido. Foi também adaptado para Visual Basic e C++ um algoritmo de interpretação de dados de *quenching* diferencial, e acoplado um processo de ajuste por mínimos quadrados. Por último, foi desenvolvida uma metodologia capaz de detectar translocação de péptidos para o interior de vesículas que aproveita o facto de uma fracção significativa de lípido estar inacessível quando se utilizam lipossomas multilamelares.

Palavras-chave:

Péptido; Microbicida; Membrana celular; Saturação; Concentração mínima inibitória.

Abstract

The antimicrobial peptides (AMPs) omiganan (ILRWPWWPWRRK–NH_2) and BP100 (KKLFKKILKYL–NH_2) were biophysically studied with bacterial and mammalian cell membrane models, essentially using optical spectroscopy techniques. Peptide-membrane binding was interpreted under a Nernst partition formalism. Both peptides strongly prefer the anionic bacterial membrane models over the zwitterionic mammalian ones, justifying, at least in part, higher antibacterial than hemolytic activities. Deviations to the expected binding behavior were observed at high bound peptide-to-lipid (P:L) ratios in the membrane whenever anionic models were used. These deviations could be ascribed to membrane saturation and occurred with both peptides. The saturation threshold could be identified for both peptides; the obtained critical P:L ratios were also consistent with membrane surface charge neutralization. Disruptive events were observed above the saturation threshold: internalization into the membrane (omiganan), leakage, membrane aggregation, membrane surface charge neutralization, and structural reorganization (BP100).

The plausibility of high membrane coverage was evaluated using a mathematical model devised to estimate the extent of binding under physiological conditions. Not only is saturation a possible phenomenon but it was also shown to be a potential requirement for peptide activity. This hypothesis could be verified using the model with published data on several AMPs. The model could be further adapted to provide a means to predict, from simple biophysical parameters (a binding constant and a critical P:L ratio), the peptide concentration at which antibacterial activity is triggered. Different methods to implement this prediction are presented.

In vivo measurements using BP100 with *Escherichia coli* were carried out to further test the correlation between membrane saturation and bacterial death. A suitable method to determine the occurrence of binding saturation with bacteria could not be devised. Nonetheless, bacterial surface charge did become neutralized by the peptide at the same concentrations that caused loss of viability, supporting a connection between the phenomena.

Keywords:

Peptide; Antimicrobial; Cell membrane; Saturation; Minimum inhibitory concentration.

Symbols & Abbreviations
and Usage Notes

In this book acronyms are expanded on first usage and whenever deemed necessary to improve clarity, although not necessarily along a description as found here. For reasons of text economy very common acronyms, scientific or not — such as DNA or US —, are not expanded nor described. Amino acid sequences are indicated using one-letter codes.

16NS 16-doxylstearic acid. Stearic acid labeled at C_{16} with a nitroxide doxyl quencher group.

5NS 5-doxylstearic acid. Stearic acid labeled at C_5 with a nitroxide doxyl quencher group.

ANTS 8-aminonaphthalene-1,3,6-trisulfonic acid. A fluorescent dye.

AMP Antimicrobial peptide. Used in this book with the same meaning as 'RAMP'.

CD Circular dichroism.

cfu Colony-forming unit. A common unit of bacterial numbers which reminds one that only bacteria that are able to form a colony will be counted when an inoculum is plated.

DPPC 1,2-dipalmitoyl-*sn*-glycero-3-phosphocholine. A zwitterionic phospholipid that forms gel-phase bilayers at room temperature.

DPPG 1,2-dipalmitoyl-*sn*-glycero-3-(phospho-rac-(1-glycerol)). An anionic phospholipid that forms gel-phase bilayers at room temperature.

D_v Concentration-ratio binding constant of a solute relative to a solid phase, such as the peptidoglycan mesh.

E. coli *Escherichia coli.*

FDA US Food and Drug Administration.

f_{PL^-} Fraction of anionic phospholipids in a mixed system.

f_{PL^c} Fraction of charged phospholipids in a mixed system.

γ_L Molar volume of phospholipids in a bilayer.

GUV Giant unilamellar vesicle. A vesicle large enough to be observed in detail using optical microscopy techniques.

I The global fluorescence intensity of a system.

IC_{50} 50% inhibitory concentration. The drug concentration leading to loss of viability of half of the cells. Preferentially used to describe toxicity against mammalian cells (see 'MIC').

I_L The global fluorescence a system would display if all the peptide molecules were bound to membranes.

IMM Institute of Molecular Medicine.

I_S The global fluorescence a system would display if all the peptide molecules were bound to membranes and in a saturation conformation.

I_W The global fluorescence a system displays when all the peptide molecules are in the aqueous phase.

K_p Partition constant of a solute among two phases, defined as a concentration-ratio.

K_{SV} Stern-Volmer constant for pure collisional quenching. The product of the bimolecular quenching kinetic constant and the fluorescence lifetime of the unquenched fluorophore.

$[L]$ Global concentration of phospholipid molecules.

L:P ratio Proportion of lipid molecules to membrane-bound peptide molecules. Inverse of the P:L ratio.

$[\boldsymbol{L}]_{\mathbf{sat}}$ Global concentration of phospholipid molecules at a saturation point.

LUV Large unilamellar vesicle. A vesicle with a diameter of the order of 10^2 nm.

MLV Multilamellar vesicle. Vesicle containing one or more smaller vesicles within. Sizes may range from those of LUVs to those of GUVs.

MIC Minimum Inhibitory Concentration. The antibiotic concentration required to achieve a 50% decrease in bacterial viability. More precisely designated MIC_{50}.

$\boldsymbol{n_L}$ Global amount of phospholipid molecules.

NMR Nuclear magnetic resonance.

$\boldsymbol{n_{\mathbf{peptide},L}}$ Amount of peptide molecules in the lipidic phase of a system.

$\boldsymbol{n_{PL^-_{\mathbf{neutralized}}}}$ Amount of anionic phospholipid molecules neutralized by the binding of a cationic peptide.

$\boldsymbol{n_{PL^-_{\mathbf{total}}}}$ Total amount of anionic phospholipid molecules in a system.

OCD Oriented circular dichroism. CD spectroscopy of chromophores embedded in a semi-solid oriented matrix, namely, oriented phospholipid bilayers.

OD Optical density. Reduction of the intensity of light transmitted through a sample due to absorption and/or scattering by particles in suspension, in absorbance units.

$[\boldsymbol{P}]$ Global concentration of peptide molecules.

$[\boldsymbol{P}]_{\boldsymbol{L}}$ Local concentration of peptide molecules in the lipidic phase of a system.

$[\boldsymbol{P}]_{\boldsymbol{L},\mathbf{MIC}}$ $[P]_L$ when $[P] = \mathrm{MIC}$ and at lipid concentrations that parallel the low amount of bacterial membrane available for binding under MIC assay conditions.

$\boldsymbol{P{:}L_{\mathbf{MIC}}}$ The P:L ratio under the same conditions as for $[P]_{L,\mathrm{MIC}}$.

P:L ratio Proportion of membrane-bound peptide molecules to lipid molecules. Inverse of the L:P ratio.

POPC 1-palmitoyl-2-oleoyl-*sn*-glycero-3-phosphocholine. A zwitterionic phospholipid that forms fluid-phase bilayers at room temperature.

POPG 1-palmitoyl-2-oleoyl-*sn*-glycero-3-(phospho-rac-(1-glycerol)). A zwitterionic phospholipid that forms fluid-phase bilayers at room temperature.

$[\boldsymbol{P}]_{\mathbf{sat}}$ Global concentration of peptide molecules at a saturation point.

$[\boldsymbol{P}]_{\boldsymbol{W}}$ Local concentration of peptide molecules in the aqueous phase of a system (usually assumed to occupy the whole volume of the system).

$[\boldsymbol{P}]_{\boldsymbol{W},\mathbf{MIC}}$ $[P]_W$ for a system under the same conditions as for $[P]_{L,\mathrm{MIC}}$.

RAMP Ribosomal AMP. An AMP that is either ribosomally assembled or a synthetic derivative of AMPs that are.

$\boldsymbol{\sigma}$ The P:L ratio at saturation.

$\boldsymbol{S}$ The bound concentration above which a saturation conformation is gradually induced, in a model that includes an intermediate state between non-saturation and saturation.

S. aureus *Staphylococcus aureus*.

SIMEXDA Acronym for 'simulated experimental data analysis'. An algorithm used to calculate in-depth fluorophore distributions from differential quenching data.

$\boldsymbol{X_L}$ Fraction of peptide molecules that are in the lipidic phase of a system.

$\boldsymbol{X_{L,ns}}$ Fraction of peptide molecules in the lipidic phase of a system, in a non-saturated conformation. Used in models that allow the coexistence of saturated and unsaturated membrane-bound conformations.

$\boldsymbol{X_{L,s}}$ Fraction of peptide molecules in the lipidic phase of a system, in a saturated conformation. Used in models that allow the coexistence of saturated and unsaturated membrane-bound conformations.

$\boldsymbol{X_W}$ Fraction of peptide molecules that are in the aqueous phase of a system.

$\boldsymbol{\zeta}$ The ζ-potential of particles in a solution or suspension.

$\boldsymbol{\zeta_0}$ The ζ-potential of a suspension of charged vesicles in the absence of peptide.

$\boldsymbol{z_{\mathbf{peptide}}}$ Global electric charge per peptide, in absolute value.

The reader will find this book divided in chapters and sections; manuscripts were incorporated under the 'Article' heading. Unpublished data that are already submitted for publication were included as an article on its own. Other unpublished data are described where fit along the text.

Both the manuscripts' and the book's page-numbering were kept, the latter being clearly labeled to prevent confusion when the two are used simultaneously. Apart from the downscaling to fit this page size, some of the included published manuscripts were slightly modified; namely, header and footer information was rearranged so as to better occupy the available space and prevent clashes with the book's page-numbering.

Contents

Part I

The Antimicrobial Peptides

Part II

Methods and Models

Preface

My PhD work, carried out under the supervision of Professor Miguel Castanho,* was projected as the study of antimicrobial peptides using mainly biophysical methodologies. However, I soon became aware that my posture as a researcher led me into a duality: I was no longer sure whether I was more interested in applying biophysical methodologies to study antimicrobial peptides or rather in using these peptides to develop and test new methodologies. The dichotomy in the perspective with which I came to face my work persists even now, and the structure of the text deliberately reflects that dual nature.

As it turned out, the work developed by me and the people with whom I collaborated contributed to the state-of-the-art both at the level of the particular peptides that were studied as well as at the level of the development of new methods and models — hopefully applicable to many other molecules. I, therefore, do not regret not having opted for any of the approaches over the other. Yet, I must admit up-front that I found the development of methods and models to be more intellectually challenging and of greater impact: it was not innocently that most results were placed in Part II, which is devoted to the developed methods, rather than in Part I, which tells the same tale from the perspective of the studied peptides. As it stands, however, neither part is completely independent of the other for the full understanding of the work, which parallels nicely the relationship between these two aspects of scientific research.

*To whom I will henceforth simply refer to as Miguel, to reflect the close professional and personal friendship we developed along these years. The reader will find in these pages some of the reasons behind this proximity.

This project began in the final, practical year of my graduation in Biochemistry, also carried out under Miguel's supervision. While I could focus this book exclusively on the work performed during the PhD proper, leaving the first year out of this description would mean that key events in my research and in my development as a scientist would have to be skipped. I, therefore, chose to cover in this text the work of roughly five years: from the beginning of my last undergraduate year to the end of my PhD. To avoid unnecessary repetition of this description, throughout the book I used simply the term 'PhD' to refer to the whole project.

This thesis is extensively based on published work, which is reproduced within: as less technical detail had to be described the writing process was significantly simplified. The downside to this approach is that theses written in this format risk becoming a collection of papers glued together by space-filling text that simply rephrases the already published introductions or repeats the theoretical bases of the used methodologies. Rather than going in that direction myself, I found it more interesting, to me as the writer and also to potential readers, to dedicate that text to the description, from a scientific standpoint, of the path that has led me through my PhD. Unlike introductions and theoretical backgrounds, this account cannot be found in the bibliography.

Because the story of my PhD is not based exclusively on the published work, and also for the sake of completeness, chapters were included to describe data and methods that have not (yet) found their way into scientific papers. Minding the above considerations I looked for a balance between descriptiveness and readability. In the end, I have tried to write a thesis as pleasant to read as my PhD work was to carry out.

Part I

The Antimicrobial Peptides

Beginning

When I joined Miguel Castanho's team — the Molecular Biophysics group, then at the Faculty of Sciences of the University of Lisbon — the choice of antimicrobial peptides (AMPs) as my subject matter fit nicely with the ongoing work. Miguel had made a strong bet on the biophysical study of novel peptide drugs and, besides the AMPs that I was going to work with, projects included the study of cell-penetrating peptides (by Sónia Henriques), peptidic HIV fusion inhibitors (by Salomé Veiga), and peptide analgesics (by Sílvia Lopes). The fact that everyone at the group was already working with peptides, but not AMPs, meant that I could tap into the group's experimental background in the field and still be independent in the execution of my project.

Miguel's invitation to study AMPs attracted me because of the relative novelty of the theme, the apparent simplicity of the peptides and model systems — the methodologies I would be using revolved mostly around the characterization of peptide-membrane interactions using liposomes — and, above all, by the ease with which such simple systems lent themselves to be mathematically modeled. I admit I may be projecting these considerations *a posteriori* but the fact is I have frequently felt fortunate for having accepted that invitation.

1. A brief introduction to AMPs

The establishment of the AMPs as a class dates back to the 80's when the discovery of the frog-skin AMP magainin spurred research in the field[1] although other peptides with antibacterial properties were already known by then.[2,3] Many more peptides from several other organisms — including humans — have been characterized in subsequent years, with the rather generic label 'AMP' providing a minimum of systematization to their classification.*

While the name 'antimicrobial peptides' clearly indicates that the grouping of these peptides is dictated by their antibiotic properties, other common characteristics have emerged and have since become close synonyms with the term 'AMP' itself. These characteristics, inevitably repeated in any self-respecting review on AMPs (see references 4 and 5 for some of the most comprehensive ones), relate mainly to peptide length, charge, and hydrophobicity: most AMPs do not exceed 30 amino acids in length; they frequently have a high cationic charge — 6+ is common, even for peptide lengths under 20 amino acids; and they usually contain, alongside with the basic residues, a high content of hydrophobic sidechains. A corollary of the last two attributes is that AMPs tend to interact strongly with phospholipid membranes, especially the anionic bacterial ones.

The observation of common traits among AMPs led to a somewhat

*Any peptide with antimicrobial properties may be classified as an AMP but the term is commonly used to denote exclusively the peptides that are either ribosomally assembled or the synthetic derivatives of these. This was the usage adopted throughout the book. The term 'RAMP' (ribosomal AMP) is also used to designate, more appropriately but much less frequently, the same subgroup; 'ribosomal' was kept in the title of this thesis, and 'RAMP' was used throughout Article II.

tacit conviction that other features, namely their mechanism of action, could be equally generalized.[6] If a complete understanding of such a general mechanism were attained very accurate antimicrobial drug design would be possible — an important advance considering the worrisome worldwide drug resistance scenario. It was not long, however, before it was realized that a unified mechanism could not even account for the differences in AMP-mediated cell membrane disruption,[7] much less for the whole antimicrobial process. Presently, and for the membrane disruptive AMPs alone, at least three distinct mechanisms of membrane perturbation have been proposed[8–11] (see Figure 1.1 for an illustration of these mechanisms; incidentally, the figure was the one intended for Article V but ended up being replaced by a much duller — if of greater scientific accuracy — editorial version). Alternatively, AMPs have been classified according to their structure when bound to membranes,[4] content of specific amino acids,[12] percursor forms,[13] or natural occurrence.[14] But, while trends in behavior have been found within such classes, an accurate prediction of an AMP's mechanism still cannot be made solely from these general characteristics.

Therapeutically, some very attractive characteristics make up for the often incomplete description of the action of the peptides: AMPs are antibiotics to which widespread resistance has not yet developed and, more importantly, AMPs are antibiotics against which bacterial resistance seems to be costlier to acquire.[15] This is presumed to be so because most AMPs target the cell membrane, a vital structure that cannot be easily modified without compromising other cellular functions.[16] In addition, the peptides often interact diffusely with the membrane without a specific binding target (for an opposite example think of β-lactam binding to their transpeptidase targets[17]); point mutations seem unlikely to prevent that unspecific interaction. Ultimately, I believe bacteria fail to effectively develop resistance to AMPs for the same reasons we find it hard to fully describe their modes of action.

The apparent absence of specific binding targets for most AMPs has earned them the nickname of "dirty drugs" in that relatively high concentrations are required for activity, which potentiates the occurrence of

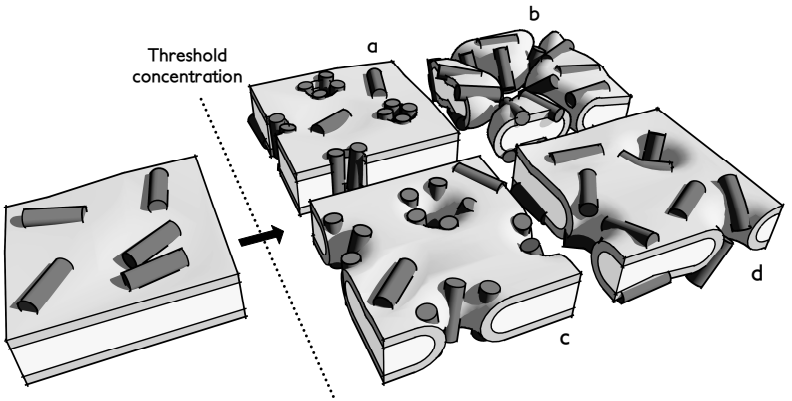

Figure 1.1 – Proposed models for AMP-mediated membrane disruption. After a threshold concentration in the membrane is reached peptides may induce: a) barrel-stave pores[8]; b) carpeting and bilayer disintegration[9]; c) toroidal pores[10]; and d) disordered toroidal pores,[11] which are a recent modification to the toroidal pore model. See the legend of Figure 1 in Article V for further details on each model.

side-effects. However, rather than just a source of undesired action, this lack of specificity may also be one of the factors behind the broad range of therapeutic applications of these peptides: besides antimicrobial activity some AMPs have been shown to possess antiviral,[18,19] antitumoral,[20] immunomodulating,[21] or cell-penetrating properties (see Article I ahead). Because of this, and because membrane interaction seems ubiquitous to these processes, Miguel is keen on seeing outside the antimicrobial box and suggests that the more abstract label 'membrane-active peptides' may better suit these drugs. Sónia, Miguel and I co-wrote a discussion paper, included at the end of the section as Article I, on the features shared by antimicrobial and cell-penetrating peptides. As argued in the review, this is more than just a conceptual proximity: AMPs, for example, have been used as templates to rationally design or improve cell-penetrating peptides.

Returning to the action of AMPs, the requirement of relatively high concentrations translates as MIC (the antimicrobial minimum inhibitory concentration) values typically lying in the low micromolar range. This

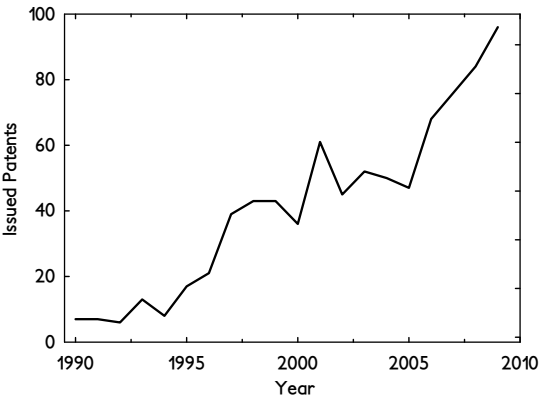

Figure 1.2 – Number of patents issued per year by the US Patent and Trademark Office with the terms 'antimicrobial peptides', 'antibiotic peptides', 'antibacterial peptides', or 'antifungic peptides'. Search conducted on the Free Patents Online database[22] for patents where the two terms occur within three words of each other.

stands somewhat midway between the nanomolar activities of target-specific drugs such as the β-lactams, and the millimolar concentrations at which many more substances can be expected to become toxic by sheer ionic and osmotic imbalance. Still, peptides can be modified so that toxicity to mammalian cells occurs only at concentrations at least one order of magnitude above the MIC,[23] which means there is a reasonably wide therapeutic window. In addition, while seemingly just a consequence of unspecific binding, the relatively high MICs will later be shown to play an important role in the development of a model of the antimicrobial mechanism of AMPs.

Twenty years of AMP research have yielded a handful of drug leads that are currently crawling their way through the approval process. Two peptides have made it as far as Phase III testing with the US Food and Drug Administration (FDA) but, to date and rather disappointingly, no one has resulted in a new drug application. This, it seems, has not discouraged researchers: a coarse search on issued patents (Figure 1.2) shows the AMPs' to be a growing field.

Article I

REVIEW ARTICLE

Cell-penetrating peptides and antimicrobial peptides: how different are they?

Sónia Troeira HENRIQUES, Manuel Nuno MELO and Miguel A. R. B. CASTANHO[1]

Centro de Química e Bioquímica, Faculdade de Ciências da Universidade de Lisboa, Ed. C8, Campo Grande, 1749-016 Lisbon, Portugal

Some cationic peptides, referred to as CPPs (cell-penetrating peptides), have the ability to translocate across biological membranes in a non-disruptive way and to overcome the impermeable nature of the cell membrane. They have been successfully used for drug delivery into mammalian cells; however, there is no consensus about the mechanism of cellular uptake. Both endocytic and non-endocytic pathways are supported by experimental evidence. The observation that some AMPs (antimicrobial peptides) can enter host cells without damaging their cytoplasmic membrane, as well as kill pathogenic agents, has also attracted attention. The capacity to translocate across the cell membrane has been reported for some of these AMPs. Like CPPs, AMPs are short and cationic sequences with a high affinity for membranes. Similarities between CPPs and AMPs prompted us to question if these two classes of peptides really belong to unrelated families. In this Review, a critical comparison of the mechanisms that underlie cellular uptake is undertaken. A reflection and a new perspective about CPPs and AMPs are presented.

Key words: antimicrobial peptide, cell-penetrating peptide, drug delivery, internalization, translocation mechanism.

INTRODUCTION

The hydrophobic nature of cellular membranes makes them impermeable for most peptides, proteins and oligonucleotides. Different strategies have been employed to penetrate the membrane barrier and deliver hydrophilic molecules inside the cell for either experimental or therapeutic purposes. So far, microinjection, electroporation, liposomes and viral vectors have been used. Most of these delivery strategies have serious drawbacks, such as low efficiency, poor specificity, poor bioavailability and extensive toxicity [1]. Moreover, they are time-consuming. The endocytic route has been used as an alternative for the import of hydrophilic macromolecules into living cells [2]. However, the proteins engaging in this mechanism stay enclosed within endosomes, and so fail to access the cytoplasm, thus missing their final target.

Peptides as vectors to introduce macromolecules into cells

An efficient strategy with which to penetrate the membrane barrier was identified by the observation that some intracellular proteins, when added to extracellular medium, were able to pass through the membrane. Tat (HIV-1 transcriptional activator protein) [3] and pAntp (*Drosophila* antennapedia transcription protein) [4] were the first proteins to be identified with this characteristic. The ability to translocate is attributed to basic amino acid sequences in these proteins, and the minimal peptide sequence necessary for the translocation to occur within Tat [5] and pAntp [6] have been elucidated. The observation that these basic peptides allow cellular delivery of conjugated molecules such as peptides [7] or proteins [8] made these molecules attractive, and a new class of vectors, initially known as PTDs (protein transduction domains) [9], but more recently re-baptized as CPPs (cell-penetrating peptides) [10], emerged. This family now includes all the peptides with the ability to translocate across membranes, regardless of whether they are natural, synthetic or chimaeric peptides.

So far, these vectors have been used to translocate a wide range of macromolecules into living cells, including proteins [8,9,11], peptides [7,12], oligonucleotides [13,14], peptide nucleic acids [15] and polysaccharides [16]. Nanoparticles [17] and liposomes [18] have also been internalized by means of CPPs.

Can AMPs (antimicrobial peptides) also work as vectors?

Most organisms produce gene-encoded AMPs as innate defences to prevent colonization and infection by several microbial pathogens [19–22]. Despite their ubiquity, AMPs can have very distinct sequences and modes of action [23,24]; nonetheless, they usually share several characteristics, such as their short length (a few tens of residues) and their cationicity, typically of charge 4+ or 5+ [25]. Other features of these peptides include their strong interaction with lipidic membranes, a usually broad killing spectrum and their ability to preserve host-cell integrity [23,24].

Clinically these peptides display antimicrobial activity at micromolar concentrations or less, and target bacteria do not seem to readily develop resistance. These properties make AMPs very promising candidates for new generations of drugs to fight antibiotic-resistant strains of pathogens [23,26].

Although most AMPs seem to act mainly at the membrane level [24,25], their translocation into the cytoplasm is not uncommon [27,28]; because of this property, membrane-crossing AMPs have also been used as templates for CPP development [29]. Thus AMPs can have clinical applications both as antibiotics and as precursors of drug transporters.

HOW DO CPPs TRANSLOCATE ACROSS THE CELL MEMBRANE?

There is no consensus regarding the mechanism of translocation of CPPs; the information available in the literature is controversial. First it was suggested that these peptides translocate by a

Abbreviations used: AMP, antimicrobial peptide; CF, carboxyfluorescein; CPP, cell-penetrating peptide; NLS, nuclear localization signal; pAntp, *Drosophila* antennapedia transcription protein; SV40, simian virus 40; Tat, HIV-1 transcriptional activator protein.

[1] To whom correspondence should be addressed (email castanho@fc.ul.pt).

© 2006 Biochemical Society

Table 1 Source, amino acid sequences and possible internalization mechanism for some examples of peptides that work as CPPs or as AMPs

Name (sequence)	Source [reference] [internalization mechanism(s), reference(s)]
Penetratin (RQIKIWFQNRRMKWKK)	pAntp homeodomain (amino acids 43–58) [6] (mainly endocytosis [39], endosomal escape mediated by pH gradient or transmembrane potential [36,53])
Tat (GRKKRRQRRRPPQ)	HIV-1 transcriptional activator Tat protein (amino acids 48–60) [5] (mainly endocytosis [40], endosomal escape mediated by pH gradient or transmembrane potential [37])
Pep-1 (Ac-KETWWETWWTEWSQPKKKRKV-cysteamine)	Amphipathic chimaeric peptide with a tryptophan-rich domain and an NLS [57] (physical mechanism mediated by peptide–membrane interaction promoted by pore formation [60] or by transmembrane potential without pores [35])
$S4_{13}$-PV (ALWKTLLKKVLKAPKKKRKV-cysteamine)	Chimaeric peptide with AMP dermaseptin S4 and an NLS [61] (mainly physical mechanism promoted by a transient membrane destabilization [62])
Magainin 2 (GIGKFLHSAKKFGKAFVGEIMNS)	AMP from the skin of the South-African clawed frog *Xenopus laevis* [101] (translocation mediated by toroidal pore formation; peptide molecules translocate stochastically as the pore disintegrates [28])
Buforin 2 (TRSSRAGLQFPVGRVHRLLRK)	AMP from the stomach of the Korean common toad *Bufo bufo gargarizans* [102] (peptide molecules translocate stochastically after the formation and disintegration of a non-permeabilizing pore-like structure [84])
Apidaecins (RP - - - - - PRPPHPR (conserved sequence among class members)	AMP from the lymph fluid of several insects [103] (receptor-dependent membrane docking and translocation into target cell [104])

mechanism independent of receptors [30] and independent of the endosomal pathway [5,6]. A physically driven mechanism was suggested, because the cellular uptake at 4 °C and 37 °C was similar [5,6,30,31].

More recent observations led to controversial results, suggesting that the cell localization observed for CPPs is an artefact and results from cell fixation for immunochemistry and cell visualization [32]. The high peptide affinity for membranes may allow CPPs to remain attached to cells during washing. During the cell fixation process, CPPs are released, and the apparent localization inside the cell results therefrom. However, direct observation of translocation in model membrane systems for some CPPs [33–35] supports the existence of physically driven mechanisms governed by spontaneous peptide–membrane interactions. The translocation mechanism issue is thus complex and may differ for different classes of CPPs (Table 1).

CPPs derived from natural proteins

The CPP derived from pAntp has 16 amino acids and is the sequence necessary and sufficient for translocation to occur [6] (Table 1) and is commonly called 'penetratin'. The Tat fragment corresponding to residues 48–60 [5] (Table 1), and a shorter fragment (residues 47–57) [18,36,37], have frequently been used in CPP research.

An endosomal pathway for internalization was initially excluded by comparison of the uptake at 4 °C and 37 °C under fixation conditions [5,6,30]. After re-evaluation for the interference of artefacts during fixation, an internalization mediated by endocytosis was concluded for both penetratin [38,39] and Tat peptide [37,40–43]. The basic amino acids are essential for translocation to occur, and membrane binding seems to be the first step prior to endocytic uptake. Heparan sulfate proteoglycans at the cell membrane were proposed to act as receptor for penetratin [42,44–46] and Tat peptide [42,47].

Although it is accepted that these CPPs can enter the cells by endocytosis, there is no consensus in the specific endocytic pathway used for the import of these arginine-rich peptides. A raft-dependent pathway involving macropinocytosis [48] or caveolae [41,49,50], or a clathrin-dependent endocytosis [47,51,52], were proposed. The dissimilarities among these results can arise from the use of different cell lines, methodologies, labelled peptides, protein-conjugated peptides and different conditions, which can inhibit some pathways while favouring others.

Even in a picture where the endosomal pathway emerges as the physiological uptake of CPPs, the escape from endosomes into the cytoplasm through a physically driven mechanism persists. An escape from endosomes due to acidification was proposed for penetratin and Tat peptide [36,37]. This hypothesis is supported by the results obtained by Gräslund and co-workers [53] with penetratin encapsulated in large unilamellar vesicles. The escape of penetratin occurred only in the presence of a pH gradient. The role of intracellular pH in the internalization of CPPs was also investigated using neutralization agents [38].

A dependence of translocation on a negative transmembrane potential was identified *in vitro* for both penetratin and Tat peptide [34] and *in vivo* for Tat peptide [54]. Terrone et al. [34] suggested that a fraction of the peptide can transverse through the membrane by a transmembrane potential-driven mechanism, whereas the other fraction is internalized by an endosomal pathway. Once inside the endosomes, the transmembrane potential (luminal side positive) drives translocation from the endosomal lumen to the cytoplasm. By contrast, Drin et al. [38] did not find any internalization of penetratin in liposomes, even in the presence of a transmembrane potential. Recently Bárány-Wallje et al. [55], following electrophysiological measurements in planar bilayers, failed to detect translocation, even in the presence of applied voltages.

Chimaeric peptides

The usefulness of peptides as vehicles to introduce macromolecules into cells led to the development of many chimaeric peptides. Pep-1 (acetyl-KETWWETWWTEWSQPKKKRKV-cysteamine) is a CPP with primary amphipathicity (i.e amphipathicity resulting from the amino acid sequence itself, not from the folding structure [56]) that comprises a tryptophan-rich so-called 'hydrophobic' domain, a hydrophilic domain derived from an NLS (nuclear localization signal) of SV40 (simian virus 40) large T-antigen, and a

© 2006 Biochemical Society

spacer between them [57]. A cysteamine group is present at the C-terminus [57] (Table 1).

Pep-1 has been used to introduce large proteins inside cell lines [57–59]. An endosomal pathway was rejected because (1) there was no difference in translocation efficiency at 37 °C and 4 °C [57] and (2) no co-localization of a delivered protein (β-galactosidase from *Escherichia coli*) with different cellular organelles (early endosomes, caveosomes and lysosomes) was detected [59]. By contrast, Weller et al. [58] proposed an endosome-mediated mechanism based on the internalization of Pep-1–protein complexes in the presence or absence of endocytic inhibitors.

Deshayes et al. [60] proposed a transient transmembrane-pore-like structure promoted by α-helix conformation of the hydrophobic domain when it interacts with membranes. This conclusion was not corroborated by other groups, because no membrane leakage was detected [35,58]. An alternative mechanism, mediated by electrostatic peptide–lipid interactions, was proposed after observation that Pep-1 translocation both *in vitro* [35] or *in vivo* [59] only occurs in the presence of a transmembrane potential.

When Pep-1 was modified at the C-terminus [lack of cysteamine group and grafting of a CF (carboxyfluorescein) group], the membrane affinity and the translocation efficiency was truly impaired, but a small uptake seems to occur by an endocytic mechanism [16].

The chimaeric peptide $S4_{13}$-PV, which results from the combination of a 13-amino-acid sequence derived from the dermaseptin S4 ($S4_{13}$ domain) with the NLS from SV40 large T-antigen (see Table 1), was proposed as a potential vehicle to introduce macromolecules into cells [61]. The uptake of this peptide under non-fixation conditions was not decreased in the presence of endocytic inhibitors [62]. An endocytic uptake was only evident at low peptide concentration [63]. The binding of the $S4_{13}$-PV peptide to the cell membrane is promoted by electrostatic interactions with negatively charged components at the cell surface, and a conformation change in the $S4_{13}$ domain upon insertion into the bilayers was detected [62]. The translocation of $S4_{13}$-PV across the cell membrane is considered to be a consequence of a transient membrane destabilization produced by peptide–membrane interactions [62]. Endosomal internalization at low peptide concentration suggests that higher peptide concentrations are necessary to induce membrane destabilization.

Translocation mechanism or mechanisms?

Considering the abovementioned examples, it is clear that the mechanism by which CPPs translocate across cell membrane and deliver their cargoes in the cytosol is far from being totally understood. Although some CPPs are able to translocate by an endocytic pathway, the escape from endosomes demands a physically driven mechanism.

The affinity of each CPP for lipid bilayers may be the key factor for their main mechanism of uptake. Penetratin, for instance, does not show a strong affinity for zwitterionic membranes [46,64,65] and does not induce significant membrane destabilization [66]. Interaction with model membranes only occurs in negatively charged lipid bilayers [46,65]. In studies of the interaction of this peptide with eukaryotic cells, negatively charged proteoglycans presented at the cell surface were regarded as essential for translocation to occur [42,44,45]. Cellular uptake of penetratin occurs via endocytosis, but requires the expression of proteoglycans [42], which demonstrates the importance of electrostatic interactions in increasing the affinity of the peptide for cell membranes [45].

By contrast, Pep-1 has a high affinity for lipidic membranes, even in the absence of negatively charged phospholipids or proteoglycans [67], and it induces significant membrane destabilization [35], which seems to favour internalization. Moreover, the introduction of a CF dye into the hydrophilic domain of Pep-1 and/or deletion of a cysteamine group decreased the peptide's affinity and, consequently, its uptake [16,58], and a slight internalization by endosomal pathway occurs [16]. This suggests that the membrane affinity and the capacity to destabilize it dictate the extent to which a peptide enters the cell by a physical mechanism (a fast process during which the endosomal pathway may be considered stationary) to the detriment of the endosomal pathway.

The hypothesis of the co-existence of endosomal and physically mediated mechanisms was also proposed by Boisseau et al. [68] in a study with maurocalcine, a CPP isolated from the Israeli gold scorpion (*Scorpio maurus palmatus*). A contribution of both mechanisms was identified where the physically driven mechanism results from a transmembrane potential. Moreover, Nakase et al. [69] showed that greater amounts of oligo-arginine were found in the cytoplasm when cells were incubated at 4 °C than at 37 °C. They proposed that, when endosomal pathways are inhibited and an alternative pathway can operate, the peptide is more efficiently translocated to the cytosol. When incubation is at 37 °C, oligo-arginine release in the cytoplasm is difficult, owing to endosome entrapment.

Translocation by a physical mechanism demands not only the existence of a high membrane affinity, but also a promoting force: pH gradients [53] and transmembrane potentials [34] are two possible driving forces. The existence of such driving forces is well understood in the cell context, where in/out media are characterized by the preservation of gradients.

HOW DO AMPs GET INSIDE CELLS?

The mechanisms by which AMPs gain access to a cell's interior can be classified as pore-dependent and pore-independent, the former being the most usual. In fact, there are relatively few AMPs that do not exert their main function via cell lysis, membrane permeabilization or other forms of bilayer disruption. Few AMPs attack internal targets, and, of those, only a small number can do so without membrane perturbation [70].

AMPs that induce membrane permeabilization

After the initial peptide–membrane interaction, mechanisms diverge; besides lysis, usually by a mechanism known as the 'carpet' model [71,72], two other models have been proposed for AMP pore formation: the barrel-stave pore and the toroidal pore (for further detailed information, see references [73,74]).

Independently of the pore type, diffusion of free peptide through the pore may not be the principal process of translocation; instead, it has been proposed that it is the peptide molecules that are involved in pore formation that stochastically translocate as the pore disintegrates [28]. Several factors support this statement, the most relevant being the fact that, for AMPs, the local concentration of membrane-bound peptide molecules is usually several orders of magnitude higher than in the aqueous phase (e.g. [75,76]); as such, there will be many more peptide molecules available for pore formation than for pore crossing. In addition, pore diameters are relatively narrow and usually not longer than the length of the peptides (alamethicin barrel stave pores have a diameter of 2–3 nm [77] and those of toroidal mellitin have a diameter of 3–4 nm [74]), preventing or hindering a free diffusion of the peptide; lastly, pore lifetimes are in the microsecond-to-millisecond range (between 40 μs for magainin and 200 ms for dermaseptins [28,78]), which is long compared with a single-molecule translocation time, but

© 2006 Biochemical Society

probably not long enough to quickly equilibrate inner and outer peptide concentrations.

Given this hypothesis, pore formation can be regarded not only as a membrane perturbation process, but also as an important intermediate step towards cellular invasion by AMPs. This is in agreement with recent findings that indicate that a synergic effect of activity at both membrane and cytoplasm levels may be required to fully explain the mechanisms of some pore-forming AMPs [79–81].

Non-lytic AMPs

For AMPs that preferentially attack internal cellular targets, similar translocation mechanisms have been reported: for buforin 2, which translocates efficiently, but with little membrane activity [70,82,83], the structure and orientation in the bilayer have been observed to be very similar to those of magainin 2 (Table 1) [83,84]. From these results a model was proposed whereby buforin 2 molecules would form a toroidal pore, just as magainin 2 does, but less stable; this would result in shorter pore lifetimes – with a concomitant decrease in permeabilization – at the same time that the translocation rate would increase because pore disintegration, which is the actual translocation step, would become more frequent [83,84]. This model is supported by results that show that the presence of bilayer components that prevent the formation of toroidal pores (such as dioleyl phosphatidylethanolamine [28]) inhibit buforin 2 translocation, whereas anionic phospholipids, which decrease the charge repulsions between the cationic peptide molecules, stabilize the pore to a point that significant leakage and flip-flop is observed [84]. Buforin 2 translocation has also been shown to withstand cargo addition, as demonstrated by the attachment of green fluorescent protein [29,85], which makes this peptide a promising candidate for its development into a CPP.

Other mechanisms of translocation

Apidaecins, which are another class of non-lytic AMPs that are able to kill bacteria with undetectable membrane permeabilization, act by binding to a cytoplasmic target (Table 1) [86]. In this case, translocation has been proposed to occur by specific interaction with a putative membrane permease or transporter in the target bacterial cell; this was suggested by the fact that the all-D enantiomers of the peptides lose the ability to cross the membrane [86]. This characteristic confers a high selectivity on these peptides, which can even be modulated [87], but, on the other hand, the need for a membrane transporter makes apidaecins unappealing as templates for CPP design.

Despite their apparent simplicity, many AMPs have been shown to possess activity-specific regions: through sequence manipulation it has been possible to regulate translocating behaviour, target specificity or antimicrobial efficiency [87–89]. By means of these alterations, it has become possible to broaden the spectrum of CPP template candidates beyond non-cytotoxic translocating AMPs. This has been taken advantage of, for example, in the derivatives of the membrane-active Bac7 peptide [29,88,90], which, unlike their precursor, are not membrane-disruptive, but have retained translocation capabilities.

CPPs AND AMPs OR JUST MEMBRANE-ACTIVE PEPTIDES?

Membrane translocation is a corollary for membrane permeabilization. Although treated differently by people interested in CPPs and AMPs, the ability to reach the inner leaflet of lipid bilayers is of crucial importance to both. Potentially, all CPPs are AMPs and all AMPs are CPPs. At high enough concentration, peptides reported as CPP perturb membranes and become membrane permeabilizers (see reference [91], in which antimicrobial activity of different CPPs is evaluated), whereas AMPs may reach cytoplasmatic targets before membrane permeabilization. This is not surprising, because both CPPs and AMPs are very similar molecules: short cationic peptides. It should be stressed that both classes cannot be differentiated on account of their structure because there is a wide diversity of conformations within each class of peptides [25,92]. The attention devoted to both CPPs and AMPs is very application-oriented, which dictates why these very similar classes of molecules are considered in such a separate fashion. CPPs are mainly studied by people focusing on gene therapy and drug delivery. AMPs are mainly regarded as tools to fight bacterial infections. However, from the molecular mechanistic point of view, the separation of these peptides into two groups is really rather academic.

Cellular membranes of target cells where the activity of these two peptides are evaluated are quite different. CPPs are generally evaluated against mammalian cells, whereas the target of AMPs is the bacterial cell. The major differences rely on anionic-lipidic and cholesterol contents. The bacterial membrane has a higher percentage of negatively charged lipids and does not contain sterols [24]. Different effects reported with CPPs and AMPs can arise from the differences in membrane composition, factors which modulate peptide affinity and membrane destabilization.

Considering the overlap between the mode of action of CPPs and AMPs, it does not seem reasonable to obstinately seek an exclusive answer to the question whether CPPs enter cells through endocytic or physical processes. As indicated above in the present Review, depending on circumstances, the same peptide may potentially use both [16,63,68]. Moreover, endocytic entrapment has to be followed by physical membrane translocation if the peptide is to reach the cytoplasm. The physical pathway can be mechanistically described by the interaction equilibrium between the peptides in the medium and the outer leaflet of membranes, perturbation of bilayers, translocation among leaflets and a second equilibrium of the peptides between the inner leaflet of the membrane and the reducing conditions of the cell interior [67,93–95] (Figure 1). A more effective or faster formation of a membrane-disturbing structure, mediated by the AMP magainin, was identified when a transmembrane potential was present [96].

Certain chimaera peptides, such as Pep-1, may even be considered a ‘blend’ between AMPs and CPPs. Although reported as a CPP, Pep-1 is a strongly amphipathic cationic peptide, rich in basic amino acids and tryptophan, having a proline residue in its sequence. These are classical characteristics attributed to AMPs. The ability to cysteine-bridge monomers, which greatly improves translocation efficiency, further increases the similarities to AMPs. Not surprisingly, Pep-1 uses mainly physical routes to translocate membranes [35,57,59]. However, this route is not always operative [16], and endocytic pathways are alternatives. The results obtained with Pep-1 confirm the co-existence of endocytic and physically mediated pathways. Such co-existence was previously proposed by other authors [97] using other CPPs, but this proposal was largely overlooked. The kinetic factor is important, as progress through physically driven pathways is rapid compared with that through endocytic pathways: when both physical and endocytic pathways are operative, the physical pathway is dominant, owing to faster kinetics [67,93].

These peptides are able to destabilize the membrane (fusion and vesicle aggregation were detected) without evidence for pore formation or flip-flop [35,66]. A ‘membrane-thinning’ effect was proposed for the AMP magainin 2 [98], in which the peptide aggregates on the surface of the membrane and the decreased local surface tension allows the peptide to intercalate the membrane.

© 2006 Biochemical Society

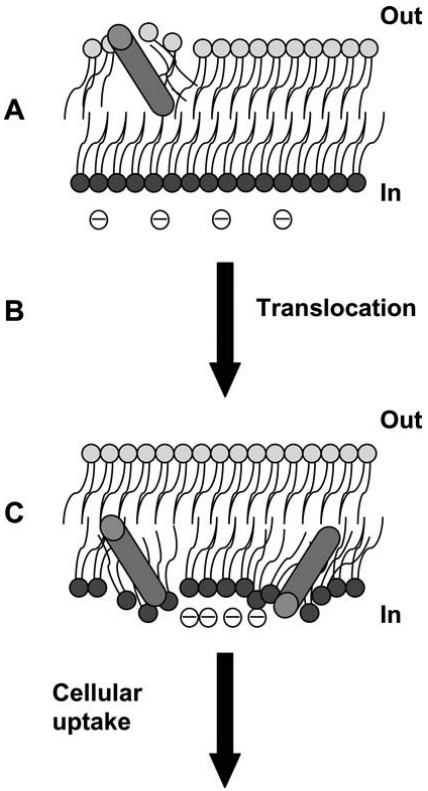

Figure 1 CPP translocation by a physically driven process can be regarded as a composite of three sequential steps

(**A**) The peptide (dark-grey cylinder) inserts in the bilayer outer interface (light-grey head-groups with fatty acid tails) and causes local membrane perturbation. (**B**) Owing to a membrane gradient (e.g. transmembrane potential, pH gradient) or concentration effects, the peptide overcomes the hydrophobic core of the bilayer by an unknown mechanism. (**C**) The peptide is released from the inner leaflet of the membrane (blue head-groups with fatty acid tails) to the cytoplasm. In a model artificial system (e.g. a vesicle) the system would tend to an equilibrium that can be accounted for by three different partition constants, one for each of the elementary steps (**A**, **B** and **C**).

Flexible sealing between peptide side groups and lipid head-groups minimize leakage during the peptide passage through the membrane [29].

A pore-formation mechanism was proposed for MPG (a 27-residue amphipathic peptide) and Pep-1 [60,99], which is also a common mechanism used by antimicrobial peptides. In the case of a transmembrane pore, a large pore would be necessary to allow the passage of attached macromolecules, a situation that compromises cell viability and all the significance of these peptides as vehicles. In some cases pore formation can explain the translocation of the peptides *per se*; however, these pores are not large enough to explain the translocation of proteins [28].

The history of CPP research can be summarized from two different periods, with a sudden change of paradigm in 2001 [32], later confirmed in 2003 [100]. First, the physical paradigm dominated. CPPs were considered to cross bilayers by a physical process. Since 2001–2003 there has been a tendency to think the opposite. Reality may not be so black-and-white, and this rather simplistic view of physically driven versus endocytic mechanisms seems inadequate. The CPP research community should go back to basics and redefine CPPs on the basis of their cargo translocation ability rather than their stand-alone peptide properties.

Most of the CPP research focuses on the peptides' membrane-translocation ability in the absence of cargoes. It is thus crucial to develop new methodologies to detect and quantify translocation of peptide-mediated cargo translocation in vesicles and cells.

As to the peptides themselves, and their interaction with lipid bilayers, it may be that the frontiers between fusogenic peptides, AMPs and CPPs become so undefined that, in the near future, only the unified broad-scope title of 'membrane-active peptides' will make sense.

REFERENCES

1 Wadia, J. S., Becker-Hapak, M. and Dowdy, S. F. (2002) Protein Transport, CRC Press, New York
2 Leamon, C. P. and Low, P. S. (1991) Delivery of macromolecules into living cells: a method that exploits folate receptor endocytosis. Proc. Natl. Acad. Sci. U.S.A. **88**, 5572–5576
3 Frankel, A. D. and Pabo, C. O. (1988) Cellular uptake of the tat protein from human immunodeficiency virus. Cell **55**, 1189–1193
4 Joliot, A., Pernelle, C., Deagostini-Bazin, H. and Prochiantz, A. (1991) Antennapedia homeobox peptide regulates neural morphogenesis. Proc. Natl. Acad. Sci. U.S.A. **88**, 1864–1868
5 Vives, E., Brodin, P. and Lebleu, B. (1997) A truncated HIV-1 Tat protein basic domain rapidly translocates through the plasma membrane and accumulates in the cell nucleus. J. Biol. Chem. **272**, 16010–16017
6 Derossi, D., Joliot, A. H., Chassaing, G. and Prochiantz, A. (1994) The third helix of the Antennapedia homeodomain translocates through biological membranes. J. Biol. Chem. **269**, 10444–10450
7 Theodore, L., Derossi, D., Chassaing, G., Llirbat, B., Kubes, M., Jordan, P., Chneiweiss, H., Godement, P. and Prochiantz, A. (1995) Intraneuronal delivery of protein kinase C pseudosubstrate leads to growth cone collapse. J. Neurosci. **15**, 7158–7167
8 Fawell, S., Seery, J., Daikh, Y., Moore, C., Chen, L. L., Pepinsky, B. and Barsoum, J. (1994) Tat-mediated delivery of heterologous proteins into cells. Proc. Natl. Acad. Sci. U.S.A. **91**, 664–668
9 Ezhevsky, S. A., Nagahara, H., Vocero-Akbani, A. M., Gius, D. R., Wei, M. C. and Dowdy, S. F. (1997) Hypo-phosphorylation of the retinoblastoma protein (pRb) by cyclin D:Cdk4/6 complexes results in active pRb. Proc. Natl. Acad. Sci. U.S.A. **94**, 10699–10704
10 Lindgren, M., Hallbrink, M., Prochiantz, A. and Langel, U. (2000) Cell-penetrating peptides. Trends Pharmacol. Sci. **21**, 99–103
11 Rojas, M., Donahue, J. P., Tan, Z. and Lin, Y. Z. (1998) Genetic engineering of proteins with cell membrane permeability. Nat. Biotechnol. **16**, 370–375
12 Rojas, M., Yao, S., Donahue, J. P. and Lin, Y. Z. (1997) An alternative to phosphotyrosine-containing motifs for binding to an SH2 domain. Biochem. Biophys. Res. Commun. **234**, 675–680
13 Allinquant, B., Hantraye, P., Mailleux, P., Moya, K., Bouillot, C. and Prochiantz, A. (1995) Downregulation of amyloid precursor protein inhibits neurite outgrowth *in vitro*. J. Cell Biol. **128**, 919–927
14 Morris, M. C., Vidal, P., Chaloin, L., Heitz, F. and Divita, G. (1997) A new peptide vector for efficient delivery of oligonucleotides into mammalian cells. Nucleic Acids Res. **25**, 2730–2736
15 Pooga, M., Soomets, U., Hallbrink, M., Valkna, A., Saar, K., Rezaei, K., Kahl, U., Hao, J. X., Xu, X. J., Wiesenfeld-Hallin, Z. et al. (1998) Cell penetrating PNA constructs regulate galanin receptor levels and modify pain transmission *in vivo*. Nat. Biotechnol. **16**, 857–861
16 Henriques, S. T., Costa, J. and Castanho, M. A. (2005) Re-evaluating the role of strongly charged sequences in amphipathic cell-penetrating peptides: a fluorescence study using Pep-1. FEBS Lett. **579**, 4498–4502
17 Lewin, M., Carlesso, N., Tung, C. H., Tang, X. W., Cory, D., Scadden, D. T. and Weissleder, R. (2000) Tat peptide-derivatized magnetic nanoparticles allow *in vivo* tracking and recovery of progenitor cells. Nat. Biotechnol. **18**, 410–414
18 Torchilin, V. P., Rammohan, R., Weissig, V. and Levchenko, T. S. (2001) TAT peptide on the surface of liposomes affords their efficient intracellular delivery even at low temperature and in the presence of metabolic inhibitors. Proc. Natl. Acad. Sci. U.S.A. **98**, 8786–8791

© 2006 Biochemical Society

19 Koczulla, A. R. and Bals, R. (2003) Antimicrobial peptides: current status and therapeutic potential. Drugs **63**, 389–406
20 Tossi, A., Mitaritonna, N., Tarantino, C., Giangaspero, A., Sandri, L. and Winterstein, K. A. (2003) Antimicrobial Sequences Database (http://www.bbcm.units.it/~tossi/pag1. htm)
21 Powers, J. P. and Hancock, R. E. (2003) The relationship between peptide structure and antibacterial activity. Peptides **24**, 1681–1691
22 Hancock, R. E. (2001) Cationic peptides: effectors in innate immunity and novel antimicrobials. Lancet Infect. Dis. **1**, 156–164
23 Zasloff, M. (2002) Antimicrobial peptides of multicellular organisms. Nature (London) **415**, 389–395
24 Yeaman, M. R. and Yount, N. Y. (2003) Mechanisms of antimicrobial peptide action and resistance. Pharmacol. Rev. **55**, 27–55
25 Hancock, R. E. (1997) Peptide antibiotics. Lancet **349**, 418–422
26 Melo, M. N., Dugourd, D. and Castanho, M. A. R. B. (2006) Omiganan pentahydrochloride in the front line of clinical application of antimicrobial peptides. Recent Pat. Anti-Infect. Drug Discov. **1**, 201–207
27 Zhang, L., Rozek, A. and Hancock, R. E. (2001) Interaction of cationic antimicrobial peptides with model membranes. J. Biol. Chem. **276**, 35714–35722
28 Matsuzaki, K., Murase, O., Fujii, N. and Miyajima, K. (1995) Translocation of a channel-forming antimicrobial peptide, magainin 2, across lipid bilayers by forming a pore. Biochemistry **34**, 6521–6526
29 Magzoub, M. and Gräslund, A. (2004) Cell-penetrating peptides: from inception to application. Q. Rev. Biophys. **37**, 147–195
30 Derossi, D., Calvet, S., Trembleau, A., Brunissen, A., Chassaing, G. and Prochiantz, A. (1996) Cell internalization of the third helix of the Antennapedia homeodomain is receptor-independent. J. Biol. Chem. **271**, 18188–18193
31 Futaki, S., Suzuki, T., Ohashi, W., Yagami, T., Tanaka, S., Ueda, K. and Sugiura, Y. (2001) Arginine-rich peptides. An abundant source of membrane-permeable peptides having potential as carriers for intracellular protein delivery. J. Biol. Chem. **276**, 5836–5840
32 Lundberg, M. and Johansson, M. (2001) Is VP22 nuclear homing an artifact? Nat. Biotechnol. **19**, 713–714
33 Thoren, P. E., Persson, D., Karlsson, M. and Norden, B. (2000) The Antennapedia peptide penetratin translocates across lipid bilayers – the first direct observation. FEBS Lett. **482**, 265–268
34 Terrone, D., Sang, S. L., Roudaia, L. and Silvius, J. R. (2003) Penetratin and related cell-penetrating cationic peptides can translocate across lipid bilayers in the presence of a transbilayer potential. Biochemistry **42**, 13787–13799
35 Henriques, S. T. and Castanho, M. A. (2004) Consequences of nonlytic membrane perturbation to the translocation of the cell penetrating peptide pep-1 in lipidic vesicles. Biochemistry **43**, 9716–9724
36 Fischer, R., Kohler, K., Fotin-Mleczek, M. and Brock, R. (2004) A stepwise dissection of the intracellular fate of cationic cell-penetrating peptides. J. Biol. Chem. **279**, 12625–12635
37 Potocky, T. B., Menon, A. K. and Gellman, S. H. (2003) Cytoplasmic and nuclear delivery of a TAT-derived peptide and a β-peptide after endocytic uptake into HeLa cells. J. Biol. Chem. **278**, 50188–50194
38 Drin, G., Cottin, S., Blanc, E., Rees, A. R. and Temsamani, J. (2003) Studies on the internalization mechanism of cationic cell-penetrating peptides. J. Biol. Chem. **278**, 31192–31201
39 Thoren, P. E., Persson, D., Isakson, P., Goksor, M., Onfelt, A. and Norden, B. (2003) Uptake of analogs of penetratin, Tat(48–60) and oligoarginine in live cells. Biochem. Biophys. Res. Commun. **307**, 100–107
40 Richard, J. P., Melikov, K., Vives, E., Ramos, C., Verbeure, B., Gait, M. J., Chernomordik, L. V. and Lebleu, B. (2003) Cell-penetrating peptides. A reevaluation of the mechanism of cellular uptake. J. Biol. Chem. **278**, 585–590
41 Fittipaldi, A., Ferrari, A., Zoppe, M., Arcangeli, C., Pellegrini, V., Beltram, F. and Giacca, M. (2003) Cell membrane lipid rafts mediate caveolar endocytosis of HIV-1 Tat fusion proteins. J. Biol. Chem. **278**, 34141–34149
42 Console, S., Marty, C., Garcia-Echeverria, C., Schwendener, R. and Ballmer-Hofer, K. (2003) Antennapedia and HIV transactivator of transcription (TAT) "protein transduction domains" promote endocytosis of high molecular weight cargo upon binding to cell surface glycosaminoglycans. J. Biol. Chem. **278**, 35109–35114
43 Lundberg, M., Wikstrom, S. and Johansson, M. (2003) Cell surface adherence and endocytosis of protein transduction domains. Mol. Ther. **8**, 143–150
44 Letoha, T., Kusz, E., Papai, G., Szabolcs, A., Kaszaki, J., Varga, I., Takacs, T., Penke, B. and Duda, E. (2006) *In vitro* and *in vivo* NF-κB inhibitory effects of the cell-penetrating penetratin. Mol. Pharmacol. **69**, 2027–2036
45 Letoha, T., Gaal, S., Somlai, C., Venkei, Z., Glavinas, H., Kusz, E., Duda, E., Czajlik, A., Petak, F. and Penke, B. (2005) Investigation of penetratin peptides. Part 2. *In vitro* uptake of penetratin and two of its derivatives. J. Peptide Sci. **11**, 805–811
46 Ghibaudi, E., Boscolo, B., Inserra, G., Laurenti, E., Traversa, S., Barbero, L. and Ferrari, R. P. (2005) The interaction of the cell-penetrating peptide penetratin with heparin, heparan sulfates and phospholipid vesicles investigated by ESR spectroscopy. J. Peptide Sci. **11**, 401–409
47 Richard, J. P., Melikov, K., Brooks, H., Prevot, P., Lebleu, B. and Chernomordik, L. V. (2005) Cellular uptake of unconjugated TAT peptide involves clathrin-dependent endocytosis and heparan sulfate receptors. J. Biol. Chem. **280**, 15300–15306
48 Wadia, J. S., Stan, R. V. and Dowdy, S. F. (2004) Transducible TAT–HA fusogenic peptide enhances escape of TAT-fusion proteins after lipid raft macropinocytosis. Nat. Med. **10**, 310–315
49 Renigunta, A., Krasteva, G., Konig, P., Rose, F., Klepetko, W., Grimminger, F., Seeger, W. and Hanze, J. (2006) DNA transfer into human lung cells is improved with Tat-RGD peptide by caveoli-mediated endocytosis. Bioconjug. Chem. **17**, 327–334
50 Ferrari, A., Pellegrini, V., Arcangeli, C., Fittipaldi, A., Giacca, M. and Beltram, F. (2003) Caveolae-mediated internalization of extracellular HIV-1 tat fusion proteins visualized in real time. Mol. Ther. **8**, 284–294
51 Vendeville, A., Rayne, F., Bonhoure, A., Bettache, N., Montcourrier, P. and Beaumelle, B. (2004) HIV-1 Tat enters T cells using coated pits before translocating from acidified endosomes and eliciting biological responses. Mol. Biol. Cell **15**, 2347–2360
52 Saalik, P., Elmquist, A., Hansen, M., Padari, K., Saar, K., Viht, K., Langel, U. and Pooga, M. (2004) Protein cargo delivery properties of cell-penetrating peptides. A comparative study. Bioconjug. Chem. **15**, 1246–1253
53 Magzoub, M., Pramanik, A. and Gräslund, A. (2005) Modeling the endosomal escape of cell-penetrating peptides: transmembrane pH gradient driven translocation across phospholipid bilayers. Biochemistry **44**, 14890–14897
54 Rothbard, J. B., Jessop, T. C., Lewis, R. S., Murray, B. A. and Wender, P. A. (2004) Role of membrane potential and hydrogen bonding in the mechanism of translocation of guanidinium-rich peptides into cells. J. Am. Chem. Soc. **126**, 9506–9507
55 Bárány-Wallje, E., Keller, S., Serowy, S., Geibel, S., Pohl, P., Bienert, M. and Dathe, M. (2005) A critical reassessment of penetratin translocation across lipid membranes. Biophys. J. **89**, 2513–2521
56 Fernandez-Carneado, J., Kogan, M. J., Pujals, S. and Giralt, E. (2004) Amphipathic peptides and drug delivery. Biopolymers **76**, 196–203
57 Morris, M. C., Depollier, J., Mery, J., Heitz, F. and Divita, G. (2001) A peptide carrier for the delivery of biologically active proteins into mammalian cells. Nat. Biotechnol. **19**, 1173–1176
58 Weller, K., Lauber, S., Lerch, M., Renaud, A., Merkle, H. P. and Zerbe, O. (2005) Biophysical and biological studies of end-group-modified derivatives of Pep-1. Biochemistry **44**, 15799–15811
59 Henriques, S. T., Costa, J. and Castanho, M. A. (2005) Translocation of β-galactosidase mediated by the cell-penetrating peptide pep-1 into lipid vesicles and human HeLa cells is driven by membrane electrostatic potential. Biochemistry **44**, 10189–10198
60 Deshayes, S., Heitz, A., Morris, M. C., Charnet, P., Divita, G. and Heitz, F. (2004) Insight into the mechanism of internalization of the cell-penetrating carrier peptide Pep-1 through conformational analysis. Biochemistry **43**, 1449–1457
61 Hariton-Gazal, E., Feder, R., Mor, A., Graessmann, A., Brack-Werner, R., Jans, D., Gilon, C. and Loyter, A. (2002) Targeting of nonkaryophilic cell-permeable peptides into the nuclei of intact cells by covalently attached nuclear localization signals. Biochemistry **41**, 9208–9214
62 Mano, M., Henriques, A., Paiva, A., Prieto, M., Gavilanes, F., Simoes, S. and Pedroso de Lima, M. C. (2006) Cellular uptake of $S4_{13}$-PV peptide occurs upon conformational changes induced by peptide-membrane interactions. Biochim. Biophys. Acta **1758**, 336–346
63 Mano, M., Teodosio, C., Paiva, A., Simoes, S. and Pedroso de Lima, M. C. (2005) On the mechanisms of the internalization of $S4_{13}$-PV cell-penetrating peptide. Biochem. J. **390**, 603–612
64 Magzoub, M., Kilk, K., Eriksson, L. E., Langel, U. and Gräslund, A. (2001) Interaction and structure induction of cell-penetrating peptides in the presence of phospholipid vesicles. Biochim. Biophys. Acta **1512**, 77–89
65 Christiaens, B., Symoens, S., Verheyden, S., Engelborghs, Y., Joliot, A., Prochiantz, A., Vandekerckhove, J., Rosseneu, M. and Vanloo, B. (2002) Tryptophan fluorescence study of the interaction of penetratin peptides with model membranes. Eur. J. Biochem. **269**, 2918–2926
66 Thoren, P. E., Persson, D., Lincoln, P. and Norden, B. (2005) Membrane destabilizing properties of cell-penetrating peptides. Biophys. Chem. **114**, 169–179
67 Henriques, S. T. and Castanho, M. A. (2005) Environmental factors that enhance the action of the cell penetrating peptide pep-1. A spectroscopic study using lipidic vesicles. Biochim. Biophys. Acta **1669**, 75–86
68 Boisseau, S., Mabrouk, K., Ram, N., Garmy, N., Collin, V., Tadmouri, A., Mikati, M., Sabatier, J. M., Ronjat, M., Fantini, J. and De Waard, M. (2006) Cell penetration properties of maurocalcine, a natural venom peptide active on the intracellular ryanodine receptor. Biochim. Biophys. Acta **1758**, 308–319

© 2006 Biochemical Society

69 Nakase, I., Niwa, M., Takeuchi, T., Sonomura, K., Kawabata, N., Koike, Y., Takehashi, M., Tanaka, S., Ueda, K., Simpson, J. C., Jones, A. T. et al. (2004) Cellular uptake of arginine-rich peptides: roles for macropinocytosis and actin rearrangement. Mol. Ther. **10**, 1011–1022

70 Cudic, M. and Otvos, Jr, L. (2002) Intracellular targets of antibacterial peptides. Curr. Drug Targets **3**, 101–106

71 Pouny, Y., Rapaport, D., Mor, A., Nicolas, P. and Shai, Y. (1992) Interaction of antimicrobial dermaseptin and its fluorescently labeled analogues with phospholipid membranes. Biochemistry **31**, 12416–12423

72 Shai, Y. (1999) Mechanism of the binding, insertion and destabilization of phospholipid bilayer membranes by α-helical antimicrobial and cell non-selective membrane-lytic peptides. Biochim. Biophys. Acta **1462**, 55–70

73 Lee, M. T., Chen, F. Y. and Huang, H. W. (2004) Energetics of pore formation induced by membrane active peptides. Biochemistry **43**, 3590–3599

74 Yang, L., Harroun, T. A., Weiss, T. M., Ding, L. and Huang, H. W. (2001) Barrel-stave model or toroidal model? A case study on melittin pores. Biophys. J. **81**, 1475–1485

75 Heerklotz, H. and Seelig, J. (2001) Detergent-like action of the antibiotic peptide surfactin on lipid membranes. Biophys. J. **81**, 1547–1554

76 Strahilevitz, J., Mor, A., Nicolas, P. and Shai, Y. (1994) Spectrum of antimicrobial activity and assembly of dermaseptin-b and its precursor form in phospholipid membranes. Biochemistry **33**, 10951–10960

77 He, K., Ludtke, S. J., Worcester, D. L. and Huang, H. W. (1996) Neutron scattering in the plane of membranes: structure of alamethicin pores. Biophys. J. **70**, 2659–2666

78 Duclohier, H. (2006) Bilayer lipid composition modulates the activity of dermaseptins, polycationic antimicrobial peptides. Eur. Biophys. J. **35**, 401–409

79 Friedrich, C. L., Moyles, D., Beveridge, T. J. and Hancock, R. E. (2000) Antibacterial action of structurally diverse cationic peptides on Gram-positive bacteria. Antimicrob. Agents Chemother. **44**, 2086–2092

80 Wu, M., Maier, E., Benz, R. and Hancock, R. E. (1999) Mechanism of interaction of different classes of cationic antimicrobial peptides with planar bilayers and with the cytoplasmic membrane of *Escherichia coli*. Biochemistry **38**, 7235–7242

81 Zhang, L., Dhillon, P., Yan, H., Farmer, S. and Hancock, R. E. (2000) Interactions of bacterial cationic peptide antibiotics with outer and cytoplasmic membranes of *Pseudomonas aeruginosa*. Antimicrob. Agents Chemother. **44**, 3317–3321

82 Park, C. B., Kim, H. S. and Kim, S. C. (1998) Mechanism of action of the antimicrobial peptide buforin II: buforin II kills microorganisms by penetrating the cell membrane and inhibiting cellular functions. Biochem. Biophys. Res. Commun. **244**, 253–257

83 Kobayashi, S., Takeshima, K., Park, C. B., Kim, S. C. and Matsuzaki, K. (2000) Interactions of the novel antimicrobial peptide buforin 2 with lipid bilayers: proline as a translocation promoting factor. Biochemistry **39**, 8648–8654

84 Kobayashi, S., Chikushi, A., Tougu, S., Imura, Y., Nishida, M., Yano, Y. and Matsuzaki, K. (2004) Membrane translocation mechanism of the antimicrobial peptide buforin 2. Biochemistry **43**, 15610–15616

85 Takeshima, K., Chikushi, A., Lee, K. K., Yonehara, S. and Matsuzaki, K. (2003) Translocation of analogues of the antimicrobial peptides magainin and buforin across human cell membranes. J. Biol. Chem. **278**, 1310–1315

86 Li, W. F., Ma, G. X. and Zhou, X. X. (2006) Apidaecin-type peptides: biodiversity, structure–function relationships and mode of action. Peptides **27**, 2350–2359

87 Casteels, P., Romagnolo, J., Castle, M., Casteels-Josson, K., Erdjument-Bromage, H. and Tempst, P. (1994) Biodiversity of apidaecin-type peptide antibiotics. Prospects of manipulating the antibacterial spectrum and combating acquired resistance. J. Biol. Chem. **269**, 26107–26115

88 Sadler, K., Eom, K. D., Yang, J. L., Dimitrova, Y. and Tam, J. P. (2002) Translocating proline-rich peptides from the antimicrobial peptide bactenecin 7. Biochemistry **41**, 14150–14157

89 Staubitz, P., Peschel, A., Nieuwenhuizen, W. F., Otto, M., Gotz, F., Jung, G. and Jack, R. W. (2001) Structure–function relationships in the tryptophan-rich, antimicrobial peptide indolicidin. J. Peptide Sci. **7**, 552–564

90 Skerlavaj, B., Romeo, D. and Gennaro, R. (1990) Rapid membrane permeabilization and inhibition of vital functions of Gram-negative bacteria by bactenecins. Infect. Immun. **58**, 3724–3730

91 Palm, C., Netzereab, S. and Hallbrink, M. (2006) Quantitatively determined uptake of cell-penetrating peptides in non-mammalian cells with an evaluation of degradation and antimicrobial effects. Peptides **27**, 1710–1716

92 Magzoub, M., Eriksson, L. E. and Gräslund, A. (2002) Conformational states of the cell-penetrating peptide penetratin when interacting with phospholipid vesicles: effects of surface charge and peptide concentration. Biochim. Biophys. Acta **1563**, 53–63

93 Hallbrink, M., Floren, A., Elmquist, A., Pooga, M., Bartfai, T. and Langel, U. (2001) Cargo delivery kinetics of cell-penetrating peptides. Biochim. Biophys. Acta **1515**, 101–109

94 Kim, J., Mosior, M., Chung, L. A., Wu, H. and McLaughlin, S. (1991) Binding of peptides with basic residues to membranes containing acidic phospholipids. Biophys. J. **60**, 135–148

95 Tamm, L. K. (1991) Membrane insertion and lateral mobility of synthetic amphiphilic signal peptides in lipid model membranes. Biochim. Biophys. Acta **1071**, 123–148

96 Vaz Gomes, A., de Waal, A., Berden, J. A. and Westerhoff, H. V. (1993) Electric potentiation, cooperativity, and synergism of magainin peptides in protein-free liposomes. Biochemistry **32**, 5365–5372

97 Scheller, A., Wiesner, B., Melzig, M., Bienert, M. and Oehlke, J. (2000) Evidence for an amphipathicity independent cellular uptake of amphipathic cell-penetrating peptides. Eur. J. Biochem. **267**, 6043–6050

98 Ludtke, S., He, K. and Huang, H. (1995) Membrane thinning caused by magainin 2. Biochemistry **34**, 16764–16769

99 Deshayes, S., Gerbal-Chaloin, S., Morris, M. C., Aldrian-Herrada, G., Charnet, P., Divita, G. and Heitz, F. (2004) On the mechanism of non-endosomial peptide-mediated cellular delivery of nucleic acids. Biochim. Biophys. Acta **1667**, 141–147

100 Fischer, R., Fotin-Mleczek, M., Hufnagel, H. and Brock, R. (2005) Break on through to the other side – biophysics and cell biology shed light on cell-penetrating peptides. ChemBioChem **6**, 2126–2142

101 Zasloff, M. (1987) Magainins, a class of antimicrobial peptides from *Xenopus* skin: isolation, characterization of two active forms, and partial cDNA sequence of a precursor. Proc. Natl. Acad. Sci. U.S.A. **84**, 5449–5453

102 Park, C. B., Kim, M. S. and Kim, S. C. (1996) A novel antimicrobial peptide from *Bufo bufo gargarizans*. Biochem. Biophys. Res. Commun. **218**, 408–413

103 Casteels, P., Ampe, C., Jacobs, F., Vaeck, M. and Tempst, P. (1989) Apidaecins: antibacterial peptides from honeybees. EMBO J. **8**, 2387–2391

104 Castle, M., Nazarian, A., Yi, S. S. and Tempst, P. (1999) Lethal effects of apidaecin on *Escherichia coli* involve sequential molecular interactions with diverse targets. J. Biol. Chem. **274**, 32555–32564

Received 19 July 2006/4 August 2006; accepted 4 August 2006
Published on the Internet 13 September 2006, doi:10.1042/BJ20061100

© 2006 Biochemical Society

2. Omiganan

The first AMP I studied was omiganan (more precisely, omiganan pentahydrochloride), which happens to be one of the two AMPs mentioned in Chapter 1 that has not continued past Phase III testing. Omiganan (sequence: ILRWPWWPWRRK–NH_2, where NH_2 indicates C-terminal amidation) was designed having the naturally occurring AMP indolicidin — itself known and studied[24] since 1992 — as a template. Omiganan was developed by MIGENIX Inc. as a topical antibiotic to prevent catheter-related infections and I would be studying it following a not-for-profit collaboration Miguel started with the company (then called Micrologix). Background on omiganan and indolicidin is provided in Article II. This article, written when I began my work with omiganan, is a review Miguel was invited to author in which we and Dominique Dugourd, our contact at MIGENIX, summarize what was then known about the two peptides.

In March 2009 the results of Phase III tests were released: the peptide met several efficiency criteria but the main result — improved performance relatively to the currently used standard — was not considered statistically significant[25] (a repetition of the less-than-optimal[26] outcome of another large-scale clinical trial in 2003). The development and commercialization partner of MIGENIX's has since quit the collaboration on the basis of insufficient commercial interest due to little advantage of omiganan over existing therapies.[27] The drug is currently orphan as MIGENIX looks for new partners. Other applications of omiganan as a treatment against acne or rosacea erythema, already in Phase II testing, were also put on hold.

While it is sad to see the subject of my study be dismissed as commercially unviable, the academic interest on omiganan and its contribution to the advancement of knowledge on AMP action persist.

Article II

Omiganan Pentahydrochloride in the Front Line of Clinical Applications of Antimicrobial Peptides

Manuel N. Melo[1], Dominique Dugourd[2,†] and Miguel A. R. B. Castanho[1,†,*]

[1]*Centro de Química e Bioquímica, Faculdade de Ciências, Universidade de Lisboa, Campo Grande C8, 1749-016 Lisboa, Portugal, and* [2]*MIGENIX Inc., 3650 Wesbrook Mall, Vancouver, BC, Canada V6S 2L2*

Abstract: Ribosomally synthesized antimicrobial peptides have very wide killing spectra and bacterial resistance to these peptides seems to be a rare phenomenon. Indolicidin is a ribosomally synthesized antimicrobial peptide that served as a template to omiganan, which is in development for the prevention of catheter-related bloodstream infections; clinical trials also proved its efficiency against acne vulgaris. Omiganan is the most advanced molecule in the front line of clinical applications of antimicrobial peptides. The mode and site of action of omiganan are not yet settled although its interaction with membranes is known to play a fundamental role. The biochemical and biophysical foundations for the action of indolicidin and its analogues are reviewed in this paper, as well as the clinical application of omiganan. The *in vitro* efficiency tests and the outcome of clinical trials are addressed. Altogether, despite the very specific use of omiganan as a topical antibiotic, it has the potential of being a pioneer of a new generation of antibiotics that carry the promise of ending the multi-resistance problem.

Keywords: Antimicrobial, peptide, membrane, peptidoglycan, lipid, clinical, therapeutic, indolicidin, catheter, acne.

1- INTRODUCTION

Nearly 100 patents can be found in worldwide databases having "antimicrobial" and "peptides" in their titles. Indolicidin derivatives raised particular interest and several compositions and methods for treating infections have been published (*e.g.*[1-3]).

Omiganan pentahydrochloride (omiganan – ILRWPWWPWRRK-amide), is a novel antimicrobial peptide (AMP) developed by MIGENIX Inc. (Vancouver, Canada) that is in development for use as a topical antimicrobial for the prevention of catheter-related bloodstream infections [4]. Omiganan is a synthetic peptide, an analogue of the naturally-occurring AMP indolicidin (ILPWKWPWWPWRR-amide), and, like indolicidin, also has a very high content of tryptophan (W) residues.

AMPs are part of non-specific host defence mechanisms and have been found in specimens from all kingdoms [5],[6],[7],[8]; in particular, indolicidin, which can be purified from the granules of bovine neutrophils [9], takes part in the process of bacterial killing inside phagocytic vesicles.

Because they are used by the innate immune system, these antibiotics often have very wide killing spectra: indolicidin is active against Gram-negative and Gram-positive bacteria [9], fungi [10], protozoa [11] and even HIV-1 (enveloped virus) [12]. Also, bacterial resistance to these peptides seems to be a rare phenomenon, which makes AMPs very interesting for the pharmaceutical industry. The studies on the structure and mode of action of omiganan are ongoing and the comparative analysis of the properties of omiganan, indolicidin, and indolicidin analogues allows for some extrapolation towards a better characterization of omiganan.

1.1 - Challenges in the Therapeutic Use of AMPs

Indolicidin, a template for omiganan's design, is included in a sub-group of AMPs called ribosomally synthesized AMPs (RAMPs or gene-encoded AMPs), which are produced by many organisms. The other group of AMPs are of the exclusive production of bacteria and fungi and are synthesized non-ribosomally (therefore termed non-RAMPs) [13]. While some non-RAMPs or their synthetic derivatives are already used as antibiotics [13,14], there is great concern towards such use of RAMPs or RAMP-related synthetic peptides, like omiganan, in case pathogen resistance develops: these peptides can be quite diverse in sequence and structure however, should microbial cross-resistance arise between them, their use as antibiotics could encourage the growth of new strains resistant to human RAMPs. Such strains would render an important part of the human innate immune system ineffective and pose serious public health threats [13].

On the other hand, the safe use of RAMPs as antibiotics is favoured by the fact that bacterial resistance is argued to be inherently hard to acquire [15,16]: these drugs usually target the cell membrane integrity and make use of fundamental characteristics of bacteria such as the overall anionic charge of the membrane phospholipids or the negative membrane potential [16-18]. For resistance to develop, bacterial membranes would have to undergo profound structural and functional changes, thus implying prohibitive costs of resistance [16]. Also, microorganisms have been subjected to attacks by human RAMPs for at least as long as *Homo sapiens* have existed; however, such a long exposure does not seem to have strengthened human pathogens to the point of making them resistant. This suggests that the mechanisms by which microbes could resist RAMPs are already at their

*Address correspondence to this author at the Centro de Química e Bioquímica, Faculdade de Ciências, Universidade de Lisboa, Campo Grande C8, 1749-016 Lisboa, Portugal; Tel: + 351 21 7500931; Fax: + 351 21 7500088; E-mail: castanho@fc.ul.pt

†*Both authors contributed equally to this work.*

© 2006 Bentham Science Publishers Ltd. 1574-891X/06 $100.00+.00

maximum efficacy and any added resistance also carries a loss of viability [19].

2- THE BIOCHEMICAL AND BIOPHYSICAL FOUNDATIONS FOR THE ACTION OF INDOLICIDIN AND ITS ANALOGUES

2.1 - Structural Characterization

The structure of indolicidin has been determined by NMR and CD [20]. While it shows no distinctive structural features in aqueous environments, indolicidin seems to adopt an approximate poly-L-proline type II helix conformation, together with β-turn behaviour, upon interaction with DOPC [20]. This is a rather uncommon secondary structure for RAMPs, the most usual being the α-helices, the β-sheets, and the disulfide bond loops [15], ordered accordingly to their relative frequencies. Extended structures, together with the helix conformation, have also been observed in the proline- and arginine- rich RAMPs bac5, bac7, and PR-39 [21-23]. Interestingly, despite the big differences in sequence and size between indolicidin and these peptides, they are part of the cathelicidin family, a mammalian subclass of RAMPs in which the antibiotics are synthesized as large propeptides, with highly conserved proregions [24]. Their common origin, together with their similar structural characteristics and expression in closely related species [22], suggests that these RAMPs could also share antimicrobial modes of action.

When interacting with micelles or liposomes, indolicidin has a relatively stretched structure that nearly spans the membrane (32 Å) despite having only 13 amino acids. This is possible because poly-L-proline type II helices have very high helical pitches (9.3 Å) when compared to α-helices (5.4 Å) [25]. The flexibility of the helix, the β-turn tendency, and a lack of order of the N-terminal residues give indolicidin a characteristic boat-shaped extended structure with positive charges on both ends, which may be important when interacting with membrane interfaces as it allows the central hydrophobic residues to be near the acyl chains of the membrane phospholipids while the charged endings remain close to the polar headgroups [6].

The secondary structure of omiganan has not yet been determined but, upon interaction with phospholipids, it may be closely related to that of indolicidin since other indolicidin analogues also share structural similarities, as indicated by CD spectra [26,27]. The differences in the primary sequence between omiganan and indolicidin include the removal of the Trp and Pro residues closest to the N-terminus, the addition of a Lys residue at the C-terminus and the substitution of Lys-5 with an Arg residue which are changes that appear to effectively centralize the hydrophobic core and increase the C-terminal cationic charge.

Omiganan should still have a poly-L-proline type II structure since its central hydrophobic segment, which is the principal constituent of the helix, has been conserved from indolicidin. Part of the peptide curvature has probably been lost with the deletion of the Pro-3 and Trp-4 residues but the peptide span might be similar to indolicidin since the deleted pair contributed little to the molecule length and an extra residue was added near the C-terminus.

Because poly-L-proline type II helices have three residues per turn, they will have a three-fold symmetry around their axis, which has been observed to occur in indolicidin [20] and should also be present in omiganan. This symmetry will cause the alignment, in pairs, of the hydrophobic core Trp and Pro residues. This leads to a segregation of Trp and Pro side chains to opposite sides of the helix axis, effectively creating a hydrophobic Trp face [28], which could be of importance to the membrane partition and activity of these peptides. A similar, yet more pronounced effect, occurs in α-helical RAMPs, where charged residues are usually positioned opposite of hydrophobic ones in the helix. This property has been shown to play a very important part in the binding of α-helical peptides to the membrane surface [29].

2.2- Mechanisms of Action Against Bacteria

– General Properties

Membrane interaction is one of the most important and most studied characteristics of RAMPs and, because most RAMPs are both amphiphilic and cationic, it is tempting to assume that a general mechanism based on these common properties could describe their modes of action towards the anionic bacterial membranes. The carpet mechanism [17], [30,31] is one such model in which an antibiotic would interact electrostatically and hydrophobically/hydro-philically with a membrane and, above a critical concentration in the bilayer, would destabilize it enough to the point that it would lose its integrity. However, several killing processes have been described besides straightforward lysis [18,32]; these include membrane attacks that lead to permeabilization through pore formation or cell depolarization and also cytoplasmic attacks such as DNA, RNA, or protein synthesis inhibition. This diversity in behaviours suggests that although the carpet model may explain the killing processes of some RAMPs, membrane surface interaction is not the only phenomenon involved in general RAMP action. It seems that the only fact that can be safely generalized is that RAMP-membrane interactions are always of great importance for activity, whether the site of action is the membrane itself or cytoplasmic targets [8].

Because such different mechanisms can potentially be found in RAMP activity, recent studies have focused more on the structural-functional relationship in these peptides and thorough reviews exist on the subject [8,18,32,33]. Nevertheless, even within the same structural subclass, various modes of action seem to coexist. New hypotheses propose alternative points of view in which, for a single antibiotic, cell death can occur through several of the aforementioned processes acting synergistically [17,34]. In addition, microenvironment changes may induce drastic behavioural changes that may lead to different antimicrobial processes from a single peptide towards different types of cells, as was reported for the bee venom RAMP mellitin [35].

Having been discovered in the early 90's [9], indolicidin has been extensively studied and several possible modes of action have been investigated. However, there is still lack of consensus regarding which process actually leads to cell death. At least three mechanisms have been proposed, namely cell depolarization [36], membrane permeabilization [37], and DNA/RNA/protein synthesis inhibition [38]. Re-

gardless of the actual mode of action, the efficiency of indolicidin, and probably of omiganan, seems to be correlated with characteristics that they share with other antimicrobial peptides [18]:

a. they are very small peptides, thus being hard to recognize and mark for proteolysis;

b. they are amidated at their C-terminus, further resisting proteolysis and eliminating the negative charge of the carboxyl group;

c. they are amphipathic, being able to interact strongly with cell membranes, which are expected to be one of their primary targets;

d. they are polycationic, which favours their preferential interaction with the negatively charged bacterial membranes, lipopolysaccharide (LPS), and peptidoglycan, rather than with the zwitterionic outer surface of mammalian membranes. Membrane potential is also more negative in bacteria than in mammalian cells, which could enhance antibiotic binding and translocation.

The last factor may be responsible for one difference between omiganan and indolicidin. Indolicidin has the clinical disadvantage of also being active against erythrocytes [26-28] while omiganan seems to be much less haemolytic [26,39]. As indicated above, the charged residues of omiganan are located closer to each end and away from the central hydrophobic segment of the peptide, and the overall positive charge of the peptide is increased from 4+ to 5+, which could account for the haemolysis reduction as these changes would not favour the peptide analogue associating with the zwitterionic mammalian membranes [31]. This is corroborated by the findings of Staubitz *et al.* [40] in which the central segment of indolicidin, conserved in omiganan, is related to activity whereas the terminal segments seem to regulate target specificity.

– Outer Membrane Interaction

Although it is probably not a lethal event for itself, the crossing of the Gram-negative outer membrane is also very important for antibiotic activity. A widely accepted mechanism of self-promoted uptake into the periplasmic space has been proposed for indolicidin and some other antimicrobial peptides [15,36]. In this model, the cationic peptide displaces the ions that equilibrate the anionic charge on the outer leaflet LPS, disturbing the bilayer and allowing the antibiotic to cross the outer membrane through transient pores or cracks. Besides the electrostatic interactions needed for the self-promoted uptake pathway, binding of indolicidin to LPS has also been proposed to be favoured by structural complementarity [26,41]. Omiganan can also be expected to follow the self-promoted uptake pathway as it is even more charged than indolicidin. Furthermore, it has been shown by the exposure of periplasmic β-lactamases that, like indolicidin [36], omiganan permeabilizes the *E. coli* outer membrane [42], which is in agreement with the destabilization required for its crossing to the periplasmic space.

– Cell Wall Interaction in Gram-Positive Bacteria

One aspect of antibiotic interaction with Gram-positive bacteria that has been neglected is the crossing of the thick peptidoglycan wall. Peptidoglycan is a negatively charged mesh that, in Gram-positives, also contains long polymers of glycerophosphate or ribitol-phosphate (termed teichoic acids) which contribute extra anionic charge to the wall [43,44]. Cationic peptides will certainly have a great affinity for the Gram-positive cell wall which will work as another target selection mechanism. However, despite being relatively small, the size of omiganan and indolicidin, and also of most RAMPs, is of the same order of magnitude as the peptidoglycan tesserae's (mesh "pores") diameter [45]. This means that the anionic charge, together with the intricate peptidoglycan mesh, could act as a peptide trap, compromising the antibiotic efficacy. Little or no study has been done in order to determine whether certain characteristics of RAMPs are required for them to cross the peptidoglycan wall and reach the membrane and other targets. Nevertheless, it has been shown that *S. aureus* strains incorporate positively charged D-alanyl-teichoic acid esters into the teichoic acid polymers, effectively lowering the antibiotic affinity, as a means of RAMP resistance [46].

– Membrane Interaction

After the interaction with the outer membrane or the peptidoglycan wall, other processes must take place before cell death occurs. Despite having been the focus of much research, the interactions of indolicidin with the bacterial cell membrane and the actual process of killing are not yet reconciled. Indolicidin, but not omiganan, permeabilized the *E. coli* inner membrane, as determined by cytoplasmic β-galactosidase exposure assays [36,42]. This could indicate that indolicidin and omiganan have different modes of action regarding lipidic bilayers. Nevertheless, care must be taken when analysing such data because β-galactosidase substrates are bulky [47] and membrane permeabilization may be underestimated if the formed pores have small diameters or are very short-lived. Should that be the case, omiganan could possibly permeabilize bacterial membranes, despite being undetected by β-galactosidase assays. In another study, indolicidin was shown to be able to induce vesicle contents leakage, at a moderate rate, as long as the liposomes were constituted by negatively charged phospholipids [37]. It should be noted that because of the charged endings and the hydrophobic core of indolicidin and omiganan, any hypothetical pores formed by these peptides are expected to be of the toroidal type rather than barrel-stave [48].

Even if omiganan does not permeabilize the inner membrane, it is at least able to disrupt its electrical potential, depolarizing the cell, as was determined by fluorescence assays with a membrane potential probe [42]. The difference in its behaviour relative to indolicidin may simply be a question of pore size or degree of membrane perturbation that does not necessarily imply a different mode of action.

EM studies also show that although lysis due to bacterial wall/membrane fragmentation does not occur upon treatment with omiganan or indolicidin, very profound membrane perturbations are induced, the most notable being the formation of multilayered membranes and membranar inclusion bodies (mesosomes) both in Gram-positive and Gram-negative bacteria, giving support for the membrane disruption hypotheses [49,50].

While membrane depolarization is not incompatible with permeabilization, little evidence for it as a killing mechanism was found by EM since significant leakage of cell contents was not observed. An exception is indolicidin analogue CP-11 acting on *S. epidermidis* [49], possibly related to hypothetically larger pores. Yet, we cannot conclude right away that depolarization is the main killing mechanism of these peptides as depolarization *per se* may be insufficient to cause death [18]. In recent work, Hancock, one of the proponents of a depolarization mechanism for the action of indolicidin against Gram-negative bacteria, reported to have observed very little correlation between cell depolarization/permeabilization and death or antimicrobial activity in Gram-positive bacteria [49]. With indolicidin for example, the majority of the cells would have died before becoming fully depolarized; there were also other antibiotics that could induce very strong and fast depolarization but were not necessarily very active or led to cell death some minutes later.

– Action on the Cytoplasm

Another mechanism proposed for the action of these peptides is based on findings that nucleic acid and protein synthesis were inhibited in bacteria treated with either indolicidin [38] or omiganan [51]. This hypothesis is consistent with the morphological effects that indolicidin or omiganan have on bacteria: *E. coli* treated with these antibiotics demonstrated filamentation, rather than lysis, as observed by EM [38,50]; this phenomenon can be a consequence of DNA damage or replication perturbation [52]. Moreover, DNA condensation seemed to occur in *S. epidermidis* [49], further suggesting that indolicidin and omiganan may attack the DNA itself or related cytoplasmic targets, which is also in agreement with predictions that poly-L-proline helices have affinity for B-DNA major grooves and may recognize certain nucleotide sequences [53].

In this last hypothesis, the peptides are required to cross the membrane to reach their targets. Translocation is expected to occur due to a number of factors. Firstly, both indolicidin and omiganan seem to have the size, when extended, to span both membrane leaflets, albeit with a small negative mismatch. Since their structure is almost symmetrical in relation to hydrophobic properties it can be assumed that if the peptides were to reversibly insert themselves perpendicularly to the membrane they would then be able, by the inverse reaction, to exit the membrane either to the external side or to the luminal side of cells/vesicles, thus effectively being able to translocate. Secondly, the negative membrane potential that is present in most cells may lower the free energy for the translocation and actively pull these cationic peptides to the cytoplasm. Lastly, although these peptides may prefer the membrane surface [20], they have a very high affinity for lipid bilayers judging by the magnitude of the water-lipid partition constant for indolicidin towards POPC and POPG liposomes [37]. Such a large extent of partition could induce the perpendicular insertion of some peptides if the membrane surface became too crowded [54]. Despite all these factors, indolicidin translocated very poorly across model membranes [55]. It should also be noted that for the reasons stated above, translocation can be a side-effect of reversible pore formation in the instances that the peptides are positioned perpendicular to the membrane. This also means that the event of translocation probably follows membrane permeabilization through pore formation.

– Multi-Targeted Action

All the proposed effects of omiganan and indolicidin have parallels in modes of action to other extended cathelicidins [22]: bac5 and bac7 permeabilize, depolarize, and inhibit the respiration of Gram-negative bacteria [23] while PR-39 seems to interfere with DNA replication but not with cell membranes [21]. This comparison corroborates the plausibility of the mechanisms proposed but is inconclusive as to which process is responsible for cell death. On the other hand, regardless of which processes take place, they seem to do so in a receptor-independent fashion, as shown by the retained activity of indolicidin analogues with inverted sequences, all D-amino acids, and both [40]. This indicates that any putative attacks on the DNA or other cytoplasmic targets must not be based on specific chiral recognition.

All these seemingly incompatible hypotheses have led to the proposition of an alternate mechanism, by Friedrich et al. [49], that encompasses all the observed facts. Because cells are not expected to die simply because they depolarize or become permeabilized, it is reasonable to assume that an intracellular target must be attacked; this putative target would be related to DNA replication or cell division mechanisms, as first proposed by Subbalakshmi and Sitaram [38] and supported by the observed effects on *E. coli* and *S. epidermidis*. The observed depolarization and permeabilization may just be consequences of the membrane interactions needed to promote the antibiotic entrance into the cell, but they are more likely to play a direct part in cell perturbation and death themselves.

3- CLINICAL APPLICATIONS OF OMIGANAN

3.1 - Omiganan is a Novel Cationic Peptide

Indolicidin was selected as the parent molecule for the design of small antimicrobial peptides for topical and for potentially systemic use because it is a relatively small peptide, it has a broad spectrum of activity and targets Gram-positive and Gram-negative bacteria, yeast, fungi, and even enveloped viruses and parasites, and is lethal to a variety of organisms [9,11,56,57]. Omiganan was initially selected for clinical development from a large panel of peptides because of its spectrum of activity, potency, killing activity, solubility in aqueous solutions, and stability. Potential advantages of omiganan over currently available prescription topical antimicrobial products include the following: its broad spectrum of activity, rapid killing action, mechanism of action, lack of cross-resistance with other currently approved antimicrobials, lack of incidence of resistance, no evidence of toxicity when applied topically at doses up to 5%, room temperature stability of its formulations, and ease of use. Omiganan's mechanisms of action and killing activity makes it an attractive candidate for the treatment or prevention of topical infections or for infections that originate from skin pathogens. In particular, omiganan's antifungal activity is an important feature given the documented risk of fungal overgrowth when conventional topical antibacterial drugs are used for prophylaxis [58]. Furthermore, omiganan may be used to protect patients from device-related infection by coating devices with omiganan before implantation. In 2003,

a Phase II clinical trial for the treatment of acne vulgaris with Omiganan was completed, where efficacy was demonstrated with statistically significant data confirming the anti-acne properties of omiganan. Omiganan is currently being investigated in a Phase III study in the USA and Europe for the prevention of local catheter infections Also in 2003, a completed Phase III study demonstrated a 49% reduction in local catheter site infection and a 21% reduction in catheter colonization.

3.2 - *In vitro* Antimicrobial Efficiency Tests

Antimicrobial potency of omiganan was investigated using various susceptibility techniques: modified agar dilution and broth microdilution with both Mueller Hinton broth (MHB) and cation-adjusted MHB (CAMHB) [4,59,60]. Omiganan's spectrum of activity was investigated against 750 clinical isolates using modified agar dilution methodology based on the NCCLS recommendation (NCCLS M7-A5) [60]. Using broth microdilution methodology, 1,437 bacterial and 214 *Candida* spp. clinical isolates [4], and 4,766 bacterial isolates from a Phase III Omiganan 1% Gel trial [59] were tested. Omiganan demonstrated a broad spectrum of antibacterial and antifungal activity with superior activity against most Gram-positive pathogens (such as *S. epidermidis*, *S. aureus*, and *Corynebacterium* spp.), and moderate activity against viridans streptococci and some Gram-negative species [4,59,60]. It is interesting to note that in general, the broth MICs of omiganan against Gram-positive bacteria were 2 to 4 times higher than the solid-phase MICs [4,59,60]. For example, the MIC_{90} of omiganan in the solid-phase assay was 4 μg/mL against *S. aureus* [60], compared with 16 μg/mL in MHB or CAMHB [4,59]. No decrease in susceptibility was observed in clinically relevant resistant pathogens including vancomycin resistant *Enterococci* spp. (VRE), methicillin resistant *S. aureus* (MRSA), or penicillin resistant streptococci [4].

3.3 - Demonstrated Benefits of Omiganan in Clinical Trials

– Acne

With the large, growing acne market, the increasing bacterial resistance seen with current acne therapies, and the clear need for a novel, first-in-class, topical treatment, omiganan represents an ideal product opportunity for further development. Omiganan has completed 5 acne clinical trials in the US: 3 Phase I studies and 2 Phase II studies. The three Phase I acne clinical studies of omiganan, performed in a total of 36 healthy volunteers and 35 acne patients, showed that the drug was very well tolerated and non-irritating over 6 weeks of treatment. There were no serious adverse events related to the study drug, and no systemic absorption of omiganan was detected after topical application of an omiganan formulation twice a day for five days.

A 6-week randomized, double-blind, multicentre Phase IIa trial was performed in 75 subjects with facial acne vulgaris to establish proof of concept for the anti-acne properties of an omiganan-containing acne solution. Omiganan diminished the severity of acne in subjects with mild to moderate disease, as shown by reduced counts of inflammatory lesions (papules and pustules), non-inflammatory lesions (comedones), and improved physician's Global Severity Assessment scores. This Phase IIa trial also confirmed the safety and local tolerability findings from the Phase I studies.

A Phase IIb, randomized, double-blind, vehicle-controlled, dose-finding study was conducted in 241 subjects with mild to moderate acne vulgaris at nine US centers to evaluate the efficacy and safety of omiganan solutions over a 12-week treatment period. After only 6 weeks of treatment, omiganan 2.5% topical acne solution demonstrated statistical superiority over the vehicle control in reducing inflammatory acne lesions ($p = 0.004$), non-inflammatory lesions ($p = 0.037$), and total lesions ($p < 0.001$) [61]. Physician's Global Severity Assessment scores also showed that omiganan 2.5% solution was clinically superior to the vehicle control [61].

– Catheter-Related Infections

At least two-thirds of the catheter-related infections are due to Gram-positive bacteria and yeasts making omiganan an attractive candidate for the prevention of these infections. Omiganan was formulated as 1% weight-weight in a gel vehicle (omiganan 1% gel). Systemic absorption and safety of omiganan 1% gel was evaluated in three randomized double-blind studies in approximately 270 healthy volunteers. No serious adverse events related to omiganan and no systemic absorption of omiganan was detected when applied on intact or abraded skin [39]. Omiganan demonstrated sustained reductions in skin colonization (> 3 $\log_{10}$ reduction for 3 days) and reduction in colonization of peripheral intravenous catheters (83% reduction versus placebo).

A Phase III, randomized, evaluation-committee-blinded study was then performed to further evaluate the efficacy and safety of omiganan 1% gel. The study enrolled over 1,400 subjects at 29 US centers. The primary objective of the Phase III trial was to demonstrate that omiganan 1% gel, administered at central venous catheter insertion sites, is superior to povidone iodine in preventing central venous catheter-related bloodstream infections. Omiganan achieved a clear, statistically significant reduction in the two secondary efficacy endpoints of the study: catheter colonization ($p=0.002$) and catheter-related local site infections ($p=0.004$) compared to povidone iodine [62]. These two endpoints, documented extensively in the published literature, correlate to the development of catheter-related bloodstream infections. The primary endpoint, a reduction in catheter-related bloodstream infections, resulted in a 15% improvement as compared to povidone iodine but this effect was not statistically significant. There were no serious drug-related adverse events reported in this trial. The product was out-licensed to Cadence Pharmaceuticals, Inc. ("Cadence", formerly Strata Pharmaceuticals, Inc.) in 2004 [63]. Cadence has submitted its request for a Special Protocol Assessment to the US FDA and plans to initiate a confirmatory pivotal Phase III trial by the end of the calendar year 2005.

CONCLUSION

The studies on the killing processes of indolicidin are far from concluded, not to mention those of the much more recently developed omiganan [64]. Because these peptides, like many RAMPs, do not have a specific binding target, there are many challenges to the unravelling of their detailed mechanism. The fact that a RAMP may, depending on the circumstances, display many modes of action and have sev-

eral cellular targets has also been a source for apparently contradictory evidence; new models describing antibiotic-pathogen interactions have been developed but the precise killing mechanisms of many RAMPs, including indolicidin, and analogues such as omiganan, still remain obscure. However, the characteristics that make RAMPs so elusive to our studies also make them so efficient at killing pathogens: the varied and complex mechanisms of RAMP action require bacteria to undergo high-cost, multi-step adaptations to become resistant; if we were able to easily pinpoint the site and mode of RAMP action we could probably expect bacteria to evolve into resistant forms just as easily.

CURRENT & FUTURE DEVELOPMENTS

Despite its very specific use as a topical antibiotic, omiganan has the potential of being a pioneer of a new generation of antibiotics that carry the promise of ending the multi-resistance problem. The difficulties in the determination of its precise bactericidal mechanism are not likely to discourage its clinical use, especially given the therapeutic qualities it has shown so far. Only time will tell whether omiganan will live up to the expectations. For the time being, it can be regarded as a successful case of rational drug design where the activity and selectivity of the parent peptide indolicidin were manipulated to best fit clinical needs.

REFERENCES

*[1] Falla, T.J., Hancock, R.E.W., Gough, M.: EP0846128 (**1998**).

[2] Friedland, H.D., Krieger, T.J., Taylor, R.; Erfle, D., Fraser, J.R., West, M.H.P.: WO9943357A1 (**1999**).

[3] Fraser, J.R., West, M.H.P., Krieger, T.J., Taylor, R., Erfle, D.: US2004009910A1 (**2004**).

[4] Sader HS, Fedler KA, Rennie RP, Stevens S, Jones RN. Omiganan Pentahydrochloride (MBI 226), a Topical 12-Amino-Acid Cationic Peptide: Spectrum of Antimicrobial Activity and Measurements of Bactericidal Activity. Antimicrobial Agents Chemother 2004; 48: 3112-8.

[5] Koczulla AR, Bals R. Antimicrobial Peptides Current Status and Therapeutic Potential. Drugs 2003; 63: 389-406.

[6] Hancock REW. Cationic Peptides: effectors in innate immunity and novel antimicrobials. Lancet Infect Dis 2001; 1: 156-64.

[7] Tossi A, Mitaritonna N, Tarantino C, Giangaspero, Sandri L, Winterstein K. A, Antimicrobial Sequences Database – Universitá degli Studi di Trieste: http://www.bbcm.univ.trieste.it/~tossi/pag1.htm - visited June 2005

[8] Powers JPS, Hancock REW. The relationship between peptide structure and antibacterial activity. Peptides 2003; 24: 1681-91.

[9] Selsted ME, Novotny MJ, Morris WL, Tang YQ, Smith W, Cullor JS. Indolicidin, a Novel Bactericidal Tridecaeptide Amide from Neutrophils. J Biol Chem 1992; 267: 4292-5.

[10] Aley SB, Zimmerman M, Hetsko M, Selsted ME, Gillin FD. Killing of *Giardia lamblia* by Cryptdins and Cationic Neutrophil Peptides. Infect Immun 1994; 62: 5397-403.

[11] Ahmad I, Perkins WR, Lupan DM, Selsted ME, Janoff AS. Liposomal entrapment of the neutrophil-derived peptide indolicidin endows it with *in vivo* antifungal activity. Biochim Biophys Acta 1995; 1237: 109-14.

[12] Robinson WE Jr, McDougall B, Tran D, Selsted ME. Anti-HIV-1 activity of indolicidin, an antimicrobial peptide from neutrophils. J Leukoc Biol 1998; 63: 94-100.

[13] Bell G, Gouyon PH. Arming the enemy: the evolution of resistance to self proteins. Microbiology 2003; 149: 1367-75.

[14] Hancock REW, Chapple DS. Peptide Antibiotics. Antimicrobial Agents Chemother 1999; 43: 1317-23

[15] Hancock REW. Peptide antibiotics. Lancet 1997; 349: 418-22.

[16] Zasloff M. Antimicrobial peptides of multicellular organisms. Nature 2002; 415: 389-95.

[17] Shai Y. Mode of Action of Membrane Active Antimicrobial Peptides. Biopolymers 2002; 66: 236-48.

[18] Yeaman MR, Yount NY. Mechanisms of Antimicrobial Peptide Action and Resistance. Pharmacol Rev 2003; 55: 27-55.

[19] Lucentini J. Antibiotic Arms Race Heats Up. Scientist 2003; 17(17): 29-30.

[20] Rozek A, Friedrich CL, Hancock REW. Structure of Bovine Antimicrobial Peptide Indolicidin Bound to Dodecylphosphocholine and Sodium Dodecyl Sulfate Micelles. Biochemistry 2000; 39: 15765-74.

[21] Boman HG, Agerberth B, Boman A. Mechanisms of Action on *Escherichia coli* of Cecropin P1 and PR-39, Two antibacterial Peptides from Pig Intestine. Infect Immun 1993; 61: 2978-84.

[22] Brogden KA, Ackermann M, McCray PB Jr, Tack BF. Antimicrobial peptides in animals and their role in host defenses. Int J Antimicrob Agents 2003; 22: 465-78.

[23] Skerlavaj B, Romeo D, Gennaro R. Rapid Membrane Permeabilization and Inhibition of Vital Functions of Gram-Negative Bacteria by Bactenecins. Infect Immun 1990; 58: 3724-30.

[24] Zanetti M, Gennaro R, Romeo D. Cathelicidins: a novel protein family with a common proregion and a variable C-terminal antimicrobial domain. FEBS Lett 1995; 374: 1-5.

[25] Arnott S, Dover SD. The structure of poly-L-proline II. Acta Crystallogr B 1968; 24: 599-601.

[26] Halevy R, Rozek A, Kolusheva S, Hancock RE, Jelinek R. Membrane binding and permeation by indolicidin analogs studied by a biomimetic lipid/polydiacetylene vesicle assay. Peptides 2003; 24: 1753-61.

[27] Subbalakshmi C, Bikshapathy E, Sitaram N, Nagaraj R. Antibacterial and Hemolytic activities of Single Typtophan Analogs of Indolicidin. Biochem Biophys Res Commun 2000; 274: 714-6.

[28] Falla TJ, Hancock REW. Improved Activity of a Synthetic Indolicidin Analog. Antimicrobial Agents Chemother 1997; 41: 771-5.

[29] Dathe M, Wieprecht T. Structural features of helical antimicrobial peptides: their potential to modulate activity on model membranes and biological cells. Biochim Biophys Acta 1999; 1462: 71-87.

[30] Papo N, Shai Y. Can we predict biological activity of antimicrobial peptides from their interaction with model phospholipid membranes? Peptides 2003; 24: 1693-703.

[31] Shai Y. Mechanism of the binding, insertion and destabilization of phospholipid bilayer membranes by α-helical antimicrobial and cell non-selective membrane-lytic peptides. Biochim Biophys Acta 1999; 1462: 55-70.

[32] Sitaram N, Nagaraj R. Interaction of antimicrobial peptides with biological and model membranes: structural and charge requirements for activity. Biochim Biophys Acta 1999; 1462: 29-54.

[33] Matsuzaki K. Why and how are peptide-lipid interactions utilized for self-defense? Magainins and tachyplesins as archetypes. Biochim Biophys Acta 1999; 1462: 1-10.

[34] Hancock REW, Scott M. The role of antimicrobial peptides in host defenses. Proc Natl Acad Sci USA 2000; 97: 8856-61.

[35] Ladokhin AS, White SH. 'Detergent-like' permeabilization of anionic lipid vesicles by melittin. Biochim Biophys Acta 2001; 1514: 253-60.

[36] Falla TJ, Karunaratne DN, Hancock REW. Mode of Action of the Antimicrobial Peptide Indolicidin. J Biol Chem 1996; 271: 19298-303.

[37] Ladokhin AS, Selsted ME, White SH. Bilayer Interactions of Indolicidin, a Small Antimicrobial Peptide Rich in Tryptophan, Proline, and Basic Amino Acids. Biophys J 1997; 72: 794-805.

[38] Subbalakshmi C, Sitaram N. Mechanism of antimicrobial action of indolicidin. FEMS Microbiol Lett 1998; 160: 91-6.

[39] Friedland HD, Sharp DD, Erfle DJ, Rubinchik E. Omiganan (MBI 226) 1% Gel: a novel topical antimicrobial agent with a favorable safety profile, in 43rd Interscience Conference on Antimicrobial Agents Chemother. 2003: Chicago, IL. p. F-1843.

[40] Staubitz P, Peschel A, Nieuwenhuizen WF, *et al.* Structure-Function Relationships in the Tryptophan-rich Antimicrobial Peptide Indolicidin. J of Pept Sci 2001; 7: 552-64.

[41] Sushma N, Kaur KJ, Jain D, Salunke DM. Plasticity in structure and interactions is critical for the action of indolicidin, an antibacterial peptide of innate immune origin. Protein Sci 2002; 11: 2158-67.

[42] Dugourd, D, Pasetka C, Erfle D, *et al*. MBI 226 Antimicrobial Peptide Interacts with Gram-Positive and Gram-Negative Cell Membranes. *ASM General meeting*, Salt Lake City, USA (**2002**).

[43] Kojima N, Araki Y, Ito E. Structure of Linkage Region between Ribitol Teichoic Acid and Peptidoglycan in Cell Walls of *Staphylococcus aureus* H. J Biol Chem 1983; 258: 9043-5.

[44] Neuhaus FC, Baddiley J. A Continuum of Anionic Charge: Structures and Functions of D-Alanyl-Teichoic Acids in Gram-positive Bacteria. Microbiol Mol Biol Rev 2003; 67: 686-723.

[45] Dmitriev BA, Toukach FV, Schaper KJ, Holst O, Rietschel ET, Ehlers S. Tertiary Structure of Bacteria Murein: the Scaffold Model. J Bacteriol 2003; 185: 3458-68.

[46] Peschel A. How do bacteria resist human antimicrobial peptides? Trends Microbiol 2002; 10: 179-86.

[47] Wu M, Maier E, Benz R, Hancock RE. Mechanism of Interaction of Different Classes of Cationic Antimicrobial Peptides with Planar Bilayers and with the Cytoplasmic Membrane of Escherichia coli. Biochemistry 1999; 38: 7235-42.

[48] Yang L, Harroun TA, Weiss TM. Barrel-Stave Model or Toroidal Model? A Case Study on Melittin Pores. Biophys J 2001; 81: 1475-85.

[49] Friedrich CL, Moyles D, Beveridge TJ, Hancock REW. Antibacterial Action of Structurally Diverse Cationic Peptides on Gram-Positive Bacteria. Antimicrobial Agents Chemother 2000; 44: 2086-92.

[50] Dugourd, D, Brinkman J, Pasetka C, Guarna M, Friedland HD, Clement J. Omiganan pentahydrochloride (MBI 226) affects *Staphylococcus aureus* cell membrane. *43rd Interscience Conference on Antimicrobial Agents and Chemotherapy*. Chicago, USA (**2003**). C1-1811.

[51] Dugourd, D, Pasetka C, Erfle D, *et al*. MBI 226 Antimicrobial Peptide Inhibits *Staphylococcus aureus* Macromolecular Synthesis. *ASM General Meeting* Salt Lake City, USA (**2002**).

[52] D'Ari R, Huisman O. Novel Mechanism of Cell Division Inhibition Associated with the SOS Response in *Escherichia coli*. J Bacteriol 1983; 156: 243-50

[53] Gresh N. Can a polyproline II helical motif be used in the context of sequence-selective major groove recognition of B-DNA? A molecular modelling investigation. J Biomol Struct Dyn 1996; 14: 255-73.

[54] Zuckermann MJ, Heimburg T. Insertion and Pore Formation Driven by Adsorption of Proteins Onto Lipid Bilayer Membrane–Water Interfaces. Biophys J 2001; 81: 2458-72.

[55] Zhang L, Rozek A, Hancock REW. Interaction of Cationic Antimicrobial Peptides with Model Membranes. J Biol Chem 2001; 276: 35714-22.

[56] Giacometti A, Cirioni O, Barchiesi F, Caselli F, Scalise G. *In-vitro* activity of polycationic peptides against *Cryptosporidium parvum*, *Pneumocystis carinii* and yeast clinical isolates. J Antimicrob Chemother 1999; 44: 403-6.

[57] Giacometti A, Cirioni O, Greganti G, Quarta M, Scalise G. *In vitro* activities of membrane-active peptides against gram-positive and gram-negative aerobic bacteria. Antimicrob Agents Chemother 1998; 42: 3320-4.

[58] Cristobal R, Edmiston CEJ, Runge-Samuelson CL, Owen HA, Firszt JB, Wackym PA. Fungal biofilm formation on cochlear implant hardware after antibiotic-induced fungal overgrowth within the middle ear. Pediatr Infect Dis J 2004; 23: 774-8.

[59] Brown SD, Traczewski MM. Omiganan pentahydrochloride (MBI 226): in-vitro spectrum and effects of environmental variation on MICs, *43rd Interscience Conference on Antimicrobial Agents and Chemotherapy*. Chicago, USA (**2003**). F-1844.

[60] Hoban DJ, Witwicki E, Zhanel G, Palatnick L, Friedland HD, McBride J. *In vitro* Activity of the Novel Topical Cationic Peptide MBI 226 Against 750 Clinical Isolates. *42nd Interscience Conference on Antimicrobial Agents and Chemotherapy*. San Diego, USA (**2002**).

[61] Press Release: Micrologix Reports Efficacy from Phase IIb Acne Study. 2004, Micrologix Biotech Inc.: Vancouver, Canada.

[62] Press Release: Micrologix Reports Phase III Trial Results of MBI 226. 2003, Micrologix Biotech Inc.: Vancouver, Canada.

[63] Press Release: Micrologix and Strata Pharmaceuticals Complete License Agreement for MBI-226. 2004, Micrologix Biotech Inc.: Vancouver, Canada.

[64] Anderegg TR, Fritsche TR, Jones RN. Quality Control Guidelines for MIC Susceptibility Testing of Omiganan Pentahydrochloride (MBI 226), a Novel Antimicrobial Peptide. J Clin Microbiol 2004; 42: 1386-7.

2.1 Early work

The initial part of my work consisted in obtaining partition constants of omiganan towards phospholipid* vesicles of different compositions. The partition constant, or K_p, is the ratio at equilibrium between the local, membrane-bound peptide concentration — 'local' denoting that only the membrane volume is considered — and the bulk aqueous phase peptide concentration. The value of K_p reflects how extensively the peptide partitions to the phospholipid membrane in question, higher values meaning a higher affinity.** Vesicles, more precisely, large unilamellar vesicles (LUVs), are spherical phospholipid bilayers made unilamellar and homogeneous in size by a process detailed in Articles III and IV, in turn adapted from reference 28. Phospholipid vesicles provide a model of cell membranes that allows a fine control over its constituents, and are extensively used in biophysical studies[29–31] as a substitute for real membranes, which are harder to obtain and prone to containing contaminants.

The purpose behind the determination of K_p values was to find differences in the partition towards vesicles modeling either bacterial or mammalian membranes. Such differences would then be used to justify, at least in part, the simultaneous activity and safety omiganan had displayed.[32,33] These were modest objectives: being highly cationic, a preference of omiganan for bacterial membrane models over mammalian ones — the first having a high content of anionic phospholipids, the latter being essentially zwitterionic — was pretty much expected. Yet, in this initial work I was able to get acquainted with the experimental protocols commonly carried out in the lab, the optical spectroscopies used to extract data from peptides and vesicles, and the mathematical formalisms that connected all that with the abstract views of peptide-membrane interaction and partition. And I did eventually find that the peptide interacted preferentially with the bacterial membrane models, which constituted on its own a minimal set of presentable results to fall back upon if later objectives failed to be met

*Throughout the book the terms 'lipid' and 'phospholipid' are interchangeably used.

**The reader is welcome to peek ahead into Section 4.1 for a more formal definition of K_p.

(these results, together with most of our later research on omiganan, are presented in Article III, included at the end of this section).

However, almost at the beginning of these studies I made a quite unexpected finding that was to deeply influence all my subsequent work.

* * *

The most common method to determine partition constants involves the titration of peptide with a suspension of vesicles. The fluorescence intensity of the peptide — in the case of omiganan due to its four tryptophans — is then monitored: peptide binding to the membrane is likely to cause an increase in the emitted fluorescence intensity due to a solvent effect of the apolar bilayer environment on the peptide's fluorescent residues. Fluorescence intensity will increase along the titration until the amount of lipid in the system is enough to have caused most peptide molecules to become membrane-bound; at this point fluorescence intensity approaches a plateau (see Figure 2.1 for a typical curve). As will be seen later, the value of K_p can be extracted from this curve — the partition curve — in the simplest case by fitting a two-parameter equation.

My first days, after an eventless characterization of the absorbance and fluorescence properties of omiganan, were spent trying to generate those hyperbolic-like curves. Eventually, such canonical curves were obtained (Figure 2.1) for vesicles made of POPC (palmitoyl-oleoyl phosphatidylcholine — a zwitterionic phospholipid that forms fluid-phase bilayers at room temperature). Following this success a clear deviation to a hyperbolic-like curve was obtained for the partition of omiganan towards DPPC (dipalmitoyl phosphatidylcholine — an also zwitterionic phospholipid that forms gel-phase bilayers below 40 °C). A somewhat sigmoidal curve was observed, with the fluorescence intensities at low lipid concentrations first decreasing, then increasing. Such a curve had already been observed by Sónia[34] when studying the cell penetrating peptide pep-1: she and Miguel had ascribed the behavior to a preferential localization of the peptide in the defects present in the gel phase phospholipid bilayer, and developed an extension to the partition model to account for

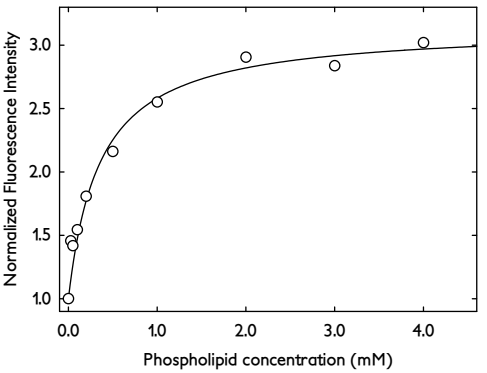

Figure 2.1 – Partition curve of 7.7 µM omiganan titrated with POPC vesicles — adapted from Article III. The line is the fit by Equation 4.5 (from Part II) to the data, from which a K_p value of $(3.7 \pm 0.4) \times 10^3$ was extracted.

the phenomenon. I gladly and successfully applied the extended model's equations to my curve, in the way learning that not only is the basic Nernst partition formalism unable to account for more complex partition behaviors, but also that its mathematical customization to suit particular needs is not necessarily difficult.

Some weeks later I performed the same experiments with POPG and DPPG (palmitoyl-oleoyl phosphatidylglycerol and dipalmitoyl phosphatidylglycerol: phospholipids with 1– charge and properties otherwise similar to those of POPC and DPPC, respectively). As predicted, a preference towards these anionic phospholipids could be seen even before any curve-fitting: much less lipid — relative to the POPC experiment — was required for the fluorescence intensity to reach a plateau. This meant that less lipid was required to bind almost all of the peptide and, thus, that the binding affinity was stronger. What was unexpected was the observation of another deviation to the hyperbolic-like behavior, visible in both POPG and DPPG curves. This deviation, unlike the one in the partition to DPPC, consisted in two or three data points at low lipid concentrations largely overshooting the expected curve, somewhat like a systematic spike (see Figure 2.2 for an example). Such observation could

be easily dismissed as casual outlying points, but the fact that both curves behaved similarly was intriguing. Little did I know that these spikes in my data, which I was not particularly happy about as they prevented a proper curve fit, were to become an important source of information on peptide action. Even more important, perhaps, than partition magnitudes.

2.2 Saturation

Analysis went on without a proper characterization of the spike phenomenon. K_p values could be obtained by ignoring the affected data points, and those were indeed higher than the ones obtained for the neutral systems. Still, because the spikes spread over the would-be rising portion of the curve, crucial for a good fit, the statistical validity of the result was weak. As remarked earlier, however, a preference for these anionic systems over zwitterionic ones could be qualitatively inferred, which supported the magnitude of the obtained values.

The following studies involved mixtures of POPC and POPG, mimicking the partly anionic, partly zwitterionic nature of the bacterial membrane. These were the bacterial membrane models to directly compare against the POPC-only mammalian model, whereas the POPG- or DPPG-only systems represented unphysiological extremes of anionic charge. Even as the results were being read already was it clear that also in these cases there were spikes present at low lipid concentrations (Figure 2.2). These turned out to be less sharp than those observed for the fully anionic systems and were also spread over a broader lipid concentration range. Furthermore, the lower the POPG content of the mixture, the flatter the spikes would become, being no longer perceptible at a 1 : 4 POPG : POPC proportion. Still, the spikes, now also dubbed humps, would prevent a proper curve-fitting, and again the preference of omiganan for these systems had to be inferred from the lower lipid concentrations required to reach the plateau. Being more physiologically relevant systems it was worth repeating the experiment several times to make sure about the deviations, and indeed they proved to be reproducible.

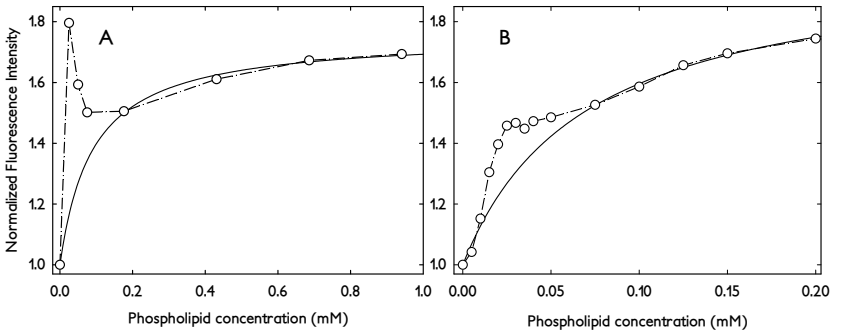

Figure 2.2 – Partition curves of 7.7 μM omiganan titrated with POPG (A) and 4 : 1 POPG : POPC (B) vesicles — adapted from Article III. The full lines represent the expected hyperbolic-like curve, fitted using only the post-deviation data points. In these cases K_p had values of $(14.6 \pm 0.3) \times 10^3$ and $(23.0 \pm 0.7) \times 10^3$, respectively, although their statistical validity is questionable.

This time Miguel and I started putting more effort into understanding the spikes. It had struck us that this phenomenon, which occurred only in the anionic bacterial model systems, could play a role in the selective activity of omiganan. Initial hypotheses to explain the observations involved multiple partitions within the membrane or aggregation of the bound peptides when in the presence of low lipid concentrations. These, however, were not straightforward to verify. Instead, in an apparent subversion of the scientific method, I tested titrations of lipid with peptide (the inverse setup of the partition curve determination) just to see if any deviations showed up under such conditions. Indeed, some breaks were faintly visible in what should be a straight line and, after some experimental optimization, namely through the use of acrylamide to clarify the breaking points (see Article III and Section 5.1 for more details on the method), a breakthrough was made: the breaking points did correspond to the conditions at which the spikes appeared in partition curves and, what was totally unexpected, they were the points above which no more peptide seemed to be able to bind the lipid. We were dealing with spatial membrane saturation!

Several new questions were raised by this finding, most regarding the validation of our interpretation of the results. But there was one question central to our understanding of the peptide's activity: could such an extreme event as the complete coverage of the membrane have physiological significance?

I addressed these questions in part of my subsequent work, along the way adapting and developing different methods (discussed in Chapter 5). In short, the correlation between the saturation points and the spikes was strengthened by observations that the association between the two held under different conditions. I was also able to further characterize the saturation phenomenon by determining the bound peptide-to-lipid proportion at saturation. To account for the overshoot of fluorescence intensity Miguel and I hypothesized that a rearrangement of the peptide's conformation or position in the membrane took place at, or close to, saturation; this rearrangement would cause an increase of the bound peptide's fluorescence quantum yield, leading to the observed spikes in the partition curves. The rearrangement hypothesis at once explained the increase of fluorescence intensity at saturation and associated the phenomenon with a molecular level event with potential macroscopic repercussions: we began thinking that saturation, a biophysically observed threshold, could be related to the *in vivo* triggering antimicrobial action of omiganan. Lastly, we were able to gradually demonstrate on theoretical grounds — partly supported by experimental evidence — that saturation is not only a physiologically plausible event but may be an actual requirement for activity.

At the time of writing of Article III some of these notions were in their infancy, and only became fully developed when I no longer was focusing my work on omiganan. In any case, even at that stage we could already put forward one of the most important hypotheses that would stem from my PhD work: *antimicrobial activity of (some) AMPs is triggered at the molecular level by events at, or close to, full membrane coverage.*

From the point of view of my scientific development I feel very fortunate for having stumbled upon an innovative idea hiding in outlying data, even if at the time I saw it more as a curse than as a blessing! — Some of

my friends may still recall my puzzled descriptions of early work, usually accompanied by several drawings of humps, spikes and hyperbolas!

2.3 Later studies

Further work with omiganan involved the characterization of several activity-related processes, such as membrane permeabilization or lysis, in-depth positioning in the membrane, translocation, or interaction with the bacterial cell wall. All of these measurements prompted, in one way or another, for methodological adaptations, and were to me more challenging in this aspect (more details in Part II) than in the interpretation of their results.

It is noteworthy, however, that the in-depth positioning tests indicated an inward movement of the peptide upon saturation, which supports the rearrangement-at-saturation hypothesis. This was only found because we specifically tested systems in and out of saturation. It is likely that if we had not encountered saturation before only one set of conditions would have been used, and an important insight missed.

Also interesting is the fact that omiganan did not induce permeabilization but was later observed to be able to translocate across anionic membranes (unpublished data; see Section 'Translocation' in the Appendix). Paradoxical as it may seem, this is in agreement with preliminary biological work carried out by the developers of the peptide, where bacterial depolarization, but not leakage, had been observed.[35]

Most of these results, together with the partition and saturation data, and tentative interaction models, compose Article III. Although I did address some loose ends on omiganan after the publication of this article my work became mainly focused on another AMP. I haven't since produced enough data on omiganan to justify a second publication.

While there may have been many reasons to sideline omiganan, one of the strongest was certainly the relative difficulty to optically study it: its four tryptophans, which at first foreboded good fluorescence measurements, were not only weakly emitting but also exquisitely sensitive to photobleaching. Moreover, because these four residues were scattered

across the sequence of omiganan, all information reported by fluorescence was an average blurred by all the residues' environments, which entailed a loss of sensitivity of many of the used methods. I am very happy for having had the chance to work with omiganan, but I did go through a few moments of despair because of it. Anyway, those troubles mustn't have been that harsh — or at least I did not take them personally — because I couldn't avoid being a bit sad at the news of the pharmaceutical mishap of the peptide.

Article III

ELSEVIER

Biochimica et Biophysica Acta 1768 (2007) 1277–1290

Biochimica et Biophysica Acta
BBA

www.elsevier.com/locate/bbamem

Omiganan interaction with bacterial membranes and cell wall models. Assigning a biological role to saturation

Manuel Nuno Melo, Miguel A.R.B. Castanho *

Centro de Química e Bioquímica, Faculdade de Ciências da UL, Campo Grande, C8, 1749-016 Lisboa, Portugal

Received 24 November 2006; received in revised form 28 January 2007; accepted 2 February 2007
Available online 17 February 2007

Abstract

Omiganan pentahydrochloride (ILRWPWWPWRRK-NH_2·5Cl) is an antimicrobial peptide currently in phase III clinical trials. This study aims to unravel the mechanism of action of this drug at the membrane level and address the eventual protective role of peptidoglycan in cell walls. The interaction of omiganan pentahydrochloride with bacterial and mammalian membrane models – large unilamellar vesicles of different POPC:POPG proportions – was characterized by UV-Vis fluorescence spectroscopy. The molar ratio partition constants obtained for the two anionic bacterial membrane models were very high ($(18.9\pm1.3)\times10^3$ and $(43.5\pm8.7)\times10^3$) and about one order of magnitude greater than for the neutral mammalian models ($(3.7\pm0.4)\times10^3$ for 100% POPC bilayers). At low lipid:peptide ratios there were significant deviations from the usual hyperbolic-like partition behavior of peptide vesicle titration curves, especially for the most anionic systems. Membrane saturation can account for such observations and mathematical models were derived to further characterize the peptide–lipid interaction under those conditions; a possible relation between saturation and MIC was deduced; this was supported by differential quenching studies of peptide internalization. Interaction with the bacterial cell wall was assessed using *Staphylococcus aureus* peptidoglycan extracts as a model. A strong partition towards the peptidoglycan mesh was observed, but not as large as for the membrane models.
© 2007 Elsevier B.V. All rights reserved.

Keywords: Antimicrobial peptide; Saturation; Partition; Membrane; Peptidoglycan

1. Introduction

Omiganan pentahydrochloride (omiganan, sequence: ILRWPWWPWRRK-amide·5Cl; predicted peptide charge at neutral pH: 5^+) is a novel cationic antibiotic peptide, currently in phase III clinical trials, designed for topical use to prevent catheter-related bloodstream infections and to reduce bacterially induced acne lesions. The sequence of omiganan is related to that of indolicidin, a ribosomally-synthesized antimicrobial peptide (RAMP) that can be purified from the granules of bovine neutrophils [1]. Besides its clinical importance – especially regarding the prevention of nosocomial infections – omiganan could become one of the first RAMP-related antibiotics to obtain market approval.

Omiganan demonstrated a broad spectrum of antimicrobial activity [2] and a favorable safety profile in clinical trials for topical use [3,4]. However, the molecular bases for these characteristics are still hypothetical and, like its structural characterization, most information comes from predictions based on studies of other RAMPs, namely the related peptides indolicidin and CP-11 [4,5]. Moreover, as with other RAMPs, bacteria exposed to omiganan seem to be unable to evolve resistance even upon repeated exposure [6,7]. This reflects the importance of the cellular components that are targeted, which have been postulated to either be the membrane or core metabolic pathways such as protein or nucleic acid synthesis. Straightforward membrane lysis, though, has been questioned as a potential killing mechanism for both omiganan and indolicidin [4,8–10].

Bilayer and cell wall interactions might not be the only microorganism killing processes of omiganan; nonetheless, even if the peptide's main activity involves cytoplasmic targets, such interactions with the membrane and cell wall

* Corresponding author. Tel.: +351 21 7500931; fax: +351 21 7500088.
E-mail address: castanho@fc.ul.pt (M.A.R.B. Castanho).

0005-2736/$ - see front matter © 2007 Elsevier B.V. All rights reserved.
doi:10.1016/j.bbamem.2007.02.005

will always be of importance for antimicrobial action, as these outer structures must necessarily be crossed. In addition, because mammalian cells display profound differences relatively to prokaryotic ones [11,12], the interactions of omiganan with membranes and cell walls of microorganisms provide a potential step to improve target specificity. Given this, the study of these interactions is essential to the full rationalization of the macroscopic properties displayed by omiganan.

While peptide–membrane interaction has been the subject of many studies [13–17], the bacterial cell wall, especially that of the Gram-positive bacteria, has been largely ignored in what concerns the mechanisms of action of RAMPs or RAMP-related antibiotics despite its likely role as a barrier to their entry into the cell. The cell wall is mainly constituted by an anionic peptidoglycan mesh with pore sizes around 4 nm in diameter [18,19]; although the exact topological disposition of the wall components is still under debate [18–20] it is clear that larger peptides will not cross it unchallenged [21,22]. Even for small peptides, such as omiganan, the wall could potentially behave, if not as a barrier, as an anionic trap.

Spectroscopic methodologies can yield detailed information about several aspects of peptide interactions [23], especially in the case of omiganan, which is intrinsically fluorescent due to its four Trp residues; however, other cellular constituents and processes often generate high degrees of noise and interference. Resorting to model systems is a workaround to these unwanted contributions: in this work large unilamellar vesicles (LUVs), of varying anionic surface charge, were used as models for both bacterial and mammalian cell membranes. Because one of the main differences between omiganan and indolicidin – which is hemolytic – is the greater cationicity of the former, the chosen models focus on the analysis of the charge effect, rather than in specific interactions with membrane components. In addition to the LUVs, a simple method was devised using *Staphylococcus aureus* (*S. aureus*) peptidoglycan extracts as a model system to clarify the omiganan–cell wall interaction.

2. Materials and methods

2.1. Reagents and apparatus

Omiganan pentahydrochloride (purity >95%) was a kind gift from MIGENIX, Inc. (Vancouver, Canada); 2-(4-(2-Hydroxyethyl)-1-piperazinyl)-ethanesulfonic acid (HEPES), sodium chloride, chloroform, ethanol (spectroscopic grade) and acrylamide were from Merck (Darmstadt, Germany); potassium iodide was from Riedel-de Haën (Seelze, Germany); 8-aminonaphthalene-1,3,6-trisulfonic acid (ANTS) was from Invitrogen Corporation (Carlsbad, California); 1-palmitoyl-2-oleoyl-*sn*-glycero-3-phosphocholine (POPC), 1-palmitoyl-2-oleoyl-*sn*-glycero-3-(phospho-*rac*-(1-glycerol)) (POPG), 1,2-dipalmitoyl-*sn*-glycero-3-phosphocholine (DPPC) and 1,2-dipalmitoyl-*sn*-glycero-3-(phospho-*rac*-(1-glycerol)) (DPPG) were from Avanti Polar-Lipids (Alabaster, Alabama); Cholesterol and Triton X-100 (TX-100) were from Sigma (St. Louis, Missouri); *S. aureus* peptidoglycan extract was from Fluka (Buchs, Switzerland) and the quenchers 5 and 16 NS (5- and 16-doxylstearic acids, respectively) were from Aldrich Chem Co. (Milwaukee, Wisconsin).

Absorbance assays were performed in a Jasco V-560 UV-vis or a Genesys 10 UV spectrophotometer; steady-state fluorescence assays were performed in a SLM Aminco 8100 spectrofluorometer (equipped with a 450WXe lamp and double monochromators) or, for the studies of omiganan–peptidoglycan interaction, in a SpectraMax GeminiEM microplate spectrofluorometer (equipped with a 1 J/flash pulsed Xenon lamp). Time resolved fluorescence measurements were as described elsewhere [24]. Lipid films were dried overnight with a *vacuubrand* vacuum pump and extruded afterwards.

All experiments were performed at room temperature and, unless otherwise stated, all solutions prepared in a 10 mM HEPES buffer, pH 7.4, containing 150 mM NaCl, which is expected to mimic physiological conditions. All steady-state omiganan fluorescence measurements were taken at an excitation wavelength of 280 nm, except for the experiments involving acrylamide where, to minimize inner filter effects due to its absorption at 280 nm, the samples were excited at 295 nm. Emission spectra were collected in the 300–450 nm wavelength range. When full spectra were not taken, single wavelength measurements were read at 353 nm in the absence of lipids and at 343 nm otherwise. ANTS fluorescence was taken by exciting at 360 nm and recording the emission at 500 nm.

2.2. Preparation of model systems

For the production of membrane model systems LUVs were prepared by extrusion of hydrated phospholipids through 400 and 100 nm pore membranes, as described elsewhere [25]; biological model systems include 100% POPC LUVs as well as 1:4, 2:1 and 4:1 POPG:POPC LUVs; the same models, except for the 2:1 proportion, were also prepared with cholesterol in a 1:2 cholesterol:phospholipid ratio. Other studied LUVs were 100% POPG, 100% DPPC and 100% DPPG systems. To produce ANTS loaded vesicles LUVs were prepared in the described buffer with the addition of 10 mM ANTS; the resulting LUVs were then passed through a 10 mL Bio-Rad Econo-Pac 10DG column (Bio-Gel P-6DG gel with 6 kDa molecular weight exclusion).

To prepare the bacterial wall model systems, peptidoglycan extracts were first softly mashed with a glass rod and then suspended in buffer. The mashing was necessary to de-aggregate some larger particles of the lyophilized extracts powder that would render the suspension inhomogeneous.

2.3. Photophysical characterization in bulk aqueous phase

The linear dependence of the absorbance and fluorescence intensity of omiganan on its concentration was tested over the 0–14.5 μM range. To check whether aggregation occurs in the aqueous phase aliquots of a 4 M acrylamide solution were sequentially added to a peptide sample while recording both the absorbance and fluorescence intensity. In this, and in all subsequent studies where a constant peptide concentration was required, 7.7 μM omiganan was used as a working concentration; this concentration is both biologically relevant – it is within the range of the MICs of omiganan against a number of strains [2] – and spectroscopically adequate – it is high enough to provide a strong fluorescence signal while having an absorbance under 0.1 at 280 nm, which ensures minimal inner filter effects.

2.4. Membrane interaction studies

The extent of membrane partition to each modeled system was determined by adding small aliquots of a LUV suspension to a peptide sample and recording its fluorescence spectrum. Membrane saturation points were determined by adding aliquots of a 205.3 μM stock peptide solution to a suspension of LUVs, in the presence of 300 mM acrylamide, and recording the fluorescence; to prevent acrylamide dilution the stock solution was also prepared with 300 mM acrylamide.

Differential quenching studies were carried out by sequentially adding aliquots of a lipophilic quencher – either 5-NS or 16-NS – to a LUV suspension previously equilibrated with peptide; for each modeled system two

different LUV concentrations were used so as to set either non-saturation or saturation states and quencher concentration was increased or reduced accordingly; both steady-state and time resolved measurements were taken (the latter only on the first and last points). Because the 5- and 16-NS stock solutions were prepared in ethanol, care was taken, while adding the quencher aliquots, to keep final ethanol concentrations below 2% (v/v) in order to prevent bilayer alterations [26].

For every addition in the described procedures, a minimum of 10 minutes was allowed for incubation before measurement.

Peptide induced leakage of vesicle contents was tested by sequentially adding 400 mM KI and 7.7 μM omiganan to ANTS containing vesicles; the ANTS fluorescence quenching by iodide was monitored (excitation at 360 nm and emission at 500 nm) and maximum leakage was assumed to be achieved by addition of 0.2% (v/v) Triton-X100.

2.5. Peptidoglycan interaction study

Different volumes of a peptidoglycan suspension were added to separate samples of omiganan at the working concentration and allowed to equilibrate for 10 minutes. The samples were then centrifuged at 4300 g for 5 minutes and the supernatant was recovered for fluorescence recording. Blanks were prepared in the same conditions but in the absence of peptide to correct for the fluorescence interference from leftover peptidoglycan in suspension.

3. Results

3.1. Photophysical characterization in bulk aqueous phase

The spectroscopic behavior of omiganan in aqueous solution resembled that of Trp, in respect to both absorbance and fluorescence (data not shown); linearity between absorbance and fluorescence intensity was observed up to 14.5 μM. The calculated absorptivity coefficient (ε) of omiganan at 280 nm was $1.72 \times 10^4\ M^{-1}\ cm^{-1}$, yielding a molar absorptivity per Trp residue of $4.3 \times 10^3\ M^{-1}\ cm^{-1}$. The quenching of omiganan by acrylamide also followed a linear Stern–Volmer relationship, with a K_{SV} of 15.5 M^{-1}. Static quenching by acrylamide originated slight upward deviations from linearity above 300 mM of quencher.

3.2. Membrane incorporation studies

Upon the partitioning of omiganan to vesicles there was, generally, an increase in fluorescence intensity as well as a spectral shift of about 10 nm to lower wavelengths (not shown). For the neutral, liquid-ordered POPC system, the increase in intensity followed a hyperbolic-like relationship, whereas the gel-phase DPPC system deviated from that behavior, inducing an intensity decrease at low concentrations, followed by a sigmoidal rise (Fig. 1A).

A deviation, or spike, in the fluorescence intensity vs. lipid concentration relationships was observed at low lipid concentrations for the most anionic systems (100% POPG, 100% DPPG, 4:1 POPG:POPC and 2:1 POPG:POPC systems) (Figs. 1B and C, and 3A; 2:1 POPG:POPC system not shown). This was not observed in the less anionic 1:4 POPG:POPC system (not shown).

Cholesterol enriched systems displayed sigmoidal curves (Fig. 2), with a behavior similar to the one displayed by the DPPC system (Fig. 1A).

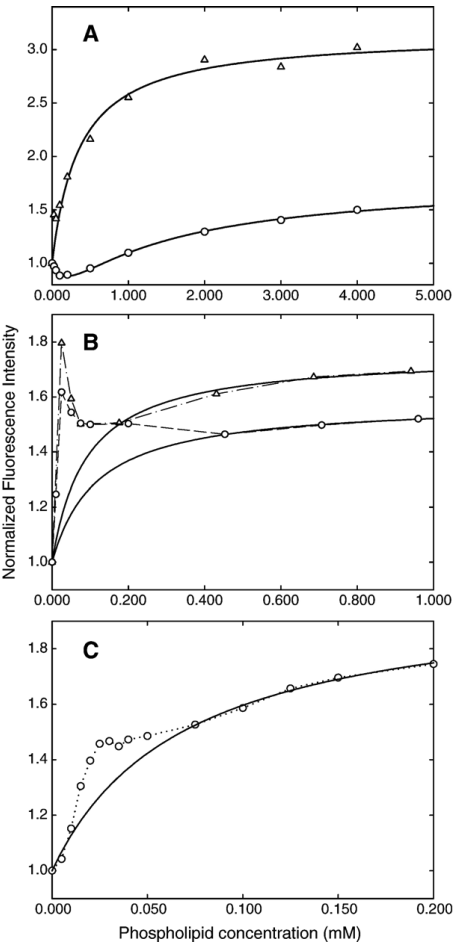

Fig. 1. Partition curves of 7.7 μM omiganan in several lipidic systems; fitted parameters are summarized in Table 1. The solid lines represent the fitting of the data to a partition model. Data points were connected to better evidence deviations from a hyperbolic behavior. (A) 100% POPC (△) and 100% DPPC (○) systems; data were fitted to the simple partition model (Eq. (1)) or to the self-quenching model (Eq. (2)), respectively. Due to possible bilayer saturation, the second and third points of the POPC partition curve were left out of the fitting. (B) 100% POPG (△) and 100% DPPG (○) systems; data were fitted to the simple partition model (Eq. (1)), but only the last four points of the POPG curve and the last three of the DPPG curve were used in the fit. (C) POPG:POPC 4:1 system. Data were fitted to the simple partition model (Eq. (1)), but only the rightmost 5 points were used for the fit. Partition towards POPG:POPC 2:1 LUVs (not shown) behaved similarly to the POPG:POPC 4:1 system, while for the POPG:POPC 1:4 system fitting to any of the models was not possible.

Membrane saturation points were successfully obtained for the 4:1 POPG:POPC system (Fig. 3B) and for the 2:1 POPG:POPC system (not shown): in a titration of vesicles with omiganan, at low peptide concentrations, a linear relationship between fluorescence intensity and peptide concentration was

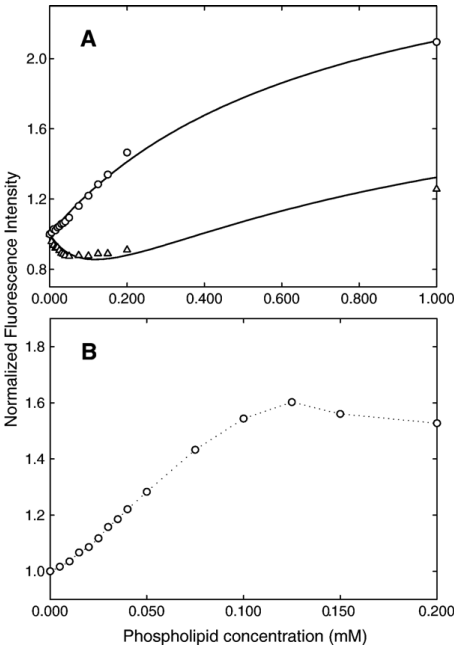

Fig. 2. Partition curves of 7.7 μM omiganan for the cholesterol containing systems; solid lines represent the fitting of the data to one of the described models. (A) 100% POPC (△) and 1:4 POPG:POPC (○) systems—because there is a clear deviation of the partition behavior towards that of the DPPC system (Fig. 1A) Eq. (2) had to be used to fit the 100% POPC system; Eq. (1) was used for the 1:4 POPG:POPC fit. Obtained partition constants are summarized in Table 1. (B) 4:1 POPG:POPC system—a distended and sigmoidal behavior was induced by cholesterol, although a deviation still occurred; because the remaining data points (two further phospholipid concentrations were used) lie almost horizontally, no information on the partition extent could be extracted.

observed; however, after a critical point, which was dependent on the used lipid concentration, a break occurred in the graph and a second linear regime, with a lower slope, followed. These breaks were assumed to represent membrane saturation, as discussed below. For the other less anionic systems, saturation points were impossible to determine since the curves did not display a clear break, although their slopes did decrease with increasing peptide concentration (data not shown).

In the membrane localization studies all biological model systems performed similarly in that relative quenching efficiencies by 5-NS and 16-NS were the same regardless of the membrane surface charge (Fig. 4). The time dependent fluorescence data were in agreement with the steady state measurements concerning 5- and 16-NS relative quenching efficiencies. The greatest observed differences were not between different systems, but between saturated and non-saturated states within the same system: the quenching efficiency of both quenchers was similar in non-saturated states whereas a clear increase of 16-NS quenching efficiency was observed in saturated systems (Fig. 4).

3.3. Omiganan induced leakage of vesicle contents

Omiganan did not seem to induce any kind of bilayer perturbation strong enough for membrane crossing by either ANTS molecules or iodide that would result in a decrease in the encapsulated ANTS fluorescence (not shown). The methodology was tested using as a control a peptide that induced leakage.

3.4. Peptidoglycan interaction study

After centrifugation of the peptidoglycan, a decrease in supernatant fluorescence, with increasing peptidoglycan concentrations, was observed (Fig. 5). This indicates that part of the peptide was dragged along with the mesh and that there is interaction between the two.

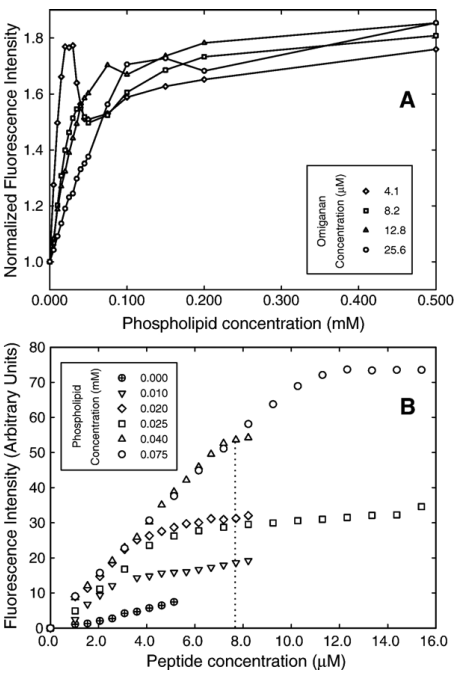

Fig. 3. (A) Partition curves of 4.1, 8.2, 12.8 and 25.7 μM omiganan in 4:1 POPG:POPC. Saturation points were taken as the maximum of the deviation in each curve and were used to determine the saturation ratio and the partition constant (Fig. 6). There is an approximately common behavior of the curves after the deviations, which is in agreement with the simulated partitions. A curve with 1.0 μM omiganan was also obtained (not shown), but a much higher I_L/I_W ratio was observed; its K_p, however, was similar to the others'. Average K_p and I_L/I_W ratio (Table 1) are in agreement with the already obtained constant and ratio for the same system (Fig. 1C). (B) Titration of different phospholipid concentrations with omiganan (4:1 POPG:POPC system) in the presence of 300 mM acrylamide. Saturation points were identified from the breaks in each curve. The dotted line indicates the peptide concentration at which the partition curve in Fig. 1C has a relative maximum (around 0.040 mM of phospholipid); this peptide concentration is very close to the saturation point in the 0.040 mM phospholipid curve.

4. Discussion

4.1. Photophysical characterization in bulk aqueous phase

The observed behavior of omiganan in aqueous phase did not reveal the presence of significant peptide–peptide interactions at the used concentrations: the obtained molar absorptivity is close to the one of free Trp^+ (5.6×10^3 $M^{-1}\cdot cm^{-1}$ [27]). The linear Stern–Volmer plot is indicative of no Trp side chain inaccessibility, the occurrence of which could be associated to peptide aggregation [28], and is also in agreement with the absence of Trp side chain protection since the K_{SV} for acrylamide quenching of free Trp^+ is 15.8 M^{-1} [29].

4.2. Membrane incorporation studies

The procedures for the membrane incorporation quantification were designed to allow the calculation of the Nernst partition constant (K_p) from fluorescence intensity (I) vs. phospholipid concentration ([L]) plots, at a constant peptide concentration ([P]), by a simple partition model, described by Santos et al. [30]. The partition constant is the ratio between the equilibrium membrane-bound and aqueous phase peptide concentrations[1] [30], thus providing an easy assessment of the extent of membrane interaction. The model used in this study regards the membrane as a volume of a separate lipidic phase within the bulk aqueous phase and treats the peptide–membrane interaction as a Nernst equilibrium; the fluorescence intensity of a peptide–lipid system, normalized by the fluorescence intensity of the peptide in aqueous phase, is then given by Eq. (1) (adapted from [30]):

$$I/I_W = \frac{1 + K_p\gamma_L[L]I_L/I_W}{1 + K_p\gamma_L[L]}, \quad (1)$$

where [L] is the total phospholipid concentration available for the peptide to interact with, K_p is the Nernst partition constant and γ_L is the phospholipids molar volume, which is 0.763 M^{-1} for liquid crystal phases [31] and 0.689 M^{-1} for gel phases [32]. I_L and I_W are the fluorescence intensities the mixture would display if all the peptide was in the lipidic or aqueous phase, respectively. I_W can be readily obtained from the measurement of I in the absence of lipid; I_L, however, is a limit value of fluorescence intensity as $[L]\rightarrow\infty$ and is determined as a system parameter together with K_p.[2]

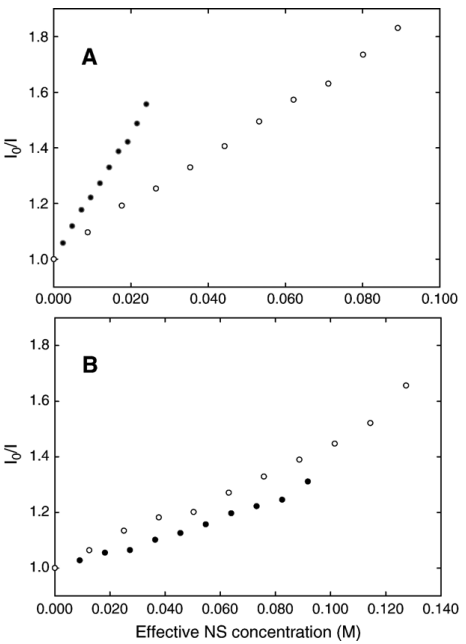

Fig. 4. Stern–Volmer representations (I_0/I vs. quencher concentration) of the quenching of 7.7 μM omiganan by the membrane quenchers 5- and 16-NS (○ and ● symbols, respectively), in the 4:1 POPG:POPC system (the quenching behavior in this system is representative of what was obtained for 2:1 and 1:4 POPG:POPC and 100% POPC systems). (A) Membrane saturation was induced by using 0.030 mM of phospholipid. (B) A phospholipid concentration of 0.3 mM was used to avoid saturation. Effective quencher concentration in the membrane was calculated using the partition constants provided by Wardlaw et al. [49]. The increase in the difference of 16-NS and 5-NS quenching efficiencies in A relatively to B is indicative of peptide burying in the bilayer, although only an average localization can be inferred, as there are four Trp residues in omiganan.

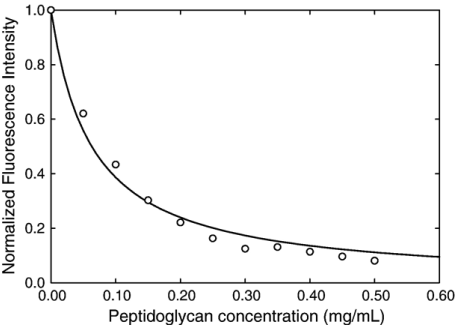

Fig. 5. Normalized omiganan fluorescence after incubation with several concentrations of peptidoglycan extracts, physically separated by centrifugation. The data were fit (solid line) to a single parameter model (Eq. (9)) and a D_g value of 15.9±1.1 mL/mg ($D_v=(3.1\pm0.2)\times10^3$) was obtained.

[1] Note that, as remarked by Santos et al., care must be taken when intercomparing K_p data from the literature since some authors define the partition constant as the ratio between the lipid and aqueous phase solute concentrations whereas others define it as the ratio between the molar fractions of the solute in each phase. Approximate conversion can be obtained by using $K_p=K_{p,x}\cdot\gamma_W/\gamma_L$, where K_p and $K_{p,x}$ are the concentration ratio and the molar fraction ratio partition constants, and γ_W and γ_L stand for the aqueous and lipidic phases molar volumes [30].

[2] More accurately, I_L should be attained when [L] reaches its maximum value of $1/\gamma_L$, which corresponds to a phospholipid only solution; for most practical cases, however, this amounts to a negligible correction. Further considerations on the subject can be found in [33].

The I/I_W vs. $[L]$ representation, termed here 'partition curve', is thus expected to be hyperbolic-like and independent of the initial peptide concentration in an ideal partition. An issue to bear in mind is that, because fluorescence emission spectral shifts can also be a consequence of peptide–lipid interaction, the integrated spectral intensity should be preferred over single wavelength intensity. In this work, full spectra were always used when possible, although the differences between following that approach and using a single wavelength were rarely significant.

In the present case, a difference between I_W and I_L was expected to occur as a consequence of an alteration in the Trp environment as the peptide enters the membrane [23,30].

4.2.1. Neutral systems

For the liquid-ordered phase POPC vesicles, which were used to model the outer leaflet of the mammalian membrane (the inner leaflet was modeled with a 1:4 POPG:POPC system), there was a good agreement of the partition curve (Fig. 1A) with the partition model, from which a K_p value of $(3.7\pm0.4)\times10^3$ and a I_L/I_W ratio of 3.09 ± 0.11 were obtained (partition parameters obtained for all lipidic systems are summarized in Table 1). For the gel phase neutral DPPC LUVs, which were used for the sake of studying the influence of membrane rigidity, initial deviations did not allow the fitting of the simple partition model (Fig. 1A). However, the intensity drop, followed by a somewhat sigmoidal behavior, was consistent with the phenomenon of peptide self-quenching: this effect is related to the accumulation of peptide molecules in membrane line defects on the borderlines between different phospholipidic crystalline organizations, favored by the rigidity of the gel phase DPPC bilayers. Eq. 1 was adapted, as deduced by Henriques et al. [34], becoming

$$\frac{I}{I_W}=\frac{K_p\gamma_L[L]I_L/I_W}{1+K_p\gamma_L[L]+k_2K_pI_L}+\frac{1}{1+K_p\gamma_L[L]}, \quad (2)$$

where k_2 is proportional to the ratio between the bimolecular self-quenching rate and the radiative decay rate. Note that the limit as $[L]\rightarrow\infty$ is not altered by the occurrence of self-quenching or by differences in the initial peptide concentration. The partition constant determined by this method was of $(4.9\pm 0.3)\times10^3$ and the I_L/I_W ratio was of 1.80 ± 0.03. While the K_p is close to the one obtained for the POPC system, the I_L/I_W ratio points towards a slightly different peptide conformation/localization.

The partition of omiganan to the neutral lipidic systems was very strong despite the absence of negative surface charge on the vesicles. Although electrostatic interactions can be expected to play a significant role in the activity of omiganan due to its 5^+ charge, it was seen that the hydrophobic effect and van der Waals forces that dominate the partition to the neutral systems can account for an important part of the peptide's membrane interaction. Hydrophobic residues such as Ile and Leu and anchoring residues such as Trp may play an important role in partition under these conditions.

4.2.2. Anionic systems

Accurate determination of the partition constant in systems containing anionic phospholipid was difficult or impossible, due to large deviations from either hyperbolic or sigmoidal partition curves (Fig. 1B and C): at variance with the partition to the neutral systems, the initial points of both liquid crystal

Table 1
Summary of the characteristics of each modeled system: constitution, partition parameters and initial behavior of the partition curve

Modeled system	Constituent phospholipids [a]	$K_p/10^3$	I_L/I_W	Used model [b]	Initial deviation [c]
100% Neutral Membrane gel phase	DPPC	4.9±0.3	1.80±0.03	SQ	–
100% Anionic membrane gel phase	DPPG	12.5±0.8	1.58±0.01	SP	+
100% Anionic membrane liquid crystal phase	POPG	14.6±1.3	1.76±0.01	SP	+
Bacterial membrane models					
Inner leaflet [d]	4:1	23.0±0.7	1.94±0.06	SP	+
Inner leaflet+cholesterol [e, f]	4:1	n.o.	n.o.	n.a.	+
Outer leaflet	2:1	43.5±8.7	1.84±0.04	SP	+
Mammalian membrane models					
Inner leaflet [f]	1:4	n.o.	n.o.	n.a.	–
Inner leaflet+cholesterol [e]	1:4	1.8±0.2	2.89±0.09	SP	–
Outer leaflet	POPC	3.7±0.4	3.09±0.11	SP	+
Outer leaflet+cholesterol [e]	POPC	8.2±1.2	2.08±0.14	SQ	–

[a] POPG:POPC mixtures are indicated by the proportion between phospholipids. All other systems are constituted by a single type of phospholipid.

[b] Used model for the fitting of the experimental results—SP: 'Simple Partition', the formalism described by Santos et al. was used (Eq. 1); SQ: 'Self-Quenching', the formalism described by Henriques and Castanho (Eq. 2) was used.

[c] Occurrence (+), or not (−), of an upward deviation in the partition curve, for low phospholipid concentrations.

[d] The parameters for this system are the average of the results of several partition curves at different peptide concentrations (Figs. 1C and 3A). The I_L/I_W ratio of the 1.0 mM curve (not shown) was not included.

[e] The system is also constituted by cholesterol in a 1:2 molar proportion relatively to the phospholipids.

[f] The extraction of partition parameters by curve-fitting was not possible for this system. Fields depending on this information are marked either 'n.o.' (not obtained) or 'n.a.' (not applicable), according to each case.

and gel phase partition curves seem to overshoot above a hypothetical hyperbolic behavior, returning to it at higher lipid concentrations, closer to the curve plateau. Nonetheless, the partition of omiganan towards these vesicles seems to be greatly enhanced relatively to their neutral counterparts, judging by the very high initial slopes of the partition curves and the little amount of lipid required to reach almost maximal interaction (notice the difference in the x axis scale of Fig. 1B and C relatively to Fig. 1A). Such an increase in the partition extent was expected because electrostatic interactions are very likely to affect the heavily charged peptide; in addition, it is possible that this very strong partition is responsible for the observed deviations from the partition model. Namely, membrane saturation may occur at low lipid concentrations when the bound peptide concentration hypothetically dictated by K_p is higher than what the membrane can accommodate. Because it considers the peptide as a volumeless entity, and thus incapable of saturating the lipidic phase, the model of Santos et al. [30] is not suited to the study of saturated systems and other models, described below, were devised to better characterize these situations. From the partition curves, K_p values could be extracted by fitting only the non-saturated points to the simple partition model (Fig. 1, Table 1). Statistical significance was, of course, hurt by this approach both because the number of available data points was reduced and because the initial rising portion of the hyperbolic partition curve, which was absent, is determinant in the calculation of K_p. Nevertheless, the obtained partition constants (Table 1), which are greater than those of the neutral systems, are consistent with the expected role of the electrostatic interactions (the partition towards the 1:4 POPG: POPC system – not shown – could not be fitted but was visibly less intense than for the other anionic systems). The same charge relationship was observed for the related peptide indolicidin [35]. The occurrence of these deviations and the hypothesis that they could represent a phenomenon not described by the simple partition model led to the discarding of the second and third points when fitting the POPC partition curve (Fig. 1A), which, upon closer inspection, seem to also deviate from the hyperbole.

The different obtained K_p's are indicative of a strong preference of omiganan towards negatively charged membranes similar to the bacterial systems (2:1 and 4:1 POPG:POPC systems, which are as anionic as the outer and inner bacterial cell membrane leaflets [11,12]), which appear to induce the highest extents of partition by providing an optimal negative surface charge. This selectivity/affinity of omiganan for prokaryotic bilayer membranes is thus one possible factor for the favorable safety profile of omiganan as a topical drug [3]: the peptide's concentration in a zwitterionic mammalian membrane does not get as high as in an anionic bacterial membrane. Partition constants of such magnitudes are commonly displayed by membrane-active peptides ([36,37] note that intercomparison of different partition constants will require an appropriate conversion), which supports the importance of the membrane interaction in omiganan's mode of action.

An observed reduction in I_L/I_W ratios is in agreement with a preferential interaction of the peptide with the membrane surface, as this may reflect an exposure of the Trp residues to a polar environment. For the models of biological membranes, peptide localization was determined with more accuracy by differential quenching methods, discussed below.

4.2.3. Cholesterol effect on the partition extent

To further assess the action of omiganan towards mammalian cells, cholesterol was added to the 100% POPC and 1:4 POPG: POPC model systems (phospholipid:cholesterol ratio of 2:1), and the presence of specific peptide–sterol interactions were investigated. These are undesirable interactions because their occurrence may increase the peptide's partition extent towards mammalian membranes (as opposed to bacterial ones, which are sterol-free) and eventually represent an increased toxicity risk, should the peptide disturb the structural properties that cholesterol confers to the bilayer [38,39].

Both partition constants for the mammalian membrane models (inner and outer leaflet) remained within the same order of magnitude as the 100% POPC, sterol-free system, which is unsupportive of the cholesterol having, per se, a very strong interaction with the peptide. The most pronounced consequence of cholesterol addition was the induction of a gel phase like behavior (Fig. 2): the partition curves deviated from the hyperbolic-like progression, indicating the occurrence of self-quenching, as with the DPPC system. Since cholesterol condenses liquid crystal bilayers, forming a liquid ordered phase [40], this observation indicates that omiganan does not have specific interactions with it, or at least not to a point where its properties are significantly altered. This was further demonstrated by testing the effect of cholesterol in the 4:1 POPG:POPC system, which has a higher charge and partition constant: the same sigmoidal behavior was observed and an apparently lower extent of partition was observed although it was impossible to calculate a K_p value because the non-hyperbolic regime dominated most of the curve (Fig. 2B).

These evidences predict a low cholesterol related toxicity of omiganan towards human cells, in agreement with its clinical safety profile [3].

4.3. Membrane saturation studies

The hypothesis of membrane saturation was tested by titrating LUV suspensions with peptide while monitoring omiganan's fluorescence intensity. Under the simple partition model, for a given lipid concentration, the relative proportions of peptide in and out of the membrane (X_L and X_W, respectively) should be constant, independently of overall peptide concentration changes [23]. In this case, the total fluorescence intensity, I, will be the sum of I_L and I_W, weighted, respectively, by X_L and X_W [23]. Because I_L and I_W, are expected to be proportional to the global peptide concentration, under these conditions $I \propto [P]$, where $[P]$ is the overall peptide concentration. The I vs. $[P]$ titrations were carried out in the presence of acrylamide, which is an aqueous phase quencher, to increase the difference between I_L and I_W, in order to better identify alterations in the phase localization of omiganan.

The behavior displayed in the peptide titrations (Fig. 3B) is consistent with the occurrence of saturation: for low membrane-

bound peptide-to-lipid ratios (P:L), which correspond to the rightmost part of the hyperbolic-like I vs. $[L]$ partition curves, the model of Santos et al. [30] is followed as I increases proportionally to $[P]$; however, with the increase of P:L the membrane will eventually run out of space and any further added peptide beyond saturation will have to remain in the aqueous phase; this is corroborated by the second slope being similar to that of the I vs. $[P]$ curve in the absence of lipid, i.e., after the saturation point the system behaves as if no lipid were present for the peptide to partition to.

The I vs. $[P]$ curve with $[L]=0.040$ mM has its saturation point close to $[P]\approx 7.7$ μM (Fig. 3B), which is precisely the peptide concentration that yields an I vs. $[L]$ curve with a deviation maximum close to 0.040 mM (Fig. 1C). In other words, the $[P]$ and $[L]$ values at the saturation point in Fig. 3B are the same than those at the end of the deviation in Fig. 1C, which is evidence for a correlation between deviations to partition curves and saturation.

To further extract information from the saturation phenomenon, a relationship between the $[P]$ and $[L]$ values at the saturation points was devised: at membrane-bound peptide concentrations below the saturation point it can be assumed that the partition is dictated by a Nernst formalism, like the one described by Santos et al. [30]. On the other hand, above the saturation threshold, the amount of peptide in the lipidic phase can be expected to be directly proportional to the total volume of the lipid phase, and thus proportional to the amount of the lipid itself. The bound peptide fraction above the saturation point ($X_{L,s}$) will be given by:

$$X_{L,s}=\frac{\sigma n_L}{n_p}=\frac{\sigma[L]}{[P]} \tag{3}$$

where σ is the P:L proportion in a saturated membrane and n_P and n_L are the total number of moles of peptide and phospholipid, respectively. At the saturation point it can be assumed that $X_{L,ns}=X_{L,s}$, $X_{L,ns}$ being the bound peptide fraction below the saturation point, and consequently:

$$X_{L,ns}=\frac{K_p\gamma_L[L]}{1+K_p\gamma_L[L]}=\frac{\sigma[L]}{[P]}=X_{L,s} \tag{4}$$

where $X_{L,ns}$ is defined as by Santos et al. [23]. This equation can be rearranged to

$$[P]=\frac{\sigma}{K_p\gamma_L}+\sigma[L] \tag{5}$$

which defines the total amount of peptide at which a saturation point occurs as a linear function of the amount of phospholipid in the system. Besides providing information on the magnitude of the partition constant, the non-zero intercept indicates that there is a minimum peptide concentration for saturation to occur, according to this model. A related equation has been used by Pott et al. [41] to define the relationship between the global peptide and phospholipid concentrations at several membrane-critical proportions of the toxin mellitin. Despite having been deduced from different starting points, Eq. (5) and the one used by Pott et al. [41] turn out to be equivalent, with the exception that Eq. (5) directly relates the intercept with the Nernst partition constant. Fig. 6 represents the saturation point ($[P]$,$[L]$) pairs for the POPG:POPC 4:1 and 2:1 systems. Eq. (5) was followed by both systems and the correlation between membrane saturation and the deviations to the partition curves was further corroborated because saturation pairs from partition curves taken at different peptide concentrations (Fig. 3A) were in agreement with the saturation pairs obtained from the I vs. $[P]$ curves (Fig. 3B). The obtained saturation P:L ratios were of 0.17 and 0.027 for the POPG:POPC 4:1 and 2:1 systems, respectively; this corresponds to 5.8 and 37.0 phospholipids per peptide at the saturation of each system.

Although the obtained saturation P:L ratios seem plausible and robust, the values for K_p have large associated errors since they are calculated from the reciprocal of a relatively small intercept, which makes this an unsuitable method for determination of very large partition constants.

4.4. Partition curve models

The initial deviations in the partition curves could be successfully attributed to membrane saturation; however, that explanation is not enough to account for the higher fluorescence intensities displayed by the saturated systems. In fact, saturation of the membrane implies that some peptide is being left out of bilayer interaction; as such, the system fluorescence intensity should decrease rather than increase. Simulated partition curves were obtained by setting the system parameters K_p, I_L/I_W and σ and taking X_L as the minimum between $X_{L,ns}$ and $X_{L,s}$ (Eq. (4)), i.e., during saturation, the amount of peptide in the membrane is limited by the saturated conditions, and afterwards by the Nernst equilibrium. The total fluorescence intensity was obtained by

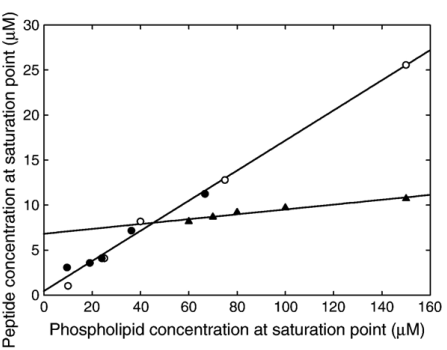

Fig. 6. Total peptide and phospholipid concentrations at saturation points for the 4:1 (● or ○) and 2:1 POPG:POPC (▲) systems, together with the respective fittings to Eq. (5) (solid lines). Saturation points were obtained from the partition curves at different peptide concentrations (Fig. 3A) (○), or from fluorescence vs. [omiganan] titrations (Fig. 3B) (●). The concordance between saturation points from fluorescence intensity vs. [omiganan] plots and from partition curves supports the relation between the deviations in the latter and membrane saturation. Obtained saturation proportions (P:L) were 0.17 for the 4:1 POPG:POPC system and 0.027 for the 2:1 POPG:POPC system; partition constants were 1.87×10^5 (but varying between 1.14×10^5 and 3.98×10^5 with the regression associated errors) and $(5.2\pm0.9)\times10^3$, respectively.

weighting I_L and I_W by X_L and $1-X_L$, respectively. These simulated curves show that the points of a partition curve that are under saturation describe a straight line below the non-saturated hyperbolic behavior (Fig. 7A). The straight initial regime is in agreement with what was observed for all systems containing anionic phospholipids, but the increase in fluorescence above the hyperbole needs further reasoning. Here we explore the simple hypothesis that, under saturation, omiganan undergoes some conformation/localization change that leads to an increase in its fluorescence quantum yield. A second set of simulated curves (Fig. 7B) were obtained by adding a fourth parameter to the system: the I_S/I_W ratio, where I_S stands for the limit fluorescence the system would display if all the peptide were in the hypothetical saturation conformation/localization. The fluorescence intensity of the system was calculated as in the previous simulations, with the exception that I_S was used in place of I_L whenever the system was saturated, i.e., $X_{L,s}<X_{L,ns}$. Simulated results under this hypothesis predict the occurrence of a discontinuity in the partition curve at the saturation point (Fig. 7B) and that increasing peptide concentrations will lead to decreasing slopes of the initial part of the curve, but constant hyperbolic portions. In addition, higher peptide concentrations should generate higher maxima before the discontinuity. All predicted characteristics were respected in partition curves taken at several peptide concentrations (Fig. 3A) except for the increase in the maxima and that sharp saturation/non-saturation transitions were only observed for low peptide concentrations. Constant post-deviation behaviors were observed, with similar resulting partition constants (average: $(2.38\pm0.78)\times10^4$) and I_L/I_W ratios (average: 1.93 ± 0.44), and, as mentioned earlier, the maxima of the deviations were successfully fit by Eq. (5) (Fig. 6). Even though this model may be too simplistic to fully describe the system behavior, it shows that saturation-related conformation/localization changes could be occurring in the membrane; these may include phenomena such as multi-merization [42], which could be involved in triggering the action of omiganan and thus represent the biophysical conditions behind its MICs against prokaryotes.

Another model was developed to deal with some limitations of the previous hypothesis, namely, the implicit, and unlikely, all-at-once conformation/localization changes undergone by the peptide at the saturation point, which lead to the discontinuity in the partition curves. In the new approach, these changes were modeled as a gradual solute saturation in the lipidic phase: for an increasing peptide concentration in the system, the peptide molecules will partition according to three different states, depicted in Figs. 7C and 8. States 1 and 3 correspond to the notions of, respectively, non-saturation and saturation. In state 2 an intermediate peptide concentration in the membrane is assumed: after the membrane-bound peptide reaches a critical concentration – correspondent to an apparent solubility product of the peptide in the lipidic phase – further interaction with the membrane requires that some peptide molecules adopt a saturated, more packed, conformation/localization, with fluorescence intensity I_S; the rest of the membrane-bound peptide remains at the concentration corresponding to the apparent solubility product. Only when all membrane-bound peptide molecules are arranged in that packed conformation does the membrane become fully saturated.

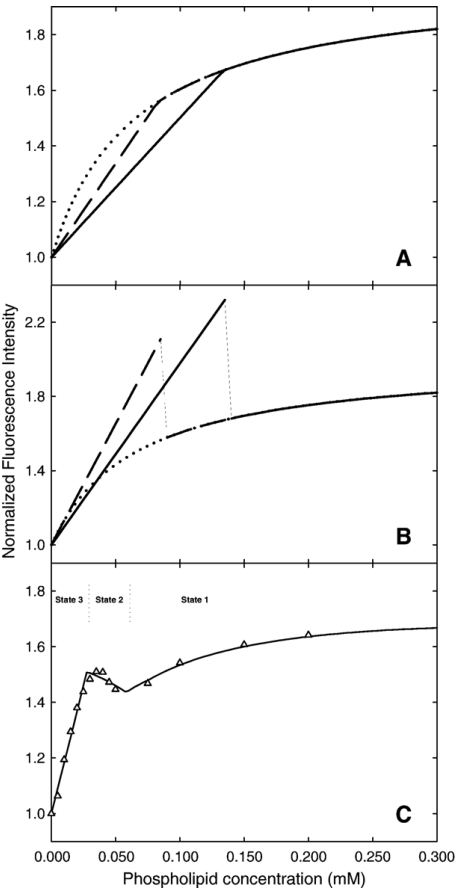

Fig. 7. (A and B) Simulated partition curves with the occurrence of saturation; the saturation points correspond to the end of the linear portions of each graph. Simulation parameters were: $\sigma=0.1$; $K_p=20000$; $I_W=1$; $I_L=2$; in B $I_S=3$ was used while in A no fluorescence change in I_L was associated with saturation (see the text for the meaning of each parameter). For the three curves in A and B 4 μM, 15 μM and 20 μM peptide concentrations were used (dotted, dashed and solid lines, respectively); the lowest of these concentrations was chosen to be below the saturation threshold (6.6 μM, under these conditions). Thinner line segments represent discontinuities. (C) Fitting of the three-state model to the 8.2 μM omiganan partition curve in 4:1 POPG:POPC; the dotted lines divide the fitted curve into the three states that were assumed (see text and appendix for a better description of each state and involved equations, respectively). It can be seen that the model is able to account for a transition between saturated and non-saturated states. Obtained system parameters were: $K_p=2.23\times10^4$; $\sigma=0.15$; solubility product=88.4 mM; $I_L/I_W=1.95$; $I_S/I_W=2.00$. K_p, σ and I_L/I_W values are in agreement with the ones determined by other methods.

The parameters of the new model are all homologous to the ones of the previous model, plus a fifth parameter, the apparent solubility product of the peptide. The equations that define the peptide proportions in each conformation (water dissolved,

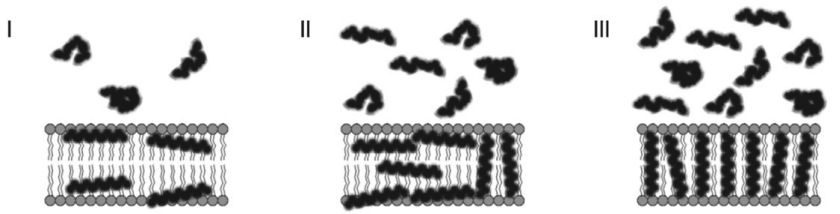

Fig. 8. Illustration of the three states of peptide–membrane interaction according to the three-state model. Notice that any depicted conformation or membrane localization of the peptide in this figure is merely illustrative (see text and appendix for a better description of each state and involved equations, respectively).

unsaturated-membrane-bound and saturated-membrane-bound; X_W, X_L, and X_S, respectively) are developed in the appendix.

This model was able to predict a transition between saturated and non-saturated membrane states (Fig. 7C), although the fitting of state 2 to the experimental data was not very good, namely due to the straight behavior of the modeled partition curve. The resulting K_p, σ and I_L/I_W values (2.23×10^4, 0.15 and 1.95, respectively) are in very close agreement with the values obtained by the other described method, which indicates that this model can be used for direct analysis of whole partition curves with saturation. The remaining two parameters, which have not been determined by other methods, should be interpreted with care since they depend largely on the few, and poorly fit, data points of state 2.

4.5. Membrane localization studies

The membrane localization of omiganan in each of the four biological model systems was probed using the lipophilic quenchers 5- and 16-NS. Time resolved fluorescence quenching data (not shown) were analyzed according to a method described by Fernandes et al. [43] which yielded two preferential peptide locations, depending on saturation: the peptide was found to be preferentially shallow into the bilayer in non-saturation conditions and very close to the membrane centre upon saturation. Because four Trp residues contribute to the global peptide fluorescence, the quenching data reflects an average localization of the central segment of the peptide.

The results obtained by differential quenching techniques are in agreement with a saturation-dependent peptide localization change. In addition, the internalization of the peptide seems a likely starting point for either membrane translocation or perturbation. In effect, the coordination of these data with the obtained different saturation proportions for the models of the inner and outer leaflets of the bacterial membrane indicates that there are membrane-bound peptide concentrations at which the outer leaflet is saturated – the peptide being internalized from the outer side of the membrane – while the inner leaflet is not – the peptide being pulled to the inner membrane surface; the saturation mediated internalization coupled to the different saturation proportions could thus represent a peptide translocation mechanism. While speculative, this hypothesis is a plausible illustration of the possible consequences of membrane saturation on the antimicrobial action of omiganan.

The dependence of the occurrence and intensity of the partition deviations on the anionic membrane charge can also be explained by the saturation-driven peptide internalization: when the system is not saturated, the peptide lies at the bilayer surface and, as mentioned, is exposed to a charged environment, resulting in a low I_L. Upon internalization, the Trp residues will be moved away from the charged phospholipid headgroups and exhibit greater quantum yields, translated in the proposed models as I_S, larger than I_L. Peptide internalization in neutral systems will not lead to such an intense increase in fluorescence because the shallow peptide was already exposed to a non-charged environment and $I_L \approx I_S$. Thus, partition curves of neutral systems behave like the modeled curves of Fig. 7A, whereas increasing anionic surface charge will induce partition curves like the ones modeled in Fig. 7B and C.

4.6. Partition, saturation and observed MICs

From a macroscopic point of view, the findings on omiganan–membrane interaction can be correlated to the MIC: at variance with [44], common MICs are not expected to be much greater than what is needed for saturation to occur. Indeed, under the hypothesized conditions by Tossi et al. [44] (phospholipid area = 0.7 nm^2; bacterium area = 10^7 nm^2; bacterial concentration = 10^6 bacteria/mL; MIC = 1 μM), one would have an overall lipid concentration accessible to the peptide of 47 nM (for the sake of simplicity, two phospholipid monolayers were assumed instead of an outer membrane model of one monolayer of lipopolysaccharide and another of phospholipid). According to Eq. (4) ($X_{L,ns}$ member), and assuming a typical partition constant of 2×10^4 [36,37], only 0.07% of the total peptide molecules are expected to be engaged in membrane interaction under these conditions. The aqueous phase peptide concentration will thus remain virtually unaltered and approximately equal to the total concentration. If we use the MIC as the total concentration, by the definition of K_p, the membrane-bound peptide concentration ($[P]_L$) will be given by K_p·MIC. With the hypothesized MIC of 1 μM, $[P]_L$ will be 20 mM. Multiplication by γ_L yields a P:L ratio of about 0.015 peptide molecules per lipid, or 66 lipid molecules per peptide, which is a far lower membrane concentration than the obtained by the calculations of Tossi et al. [44] (40 peptide molecules per phospholipid) where implicit infinitely high partition constants were used. The local membrane concentration of a peptide

predicted by these calculations is probably insufficient for saturation to occur, but by a narrow margin; this means that peptides with slightly higher K_p's or MICs may indeed be in saturation: in the previously hypothesized conditions, omiganan, which has a typical MIC_{50} of about 8 to 16 μM against *S. aureus* [2] and a K_p of 23.0×10^3 (Table 1), would have a local concentration in the membrane of 184 mM, correspondent to about 7 phospholipid molecules per peptide. This is clearly a saturation situation and is in close agreement with the obtained saturation proportions (Fig. 6). This relation between MIC and saturation supports the existence of possible saturation-triggered antimicrobial mechanisms not exclusive of omiganan but potentially shared by many other peptides with high enough K_p and MIC.

4.7. Omiganan induced leakage of vesicle contents

Lack of leakage is in agreement with previous studies [10] where the maximum observed effect of membrane perturbation was depolarization. Together with the high extents of partition towards the bilayer, the absence of severe membrane perturbation favors a translocation mediated peptide action, in agreement with the hypothesis from membrane saturation studies.

4.8. Peptidoglycan interaction study

The extent of interaction between omiganan and the bacterial cell wall was assessed by a method similar to the one used for the partition curves, with the difference that physical separation by centrifugation was used and the peptide was quantified in the supernatant only. This was needed because the peptidoglycan extracts exhibited intense, Trp characteristic, fluorescence – very likely from wall proteins that were not washed away during the extraction process – which prevented an integrated approach.

By comparing the fluorescence intensity of the peptide that remained on the supernatant (I) with the initial peptide fluorescence in the absence of added peptidoglycan (I_W), the aqueous phase fraction can be readily calculated:

$$I/I_W = X_W \tag{6}$$

X_W can be defined as $(1-X_p)$, where X_p is the peptide fraction that was held in the peptidoglycan. To relate X_p with the extent of peptidoglycan partition, it was considered that this interaction behaved similarly to a solute–resin interaction, like the ones involved in ion chromatography; the following relationship was then applicable, as described elsewhere [45]:

$$D_g = \frac{\frac{n_{Omg,PG}}{m_{PG}}}{[Omg]_W} \tag{7}$$

where D_g (in volume per mass units), also called the column constant, is a system parameter that, like K_p, dictates the peptide–peptidoglycan degree of interaction; $n_{Omg,PG}$ is the number of peptide molecules in the peptidoglycan mesh, m_{PG} is the mass of the mesh and $[Omg]_W$ is the water dissolved peptide concentration. D_g can be converted to a molar ratio (usually represented D_v) after multiplication by the fully hydrated peptidoglycan density (H_2O mass excluded) [45]. Obviously, the peptidoglycan is not a solvent; however, a spatial concentration of the peptide in the mesh can be considered. A reported value of 196.1 mg/mL for the *S. aureus* wall was used in this conversion [46]. However, due to possible peptidoglycan volume changes, D_v must be carefully used [46]; it is, nonetheless, a much more useful parameter than D_g since it has a more intuitive meaning and can be directly compared to K_p values.

Because X_p is given by the ratio of the peptidoglycan-bound peptide and the total amount of peptide, it can be defined as a function of D_g:

$$X_P = \frac{n_{Omg,PG}}{n_{Omg,PG}+n_{Omg,W}} = \frac{D_g\cdot C_{PG}}{1+D_g\cdot C_{PG}}, \tag{8}$$

where C_{PG} stands for the mass concentration of the peptidoglycan and $n_{Omg,W}$ for the moles of aqueous peptide. The fluorescence intensity is then given by:

$$I/I_W = X_W = (1-X_P) = \frac{1}{1+D_g\cdot C_{PG}}. \tag{9}$$

A good fit was obtained (Fig. 5) with $D_g = 15.9\pm1.1$ mL/mg ($D_v=(3.1\pm0.2)\times10^3$); which suggests that the omiganan molecules will be much more concentrated in the mesh than in the water. Despite this large partition towards the peptidoglycan, in a biological system the highest local peptide concentration will still be in the membrane ($K_p > D_v$), nevertheless, because peptidoglycan occupies a much larger volume than the bilayer does (typically, 20 to 80 nm thick in gram-positive bacteria [47], about 5 to 20 times the width of a bilayer) the relative difference of K_p over D_v (approximately 7 to 13 fold) is compensated for, and the absolute amount of peptide can be expected to be similar in both locations and possibly even greater in the cell wall. While these results could, at a first glance, lead to the conclusion that the cell wall is able to compete with the membrane for the antibiotic and possibly act as reservoir/trap that would reduce the peptide's efficiency, it must not be forgotten that, as mentioned earlier, both the membrane and the cell wall exist in minute concentrations under MIC assay conditions, which results in the wall and membrane-bound peptide fractions being negligible. Under these circumstances, both predicted aqueous phase and membrane bound peptide concentrations should remain the same in the presence or absence of the cell wall, defeating its role as a peptide trap. The observed thermodynamic impossibility for the wall to become such an ionic peptide trap is in agreement with the report that *S. aureus* adapt by incorporating D-alanine esters into the teichoic acid to lower the overall anionic charge of the wall as a means of repelling cationic antibiotics [48], rather than entrapping them. This does not invalidate the hypothesis that other components of the system, such as anionic species in solution, can be involved in peptide association and consequent reduction of membrane interaction [44], however, such components must be in a relatively large concentration for their influence to be significant; likewise, other membrane constituents, which are

usually in high local concentrations, may affect omiganan's partition.

It should also be noted that these findings refer to thermodynamic properties of the peptide–wall interaction; the ability, or lack thereof, of the peptidoglycan to restrict the diffusion of the peptide cannot be inferred from the used method.

Acknowledgements

Omiganan pentahydrochloride was a kind gift from MIGENIX Inc. (Vancouver, Canada). Fundação para a Ciência e Tecnologia (Portugal) is acknowledged for a grant to M. Melo (SFRH/BD/24778/2005).

Appendix

The three-state model is defined by the equation sets described below, where $X_{L,ns}$, $X_{L,s}$ and X_W represent the non-saturated membrane-bound, the saturated membrane-bound and the aqueous phase peptide fractions, respectively; $[P]$ and $[L]$ are the total peptide and lipid concentrations and $[L]_f$ is the free lipid concentration (not involved in saturation); The parameters K_p, σ and S are the Nernst partition constant, the saturation P:L ratio and the apparent solubility product of the peptide, respectively. The total fluorescence intensity I of the system is given by the weighted sum of the fluorescence contribution of each peptide population (I_W, I_L and I_S, for the aqueous phase, non-saturated membrane-bound and saturated membrane-bound populations, respectively): $I=X_W I_W+X_{L,ns}I_L+X_{L,s}I_S$.

State 1—Low overall peptide concentrations—Because the membrane-bound peptide concentration is insufficient to cause saturation, $X_{L,s}$ is zero and no lipid is occupied by saturated peptide molecules. The peptide fraction in the membrane is dictated by the partition constant, as in the $X_{L,ns}$ member of Eq. (4). The set of equations for this state is:

$$X_{L,s} = 0 \tag{A1}$$

$$X_W = 1 - X_{L,ns} \tag{A2}$$

$$X_{L,ns} = \frac{K_p \gamma_L [L]}{1 + K_p \gamma_L [L]} \tag{A3}$$

$$[L]_f = [L] \tag{A4}$$

State 2—Intermediate peptide concentrations—The peptide concentration in the membrane exceeds the threshold of the solubility product and two populations now coexist in the membrane: peptide in non-saturated and saturated conformations/localizations, the concentration of the former being constant and equal to the solubility product. Assuming, for simplicity that exchanges between membrane-bound and aqueous phase peptide concern only the non-saturated form and still follow the Nernst equilibrium it can be seen that that the aqueous phase peptide concentration should also be constant and equal to (S/K_p). Considering that the aqueous phase volume is approximately equal to the total system volume, X_W can be obtained as:

$$X_W = \frac{S}{K_p \cdot [P]} \tag{A5}$$

$X_{L,ns}$ can be obtained in a similar manner, but prior to division by $[P]$, the concentration of non-saturated membrane-bound peptide molecules over the total volume must be calculated; this can be done by multiplying S by the membrane volume and dividing by the total volume (note that the membrane volume concerns only the portion of the bilayer that is not saturated):

$$X_{L,ns} = \frac{S \cdot V_{L,f}}{V_{total}[P]} \tag{A6}$$

where $V_{L,f}$ is the non-saturated membrane volume and V_{total} is the total volume of the system. $V_{L,f}$ is given by $[L]_f \cdot V_{total} \cdot \gamma_L$, and thus

$$X_{L,ns} = \frac{S \cdot [L]_f \cdot \gamma_L}{[P]} \tag{A7}$$

$[L]_f$ can be calculated from the difference between the global phospholipid concentration and the concentration of saturation involved phospholipids. The latter is equal to $\frac{X_{L,s}[P]}{\sigma}$, and thus

$$[L]_f = [L] - \frac{X_{L,s}[P]}{\sigma} \tag{A8}$$

$X_{L,s}$ can be obtained by mass conservation:

$$X_{L,s} = 1 - X_W - X_{L,ns} \tag{A9}$$

However, with only this set of equations, $X_{L,ns}$ is recursively dependent on itself. Eqs. (A7), (A8) and (A9) can be combined to yield an independent definition of $X_{L,ns}$:

$$X_{L,ns} = \frac{S \cdot \gamma_L}{\sigma - S \cdot \gamma_L} \left(\frac{[L] \cdot \sigma}{[P]} + X_W - 1 \right) \tag{A10}$$

State 3—High overall peptide concentrations—The membrane becomes fully saturated with peptide. Only the aqueous phase and the saturated conformation/localization peptide populations coexist; the fraction of peptide in the membrane is given by the $X_{L,s}$ member of Eq. (4):

$$X_{L,s} = \frac{\sigma [L]}{[P]} \tag{A11}$$

$$X_W = 1 - X_{L,s} \tag{A12}$$

$$X_{L,ns} = 0 \tag{A13}$$

$$[L]_f = 0 \tag{A14}$$

The equations for each state were solved for a range of lipid concentrations and the parameters were fit to experimental data by a least squares method, based on the Solver add-in of Microsoft Excel 2003 (Microsoft, Seattle, WA).

References

[1] M.E. Selsted, M.J. Novotny, W.L. Morris, Y.Q. Tang, W. Smith, J.S. Cullor, Indolicidin, a novel bactericidal tridecapeptide amide from neutrophils, J. Biol. Chem. 267 (1992) 4292–4295.

[2] H.S. Sader, K.A. Fedler, R.P. Rennie, S. Stevens, R.N. Jones, Omiganan pentahydrochloride (MBI 226), a topical 12-amino-acid cationic peptide: spectrum of antimicrobial activity and measurements of bactericidal activity, Antimicrob. Agents Chemother. 48 (2004) 3112–3118.

[3] H.D. Friedland, D.D. Sharp, D.J. Erfle, E. Rubinchik, 43rd Interscience Conference on Antimicrobial Agents and Chemotherapy, Chicago, IL, 2003, p. F-1843.

[4] M.N. Melo, D. Dugourd, M.A. Castanho, Omiganan pentahydrochloride in the front line of clinical applications of antimicrobial peptides, Recent Pat. Anti Infect. Drug Discov. 1 (2006) 201–207.

[5] A. Rozek, C.L. Friedrich, R.E. Hancock, Structure of the bovine antimicrobial peptide indolicidin bound to dodecylphosphocholine and sodium dodecyl sulfate micelles, Biochemistry 39 (2000) 15765–15774.

[6] P.J. McNicol, E. Rubinchik, C. Pasetka, R. Baber, J. Lopez, H.D. Friedland, 41st Interscience Conference on Antimicrobial Agents and Chemotherapy, Chicago, IL, 2001.

[7] D.J. Hoban, E. Witwicki, G. Zhanel, L. Workman, J. Clement, H.D. Friedland, D. Dugourd, 43rd Interscience Conference on Antimicrobial Agents and Chemotherapy, Chicago, IL, 2003.

[8] C. Subbalakshmi, N. Sitaram, Mechanism of antimicrobial action of indolicidin, FEMS Microbiol. Lett. 160 (1998) 91–96.

[9] T.J. Falla, D.N. Karunaratne, R.E. Hancock, Mode of action of the antimicrobial peptide indolicidin, J. Biol. Chem. 271 (1996) 19298–19303.

[10] D. Dugourd, C. Pasetka, D. Erfle, E. Rubinchik, K. Lee, H.D. Friedland, P.J. McNicol, ASM General meeting, Salt Lake City, UT, 2002.

[11] A.J. Verkleij, R.F. Zwaal, B. Roelofsen, P. Comfurius, D. Kastelijn, L.L. van Deenen, The asymmetric distribution of phospholipids in the human red cell membrane. A combined study using phospholipases and freeze-etch electron microscopy, Biochim. Biophys. Acta 323 (1973) 178–193.

[12] M.T. Madigan, J.M. Martinko, J. Parker, Brock's biology of microorganisms, in: M.T. Madigan, J.M. Martinko, J. Parker (Eds.), 9th ed., Prentice Hall International, London, 2000.

[13] U.H. Durr, U.S. Sudheendra, A. Ramamoorthy, LL-37, the only human member of the cathelicidin family of antimicrobial peptides, Biochim. Biophys. Acta 1758 (2006) 1408–1425.

[14] S. Thennarasu, D.K. Lee, A. Tan, U. Prasad Kari, A. Ramamoorthy, Antimicrobial activity and membrane selective interactions of a synthetic lipopeptide MSI-843, Biochim. Biophys. Acta 1711 (2005) 49–58.

[15] A. Ramamoorthy, S. Thennarasu, D.K. Lee, A. Tan, L. Maloy, Solid-state NMR investigation of the membrane-disrupting mechanism of antimicrobial peptides MSI-78 and MSI-594 derived from magainin 2 and melittin, Biophys. J. 91 (2006) 206–216.

[16] A. Ramamoorthy, S. Thennarasu, A. Tan, K. Gottipati, S. Sreekumar, D. L. Heyl, F.Y. An, C.E. Shelburne, Deletion of all cysteines in tachyplesin I abolishes hemolytic activity and retains antimicrobial activity and lipopolysaccharide selective binding, Biochemistry 45 (2006) 6529–6540.

[17] V. Dhople, A. Krukemeyer, A. Ramamoorthy, The human beta-defensin-3, an antibacterial peptide with multiple biological functions, Biochim. Biophys. Acta 1758 (2006) 1499–1512.

[18] B.A. Dmitriev, F.V. Toukach, K.J. Schaper, O. Holst, E.T. Rietschel, S. Ehlers, Tertiary structure of bacterial murein: the scaffold model, J. Bacteriol. 185 (2003) 3458–3468.

[19] B.A. Dmitriev, F.V. Toukach, O. Holst, E.T. Rietschel, S. Ehlers, Tertiary structure of *Staphylococcus aureus* cell wall murein, J. Bacteriol. 186 (2004) 7141–7148.

[20] W. Vollmer, J.V. Holtje, The architecture of the murein (peptidoglycan) in gram-negative bacteria: vertical scaffold or horizontal layer(s)? J. Bacteriol. 186 (2004) 5978–5987.

[21] P. Demchick, A.L. Koch, The permeability of the wall fabric of *Escherichia coli* and *Bacillus subtilis*, J. Bacteriol. 178 (1996) 768–773.

[22] A.J. Dijkstra, W. Keck, Peptidoglycan as a barrier to transenvelope transport, J. Bacteriol. 178 (1996) 5555–5562.

[23] N.C. Santos, M.A. Castanho, Fluorescence spectroscopy methodologies on the study of proteins and peptides. On the 150th anniversary of protein fluorescence, Trends Appl. Spectrosc. 4 (2002) 113–125.

[24] L.M. Loura, A. Fedorov, M. Prieto, Resonance energy transfer in a model system of membranes: application to gel and liquid crystalline phases, Biophys. J. 71 (1996) 1823–1836.

[25] L.D. Mayer, M.J. Hope, P.R. Cullis, Vesicles of variable sizes produced by a rapid extrusion procedure, Biochim. Biophys. Acta 858 (1986) 161–168.

[26] D.B. Chalpin, A.M. Kleinfeld, Interaction of fluorescence quenchers with the n-(9-anthroyloxy) fatty acid membrane probes, Biochim. Biophys. Acta 731 (1983) 465–474.

[27] G.D. Fasman, 3rd ed., Handbook of Biochemistry and Molecular Biology: Proteins, vol. 1, CRC Press, Cleveland, OH, 1976.

[28] S.S. Lehrer, Solute perturbation of protein fluorescence. The quenching of the tryptophyl fluorescence of model compounds and of lysozyme by iodide ion, Biochemistry 10 (1971) 3254–3263.

[29] F. Moro, F.M. Goni, M.A. Urbaneja, Fluorescence quenching at interfaces and the permeation of acrylamide and iodide across phospholipid bilayers, FEBS Lett. 330 (1993) 129–132.

[30] N.C. Santos, M. Prieto, M.A. Castanho, Quantifying molecular partition into model systems of biomembranes: an emphasis on optical spectroscopic methods, Biochim. Biophys. Acta 1612 (2003) 123–135.

[31] S.W. Chiu, E. Jakobsson, S. Subramaniam, H.L. Scott, Combined Monte Carlo and molecular dynamics simulation of fully hydrated dioleyl and palmitoyl-oleyl phosphatidylcholine lipid bilayers, Biophys. J. 77 (1999) 2462–2469.

[32] J.F. Nagle, M.C. Wiener, Structure of fully hydrated bilayer dispersions, Biochim. Biophys. Acta 942 (1988) 1–10.

[33] M.A. Castanho, M.X. Fernandes, Lipid membrane-induced optimization for ligand–receptor docking: recent tools and insights for the "membrane catalysis" model, Eur. Biophys. J. 35 (2006) 92–103.

[34] S.T. Henriques, M.A. Castanho, Environmental factors that enhance the action of the cell penetrating peptide pep-1 A spectroscopic study using lipidic vesicles, Biochim. Biophys. Acta 1669 (2005) 75–86.

[35] A.S. Ladokhin, M.E. Selsted, S.H. White, Bilayer interactions of indolicidin, a small antimicrobial peptide rich in tryptophan, proline, and basic amino acids, Biophys. J. 72 (1997) 794–805.

[36] N. Rochel, J.A. Cowan, Dependence of the lytic activity of the N-terminal domain of human perforin on membrane lipid composition—Implications for T-cell self-preservation, Eur. J. Biochem. 249 (1997) 223–231.

[37] H. Heerklotz, J. Seelig, Detergent-like action of the antibiotic peptide surfactin on lipid membranes, Biophys. J. 81 (2001) 1547–1554.

[38] R.F. Epand, A. Ramamoorthy, R.M. Epand, Membrane lipid composition and the interaction of pardaxin: the role of cholesterol, Protein Pept. Lett. 13 (2006) 1–5.

[39] F. Porcelli, B. Buck, D.K. Lee, K.J. Hallock, A. Ramamoorthy, G. Veglia, Structure and orientation of pardaxin determined by NMR experiments in model membranes, J. Biol. Chem. 279 (2004) 45815–45823.

[40] R.F. de Almeida, A. Fedorov, M. Prieto, Sphingomyelin/phosphatidylcholine/cholesterol phase diagram: boundaries and composition of lipid rafts, Biophys. J. 85 (2003) 2406–2416.

[41] T. Pott, M. Paternostre, E.J. Dufourc, A comparative study of the action of melittin on sphingomyelin and phosphatidylcholine bilayers, Eur. Biophys. J. 27 (1998) 237–245.

[42] F. Porcelli, B.A. Buck-Koehntop, S. Thennarasu, A. Ramamoorthy, G. Veglia, Structures of the dimeric and monomeric variants of magainin antimicrobial peptides (MSI-78 and MSI-594) in micelles and bilayers, determined by NMR spectroscopy, Biochemistry 45 (2006) 5793–5799.

[43] M.X. Fernandes, J. Garcia de la Torre, M.A. Castanho, Joint determination by Brownian dynamics and fluorescence quenching of the in-depth location profile of biomolecules in membranes, Anal. Biochem. 307 (2002) 1–12.

[44] A. Tossi, L. Sandri, A. Giangaspero, Amphipathic, alpha-helical antimicrobial peptides, Biopolymers 55 (2000) 4–30.

[45] D.T. Gjerde, J.S. Fritz, Ion Chromatography, 2nd ed.Alfred Hüthig Verlag, Heidelberg, 1987.
[46] L.T. Ou, R.E. Marquis, Electromechanical interactions in cell walls of gram-positive cocci, J. Bacteriol. 101 (1970) 92–101.
[47] M.T. Cabeen, C. Jacobs-Wagner, Bacterial cell shape, Nat. Rev., Microbiol. 3 (2005) 601–610.
[48] A. Peschel, M. Otto, R.W. Jack, H. Kalbacher, G. Jung, F. Gotz, Inactivation of the dlt operon in *Staphylococcus aureus* confers sensitivity to defensins, protegrins, and other antimicrobial peptides, J. Biol. Chem. 274 (1999) 8405–8410.
[49] J.R. Wardlaw, W.H. Sawyer, K.P. Ghiggino, Vertical fluctuations of phospholipid acyl chains in bilayers, FEBS Lett. 223 (1987) 20–24.

3. BP100

Two years into my PhD project, and after having done most of the work with omiganan that would be published as Article III, I started working with the peptide BP100. This addition to my project resulted from a collaboration Miguel started with the group of Eduard Bardají, from the University of Gerona. BP100 had been designed by Eduard's group shortly before the beginning of our collaboration and its primary development was being targeted at fighting crop diseases caused by Gram-negative bacteria. The partnership was profitable for both groups: the people in Gerona were essentially dedicated to synthesis and benefitted from the insights our methodologies could provide on peptide action, in turn, we benefitted from what they did best, which was to design and produce peptides. The symbiosis was extended beyond the mere exchange of information or peptides: Rafael Ferre, the PhD student that synthesized BP100, visited our lab to perform part of the work with the peptide; shortly after, Marta Ribeiro, a biochemist that had by then started her PhD in our group, would visit Gerona to receive training in the synthesis of the analgesic peptide she is studying.

3.1 Genesis of BP100

BP100 can be thought of as a fourth generation AMP: it results from the modification of a peptide, called Pep3, itself a shorter version of another peptide, termed CA(1-7)M(2-9), in turn designed from naturally occurring templates.

CA(1-7)M(2-9) was first synthesized in the early 90's as the result of a strategy to shorten naturally occurring peptides for use as drugs.[36] Briefly,

a segment of the bee-venom AMP mellitin was appended to a segment of the moth AMP cecropin A in order to broaden the latter's spectrum while reducing the former's cytotoxicity (the designation CA(1-7)M(2-9) reflects the chimeric origin of the peptide: the first seven residues of cecropin A followed by the second through the ninth residues of melittin; its actual sequence is KWKLFKKIGAVLKVL–NH_2, also C-terminally amidated like most AMPs). The shortening of active peptides is an important objective mainly because the synthesis of long sequences — and the 38 amino-acid-long sequence of cecropin A can be considered *very* long — is unfeasibly expensive in a pharmaceutical mass production context.[36,37] Pep3 was designed some years after CA(1-7)M(2-9), its sequence, WKLFKKILKVL–NH_2, resulting from further shortening.[38] Overall, the size reduction strategy can be considered to have been successful as both CA(1-7)M(2-9) and Pep3 possess good activities against fungi and Gram-negatives[36,38] (although only a slightly modified version of CA(1-7)M(2-9) has been tested for fungicidal activity). There was, nonetheless, a tradeoff in the process of obtaining manageable sequence lengths: the two peptides are still outperformed by cecropin A — against Gram-negatives — and melittin — against Gram-positives.

BP100 was synthesized as part of a library of Pep3 analogs. The objective behind the design of this library was no longer to obtain shorter sequences, but to improve the activity of the parent peptide against Gram-negatives. However, unlike a random combinatorial chemistry approach, the elements of this library are not the result of just any changes to the sequence of Pep3. Instead, a very elegant — and successful — process to enhance Pep3's activity by targeting specific amino acid positions was devised. It had already been remarked that upon the adoption of an α-helix structure the charged and the apolar residues of Pep3 segregated along the helix's diameter[38]; this is evident in the the Edmunson's projection of the Pep3's α-helix (Figure 3.1). It is widely accepted that this feature, common in α-helical AMPs, stabilizes the parallel adsorption and burying of peptides into membranes by simultaneously allowing the charged and apolar residues to interact with the phospholipids' headgroups and acyl chains, respectively.[5,39] Focus was put on modifying the residues that lie on

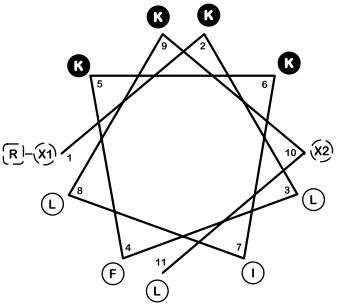

Figure 3.1 – Edmunson wheel projection of the α-helical template for the library of Pep3 analogs. Cationic residues are shown in a full circle and apolar residues in an empty one; positions that were scanned are labeled X1 and X2, in dashed circles; the N-terminal modification is denoted R in a dashed square (for Pep3 X1=W and X2=V; for BP100 X1=K and X2=Y; none of the peptides was N-terminally modified). When bound to membranes, Pep3 is expected to adopt an α-helical conformation, parallel to the bilayer, with approximately diametral separation of cationic and hydrophobic residues. Adapted from Article IV

the interface between the charged and the apolar patches of the helix, as these were more likely to influence its insertion properties. The relevant residues can be clearly seen, from Figure 3.1, to be those at postitions 1 and 10. Rafael constructed the library by scanning these positions with different amino acids. In addition, because the N-terminal residue was one of the target positions, several types of N-terminal substitution were also performed.[40–42]

BP100 was selected from the library for displaying the best compromise between hemolysis and antibacterial activity against a panel of Gram-negative plant pathogens. In its sequence, relatively to Pep3, W1 was replaced by a lysine residue and V10 by a tyrosine one; the N-terminus was not derivatized (final sequence: KKLFKKILKYL–NH_2). BP100 improves significantly on the activity of Pep3 against these Gram-negatives but it is still somewhat weaker than the full-length cecropin A.[41] Yet, its creation does demonstrate the possibility of successfully using naturally occurring peptides to design new AMPs — in this particular case better suited for mass production.

3.2 First results

The study of BP100 began, much in the same way as with omiganan, by the construction of partition curves towards several systems. This time the observed fluorescence was emitted by the tyrosine residue in position 10 as no tryptophans were present in the sequence. Fortunately, BP100 was one of the peptides in the library in which such a fluorescence residue had been substituted in; otherwise, work would have had to be carried out using the much fainter phenylalanine fluorescence of position 4. Also fortunately, the fact that tyrosine has a lower quantum yield than tryptophan did not mean data acquisition was harder with BP100 than with omiganan: in general, results were much less prone to artifacts with the single tyrosine of BP100 than with the four tryptophans of omiganan, and this is one of the reasons why I later focused almost exclusively on BP100 for testing new methods.

Having observed saturation with omiganan I paid particular attention to the occurrence of similar events with BP100. And occur they did! As with omiganan, anionic membrane models caused partition curves to spike at low lipid concentrations. This observation corresponded to some of the predictions we had made about AMP action and saturation, which was very exciting (findings on BP100 are presented in Article IV, included at the end of the chapter). But at the same time I was a bit apprehensive about the similarities with the case of omiganan, afraid that such a coincidence could be the result of some kind of experimenter error.

Before any further characterization of the deviations in the BP100 partition curves — even before an unequivocal assignment to saturation — I travelled to Brazil for a six months' collaboration at the Federal University of Rio de Janeiro (briefly described in Chapter 'Other work'). During this meantime Rafael Ferre came to Lisbon to learn our methodologies and picked up the studies on BP100 where I had left, having the previous work done with omiganan as a reference. Across the ocean I was very glad, and relieved, when I heard that he obtained partition curves with deviations just like mine, and also that he was able to successfully apply to BP100 the method I had developed to identify the saturation points of

omiganan. To top it off, the results were consistent with our hypothesis of an activity triggered at high peptide concentrations; and this with an AMP with sequence and origin completely distinct from those of omiganan. Our confidence on a model of interaction applicable to more than a handful of AMPs was growing stronger.

3.3 More on saturation

As Rafael would only return to Gerona a couple of months after I came back from Rio, I got the chance to team up with him for that part of the work — it is thus in all fairness that we share the first authorship of Article IV. In the process I made a good friend and got to learn Spanish! Like I stated earlier this collaboration extended far past the mere exchange of scientific knowledge, and I hope to have many such partnerships in the future.

While I was in Brazil, Rafael carried out with BP100 most of the methodologies that had been adapted to study saturation with omiganan. Upon my return, with that batch of work out of the way, we were able to focus on new approaches to understand the saturation phenomenon and to try to verify its link to antibacterial activity. Rafael made an important breakthrough when he remarked that vesicle suspensions seemed to get more turbid under saturation conditions: following this lead we were able to correlate the occurrence of saturation with a sudden increase of the optical density (OD) of the suspensions, which I could later ascertain to be due to vesicle aggregation (or disintegration followed by phospholipid aggregation). And before Rafael left we were still able to correlate saturation with an increase in BP100-induced vesicle leakage.

* * *

During the second year of my work with BP100 the whole team moved to the Institute of Molecular Medicine (IMM) at the medical school of the University of Lisbon — a mere half-mile from our lab at the Faculty of Sciences. At the IMM we formed the Physical Biochemistry Unit.

The move followed Miguel's taking over the chair of Biochemistry at the Faculty of Medicine and allowed us to come in contact with a much larger and more biology-oriented research environment. This would significantly influence my work, especially in the later stages of the studies with BP100. Immediate plans, however, were maintained.

This was a very productive period. I had become very motivated as I was decidedly exploring uncharted territories of AMP science: membrane saturation had been proposed before, but only for non-peptide anti-inflammatory drugs[43] (incidentally, by the group of Margarida Bastos, a biophysicist that also studies AMPs and with whom I had very enriching exchanges of ideas over these years). And I wasn't just exploring the possibility of the occurrence of saturation, I was actually finding very convincing evidence that this would be the membrane-level threshold corresponding to the MIC with bacteria.

More than supporting a mechanism of AMP action these ideas bridged the gap between biophysical concepts and macroscopic events at the cell level. This is a very important aspect in a biophysical context, where one is always in danger of losing contact with physiological meaning when dealing with model versions of reality. At the same time, a quantitative perspective is brought to the processes underlying the biological event of bacterial killing by AMPs. A full chapter in Part II is devoted to exploring the consequences of the convergence in this point of the molecular- and cellular-level interpretations of AMP action.

Although the concept I proposed was new to the field of AMPs, it was not at all incompatible with existing views: most of the proposed disruption models implicitly assumed, in one way or another, the crossing of a threshold (see Figure 1.1 and references therein). The carpet model, which postulates that a given degree of membrane coverage is required for activity to be triggered, is particularly close to my hypothesis. This would be remarked by the very proponent of the model, Yechiel Shai, as he saw my results when we met at the 30th European Peptide Symposium in Helsinki.

* * *

Subsequent work with BP100 involved mostly the creation or the adaptation of methods to better characterize its interaction with membranes. Dynamic light-scattering methods were very important at this stage and I am indebted to Marco Domingues, from the Biomembranes Unit at the IMM, for having assisted me with this technique in which I had no practice. Using light-scattering I was able to confirm that the sudden increase in OD at saturation corresponded to vesicle aggregation. The same technique also allowed the determination of the surface charge of vesicles (as the ζ-potential — technical details in Section 4.3) upon BP100 binding. Initial characterization had pointed to very high peptide-to-lipid (P/L) ratios at saturation (1 : 5.9 for omiganan and 1 : 8.4 for BP100); interestingly, those values were consistent with a balance in the membrane between the peptides' and the phospholipids' charges. Indeed, ζ-potential measurements indicated a neutralization of membrane charge at saturation and were a very welcome confirmation of that prediction (see Article IV).

It was also at this stage that I managed to successfully create and employ a method to detect peptide translocation into the vesicular lumen, an objective that I had pursued since the study of omiganan (BP100 did translocate, irrespectively of the membrane-bound concentration, which was an expected behavior given the peptide's leakage- and aggregation-inducing properties). I also perfected the method used for measuring the depth of peptide insertion in the membrane and even started outsourcing it to other group members. Unlike omiganan, no movement of BP100 was observed upon saturation; rather, the peptide's tyrosine residue — the reporter in this method — seems to sit at a constant depth. In spite of their significance regarding the action of the peptide, these weren't exactly thrilling results, but for me, as had happened with the advanced studies of omiganan, the excitement was in the development of the methodologies.

3.4 Karlsruhe

In 2007, following the 2nd Workshop on the Biophysics of Membrane-Active Peptides — which our group co-organized — Miguel started a prospective collaboration with the group of Anne Ulrich, from the

University of Karlsruhe, Germany. The collaboration would become effective shortly after, when a joint application won a grant created to promote scientific interchange between both countries.

The planned work consisted chiefly in applying nuclear magnetic resonance (NMR) and circular dichroism (CD) methodologies developed in Karlsruhe to gain structural insight on the interaction of BP100 with membranes. As one of the methods relied on the use of ^{19}F-NMR, fluorinated analogs of BP100 had to be synthesized, which involved the replacement of some residues with a fluorine-containing amino acid probe developed in Karlsruhe.[44] Synthesis was carried out by Christian Mink, who was then a PhD student at the Ulrich group, and with whom I would team up in this collaboration.

The first part of the work, important though not very informative on BP100 action, was devoted to validating the use of the analogs: activity tests were performed in Karlsruhe and in Gerona (all the analogs displayed activities close to those of BP100, with MICs within 5 μM), and Christian came to Lisbon to test if the fluorinated peptides behaved similarly to the native BP100 under our biophysical methodologies. Five analogs had been synthesized, and these were simply too many to allow individual in-depth partition and saturation studies: we settled on obtaining the partition curves for each peptide in zwitterionic (POPC) and anionic (2 : 1 POPG : POPC) vesicles and checking for similar partition behavior and the occurrence of saturation-dependent deviations. Remarkably, all the analogs displayed deviations at roughly the same conditions and the partitions could be seen to lie in the same order of magnitude — although only in some cases was there an almost perfect superposition of results (see Figure 3.2). It was important that the analogs displayed saturation-dependent effects, and I was hopeful that we would arrive at the structural characterization of such phenomena. So far, studies of the fluorinated analogs had green light.

My turn to travel to Karlsruhe would come a few months after Christian's visit. There, I found that most of the group's effort was focused on the application of two powerful techniques to extract information on peptide membrane interactions: solid-state ^{19}F-NMR,[45] and CD of

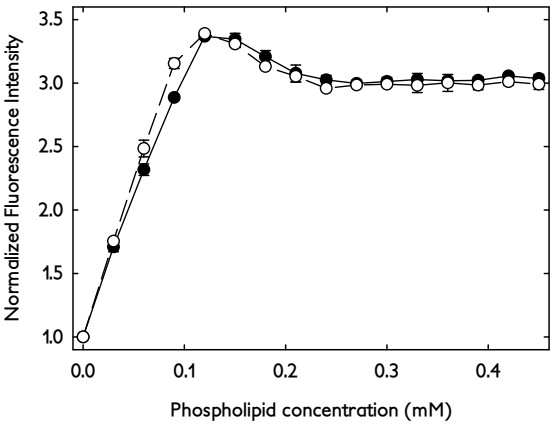

Figure 3.2 – Partition curves of native BP100 (full symbols) and of the analog fluorinated at position 11 (empty symbols) with 2 : 1 POPG : POPC vesicles (unpublished). The fluorinated analog reproduces faithfully the behavior of the native BP100, including the saturation-dependent deviation.

oriented* phospholipid bilayers[46] (this type of CD will be denoted OCD — oriented circular dichroism). In my opinion however, it was the chance to use the more common solution CD that yielded the most interesting results of my stay. Before any description of results I must acknowledge Christian's contribution to the work: not only did he synthesize the peptides, he also carried out practically all the NMR and a large part of the OCD measurements — while in Karlsruhe I became able to perform sample preparation and CD and OCD experiments independently, but much more time is necessary before I would get properly acquainted with NMR acquisition.

From NMR and OCD data the peptide was found to lie mostly parallel to the membrane surface. However, none of these techniques was able to see past the saturation threshold because, as could have been predicted from previous results, the peptide got disruptive by then and disintegrated our carefully crafted oriented bilayers. In turn, solution CD — employed mainly to make sure the peptide indeed assumed an

*Oriented bilayers are obtained by allowing phospholipids to assemble in a flat surface, usually by solvent (aqueous or organic) evaporation. Resulting bilayers stack parallel to the surface.

α-helical structure when bound to membranes (knowledge of the bound structure is a prerequisite of the NMR method) — is not affected by loss of anisotropic membrane integrity. By using it to characterize the BP100-vesicle interaction I was able to identify a second membrane-bound peptide structure/aggregation state that showed up precisely along saturation! (Figure 3.3) This was a very important observation: up to that point the existence of an alternate structure or aggregation state had been a postulate required to conciliate saturation with fluorescence data but this assumption had only been supported, very indirectly, from the observation of omiganan's internalization (see Section 2.3, and Section 'Differential quenching' in the Appendix). I must here thank the precious help I received from Jochen Bürck, the CD expert at Karlsruhe: he spent quite some time teaching me the theoretical and practical bases of CD spectroscopy, which allowed me to design my own procedures and eventually make that important find.

The precise structural characteristics of the saturation conformer of BP100 are still unknown: its CD spectrum always overlaps with either the random coil features the peptide displays when in the aqueous phase, or the α-helix spectrum when membrane-bound and out of saturation. Tentative deconvolutions[47,48] indicate the presence of β-turns together with β-strands; from these results I am inclined to imagine the formation of some sort of aggregates, since it is not likely that an eleven-amino-acid peptide has enough length to consistently fold into a β-strand. (Now that the existence of this elusive intermediate has been ascertained, and after my stay in Rio, I believe solution NMR would be the tool of choice to accurately characterize it.) Still, irrespectively of the actual structure of the intermediate, a major reorganization has been shown occur at, or close to, saturation, and this is strong evidence supporting a link between this molecular-level threshold and an activity-triggering mechanism.

3.5 Stepping into biological studies

While at the IMM, my work shifted from the lifeless *in vitro* models I had used so far towards experiments closer to *in vivo* situations. Ana

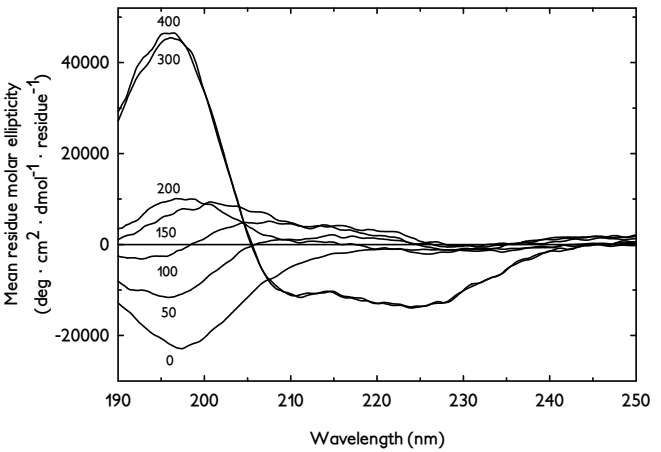

Figure 3.3 – CD spectra of 13.4 μM BP100 with increasing concentrations of 2 : 1 POPG : POPC, indicated in micromolar units next to each trace (unpublished). The spectra at zero and maximum lipid concentrations are typical of random coil and α-helical, structures, respectively, but intermediate spectra (from 50 to 200 μM of lipid) display features that cannot be ascribed to a linear combination of the first two, namely, a positive elipticity in the 208 – 215 nm region.

Correia, the biologist that joined the group upon our arrival at the IMM, partnered with me in these studies, the first being to gauge the cytotoxicity of the peptide against more complex eukaryotic models — hemolysis had already been tested in Gerona as part of the peptide selection process. The fact that the peptide was about five-fold more active against our cells than erythrocytes raised some questions, and a corresponding number of hypotheses. The description of our findings and of the mishaps that, unfortunately, prevented a successful approach can be found in Chapter 'Unfinished business'.

In subsequent studies focus was put on using live bacteria to verify our hypotheses of AMP action: no matter how well our models on membrane saturation and possible subsequent neutralization fit available data, if the predicted phenomena are not actually observed *in vivo* those will never be more than interesting theoretical possibilities. This time, work with

live cells would prove not to be as hard as the first attempt had led me to believe.

Once again, being at the IMM facilitated the transition to biological experiments: both Catarina Laborinho and Isa Serrano, a lab technician and a post-doc that joined the group during my third PhD year, had an extensive background in microbiology and provided important input on the implementation of experiments with bacteria. But it has been Carla Alves, the visiting PhD student from the University of Madeira, that has contributed the most by carrying out a great part of the experimental execution, especially since I started dedicating most of my time to writing this book. Were it not for her, all the following description would have had to be relegated to the 'Unfinished business' chapter.

Carla and I were able to successfully implement the MIC assay protocol used in Gerona and gauged the MIC of BP100 against *Escherichia coli* to be between 2 and 4 μM. This is not only in the same range that had been obtained in Gerona against other Gram-negatives,[41] but also in good agreement with as of yet unpublished tests carried out by colleagues of Christian's in Karlsruhe also against *E. coli*. *Staphylococcus aureus* were remarkably unsusceptible to the antibiotic — a likely consequence of a significant overlap between the sequence of BP100 with that of cecropin A, itself inactive against Gram-positives[36] (melittin does perform well against Gram-positives[36] but after all the shortening and optimization steps in the design of BP100 the two sequences have only weak resemblances).

Having established a consistent system for working with *E. coli*, we proceeded to testing the hypothesis of the co-occurrence of bacterial membrane surface neutralization and death. Using an adaptation of the light scattering method used to measure vesicles' ζ-potential very exciting results were obtained: the ζ-potential of *E. coli* was observed to increase from −20 mV in the absence of peptide, to close to zero at a BP100 concentration equal to the MIC (Figure 3.4). While this does not imply the existence of a neutralization-mediated killing mechanism it does confirm our prediction that neutralization should occur close to the MIC. In turn, this supports our hypothesis that bacterial surfaces are indeed saturated at the MIC. And even if the ζ-potential reflects only the bacterial surface

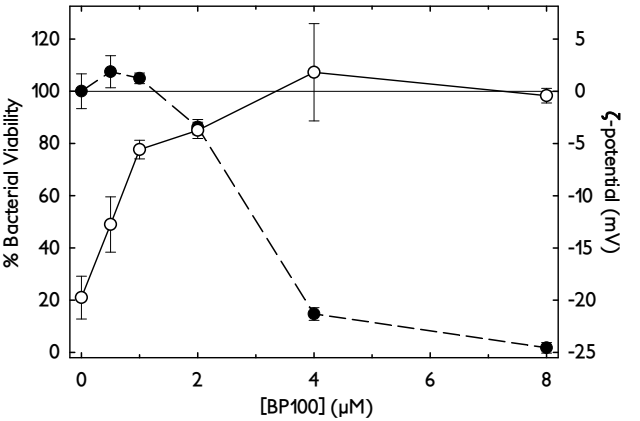

Figure 3.4 – Bacterial viability (full symbols) and ζ-potential (empty symbols) of *E. coli* after exposure to different concentrations of BP100 (unpublished). Bacteria lose viability over the same peptide concentration range that causes the neutralization of their surface charge.

charge of *E. coli* — and not that of any inner structure such as the plasma membrane — a neutralization of the also anionic outer membrane can still be inferred, showing that peptide molecules do indeed reach very high concentrations when bound to bacterial membranes.

Following the success of the ζ-potential measurements, the test of the saturation hypothesis was the logical path to follow (actually, it was even more logical to have started the *in vivo* experiments by testing this hypothesis but the experimental setup for the ζ-potential determination was much simpler to design and execute). However, though Carla and I put a great effort into it, we could not get conclusive results due to a number of methodological limitations (both the used method and its shortcomings are described in Chapter 'Unfinished business'). These were the last experiments I performed with BP100, or with anything else for that matter, before starting writing full-time.

ARTICLE IV

Synergistic Effects of the Membrane Actions of Cecropin-Melittin Antimicrobial Hybrid Peptide BP100

Rafael Ferre,[†] Manuel N. Melo,[‡] Ana D. Correia,[‡] Lidia Feliu,[†] Eduard Bardají,[†] Marta Planas,[†] and Miguel Castanho[‡*]

[†]Laboratori d'Innovació en Processos i Productes de Síntesi Orgànica, Departament de Química, Universitat de Girona, Girona, Spain; and [‡]Instituto de Medicina Molecular, Faculdade de Medicina, Universidade de Lisboa, Lisbon, Portugal

ABSTRACT BP100 (KKLFKKILKYL-NH_2) is a short cecropin A-melittin hybrid peptide, obtained through a combinatorial chemistry approach, which is highly effective in inhibiting both the in vitro and in vivo growth of economically important plant pathogenic Gram-negatives. The intrinsic Tyr fluorescence of BP100 was taken advantage of to study the peptide's binding affinity and damaging effect on phospholipid bilayers modeling the bacterial and mammalian cytoplasmic membranes. In vitro cytotoxic effects of this peptide were also studied on mammalian fibroblast cells. Results show a stronger selectivity of BP100 toward anionic bacterial membrane models as indicated by the high obtained partition constants, one order of magnitude greater than for the neutral mammalian membrane models. For the anionic systems, membrane saturation was observed at high peptide/lipid ratios and found to be related with BP100-induced vesicle permeabilization, membrane electroneutrality, and vesicle aggregation. Occurrence of BP100 translocation was unequivocally detected at both high and low peptide/lipid ratios using a novel and extremely simple method. Moreover, cytotoxicity against mammalian models was reached at a concentration considerably higher than the minimum inhibitory concentration. Our findings unravel the relationships among the closely coupled processes of charge neutralization, permeabilization, and translocation in the mechanism of action of antimicrobial peptides.

INTRODUCTION

Antimicrobial peptides (AMPs) form an essential part of the innate immune system of virtually all forms of life (1–7). During the last decades, AMPs have been widely studied, as they may become an alternative to conventional antibiotics, especially for the treatment of drug-resistant infections (8, 9). Hundreds of AMPs have been isolated (see a comprehensive list at http://www.bbcm.univ.trieste.it/~tossi/pag1.htm) and several thousands have been de novo designed and synthetically produced. They display a wide range of biological activities against bacteria, fungi, protozoa, enveloped viruses, and even tumor cells (9–14). Interestingly, they retain activity against antibiotic-resistant strains and do not readily elicit resistance (15–17).

Despite displaying extensive sequence heterogeneity, most AMPs share two functionally important features: a net positive charge and the ability to assume an amphipathic structure. These structural characteristics are essential for the mode of action of most AMPs, which target the microbial membrane. The net positive charge promotes their binding to the anionic microbial surface, while the amphipathic structure favors peptide insertion into the membrane (10–12,15,16,18–20). Despite extensive studies, the precise mechanism of peptide-membrane interaction and cell killing has not been firmly established for many AMPs. Several models have been proposed to account for the morphological changes involved in AMPs-mediated membrane disruption, such as pore formation (21), cell lysis (22), or peptide translocation into the cytoplasm (23). Recently, some studies have shown that, apart from membrane damage, other mechanisms may be involved including intracellular targets (9,15,16). However, in such mechanisms, peptides still must traverse the cell membrane to reach their site of action, which stresses the relevance of peptide-membrane interactions for AMP activity.

Cecropins, first isolated from the hemolymph of the giant silk moth *Hyalophora cecropia*, are some of the best studied AMPs (24–26). They represent a family of peptides composed of 31–39 amino acids with antibacterial activity against both Gram-negative and Gram-positive bacteria. Cecropins do not exhibit cytotoxic effects against human erythrocytes and other eukaryotic cells, but are susceptible to protease degradation (24,27,28). In an effort to overcome the high production costs of such long peptides and to improve their biological properties, short peptide analogs have been designed and synthesized. These studies have led to the identification of nontoxic and more stable peptide sequences displaying a broader and higher activity than their natural counterparts (29–36). In particular, the undecapeptide WKLFKKILKVL-NH_2 (Pep3), derived from the well-known cecropin A(1–7)-melittin(2–9) hybrid (30,33,34), has been found to be sufficient for antifungal and antibacterial activities, while displaying low cytotoxicity (32,37–40).

Recently, we have identified cecropin A-melittin hybrid undecapeptides derived from Pep3 which inhibit in vitro growth of economically important plant pathogenic bacteria such as *Erwinia amylovora*, *Pseudomonas syringae*

Submitted August 22, 2008, and accepted for publication November 17, 2008.

*Correspondence: macastanho@fm.ul.pt

Rafael Ferre and Manuel N. Melo contributed equally to this work.

Editor: Huey W. Huang.

© 2009 by the Biophysical Society

0006-3495/09/03/1815/13 $2.00

doi: 10.1016/j.bpj.2008.11.053

pv. *syringae*, and *Xanthomonas axonopodis* pv. *vesicatoria* (38–40). In particular, KKLFKKILKYL-NH_2 (BP100), obtained through a combinatorial chemistry approach, displays a bactericidal effect against these bacteria as well as minimized cytotoxicity and low susceptibility to proteinase K degradation (38). Moreover, BP100 is highly effective to prevent infections of *E. amylovora* in pear and apple flowers, being only slightly less potent than streptomycin, which is the most active compound currently used in fire blight control (38).

Although it has been proposed that the mode of action of cecropins and melittin depends on the peptide concentration and membrane composition (41–45), the mechanisms involved in the action of cecropin-melittin hybrid peptides, and especially that of short undecapeptides, are very far from being completely understood. Insights into the mode of action of BP100 are essential for the full rationalization of the biological properties of this peptide as well as for their further improvement. In this study, we investigated the interaction of BP100 with different model membranes using spectroscopic methodologies, which can afford valuable information about peptide-membrane interaction. A comprehensive study was carried out to ascertain the conditions under which BP100 disrupts membranes or, alternatively, translocates across them to reach the lumen of vesicles. Moreover, the in vitro cytotoxic effects of this peptide were also studied on mammalian fibroblast cells.

MATERIALS AND METHODS

Reagents and apparatus

The ultraviolet-visible absorption and steady-state fluorescence emission assays were performed at room temperature in a model No. V-560 UV-Vis spectrophotometer (JASCO, Hachioji, Japan) and in a model No. IBH FL3-22-time-correlated single photon-counting (TCSPC) spectrofluorometer (Horiba Jobin Yvon, Longjumeau, France), equipped with a 450 W Xe lamp and double monochromators, or in a Cary Eclipse Thermo Spectronic spectrofluorometer (Varian, Palo Alto, CA), equipped with a 75 kW pulsed Xe lamp. Multiwell absorption measurements were performed in a Multiskan RC plate reader (Labsystems, Helsinki, Finland). Time-resolved fluorescence decays were collected in the FL3-22-TCSPC spectrofluorometer using a time-correlated single photon counting (TCSPC) technique with a 279-nm nanoLED source (IBH, Glasgow, UK); reduction of scattered light contribution to the decays was achieved by horizontally polarizing the excitation light with a Glan-Thompson polarizer; lifetimes were calculated from time-resolved fluorescence intensity decays using at least 10 K counts in the peak channel; fluorescence intensity decay curves were deconvoluted with the software package DAS 6.1 from IBH.

Dynamic light scattering and ζ-potential measurements were taken in a Zetasizer Nano-ZS (Malvern Instruments, Worcestershire, UK), equipped with a 633-nm HeNe laser.

We used 2-(4-(2-hydroxyethyl)-1-piperazinyl)-ethanesulfonic acid (HEPES), sodium chloride, chloroform, ethanol (spectroscopic grade), acrylamide, dimethyl sulfoxide, and trypan blue (Merck, Darmstadt, Germany). Phospholipids 1-palmitoyl-2-oleoyl-*sn*-glycero-3-phosphocholine (POPC) and 1-palmitoyl-2-oleoyl-*sn*-glycero-3-(phosphor-rac-(1-glycerol)) (POPG) were from Avanti Polar Lipids (Alabaster, AL). Cholesterol, cell culture media, serum, antimicrobials, trypsin/versine, 3-(4,5-dimethylthiazol-2-yl)-2,5-diphenyl-2*H*-tetrazolium bromide (MTT), and crystal violet stain were from Sigma (St. Louis, MO). Lipophilic quenchers 5- and 16-NS (5- and 16-doxylstearic acids, respectively) were from Aldrich Chemical (Milwaukee, WI).

All the 9-fluorenylmethoxycarbonyl (Fmoc)-amino acid derivatives, reagents, and solvents used in the peptide synthesis were obtained from Senn Chemicals International (Gentilly, France). Fmoc-Rink-4-methylbenzhydrylamine resin (0.64 mmol/g) was purchased from Novabiochem (Darmstadt, Germany). Trifluoroacetic acid, *N*-methyl-2-pyrrolidinone, and triisopropylsilane were from Sigma-Aldrich (Madrid, Spain). Piperidine and *N*,*N*-diisopropylethylamine were purchased from Fluka (Buchs, Switzerland). Solvents for high-performance liquid chromatography (HPLC) were obtained from J.T. Baker (Deventer, Holland).

Solutions were prepared in a 10 mM HEPES buffer at pH 7.4, containing 150 mM NaCl (the so-called physiologic ionic strength). All BP100 fluorescence measurements were recorded at an excitation wavelength of 275 nm, except for the experiments involving acrylamide in which the peptide was excited at 285 nm to minimize the relative quencher/fluorophore light absorption ratio.

Peptide synthesis

BP100 was synthesized as a C-terminal carboxamide on a Rink *p*-methylbenzhydrylamine resin by the solid-phase synthesis method using standard 9-fluorenylmethoxycarbonyl (Fmoc) chemistry (38). The peptide was purified by reverse-phase semipreparative HPLC on a 5 μm, 1.0 $\times$ 25 cm C18 Tracer column (Teknokroma, Barcelona, Spain) using a linear gradient from 10 to 60% acetonitrile in water with 0.1% trifluoroacetic acid over 50 min. The peptide was obtained with >95% HPLC purity. Electrospray ionization mass spectrometry was used to confirm peptide identity.

Preparation of model membrane vesicles

Large unilamellar vesicles (LUVs) of 100-nm diameter and multilamellar vesicles (MLVs) of different phospholipid composition were used as biological membrane models. MLVs were obtained by hydration of dried phospholipid films under vortex agitation; when required, multilamellarity was enhanced by first hydrating the films in a fraction of the final volume. LUVs were prepared by freezing-thawing and extruding MLVs, as described elsewhere (46). Sonication of vesicles, when needed, was carried out in an Ultrasound Technology UP200S power sonicator (Hielscher Ultrasonics, Teltow, Germany). Mammalian model systems included 100% POPC LUVs and 2:1 POPC/cholesterol LUVs. Bacterial model systems included 2:1 and 4:1 POPG/POPC LUVs.

Photophysical characterization of BP100 in aqueous solution

The linear dependence of the absorbance and fluorescence intensity of BP100 on its concentration was tested over the 0–140 μM range. To check whether peptide aggregation occurs in the aqueous phase, the Tyr fluorescence was quenched by sequentially adding aliquots of a 4 M acrylamide solution to a 15 μM peptide sample, while recording both the absorbance and fluorescence intensity. Quenching assays data were analyzed according to the Stern-Volmer formalism (47) and were corrected for simultaneous light absorption of fluorophore and quencher (48).

Peptide-membrane incorporation studies

The extent of the partition of BP100 to each model membrane was evaluated by titrating a 15 μM peptide solution with the corresponding LUVs suspension and recording the fluorescence emission. Samples were incubated for 10 min after each addition of lipid suspension. The molar ratio partition constants, K_P, were calculated by fitting the experimental data with Eq. 1, as described elsewhere (49). The quantities I_W and I_L are the fluorescence intensities the mixture would display if all the peptide is in the aqueous or

the lipidic phase, respectively; γ_L is the phospholipid molar volume, which is considered to be 0.763 M^{-1}, corresponding to the typical value for liquid crystalline lipid bilayers (50); and [L] is the phospholipid concentration. Fluorescence data were corrected both for dilution and scattered light (51),

$$\frac{I}{I_W} = \frac{1 + K_p\gamma_L\frac{I_L}{I_W}[L]}{1 + K_p\gamma_L[L]}, \quad (1)$$

$$K_p = \frac{[BP100]_L}{[BP100]_W}, \quad (2)$$

where $[BP100]_L$ and $[BP100]_W$ are the peptide concentrations in the lipid volume or in the aqueous phase, respectively. It should be noted that because K_p implicitly includes electrostatic contributions that may be dependent upon the global peptide concentration, it should be taken as an apparent partition constant (52).

Membrane saturation studies were carried out with 2:1 POPG/POPC LUVs. Saturation points were determined by adding small aliquots of a 750 μM stock peptide solution to an LUV suspension (phospholipid concentrations of 0, 40, 75, 125, 175, and 250 μM) containing 100 mM acrylamide. The fluorescence emission was recorded after 10 min of each peptide addition. To prevent dilution of acrylamide, the stock peptide solution also contained 100 mM of this aqueous phase quencher. The peptide/lipid (P/L) ratio at saturation (σ) and K_p were calculated by fitting the obtained saturation points with Eq. 3, as described elsewhere (53):

$$[P] = \frac{\sigma}{K_p\gamma_L} + \sigma[L]. \quad (3)$$

In-depth membrane localization studies

Differential quenching studies were carried out by sequentially adding aliquots of a lipophilic quencher—either 5-NS or 16-NS—to a LUV suspension previously equilibrated with 10 μM BP100; two different LUV concentrations—125 and 250 μM—were used so as to set either saturation or nonsaturation states and quencher concentration was increased or reduced accordingly; time-resolved fluorescence measurements of the Tyr in BP100 were taken. To prevent bilayer alterations while adding the 5- and 16-NS quencher aliquots, prepared in ethanol, care was taken to keep final ethanol concentrations below 2% (v/v) (54). Results were analyzed with a methodology based on the knowledge of the quenchers' in-depth distributions in the membrane (55), modified to implement a least-squares fitting to the data.

Vesicle permeabilization studies

The kinetics of BP100-induced vesicle leakage was monitored by Co^{2+} quenching of the fluorescence of 1% N-NBD-PE (56) incorporated into 125 μM 2:1 POPG/POPC vesicles, at BP100 concentrations ranging from 0 to 25 μM. Briefly, experiments were carried out by adding aliquots of BP100 to a suspension of vesicles in the presence of 20 mM $CoCl_2$. The $CoCl_2$, which is unable to permeate phospholipid membranes, was added to the vesicles shortly before the measurement, quenching the outer leaflet N-NBD-PE fluorescence. The kinetics were started with the addition of BP100. Permeabilization of the membrane to the Co^{2+} ions results in further quenching of the inner leaflet N-NBD-PE population. The decrease of NBD fluorescence emission intensity at 515 nm was monitored with excitation at 460 nm. The percentage of leakage at time t after peptide addition was determined from Eqs. 4–6,

$$\%\ \text{leakage}\ (t) = \left[Co^{2+}\right]_{in}(t)/\left[Co^{2+}\right]_{out}(t) \approx [Co^{2+}]_{in}(t)/[Co^{2+}]_{TOTAL}, \quad (4)$$

where $[Co^{2+}]_{TOTAL}$, $[Co^{2+}]_{in}$, and $[Co^{2+}]_{out}$ correspond to the global, luminal, and external quencher concentrations, respectively. The approximation of $[Co^{2+}]_{out}(t)$ as $[Co^{2+}]_{TOTAL}$ can be made because no significant decrease of external quencher concentration is expected upon leakage: at these lipid concentrations, the total internal vesicle volume can be calculated to be <0.005% of the sample volume (57). From the collisional quenching Stern-Volmer formulation (58), quencher concentrations can be related with fluorescence intensities,

$$\%\,\text{leakage}\,(t) = \frac{-\Delta I_{in}(t)}{I_{in}(t) \times K_{SV}} \div \frac{-\Delta I_{max}}{I_c \times K_{SV}} = \frac{I_c \times \Delta I_{in}(t)}{I_{in}(t) \times \Delta I_{max}} \quad (5)$$

where K_{SV} is the Stern-Volmer quenching constant, I_{in} is the contribution of inner leaflet fluorophores to the global fluorescence intensity, ΔI_{in} is the change in I_{in} after peptide addition, ΔI_{max} is the maximum change in global fluorescence from before quencher addition to complete leakage, and I_c corresponds to the minimum fluorescence intensity at 100% leakage, obtained by vesicle sonication. There are two populations contributing to the global fluorescence: the inner and outer leaflet fluorophores; because the external quencher concentration remains virtually constant, the fluorescence intensity of the outer fluorophore fraction will also be approximately constant and $\Delta I = \Delta I_{in}$, where ΔI is the change in global intensity upon peptide addition. In addition, from the moment of quencher addition, the external fraction decreases to its minimum possible fluorescence intensity which, given the large size of a vesicle, is roughly one-half of I_c. This allows the substitution of $I_{in}(t)$ as $I(t) - 0.5 \times I_c$,

$$\%\ \text{leakage}\ (t) = \frac{I_c \times \Delta I(t)}{\left(I(t) - 0.5I_c\right) \times \left(I_c - I_{pre}\right)}, \quad (6)$$

where I_{pre} is the global fluorescence intensity before quencher addition.

Leakage kinetics were tentatively fitted with the system of ordinary differential equations described in Gregory et al. (59).

Membrane translocation studies

To determine the occurrence and extent of peptide translocation across the membrane a novel method was devised: the increase of BP100 fluorescence upon membrane interaction was followed after MLV addition. A control experiment was performed in which the interaction kinetic was instead initiated with LUVs produced from the same suspension of MLVs. In the occurrence of translocation, the interaction kinetic with the MLVs would be slowed down with respect to LUV interaction due to the multiple membrane crossing steps. In the absence of translocation, although the lipid concentration is the same in MLV and LUV suspensions, the peptide would sense an apparently lower concentration of lipid in an MLV suspension, as only the outer lipid shell is accessible; as such, fluorescence would never increase as much with MLVs as with LUVs (see Fig. 1 for details). A quantity of 40 μM 2:1 POPG/POPC LUVs and MLVs were used. The sensitivity in the detection of peptide-lipid interaction was improved by adding aliquots of 200 mM of acrylamide to increase the fluorescence change upon binding. Potential artifactual increases of BP100 emission due to scattered light contribution were controlled by monitoring the ratio of fluorescence intensities at 303 and 330 nm.

Vesicle aggregation and charge studies

Turbidity studies were carried out by monitoring the changes induced by BP100 in the optical density (OD) of a vesicle suspension. Briefly, aliquots of a 1 mM BP100 stock solution were added to 125 μM 2:1 POPG/POPC vesicle suspensions. Peptide concentrations tested ranged from 0 to 21 μM. The OD was recorded at 450 nm every 2 s for 30 min after peptide addition.

Dynamic light scattering measurements were carried out in similar conditions as the OD measurements. BP100 concentrations ranged from 0 to 16.5 μM. The ζ-potential measurements were performed at 250 μM lipid and at BP100 concentrations up to membrane saturation.

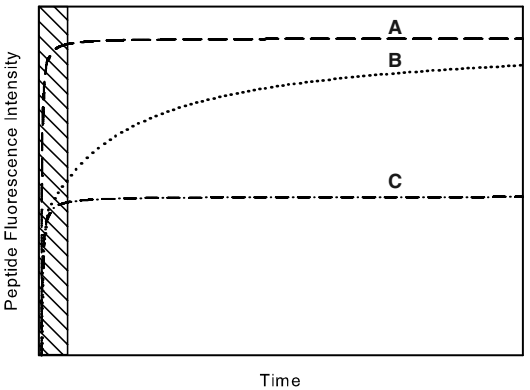

FIGURE 1 Expected fluorescence increase kinetics of BP100 in interaction with LUVs or MLVs. (*A*) LUVs with or without the occurrence of translocation: the entire lipid is accessible to the peptide at time 0 resulting in a fast interaction kinetics. (*B*) MLVs, with peptide translocation: at time 0, only a fraction of the lipid is accessible to the peptide, resulting in a fast, but partial, increase in fluorescence; as the peptide translocates, more lipid becomes accessible, and a full fluorescence increase is eventually reached at a lower rate. (*C*) MLVs, without translocation: there is a fast interaction with the accessible fraction of lipid, but no subsequent increase is expected, as no more lipid becomes accessible. The hatched region indicates the approximate relative measurement dead time for BP100 under our setup.

Cytotoxicity assays

Cell culture

V79 Chinese hamster lung fibroblast cells (MZ subline (60)) were used for the cytotoxicity assays (61). They were routinely cultured in 175 cm^2 tissue flasks in Ham's F-10 medium, supplemented with 10% newborn calf serum and 1% penicillin/streptomycin, in a humidified incubator at 37°C with 5% CO_2. Cells were routinely subcultured in the semiconfluent state over a maximum of eight passages and regularly tested negative for *Mycoplasma*. The V79 cells used in this study were kindly obtained from Prof. H. Glatt (German Institute of Human Nutrition, Germany) and were routinely maintained and kindly provided by Dr. Nuno Oliveira (University of Lisbon, Portugal).

Exposure conditions in the assays

V79 cells were suspended in 180 μL culture medium in 96-well plates, at a density of 5×10^3 cells/well, optimized to keep the cultures in optimal growth during the whole experiment. After seeding, the plates were incubated for 24 h before the experiment. BP100 was dissolved in HEPES and added to 20 μL of the medium to obtain final concentrations of 90, 60, 40, 30, and 10 μM. Two replicates for each peptide concentration were used. Each plate contained a negative control (culture medium + 10% HEPES) and a positive control (culture medium + 10 mM H_2O_2). Cell viability was measured after incubation for 24 h at 37°C with 5% CO_2.

Cell viability assays

Three assays were performed to test the cell viability. The MTT assay was used to investigate the effect of BP100 on the mitochondrial dehydrogenase activity, measured as the ability of viable cells to produce formazan crystals (62). The cells were rinsed once with phosphate-buffered saline and then 200 μL MTT solution (5 mg/ml) were added to each well. After 2.5 h incubation at 37°C, 200 μL dimethyl sulfoxide were added to each well to dissolve the purple formazan crystals (63). The absorbance of the resulting dispersion was determined at 595 nm in the multiwell scanning spectrophotometer.

Crystal violet is a dye that accumulates in the cell nucleus and was applied in this study as an indicator for cell viability (62). The fixed dye correlates directly with the nuclear DNA content, and thus also with the cell number. After its application, nonviable, nonadherent cells were washed. The fixed crystal violet was solubilized in 10% SDS for 20 min and the OD of the solution was measured at 595 nm.

The ability of cells to stain with trypan blue was used to investigate the loss of plasma membrane integrity (64). The cells were washed with phosphate-buffered saline, dispersed with 40 μL trypsin EDTA and the resulting cell suspension was diluted in 10 μL of culture medium. 20 μL of the mixed cell suspension were added to 20 μL of 0.4% trypan blue fresh solution, prepared in NaCl 0.9%, to stain nonviable cells. Cell viability was expressed as the percentage of unstained cells (65).

Statistical analysis and regression modeling

To account for the interplate variability, the absolute values of the cell viable parameters were normalized to the average of the negative controls (100% viability) and the positive controls (0% viability, corresponding to 100% cell death) (64). Statistical concentration-response analyses were performed in the same way for all three in vitro tests by fitting a three-parameter nonlinear regression Logit model to the data (66). Dunnett's test (α = 5%) was employed to determine statistical significant differences between the treated groups and the negative controls. IC_{50} values were determined as the midpoint of the fitted curves.

RESULTS

Photophysical characterization in aqueous solution

Both the absorbance and fluorescence intensities of BP100 depended linearly on concentrations up to 140 μM (data not shown). The obtained photophysical parameters were similar to those of free Tyr: the excitation maximum for BP100 was at 275 nm (λ_{em} = 306 nm), which is coincident with the wavelength of maximal electronic absorption. The calculated absorptivity coefficient (ε) at this wavelength was 1.40×10^3 M^{-1} cm^{-1}. The quenching of BP100 by acrylamide followed a linear Stern-Volmer relationship up to 250 mM of quencher, with a K_{SV} of 15.1 M^{-1} (not shown).

Membrane insertion studies

For all the membrane models tested, an increase of fluorescence intensity was observed upon the partition of BP100 between the aqueous buffered phase and the lipidic membrane studied (Fig. 2). Partition parameters are summarized in Table 1.

For the neutral systems, liquid-crystal POPC and liquid-ordered 2:1 POPC-cholesterol LUVs, the increase of fluorescence followed a hyperbolic-like relationship (Fig. 2 *A*). In contrast, the anionic systems 2:1 POPG/POPC and 4:1 POPG/POPC deviated from this behavior (Fig. 2 *B*). At low lipid concentrations, an overshoot of the fluorescence intensity was detected. This result was assigned to reflect membrane saturation. To confirm this hypothesis, membrane saturation studies were carried out for the 2:1 POPG/POPC system (Fig. 3). Saturation points were identified from the

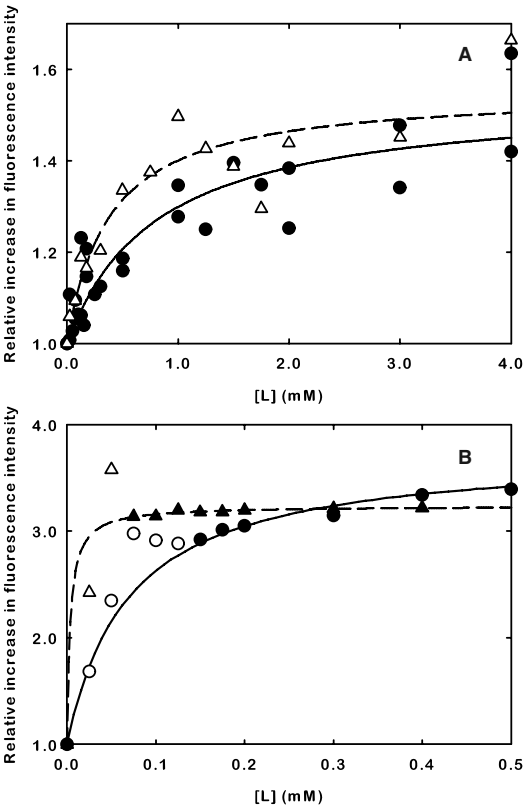

FIGURE 2 Lipid titrations of 15 μM BP100 with different LUV systems. Lines represent the fitting parameters of the data to the partition model in Eq. 1. (*A*) POPC (•, *solid line*) and 2:1 POPC/cholesterol (△, *dashed line*) LUVs. (*B*) 4:1 POPG/POPC (•, *solid line*) and 2:1 POPG/POPC (▲, *dashed line*) LUVs; deviations occurred at low lipid concentrations and those data points (*empty*) were removed from the fittings. The difference in the required amounts of lipid for the titrations in panels *A* and *B* indicates a much higher partition toward the anionic models; this is confirmed by the obtained partition constants. Fit parameters are summarized in Table 1.

breaks observed in the curves obtained from titration of vesicles with BP100 and were fitted with Eq. 3 (Fig. 3, *inset*). A K_p value of 8.41×10^4 was obtained and a σ of 0.118 was determined, which corresponds to 8.4 phospholipids per peptide at the saturation of the vesicles.

The depth of membrane internalization was probed using stearic acid molecules labeled at different carbon positions (carbons 5 and 16 for 5- and 16-NS, respectively) with tyrosine quenching nitroxyl groups. With previous knowledge of the in-depth distribution of each quencher, an integrated approach was used to infer the distribution of the tyrosine residue of the peptide from each quencher's quenching profile (based on (55)). These profiles did not change significantly upon saturation (not shown), indicating little change in the in-depth localization of the peptide. This was

TABLE 1 Summary of the characteristics of each studied system: constitution and partition parameters determined using Eq. 1

Modeled system	Constituent phospholipids	$K_p/10^3$	I_L/I_W
Bacterial membrane models			
Outer leaflet	2:1 POPG/POPC	30.8 ± 6.2	3.59 ± 0.06
Inner leaflet	4:1 POPG/POPC	87.6 ± 9.8	3.58 ± 0.02
Mammalian membrane models			
Outer leaflet	100% POPC	1.6 ± 0.5	1.54 ± 0.06
Outer leaflet + cholesterol	2:1 POPC/cholesterol	3.5 ± 1.3	1.55 ± 0.06

confirmed after analysis: in the absence of saturation, the average in-depth localization from the bilayer center was 10.5 Å and the distribution half-width at half maximum was 3.2 Å (a Lorentzian distribution was assumed); under saturation, these parameters were 11.2 Å and 2.4 Å, respectively.

Vesicle permeabilization studies

Fig. 4 displays the leakage kinetics induced by increasing BP100 concentrations. BP100 induced vesicle leakage in a dose-dependent manner. It should be noticed that from 15 μM peptide the kinetics display a markedly sigmoidal rise; this is evident in Fig. 4. A transition at 15 μM of BP100 is also clearly observed in the leakage percentage at 390 s (Fig. 4, *inset*). Thus, for 125 μM lipid, 15 μM is a critical BP100 concentration dictating the transition between two different regimes of peptide-lipid interactions.

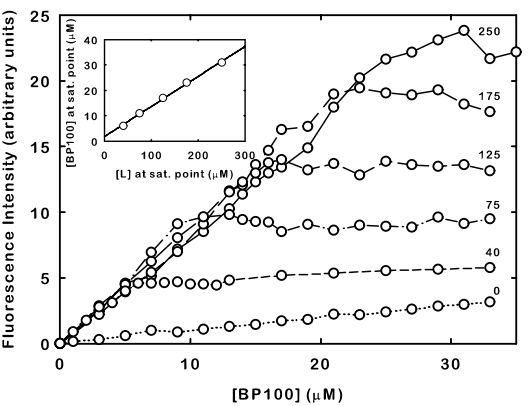

FIGURE 3 Titration of several concentrations of 2:1 POPG/POPC LUVs with BP100 in the presence of 100 mM acrylamide (lipid concentration is indicated in μM for each set of points). Saturation points were identified from the breaks in each curve. (*Inset*) Linear dependence of the global peptide and lipid concentrations at the saturation points, fitted according to Eq. 3, yielding a saturation proportion of 8.4 phospholipids per peptide and a partition constant of 8.41×10^4.

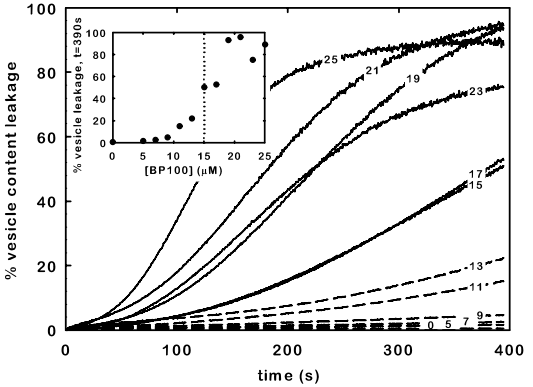

FIGURE 4 Time course of BP100-induced vesicle leakage to Co^{2+} with 125 μM 2:1 POPG/POPC LUVs doped with 1% N-NBD-PE; each curve corresponds to a different BP100 concentration, indicated in the figure in μM. Dashed lines correspond to subsaturation conditions. (*Inset*) Leakage percentage at 390 s in which a transition in behavior with BP100 concentration is evident; this transition occurs close to the expected membrane saturation point for the used lipid concentration, indicated by the dotted line.

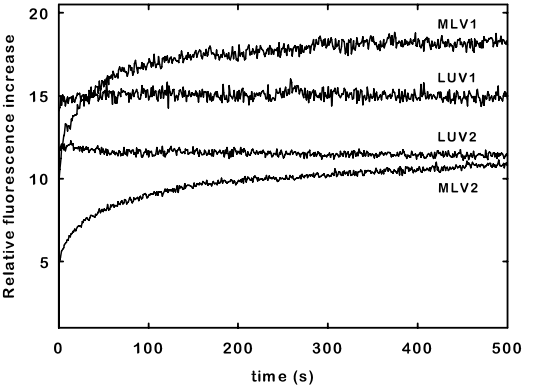

FIGURE 5 Time course of BP100 interaction with 40 μM 2:1 POPG/POPC LUVs and MLVs. LUV1 and MLV1: 4 μM BP100. LUV2 and MLV2: 12 μM BP100. Chosen BP100 concentrations are below and above membrane saturation, as per Eq. 3. Comparison with the expected kinetic profiles (Fig. 1) indicates the occurrence of peptide translocation in both cases.

The sigmoidal curves could be fitted with the model described by Gregory et al. (59) (not shown), even though in their work only hyperbolic-like kinetics were fit. Both rate constants of pore formation/dissipation needed to be two-to-three orders-of-magnitude lower than those observed by Gregory et al. (59) to generate a sigmoidal behavior comparable to the one observed in Fig. 4. Further quantitative analysis of leakage parameters is, however, not reliable, due to multiple minima in the solution space and some degree of correlation.

Membrane translocation studies

There were marked differences between the peptide-MLV and peptide-LUV interaction kinetics (Fig. 5). Whereas the increase in peptide fluorescence intensity upon LUV addition was almost instantaneous, the MLV-induced increase spanned several minutes. Fluorescence intensity for the MLV additions started out lower than that induced by LUV additions of the same lipid concentration, but rose to approximately the same relative level, as expected for the occurrence of translocation (Fig. 1). To better compare the fluorescence change at both peptide concentrations, Fig. 5 depicts the relative increase in fluorescence upon lipid addition. As a consequence there are small differences in the endpoint of the kinetics at low BP100 concentrations (Fig. 5—MLV1 and LUV1), attributable to error introduced by the low initial Tyr fluorescence signal and further aggravated by the use of acrylamide.

Vesicle aggregation and surface charge studies

Apart from a transient initial increase in turbidity, no significant changes in vesicle OD were observed at peptide concentrations <15 μM (Fig. 6). For peptide concentrations at or >15 μM, however, there was a remarkable time-dependent increase of the OD due to liposome aggregation induced by BP100 (Fig. 6, *inset*).

A related change was also observed with light scattering measurements where the average particle diameter of the LUV suspension increased by ~10-fold (Fig. 7). Similarly to permeabilization, the BP100-induced increase of vesicle turbidity/aggregation displays a transition between two regimes close to 15 μM, with 125 μM of lipid.

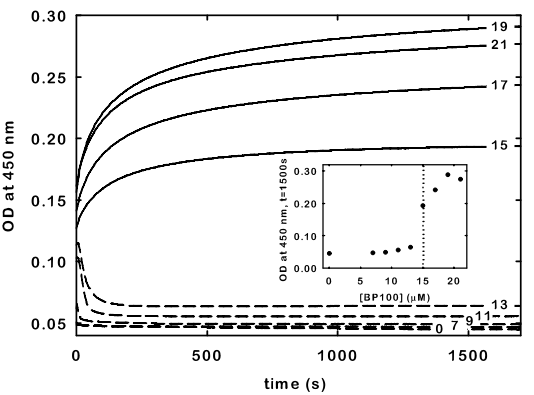

FIGURE 6 Time course of BP100-induced OD change ($\lambda = 450$ nm) of 125 μM 2:1 POPG/POPC LUVs; each curve corresponds to a different BP100 concentration, indicated in the figure in μM. Two different kinetic behaviors are evident. Dashed lines correspond to subsaturation conditions. (*Inset*) OD_{450} at 1500 s. The transition in behavior is evident above 15 μM; as with vesicle leakage (Fig. 4), this transition occurs close to the expected membrane saturation point for the used lipid concentration, indicated by the dotted line.

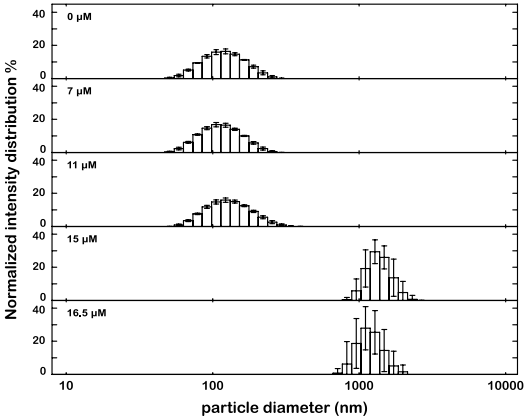

FIGURE 7 Normalized intensity distribution determined by dynamic light scattering of the particle sizes of a 125 μM 2:1 POPG/POPC LUV suspension in the presence of increasing BP100 concentrations (*error bars* represent SD). Above membrane saturation, which is expected at ~15 μM BP100 at this lipid concentration, a significant increase in particle size and heterogeneity is observed, in agreement with the occurrence of vesicle aggregation. This result correlates with the observed distinct behavior of BP100-induced OD change below and above saturation (Fig. 6).

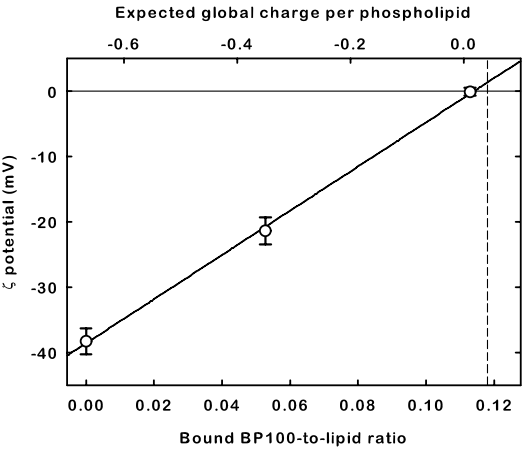

FIGURE 8 The ζ-potential of 250 μM 2:1 POPG/POPC LUV in the presence of different BP100 concentrations (*error bars* represent SD). Peptide concentrations are displayed either as bound peptide/lipid ratios (calculated with the partition constant obtained from Eq. 3) or as the estimated global charge per phospholipid assuming a 6^+ charge on the peptide. A linear regression of the points is displayed as a guide to the eye. The saturation ratio is indicated by the dashed line. A neutralization of the LUV charge at the saturation point was observed, in agreement with what was expected from the saturation proportion (Fig. 3), the peptide charge, and the composition of the system.

The particles' ζ-potential was -38.3 mV in the absence of peptide but was brought close to zero (-0.1 mV) at saturation (Fig. 8); aggregation and increase in turbidity prevented ζ-potential measurement at higher peptide concentrations.

Effects of BP100 exposure on cell viability

Fig. 9 depicts the effects of BP100 on the mitochondrial activity, cell monolayer adherence, and membrane integrity of cultured hamster fibroblasts. All cell viability parameters responded to the peptide (10–90 μM) in a clear dose-dependent way. At the highest tested concentration (90 μM), low cell viability (<10%) was observed. The peptide concentrations, at which 50% inhibition was expected (IC_{50}), were interpolated from the regressions for each viability assay, and ranged from 51.1 μM, for the crystal violet stain, to 64.3 μM for the trypan blue assay.

DISCUSSION

The biological activity of small, cationic antimicrobial peptides has been largely associated with their interaction with membranes. It is widely believed that for many of these peptides, membrane disruption is the primary mechanism of cell killing (10–12,15,16,18–20). However, their exact mode of action is still poorly understood. Elucidating their mechanism of action and their specific membrane damaging properties is crucial for the rational design of novel antibiotic peptides with high antibacterial activity and low cytotoxicity. With these observations in mind, and considering that BP100 contains a Tyr residue, which makes it intrinsically fluorescent, we have exploited its photophysical properties to obtain information about its binding affinity and damaging effect on bilayers having a lipid composition

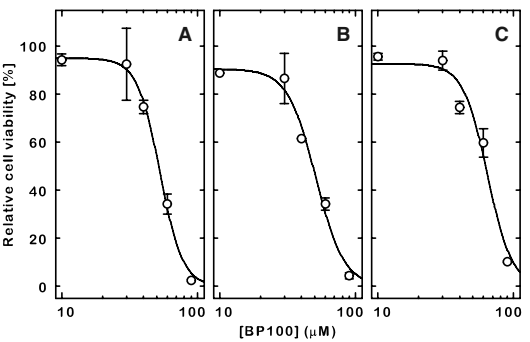

FIGURE 9 Effects of BP100 on the viability of V79 Chinese hamster lung fibroblast cells after 24 h exposure (*error bars* represent SE). (*A*) Mitochondrial activity determined by the MTT assay; $IC_{50} = 52.9$ μM. (*B*) Loss of monolayer adherence estimated by the crystal violet assay; $IC_{50} = 51.1$ μM. (*C*) Plasma membrane integrity estimated by the trypan blue assay; $IC_{50} = 64.3$ μM. Logit curves were fitted to the data and are shown as lines. The IC_{50} values are proportionally greater-than the MIC, by approximately the same factor as the partition constants toward the anionic bacterial models are greater-than toward the neutral mammalian models, suggesting a concentration-dependent disruption mechanism.

similar to that of the bacterial and mammalian cytoplasmic membranes.

Photophysical characterization of BP100 in aqueous solution

The photophysical characterization of peptides in aqueous solution is a prerequisite to understand their interaction with phospholipid model membranes. The observed behavior of BP100 in aqueous solution reflects that peptide aggregation does not occur at the studied peptide concentration range. This is supported by the linear dependencies of fluorescence emission intensity and electronic absorption on concentration and by the obtained λ_{exc}, λ_{em}, and ε-values as they are similar to those of free Tyr (275, 303, and 1400, respectively (47)), indicating that the Tyr in BP100 is exposed to an aqueous environment (47). Moreover, a linear Stern-Volmer plot for the fluorescence quenching of BP100 with acrylamide is observed up to 250 mM (not shown). In addition, there are no significant differences between the obtained K_{SV} and the one for acrylamide quenching of free Tyr, evidencing that Tyr is totally accessible to the aqueous phase. The absence of aggregation observed for BP100, together with its overall positive charge (+6), could account for its high solubility in aqueous solution and facilitates the interpretation of the peptide-membrane interaction results.

Membrane insertion studies

The extent of the partition of BP100 into model membranes was studied using a partition model described by Santos et al. that allows the calculation of the Nernst partition constant (K_p) from fluorescence intensity (I) versus phospholipid concentration ([L]) plots at a constant peptide concentration ([P]) (49). The K_p, defined as the ratio between the equilibrium membrane-bound and aqueous phase peptide concentrations, provides an easy assessment of the extent of peptide-membrane interaction (Eq. 2). For both neutral systems POPC and 2:1 POPC/cholesterol LUVs, used as models of the outer leaflet of mammalian membranes, the fluorescence intensity increased following an hyperbolic-like relationship (Fig. 2 *A*). The moderate K_p values obtained for vesicles composed of 100% POPC and POPC/cholesterol mixtures (Table 1) could be attributed to the hydrophobic effect and the van der Waals forces that are likely to dominate the interactions between the neutral lipids and the hydrophobic residues of BP100. In this case, no specific interaction with cholesterol was observed, which is an indicator of low toxicity toward mammalian cells. Furthermore, cholesterol seems to play an important role in preventing the intercalation of AMPs into eukaryotic cell membranes (67); its presence and the absence of acidic phospholipids in the eukaryotic membranes could account for the low cytotoxicity displayed by BP100 against erythrocytes (38).

For the anionic liquid-crystalline 2:1 and 4:1 POPG/POPC vesicles, which served as models for bacterial cell membranes, the partition curves deviated from the hyperbolic-like progression at low lipid concentrations (Fig. 2 *B*). A similar behavior has been recently reported for the antimicrobial peptide omiganan and has been attributed to a membrane saturation process: at low phospholipid concentrations, membrane saturation may occur when the bound peptide concentration, hypothetically dictated by K_p, is higher than what the membrane can accommodate (53); under these conditions, interaction changes may occur, as has also been described for other AMPs upon the crossing of threshold P/L ratios (68,69). Since the model of Santos et al. (49) is not well suited to study these saturated systems, the K_p values were obtained by fitting only the nonsaturated points to the partition model (Fig. 2 *B* and Table 1). This approach is obviously subject to error because the initial points of the curve, which are important for the accurate calculation of K_p, cannot be used. However, even with great associated errors, the obtained partition constants were one or more orders-of-magnitude higher than those of the neutral systems (Table 1). These results are consistent with the expected preference of cationic peptides for negatively charged membranes as a consequence of the strong electrostatic interaction.

To ensure that the deviation observed in the partition curves of the anionic vesicles was due to a saturation of the system, membrane saturation studies were carried out using 2:1 POPG/POPC LUVs. LUV suspensions were titrated with peptide in the presence of acrylamide while monitoring BP100's fluorescence intensity. Acrylamide is an aqueous quencher that facilitates the identification of alterations in the phase localization of peptides. In a nonsaturation regime, a linear increase of the fluorescence intensity is expected: as per the formalism behind Eq. 1, the fractions of the peptide in each phase are constant with constant [L]; therefore, any variation in peptide concentration will result in a proportional increase in each of these fractions and, also therefore, in a global proportional increase of the fluorescence intensity (53). Conversely, if saturation occurs, the membrane will not be able to accommodate any more peptide, which will then remain in the aqueous phase. Because acrylamide quenches preferentially the fluorescence of the aqueous phase peptide population, a weaker progression of the fluorescence intensity, relatively to a nonsaturation state, should then be detected (53). This behavior was indeed observed in the BP100 titrations (Fig. 3), showing the occurrence of saturation: two different slopes were obtained for each I versus [P] curve. The first slope corresponds to a nonsaturated state while the second one, which is similar to that of the curve in the absence of lipid, can be ascribed to a saturation of the system. The saturation points could be easily obtained from the breaks of the initial slopes of each titration curve. It was observed that the I versus [P] curve with [L] = 125 μM had its saturation point close to [P] = 17 μM (Fig. 3), which is slightly higher than the peptide concentration that yielded an I versus [L] curve

with a deviation maximum close to [L] = 125 μM (Fig. 2 *B*). This result supports the hypothesis that the deviations observed in the partition curves correspond to a saturation of the membrane.

Further information from the saturation phenomenon was obtained by representing the saturation point ([P],[L]) pairs for the 2:1 POPG/POPC LUVs (Fig. 3, *inset*). This system followed Eq. 3, which defines the total amount of peptide at which a saturation point occurs as a linear function of the amount of lipid in the system, and allows the calculation of σ—the P/L ratio at saturation—and the Nernst partition constant K_p. However, it should be noticed that the values for K_p have large associated errors because they are calculated from the reciprocal of a small intercept. Despite that, the obtained K_p (8.41×10^4) had the same order of magnitude as that determined from the partition curve using the model of Santos et al. (49) (3.08×10^4). In addition, the saturation P/L ratio was 0.118, which corresponds to 8.4 phospholipids per peptide directly in contact with the membrane at the saturation. Because there are 2/3 anionic phospholipids in the used system, there will be 5.6 negatively charged phospholipids per peptide at saturation. Interestingly, this number is very close to the expected charge of the peptide (+6) at pH 7.4, which suggests that electroneutrality is reached at the saturation of the system.

There was no significant alteration in the tyrosine in-depth location upon saturation, indicating that most of BP100 molecules maintain their positioning within the membrane. The location of the tyrosine residue, approximately halfway across the membrane leaflet, is coherent with a relatively deep burying of the peptide if it adopts, as expected (40), a horizontally oriented α-helical structure. The lysines have the ability to snorkel and keep their charged amino groups near the headgroup region (70,71) while the hydrophobic side chains could go as far as the bilayer center. This localization within the bilayer is likely responsible, at least in part, for the membrane destabilizing capabilities of BP100.

Vesicle permeabilization studies

Investigations on the mode of action of AMPs, such as cecropins and melittin, have shown that they exert their activity by inducing the formation of transmembrane pores or by causing cell lysis, depending on both the peptide concentration and the membrane composition (41–45). Moreover, it has been reported that cecropin-melittin hybrids are also able to cause membrane permeabilization (72,73). These findings prompted us to test BP100-induced permeabilization of model lipidic membranes.

Results showed that BP100 has an important permeabilizing effect dependant on peptide concentration. The increase in the permeabilization rate with BP100 concentration is, however, not linear (Fig. 4). The clear change of behavior at ~15 μM peptide, toward faster, sigmoidal, and more intense leakage kinetics—visible both in the permeabilization kinetics (Fig. 4) and in the leakage percentage profile at 390 s (Fig. 4, *inset*)—occurs very close to the peptide concentration expected to cause membrane saturation for the 125 μM lipid concentration (Fig. 3). These results show that membrane saturation affects more than just the amount of bound peptide: high P/L ratios at, or close to, membrane saturation are able to induce a change in a functional property of the peptide. The sigmoidal leakage kinetic induced by BP100 is uncommon, as such profiles are usually hyperbolic-like (74). Nevertheless, a similar kinetic was recently observed for an unrelated AMP (74). In both these cases, because the interaction with LUVs is not a limiting step (Fig. 5, LUV *traces*), the lag involved in the sigmoidal behavior may be related to postbinding events in the membrane (74).

Further information was extracted by fitting the data with the model used by Gregory et al. (59) to describe cecropin A-induced leakage. This model was only used to fit hyperbolic-like kinetics, but, even in those cases (59), close inspection of the model in the first seconds of each kinetics does reveal a brief sigmoidal behavior. Upon fitting, the magnitude of this behavior could only be manipulated to match the timescale of BP100-induced leakage kinetics by lowering the k_1 and k_2 constants of the model two-to-three orders of magnitude, relative to the values obtained in Gregory et al. (59). As these parameters are the rate constants of pore forming/dissipation, this result suggests that, after binding, BP100 becomes disruptive at a slower rate than cecropin A.

The high degree of peptide-induced leakage after saturation may reflect severe membrane damage or lysis, whereas the lower permeabilization before saturation could reflect a lesser destabilization of the membrane upon peptide binding. High P/L ratios close to saturation would then act as the trigger between these two states, and could be the biophysical parallel to the in vivo onset of antibacterial activity. This is supported by the fact that the threshold dependence on peptide concentration (Fig. 4, *inset*) could not be accounted for with data fitting without assuming some kind of parameter change with increasing BP100 concentration—such as an increase in the mentioned k_1 and k_2 disruption rates. Although hypothetical, this scenario is plausible, and stresses the importance of high local peptide concentrations in the membrane.

Membrane translocation studies

The determination of the occurrence of membrane translocation is an important functional characterization: a nontranslocating peptide can only exert its activity at the extracellular/membrane level, whereas one crossing a membrane may also have cytoplasmic targets. However, detection of translocation can be troublesome, and, although there are several methods available, many require peptide derivatization or have limited applicability (75).

Despite there being other published methods where MLVs are used to enhance an internalization effect (75,76), the method developed in our work is extremely simple and requires only that the peptide has intrinsic fluorescence and that its interaction kinetics with LUVs are significantly faster than its translocation kinetics; quencher enhancement is not an absolute requirement. The results clearly showed a translocation behavior at both high and low P/L ratios (Fig. 5). As predicted in Fig. 1 for a translocating peptide, the interaction with MLVs was slower than with LUVs, but eventually reached the same fluorescence increase. Occurrence of translocation is unequivocal and, together with the permeabilization assays, constitutes a further proof of the membrane activity of the peptide.

Vesicle aggregation and surface charge studies

Turbidity measurements have been described as an useful tool to investigate the affinity of cationic peptides toward charged vesicles (77). The stability of a dispersion of charged vesicles is mainly governed by three types of forces: electrostatic repulsion, van der Waals attraction, and hydration (77). Cationic peptides can alter the charge density of the vesicle surface inducing vesicle aggregation, which can be followed as an increase of the OD. Turbidity results showed two different kinetic patterns depending on BP100 concentration (Fig. 6). For 125 μM lipid (2:1 POPG/POPC LUV) and peptide concentrations <15 μM, which correspond to a nonsaturated state, no significant changes in turbidity were observed. However, when membrane saturation occurs (≥ 15 μM peptide), the optical density of the solution increased until a plateau was reached, ~30 min after the addition of BP100. This increase is likely due to vesicle aggregation induced under membrane saturation conditions. These results confirm the affinity of BP100 for acidic phospholipids and reinforce the hypothesis that electroneutrality is reached at the membrane saturation point.

These conclusions were confirmed using light scattering methodologies: the change in the LUV suspension OD is related to an increase in the average particle size from 100 nm—in the absence of peptide and up to saturation—to >1 μm upon saturation (Fig. 7). In addition, ζ-potential measurements in this range showed that BP100 brings the LUV charge to approximate electroneutrality at saturation, confirming the prediction based on the saturation proportion (Fig. 8). This effect is certainly favoring vesicle aggregation by canceling the electrostatic repulsion between them.

Partition, saturation, and prediction of MIC

During our recent investigations, we have found that minimum inhibitory concentration, MIC, and saturation can be correlated for peptides, such as omiganan (53). For this peptide, MICs were found to be similar to the peptide concentration needed to reach the saturation state, reflecting the existence of possible saturation-triggered antimicrobial mechanisms. Since findings from BP100-membrane interaction studies also suggest that membrane saturation is important for the activity of this peptide, we examined whether the results obtained are in agreement with the experimental MIC values.

As previously reported (53), under typical bacterial titers and using the MIC as the total peptide concentration, the membrane-bound peptide concentration ($[P]_L$) is given by $K_p \times$ MIC. On the other hand, σ can be determined as $[P]_L \times \gamma_L$. Combining both expressions, the MIC can be readily calculated as $\text{MIC} = \sigma/(K_p \times \gamma_L)$. Using the obtained σ (0.118) and K_p (3.08×10^4 or 8.41×10^4, from the partition and saturation studies, respectively) values, and considering γ_L as 0.763 M^{-1} (50), this equation leads to MIC values of 2 or 5 μM, depending on the selected K_p. These values are consistent with the antibacterial activity displayed by BP100, which inhibited in vitro growth of the bacteria *E. amylovora*, *X. vesicatoria*, and *P. syringae* at 2.5–7.5 μM (38). In addition to validating the obtained values for K_p and σ, these results strongly support the correlation between these constants and the MIC, evidencing the importance of the saturation point in the mode of action of this peptide.

Physiological significance of saturation-induced activity

The obtained results clearly point toward the occurrence of different membrane-disrupting events as saturation is reached. Given the plausible correlation between saturation and the onset of antibacterial activity of BP100, an extrapolation of these events to an in vivo setting was sought.

Surface charge neutralization at saturation was found to be an important occurrence, triggering the observed vesicle aggregation, and probably being responsible for the destabilization that led to an increase in membrane permeabilization, as leakage enhancement correlates with vesicle aggregation. The bacterial metabolism will certainly be sensitive to the neutralization-induced loss of the membrane surface potential, as this will disturb the charge environment of the outer leaflet proteins. The observed coupled permeabilization (if not lysis) entails even further damage to the cell, namely the dissipation of the transmembrane potential which, among other effects, will halt ATP synthesis. Vesicle aggregation may not have a parallel in vivo, as bacterial membranes have additional layers of protection (LPS, peptidoglycan, capsule) preventing direct membrane contact between bacteria; its occurrence in vitro does, however, stress the importance of the surface potential for membrane stability. The observed translocation could be a consequence of the permeabilization or can be an independent event; either way, direct interaction with cytoplasmic targets is yet another possible cause of bacterial death.

Effects of BP100 exposure on cell viability

The experimental results from our studies show cytotoxic effects in the cultured mammalian fibroblast cells at

concentrations of BP100 above 50–60 μM (Fig. 9). This is in good agreement with similar findings in human erythrocytes (38), where an increased release of hemoglobin was observed above 150 μM. Although the membrane integrity in our V79 cells was affected at lower concentrations (IC_{50} = 51.1 μM), it probably just reflects the different cell lines: different sensibilities to antibacterial peptides were also found between human erythrocytes and mammalian COS-7 kidney cells (65), and might indicate a better resistance of the human erythrocytes to this class of peptides (78). Results from the MTT assay (Fig. 9) demonstrated changes in the metabolic activity of mitochondria V79 cells, as the dehydrogenase enzymes started to be less active to convert the yellow water-soluble salt into insoluble formazan crystals at increasing peptide concentrations. Whether this means that there is a direct action on the mitochondria, or indirect loss of mitochondrial activity, cannot be ascertained without further investigation.

A successful application of this peptide as a bactericide demands a high therapeutic index, i.e., a high antimicrobial activity but low cytotoxicity. The high antimicrobial potency (MIC = 2.5–7.5 μM) and relatively low cytotoxicity in human erythrocytes (38) reveals promising values for BP100. Although cytotoxic effects were observed in V79 cells at peptide concentrations above 50–60 μM, this range is still far above the anticipated antimicrobial application levels.

Cytotoxicity against mammalian models is reached at a concentration higher than the MIC by roughly the same proportion that K_p values toward mammalian model bilayers are lower than toward bacterial ones. This observation suggests that cell killing may be dependent on a constant local membrane-bound concentration, independently of the considered lipid system.

CONCLUSION

This work clearly points out a correlation between high membrane concentrations (possibly even saturation) of BP100 and bacterial death. Three different potential causes of activity of AMP, i.e., charge neutralization, permeabilization, and translocation, were identified. In addition, a concentration dependence of the killing phenomena, in bacteria and in mammalian cells, was suggested. While the exact mechanism of action of the peptide may remain elusive in vivo, and depend on the peptide and bacteria species, our findings unravel the bases of the closely coupled occurrence of those causes, as experimentally observed by Friedrich et al. (79).

Fundação para a Ciência e a Tecnologia (Portugal) is acknowledged for a grant to M.N.M. (No. SFRH/BD/24778/2005). R.F. is the recipient of a predoctoral fellowship from the Ministry of Education and Science of Spain. This work was supported by grants from the Ministry of Education and Science of Spain (No. AGL2006-13564/AGR), and from the Catalan Government (No. 2005SGR00275).

REFERENCES

1. Brogden, K. A., M. Ackermann, P. B. McCray, Jr., and B. F. Tack. 2003. Antimicrobial peptides in animals and their role in host defenses. *Int. J. Antimicrob. Agents.* 22:465–478.
2. Bulet, P., R. Stocklin, and L. Menin. 2004. Antimicrobial peptides: from invertebrates to vertebrates. *Immunol. Rev.* 198:169–184.
3. Ganz, T., and R. I. Lehrer. 1998. Antimicrobial peptides of vertebrates. *Curr. Opin. Immunol.* 10:41–44.
4. Garcia-Olmedo, F., A. Molina, J. M. Alamillo, and P. Rodriguez-Palenzuela. 1998. Plant defense peptides. *Biopolymers.* 47:479–491.
5. Otvos, L., Jr. 2000. Antibacterial peptides isolated from insects. *J. Pept. Sci.* 6:497–511.
6. Zasloff, M. 2002. Antimicrobial peptides of multicellular organisms. *Nature.* 415:389–395.
7. Broekaert, W. F., B. P. A. Cammue, M. F. C. DeBolle, K. Thevissen, G. W. DeSamblanx, et al. 1997. Antimicrobial peptides from plants. *Crit. Rev. Plant Sci.* 16:297–323.
8. Hancock, R. E., and A. Patrzykat. 2002. Clinical development of cationic antimicrobial peptides: from natural to novel antibiotics. *Curr. Drug Targets Infect. Disord.* 2:79–83.
9. Hancock, R. E., and H. G. Sahl. 2006. Antimicrobial and host-defense peptides as new anti-infective therapeutic strategies. *Nat. Biotechnol.* 24:1551–1557.
10. Boman, H. G. 2003. Antibacterial peptides: basic facts and emerging concepts. *J. Intern. Med.* 254:197–215.
11. Hancock, R. E. 2001. Cationic peptides: effectors in innate immunity and novel antimicrobials. *Lancet Infect. Dis.* 1:156–164.
12. Jenssen, H., P. Hamill, and R. E. Hancock. 2006. Peptide antimicrobial agents. *Clin. Microbiol. Rev.* 19:491–511.
13. Montesinos, E. 2007. Antimicrobial peptides and plant disease control. *FEMS Microbiol. Lett.* 270:1–11.
14. Zhang, L., and T. J. Falla. 2006. Antimicrobial peptides: therapeutic potential. *Expert Opin. Pharmacother.* 7:653–663.
15. Brogden, K. A. 2005. Antimicrobial peptides: pore formers or metabolic inhibitors in bacteria? Nat. Rev. Microbiol. 3:238–250.
16. Yeaman, M. R., and N. Y. Yount. 2003. Mechanisms of antimicrobial peptide action and resistance. *Pharmacol. Rev.* 55:27–55.
17. Perron, G. G., M. Zasloff, and G. Bell. 2006. Experimental evolution of resistance to an antimicrobial peptide. *Proc. Biol. Sci.* 273:251–256.
18. Shai, Y. 2002. Mode of action of membrane active antimicrobial peptides. *Biopolymers.* 66:236–248.
19. Tossi, A., L. Sandri, and A. Giangaspero. 2000. Amphipathic, α-helical antimicrobial peptides. *Biopolymers.* 55:4–30.
20. Bechinger, B. 2004. Structure and function of membrane-lytic peptides. *Crit. Rev. Plant Sci.* 23:271–292.
21. Yang, L., T. A. Harroun, T. M. Weiss, L. Ding, and H. W. Huang. 2001. Barrel-stave model or toroidal model? A case study on melittin pores. *Biophys. J.* 81:1475–1485.
22. Shai, Y. 1999. Mechanism of the binding, insertion and destabilization of phospholipid bilayer membranes by α-helical antimicrobial and cell non-selective membrane-lytic peptides. *Biochim. Biophys. Acta.* 1462:55–70.
23. Kobayashi, S., A. Chikushi, S. Tougu, Y. Imura, M. Nishida, et al. 2004. Membrane translocation mechanism of the antimicrobial peptide buforin 2. *Biochemistry.* 43:15610–15616.
24. Hultmark, D., A. Engstrom, H. Bennich, R. Kapur, and H. G. Boman. 1982. Insect immunity: isolation and structure of cecropin D and four minor antibacterial components from *Cecropia pupae*. *Eur. J. Biochem.* 127:207–217.
25. Hultmark, D., H. Steiner, T. Rasmuson, and H. G. Boman. 1980. Insect immunity. Purification and properties of three inducible bactericidal proteins from hemolymph of immunized pupae of *Hyalophora cecropia*. *Eur. J. Biochem.* 106:7–16.

26. Sato, H., and J. B. Feix. 2006. Peptide-membrane interactions and mechanisms of membrane destruction by amphipathic α-helical antimicrobial peptides. *Biochim. Biophys. Acta.* 1758:1245–1256.
27. Andreu, D., R. B. Merrifield, H. Steiner, and H. G. Boman. 1983. Solid-phase synthesis of cecropin A and related peptides. *Proc. Natl. Acad. Sci. USA.* 80:6475–6479.
28. Steiner, H., D. Hultmark, A. Engstrom, H. Bennich, and H. G. Boman. 1981. Sequence and specificity of two antibacterial proteins involved in insect immunity. *Nature.* 292:246–248.
29. Alberola, J., A. Rodriguez, O. Francino, X. Roura, L. Rivas, et al. 2004. Safety and efficacy of antimicrobial peptides against naturally acquired *Leishmaniasis*. *Antimicrob. Agents Chemother.* 48:641–643.
30. Andreu, D., J. Ubach, A. Boman, B. Wahlin, D. Wade, et al. 1992. Shortened cecropin A-melittin hybrids. Significant size reduction retains potent antibiotic activity. *FEBS Lett.* 296:190–194.
31. Boman, H. G., D. Wade, I. A. Boman, B. Wahlin, and R. B. Merrifield. 1989. Antibacterial and antimalarial properties of peptides that are cecropin-melittin hybrids. *FEBS Lett.* 259:103–106.
32. Cavallarin, L., D. Andreu, and B. San Segundo. 1998. Cecropin A-derived peptides are potent inhibitors of fungal plant pathogens. *Mol. Plant Microbe Interact.* 11:218–227.
33. Chicharro, C., C. Granata, R. Lozano, D. Andreu, and L. Rivas. 2001. N-terminal fatty acid substitution increases the leishmanicidal activity of CA(1–7)M(2–9), a cecropin-melittin hybrid peptide. *Antimicrob. Agents Chemother.* 45:2441–2449.
34. Giacometti, A., O. Cirioni, W. Kamysz, G. D'Amato, C. Silvestri, et al. 2004. In vitro activity and killing effect of the synthetic hybrid cecropin A-melittin peptide CA(1–7)M(2–9)NH_2 on methicillin-resistant nosocomial isolates of *Staphylococcus aureus* and interactions with clinically used antibiotics. *Diagn. Microbiol. Infect. Dis.* 49:197–200.
35. Lee, D. G., Y. Park, I. Jin, K. S. Hahm, H. H. Lee, et al. 2004. Structure-antiviral activity relationships of cecropin A-magainin 2 hybrid peptide and its analogues. *J. Pept. Sci.* 10:298–303.
36. Wade, D., D. Andreu, S. A. Mitchell, A. M. Silveira, A. Boman, et al. 1992. Antibacterial peptides designed as analogs or hybrids of cecropins and melittin. *Int. J. Pept. Protein Res.* 40:429–436.
37. Ali, G. S., and A. S. Reddy. 2000. Inhibition of fungal and bacterial plant pathogens by synthetic peptides: in vitro growth inhibition, interaction between peptides and inhibition of disease progression. *Mol. Plant Microbe Interact.* 13:847–859.
38. Badosa, E., R. Ferre, M. Planas, L. Feliu, E. Besalu, et al. 2007. A library of linear undecapeptides with bactericidal activity against phytopathogenic bacteria. *Peptides.* 28:2276–2285.
39. Bardají, E., E. Montesinos, E. Badosa, L. Feliu, M. Planas, et al. 2006. Antimicrobial linear peptides. P200601098; priority date: April 28th, 2006; Oficina Española de Patentes y Marcas, Spain.
40. Ferre, R., E. Badosa, L. Feliu, M. Planas, E. Montesinos, et al. 2006. Inhibition of plant-pathogenic bacteria by short synthetic cecropin A-melittin hybrid peptides. *Appl. Environ. Microbiol.* 72:3302–3308.
41. Christensen, B., J. Fink, R. B. Merrifield, and D. Mauzerall. 1988. Channel-forming properties of cecropins and related model compounds incorporated into planar lipid membranes. *Proc. Natl. Acad. Sci. USA.* 85:5072–5076.
42. Ladokhin, A. S., M. E. Selsted, and S. H. White. 1997. Sizing membrane pores in lipid vesicles by leakage of co-encapsulated markers: pore formation by melittin. *Biophys. J.* 72:1762–1766.
43. Ladokhin, A. S., and S. H. White. 2001. "Detergent-like" permeabilization of anionic lipid vesicles by melittin. *Biochim. Biophys. Acta.* 1514:253–260.
44. Silvestro, L., K. Gupta, J. N. Weiser, and P. H. Axelsen. 1997. The concentration-dependent membrane activity of cecropin A. *Biochemistry.* 36:11452–11460.
45. Steiner, H., D. Andreu, and R. B. Merrifield. 1988. Binding and action of cecropin and cecropin analogues: antibacterial peptides from insects. *Biochim. Biophys. Acta.* 939:260–266.
46. Mayer, L. D., M. J. Hope, and P. R. Cullis. 1986. Vesicles of variable sizes produced by a rapid extrusion procedure. *Biochim. Biophys. Acta.* 858:161–168.
47. Santos, N. C., and M. A. Castanho. 2002. Fluorescence spectroscopy methodologies on the study of proteins and peptides. On the 150th anniversary of protein fluorescence. *Trends Appl. Spectrosc.* 4:113–125.
48. Coutinho, A., and M. Prieto. 1993. Ribonuclease-T_1 and alcohol-dehydrogenase fluorescence quenching by acrylamide—a laboratory experiment for undergraduate students. *J. Chem. Educ.* 70:425–428.
49. Santos, N. C., M. Prieto, and M. A. Castanho. 2003. Quantifying molecular partition into model systems of biomembranes: an emphasis on optical spectroscopic methods. *Biochim. Biophys. Acta.* 1612:123–135.
50. Nagle, J. F., and M. C. Wiener. 1988. Structure of fully hydrated bilayer dispersions. *Biochim. Biophys. Acta.* 942:1–10.
51. Ladokhin, A. S., S. Jayasinghe, and S. H. White. 2000. How to measure and analyze tryptophan fluorescence in membranes properly, and why bother? Anal. Biochem. 285:235–245.
52. Wenk, M. R., and J. Seelig. 1998. Magainin 2 amide interaction with lipid membranes: calorimetric detection of peptide binding and pore formation. *Biochemistry.* 37:3909–3916.
53. Melo, M. N., and M. A. Castanho. 2007. Omiganan interaction with bacterial membranes and cell wall models. Assigning a biological role to saturation. *Biochim. Biophys. Acta.* 1768:1277–1290.
54. Chalpin, D. B., and A. M. Kleinfeld. 1983. Interaction of fluorescence quenchers with the *n*-(9-anthroyloxy) fatty acid membrane probes. *Biochim. Biophys. Acta.* 731:465–474.
55. Fernandes, M. X., J. Garcia de la Torre, and M. A. Castanho. 2002. Joint determination by Brownian dynamics and fluorescence quenching of the in-depth location profile of biomolecules in membranes. *Anal. Biochem.* 307:1–12.
56. Chattopadhyay, A., and E. London. 1988. Spectroscopic and ionization properties of *N*-(7-nitrobenz-2-oxa-1,3-diazol-4-yl)-labeled lipids in model membranes. *Biochim. Biophys. Acta.* 938:24–34.
57. Pokorny, A., and P. F. Almeida. 2004. Kinetics of dye efflux and lipid flip-flop induced by δ-lysin in phosphatidylcholine vesicles and the mechanism of graded release by amphipathic, α-helical peptides. *Biochemistry.* 43:8846–8857.
58. Lakowicz, J. R. 1999. Quenching of fluorescence. Principles of Fluorescence Spectroscopy, 2nd Ed. Kluwer Academic/Plenum, New York; London.
59. Gregory, S. M., A. Cavenaugh, V. Journigan, A. Pokorny, and P. F. Almeida. 2008. A quantitative model for the all-or-none permeabilization of phospholipid vesicles by the antimicrobial peptide cecropin A. *Biophys. J.* 94:1667–1680.
60. Rueff, J., C. Chiapella, J. K. Chipman, F. Darroudi, I. D. Silva, et al. 1996. Development and validation of alternative metabolic systems for mutagenicity testing in short-term assays. *Mutat. Res.* 353:151–176.
61. Zucco, F., I. De Angelis, and A. Stammati. 1998. Cellular models for in vitro toxicity testing. *In* Animal Cell Culture Techniques. M. Clynes, editor. Springer, Berlin; London.
62. Mickuviene, I., V. Kirveliene, and B. Juodka. 2004. Experimental survey of non-clonogenic viability assays for adherent cells in vitro. *Toxicol. In Vitro.* 18:639–648.
63. Mitchell, J. B. 1988. Potential applicability of nonclonogenic measurements to clinical oncology. *Radiat. Res.* 114:401–414.
64. Brink, C. B., A. Pretorius, B. P. van Niekerk, D. W. Oliver, and D. P. Venter. 2008. Studies on cellular resilience and adaptation following acute and repetitive exposure to ozone in cultured human epithelial (HeLa) cells. *Redox Rep.* 13:87–100.
65. Cudic, M., C. V. Lockatell, D. E. Johnson, and L. Otvos, Jr. 2003. In vitro and in vivo activity of an antibacterial peptide analog against uropathogens. *Peptides.* 24:807–820.
66. Scholze, M., W. Boedeker, M. Faust, T. Backhaus, R. Altenburger, et al. 2001. A general best-fit method for concentration-response curves and the estimation of low-effect concentrations. *Environ. Toxicol. Chem.* 20:448–457.

67. Zhao, H., R. Sood, A. Jutila, S. Bose, G. Fimland, et al. 2006. Interaction of the antimicrobial peptide pheromone Plantaricin A with model membranes: implications for a novel mechanism of action. *Biochim. Biophys. Acta.* 1758:1461–1474.

68. Huang, H. W. 2000. Action of antimicrobial peptides: two-state model. *Biochemistry.* 39:8347–8352.

69. Huang, H. W. 2006. Molecular mechanism of antimicrobial peptides: the origin of cooperativity. *Biochim. Biophys. Acta.* 1758:1292–1302.

70. Segrest, J. P., H. De Loof, J. G. Dohlman, C. G. Brouillette, and G. M. Anantharamaiah. 1990. Amphipathic helix motif: classes and properties. *Proteins.* 8:103–117.

71. Kandasamy, S. K., and R. G. Larson. 2006. Molecular dynamics simulations of model trans-membrane peptides in lipid bilayers: a systematic investigation of hydrophobic mismatch. *Biophys. J.* 90:2326–2343.

72. Abrunhosa, F., S. Faria, P. Gomes, I. Tomaz, J. C. Pessoa, et al. 2005. Interaction and lipid-induced conformation of two cecropin-melittin hybrid peptides depend on peptide and membrane composition. *J. Phys. Chem. B.* 109:17311–17319.

73. Juvvadi, P., S. Vunnam, E. L. Merrifield, H. G. Boman, and R. B. Merrifield. 1996. Hydrophobic effects on antibacterial and channel-forming properties of cecropin A-melittin hybrids. *J. Pept. Sci.* 2:223–232.

74. Rathinakumar, R., and W. C. Wimley. 2008. Biomolecular engineering by combinatorial design and high-throughput screening: small, soluble peptides that permeabilize membranes. *J. Am. Chem. Soc.* 130:9849–9858.

75. Henriques, S. T., M. N. Melo, and M. A. Castanho. 2007. How to address CPP and AMP translocation? Methods to detect and quantify peptide internalization in vitro and in vivo. (Review). *Mol. Membr. Biol.* 24:173–184.

76. Matsuzaki, K., S. Yoneyama, O. Murase, and K. Miyajima. 1996. Transbilayer transport of ions and lipids coupled with mastoparan X translocation. *Biochemistry.* 35:8450–8456.

77. Persson, D., P. E. Thoren, and B. Norden. 2001. Penetratin-induced aggregation and subsequent dissociation of negatively charged phospholipid vesicles. *FEBS Lett.* 505:307–312.

78. Otvos, L., Jr., K. Bokonyi, I. Varga, B. I. Otvos, R. Hoffmann, et al. 2000. Insect peptides with improved protease-resistance protect mice against bacterial infection. *Protein Sci.* 9:742–749.

79. Friedrich, C. L., D. Moyles, T. J. Beveridge, and R. E. Hancock. 2000. Antibacterial action of structurally diverse cationic peptides on Gram-positive bacteria. *Antimicrob. Agents Chemother.* 44:2086–2092.

My work and the AMPs

Work with omiganan and BP100 prompted the hypothesis that saturation, or otherwise high membrane coverage, is somehow a requirement for AMP activity in a general sense. But, from a functional perspective, why should it be so? What is there that is intrinsically disruptive in the full coverage of a bacterium? One can imagine several possible scenarios, even ones in which bacteria become smothered by the peptide molecules, which then clog any metabolite exchange routes in and out of the cell.

My view, however, after reading some of the work by Huey Huang on threshold effects,[49,50] is that a high degree of membrane coverage is needed to overcome the energy barrier involved in bringing together the bound peptide molecules — this makes sense since the peptides are heavily charged and likely to drift apart if there is room to. In turn, peptide proximity increasingly destabilizes the bilayer: bound peptide molecules can cause a local membrane thinning,* an effect that is amplified, potentially to the point of disruption, when several molecules are forced together.[50] This explanation has the advantage of not requiring the assumption of any kind of specific peptide-peptide interactions in the membrane.

Under this perspective, the role of surface charge is that of the driving force that brings peptide molecules to the membrane even when the already bound molecules have to lie close to each other. Charge neutralization marks the limit upon which this force ceases to act. Rafael remarked that the most charged peptides in the library he developed were not

*Membrane insertion of peptides, even if shallow, will cause separation of the phospholipid molecules; as a consequence, either the involved acyl chains spread out and flatten to remain in contact with each other, or the phospholipids from the opposing leaflet draw closer to fill in the gap, or both.[50] In any case, a local thinning of the bilayer is expected.

necessarily the most active; that may be due to the fact that in those cases the bacterial surface charge was neutralized before a high enough bound concentration of peptide was reached. Interesting possibilities arise from these considerations, namely that peptide action is ultimately dictated by their charge, their membrane interaction properties, and their size.

In addition to this, the event of charge neutralization is also potentially disruptive by itself: the complex environment of the membrane, where important metabolic processes take place, will definitely be perturbed by the loss of surface charge and the associated potentials, which will certainly contribute to bacterial death.

* * *

A point I have not yet addressed is that of the model membrane composition. In my work with both peptides highly anionic phospholipid mixtures have been used as models for bacterial membranes — 2 : 1 POPG : POPC and even 4 : 1 POPG : POPC. Reported values[51] for the *in vivo* membrane content of anionic and phospholipids are lower than those I used, lying between 30% and 40% — 3 : 7 is an anionic : zwitterionic phospholipid ratio that seems to be growing in acceptance as a standard for biophysical studies.[52–54] The reason why I insisted on the use of highly anionic models is of a practical nature: in less charged systems deviations at high bound peptide concentrations simply become too faint for detection. In the end, some physiological significance was traded off for insight into the threshold events of the peptides' action. Of course, departure from physiological conditions may invalidate this insight. However, if the saturation-neutralization correlation holds for less charged models then the effect of using highly anionic membranes amounts to having a proportionally higher P:L ratio at saturation: for omiganan and BP100 the expected saturation proportions at a 3 : 7 anionic : zwitterionic ratio are, respectively, 1 : 16.7 and 1 : 20. These values still correspond to relatively high concentrations and to high degrees of membrane coverage. The overall conclusions of the work can thus be shown to withstand the use of a less-than-optimal membrane model system.

Lastly, the possibility that the activity of many AMPs depends on conditions at, or close to, saturation, is indeed corroborated by data published on several peptides. Miguel, Rafael and I published a review (Article V, included ahead) on how our hypothesis successfully fits those data. Ultimately, I hope that more than reporting a finished research our work, reflected on that review, conveys the notion that there is now a void in AMP characterization that must be filled.

End of Part I

Part II

Methods and Models

The other side

I have honored the commitment made in the thesis' title and devoted Part I entirely to my research on AMPs. Now, I will recount my PhD work from an entirely distinct perspective. Much like some points in the previous part, where omiganan and BP100 were regarded not as the fulcrum of the research but as means to reach a more encompassing knowledge on AMPs, the following text will describe how the two were used to develop methods applicable beyond their immediate study.

The emergence of this side of my work was not specifically planned for at the beginning of my PhD. Rather, I developed along the way — at first unconsciously — a preference for the intellectual challenge in the devising of new means to experimentally and mathematically wring information from the studied systems.

The creation of new methods impacted more than just my work, as I began assisting my colleagues in applying them to their peptides. This was a very rewarding aspect because of both the recognition and the opportunity to contribute to other people's projects.

I am deeply thankful to Miguel for having let me foray into the methodological side of research, instead of limiting my work to the application of established protocols. Throughout this process I always felt trusted by him and this enabled me to become confident on the abilities I was acquiring. I was extremely fortunate to begin my career under the supervision of such a scientist and professor.

4. Partition

Much of my work revolves around the notion of partition, which is nothing more than the application of the concept of chemical equilibrium to the distribution of a solute between immiscible phases. According to the view we follow at the lab, the same principles can be used to interpret the interaction of peptide molecules with the phospholipid bilayers of vesicles. It does take a leap of faith to consider the thin bilayers to be equivalent to spherical shells of an immiscible liquid phase but I believe it to be a short leap compared with other approaches where specific lipid-peptide binding stoichiometries are assumed.

4.1 The partition constant

The formalism of partition is rooted on thermodynamic grounds and provides an equilibrium constant with which one can characterize a system. This constant is termed 'partition constant' and the definition that I will follow is based on the studies Marcelin Berthelot and Emile Jungfleisch;[55,56] and later Walther Nernst;[57] carried out in the 19th century. According to their work, the ratio, at equilibrium, of the concentrations of a solute in each of two immiscible phases is a constant; these phases are here realized as a lipidic one — the vesicles' membranes — and an aqueous one — the bulk phase, the peptide being the solute:

$$K_p = \frac{[P]_L}{[P]_W} \tag{4.1}$$

K_p is the partition constant of the peptide for the membrane-water system. $[P]_L$ and $[P]_W$ are the concentration of peptide in the lipidic and aqueous

phases, respectively. Note that these are local concentration in each phase, not concentrations over the whole system volume.

The physical meaning of K_p is quite easy to understand from Equation 4.1. The partition constant reports how much more, or less, concentrated the membrane-bound peptide gets relative to the peptide in the aqueous phase. AMPs have K_p values in the order of 10^4 to 10^5 towards vesicles that mimic bacterial membranes (see Article V for some examples), which means the peptides get 10^4- to 10^5-fold more concentrated in those bilayers than in the bulk aqueous phase.

By manipulation of Equation 4.1 we arrive at another important relationship:

$$X_L = \frac{K_p \gamma_L [L]}{1 + K_p \gamma_L [L]} \tag{4.2}$$

X_L is the membrane-bound peptide fraction, or the ratio of the lipid-bound peptide molecules over the total peptide; $[L]$ is the global phospholipid concentration, obtained after approximating the aqueous phase volume as the total system volume — an acceptable shortcut even for the most concentrated vesicle suspensions used in studies with peptides. Equation 4.2 establishes a bridge between K_p, the bound peptide fraction, and the lipid concentration, which is an independent variable of the system. As such, Equation 4.2 is frequently at the core of methods to experimentally determine K_p. The equation also emphasizes an important property of peptide-membrane interaction: for a given lipid concentration the bound and unbound fractions are constant and *do not depend on the global amount of peptide*. The consequence is that if we increase the amount of peptide (all other variables remaining constant) in a water-vesicle-peptide system, the number of peptide molecules in both phases will rise proportionally to the increase, and so will the local concentrations. These implications will be explored later on.

Also of importance are the conditions for which Equation 4.1 holds. Nernst pointed out that Equation 4.1 was only valid so long as the solute under consideration does not establish significant secondary equilibria in either phase — for example by ionization, oligomerization or even

change of conformation.[57] When such equilibria do take place each species must be considered as having a K_p value of its own. For simplicity, AMP-membrane binding studies do not usually take these aspects into consideration, implicitly assuming that peptide molecules either exist in a single ionization state or that all different states will partition with the same affinity. Changes in peptide conformation or multimerization — usually taking place in the membrane — are dealt with differently: in my work the assumption that only one of the forms of the peptide is able to partition in and out of the membrane yielded good results (see Section 5.3), but in other cases that might not be valid. A last requirement of Equation 4.1, not explicitly stated in the seminal works of Berthelot, Jungfleisch and Nernst, is that both phases are ideally dilute solutions (meaning that solute-solute interactions are negligible), and therefore that the chemical potential of the solute changes linearly with the logarithm of its molar fraction.[58] It is only then that the partition constant really is constant.* As will be seen later, violation of the precondition of ideally dilute solutions led to very interesting results.

4.2 Determining K_p

The methods for experimentally determining partition constants were, like the formalism of partition, the basis of much of my work. It is thus important that I describe the general approach for obtaining K_p even though I had no actual role in its design.

At the lab we traditionally use fluorescence spectroscopy to measure partition constants. This is well suited to study peptides, which are frequently natively fluorescent due to the presence of tryptophan, tyrosine, or phenylalanine residues. Fluorescence can be used to track the binding of the peptides because the fluorescent moieties are sensitive to the polarity

*The thermodynamic basis of the partition equilibrium further states that it is the ratio of the solute molar fractions in each phase that is constant, not the ratio of its molarities.[58] Conversion to a concentration ratio constant is also based on the assumption of ideally dilute solutions (see the Supplementary Material of Article VI for an assessment of the error introduced when that assumption is not valid); the two constants, however, are not equivalent.[31]

of the environment the peptide is in: as the peptide binds the membrane and comes into contact with the apolar portion of the bilayer there will be a solvent effect that destabilizes the excited state, increasing its energy (the slow-moving acyl chains cannot reorganize as fast as water in response to the change in the molecule's dipole moment upon excitation). Interaction with the membrane also means the fluorescent groups are less likely to be exposed to collisions by ions or the polar water molecules, which prolongs their fluorescence lifetime and increases their quantum yield. Thus, the fluorescence emitted by the peptide is expected, as a result of binding, to increase in intensity and to shift to shorter wavelengths (the shift being usually only observed with tryptophan). Other less common cases, such as a reduction in the fluorescence intensity, are possible — imagine, for example, a fluorescence residue that sits in a hydrophobic pocket of a peptide or protein and that becomes exposed after a conformation change that takes place in the membrane. To the determination of K_p, however, all is needed is that there is a measurable difference in the fluorescence emission of the peptide upon interaction with the membrane.

The fact that the populations of peptide in each phase have distinct fluorescent behavior allows the whole ensemble to be observed simultaneously; there is no need to physically separate the phases to proceed to the quantification of the peptide in each one. The global fluorescence intensity* I is given by:

$$I = X_L I_L + X_W I_W \tag{4.3}$$

I_L and I_W are the fluorescence intensities the peptide would display if all its molecules were in either the lipidic or the aqueous phase; X_W is the water counterpart of X_L (because only two phases are assumed $X_W = 1 - X_L$). Equation 4.3 simply states that the observed fluorescence intensity is the sum of the maximum intensities from the two phases, weighed by the fraction of peptide in each. Equation 4.2 can be combined

*It must be noted that the method involves fluorescence intensities but not wavelengths, which means that the frequent spectral shifts are not accounted for. To avoid the introduction of an error the area of the whole spectrum should be taken for the fluorescence intensity, instead of the value at a single wavelength.

with Equation 4.3 to link, through K_p, the observable (the fluorescence intensity) to the independent variable (the lipid concentration):

$$I = \frac{I_W + K_p \gamma_L [L] I_L}{1 + K_p \gamma_L [L]} \tag{4.4}$$

Equation 4.4 is appropriate for experimental determination of K_p. However, besides K_p, I_L is also an unknown parameter. This means that at least two data points at different values of $[L]$ must be collected (I_W can be obtained experimentally and $0.76\,\text{M}^{-1}$ was taken from reference 59 as an approximation of γ_L for fluid membranes). The preferred setup at the lab involves the titration of a peptide solution with vesicles. This has several advantages, namely by saving peptide and by including the measurement of I_W, which is the point before any addition of lipid.

Still, the fact that Equation 4.4 depends on I_W and I_L makes the data points also dependent on the amount of peptide. By representing the normalization of Equation 4.4 to I_W the points become robust to the peptide concentration and the results of separate titrations will be superimposable, even if the peptide concentrations differ:

$$\frac{I}{I_W} = \frac{1 + K_p \gamma_L [L] \frac{I_L}{I_W}}{1 + K_p \gamma_L [L]} \tag{4.5}$$

Normalization to I_W also transforms I_L — which has little meaning on its own — in the I_L/I_W ratio. This is a much more informative value that reflects the change of the fluorescence quantum yield of the peptide upon binding the membrane. Although I haven't frequently done so, the I_L/I_W ratio can be used, along K_p, to characterize a peptide-membrane interaction.

The extraction of K_p from titration data points can be done in many ways, but the most common is to directly perform a non-linear fit of Equation 4.5 to the data. According to Equation 4.5 the dependence of I/I_W on $[L]$ is translated into a hyperbolic-like curve (see Figure 2.1), unsurprisingly called a partition curve. The shape of this curve results from the increase in fluorescence of the peptide as the adding of vesicles

drives more and more molecules to the lipidic phase. An asymptotic plateau (I_L/I_W) is approached when most of the peptide is already bound; there is no more peptide available to bind the membrane even if much more lipid is added.

Another aspect of the titration process is that for every addition of lipid (disregarding any changes in volume) and consequent binding of peptide molecules, there will be a decrease in their bulk phase concentration. From the definition of K_p in Equation 4.1 we can see that such a reduction of $[P]_W$ must be accompanied by a proportional drop in $[P]_L$. Thus, adding lipid to a system will lower the peptide concentration of *both* phases. A consequence of this fact is that the peptide will be most concentrated in the lipidic phase when $[L] \to 0$. This means that partition curves start out with high local peptide concentrations in the membrane, which are then gradually diluted as $[L]$ increases.

* * *

Up to this point I have addressed the long established theoretical and experimental bases of the partition formalism as it is adapted to the characterization of peptide-membrane interactions. From here on I will describe mostly those methods in whose development I was involved.

4.3 Alternative methods

A different way to obtain the partition constant from peptide-lipid systems was devised by Miguel (I admit that my contribution here amounted to the validation of Miguel's conclusions using my data). It is a method based on the light-scattering measurements of the ζ-potential of peptide-vesicle mixtures. I include this description here for consistency with the chapter's contents, but rather anachronistically as the actual development of the idea took place well into the last year of my PhD.

The ζ-potential can be understood as the susceptibility of a particle to be electrophoretically displaced. It reflects the global surface charge of that particle, taking into account the exchange of each counterion — the

tighter a counterion binds the particle, the more effectively will it mask its charges. Negative potentials correspond to anionic surfaces and positive potentials to cationic ones.

ζ-potential measurements are frequently used to assess the importance of electrostatic interactions in the binding of peptides to charged vesicles. In this case, the particles in suspension whose ζ-potential is measured are the vesicles as their size makes them much better scatterers than the peptide molecules. Measurements are usually carried out for several concentrations of peptide, while the vesicles' concentration is kept constant.

Vesicles containing anionic phospholipids typically display a markedly negative ζ-potential that increases with the peptide concentration (this description assumes the most common case of the interaction of a cationic peptide with an anionic vesicle) until a plateau is reached close to 0 mV. Miguel set out to extract partition constants from this kind of data. I, however, was skeptical: there is not enough information in a titration of lipid with peptide to allow K_p determination from fluorescence measurements. This is so mainly because there is a second unknown in the system, I_L. I thought the same would apply to ζ-potential but Miguel proved me wrong. In these experiments we know the charge of the peptide and the charge and proportion of the anionic phospholipids; there is no I_L or analogous unknown parameter involved.

From the vesicles' potential in the presence and absence of peptide a relative reduction of the surface charge can be calculated. Miguel pointed out that this reduction (in absolute value) reflects the proportion of anionic phospholipid charges that is neutralized. This is translated by Equation 4.6:

$$\left|\frac{\Delta\zeta}{\zeta_0}\right| = \frac{n_{PL^-_{\text{neutralized}}}}{n_{PL^-_{\text{total}}}} \tag{4.6}$$

where $\frac{\Delta\zeta}{\zeta_0}$ is the relative reduction in potential (as a function of the global peptide concentration, $[P]$), $n_{PL^-_{\text{neutralized}}}$ is the number of anionic phospholipids whose charge has been masked, and $n_{PL^-_{\text{total}}}$ is the total number of anionic phospholipids.

If we make the (somewhat risky, but necessary) assumption that each cationic charge of a bound peptide molecule completely masks one of the phospholipids' anionic charges, we can convert $n_{PL^-_{\text{neutralized}}}$ into the number of bound peptide molecules ($n_{\text{peptide},L}$):

$$n_{PL^-_{\text{neutralized}}} = n_{\text{peptide},L} \cdot z_{\text{peptide}} \tag{4.7}$$

where z_{peptide} is the global charge per peptide, in absolute value. The denominator of Equation 4.6 can be replaced by the total amount of phospholipids (n_L) multiplied by the proportion of anionic ones (f_{PL^-}); the resulting expression can be readily transformed to include X_L (dividing numerator and denominator by $[P]$):

$$\left|\frac{\Delta\zeta}{\zeta_0}\right| = \frac{n_{\text{peptide},L} \cdot z_{\text{peptide}}}{f_{PL^-} \cdot n_L} = \frac{X_L \cdot z_{\text{peptide}}}{f_{PL^-} \cdot [L]} \cdot [P] \tag{4.8}$$

The bridge between ζ-potential and K_p is finally established by combining Equation 4.8 with Equation 4.2:

$$\left|\frac{\Delta\zeta}{\zeta_0}\right| = \frac{K_p \cdot \gamma_L \cdot z_{\text{peptide}}}{f_{PL^c}(1 + K_p \cdot \gamma_L \cdot [L])} \cdot [P] \tag{4.9}$$

The symbol f_{PL^-} was replaced by f_{PL^c}, to mean 'fraction of charged phospholipids', making the equation independent of the assumption of an anionic vesicle. Equation 4.9 represents a straight line that crosses the origin. K_p can be obtained from its slope. It should be noted that the equation is only applicable to the rising portion of the ζ-potential *vs* peptide curves: the reaching of a plateau usually signifies complete charge neutralization, which is not contemplated in this model.

Equation 4.9 proved adequate to describe the data. Its application to the ζ-potential data of BP100 returned a value of K_p of $(56.4 \pm 0.9) \times 10^3$, within less than 10% of my most thorough determination by fluorescence. It is a shame that this method was only developed after the publication of Article IV, which does include the ζ-potential data.

The successful application of the method leads us to suspect that the assumption 'one peptide charge – one neutralized phospholipid' is actually

valid. The obtained value of K_p, with a magnitude of 10^4, represents a strong binding, and this too contributes to the validity of the assumption: tightly-bound counterions mask the particles' charges more completely. This, however, raises the possibility that the approach may not be as successful when applied to weakly-binding peptides.

* * *

At the end of my work with omiganan Miguel and I set out to better characterize the influence of the bacterial peptidoglycan on the interactions of the peptide. This was particularly important for omiganan's action because, unlike BP100, it can also target Gram-positives. These bacteria have the thickest cell walls,[60] in some cases with peptidoglycan widths up to 80 nm. We wanted to know if this huge anionic structure (I can now say I have worked with the largest naturally-occurring covalent molecule!) could in any way sequester the peptide and prevent its interaction with the membrane. To answer this question I tried to obtain something akin to a K_p to quantify the affinity of omiganan towards the peptidoglycan. I learned that if the peptidoglycan is considered a solid phase, similar to a chromatography resin, the binding equilibrium is subject to pretty much the same rules as the partition to vesicles.[61] After finding a value for the peptidoglycan mesh density[62] I was even able to arrive at a concentration-ratio binding constant (termed D_v) comparable to K_p (see Article III).

I soon discovered that an approach to obtain D_v based on the titration of the peptide with peptidoglycan would not work: the interior of the peptidoglycan mesh, being flooded with water, is not a very different environment from the outer bulk phase. The behavior of the peptide's fluorescence was little affected by binding, which prevented the application of the method. In addition, I faced a practical problem: I was working with *S. aureus* peptidoglycan extracts that, judging from their intense tryptophan-like fluorescence, had a lot of residual protein. Even if the peptide fluorescence changed upon binding, this would most likely be masked by the intense background.

The solution was to separate the solid and liquid phases by centrifugation and proceed to the quantification of the peptide in one of them. When needed, the application of this approach to vesicles is quite troublesome because their density is too close to that of the water to allow a successful centrifugation. Peptidoglycan, however, readily sinks to the bottom of a vessel, even at room g's.

Before I could put the method into practice I had to find a way to make the peptidoglycan suspension more homogeneous. The size differences in the particles were clearly visible to the naked eye, with actual chunks floating about. Both bath- and power sonications did not work; besides, I was afraid this technique would promote the release of protein contaminants from the mesh. Crushing of the powder between glass plates yielded better results. Still, much of the powder would stick to the glass, interfering with quantification, and other portions would form planar chunks, defeating the purpose of the process. After a few weeks, the solution was provided by Margarida Rodrigues — my good friend and scientific neighbor, then at the Free Radicals, Health, and Nutrition Group, in the Faculty of Sciences, and now at the Biomembranes Unit, in the IMM — who spent some hours helping me mold glass rods into the appropriate shape to softly mash the peptidoglycan powder at the bottom of a conical plastic tube.

After a homogeneous suspension was obtained, it was just a matter of incubating different volumes of it with aliquots of omiganan and centrifuging. The peptide could be successfully detected in the supernatant, even though some contaminant fluorescence did creep up (the use of controls without peptide was enough to correct it). The results could be well fit by a simplified version of Equation 4.3 where only the aqueous phase is considered. The mathematical link between D_v and X_W is deduced in Article III. The fitting equation is significantly simplified relative to Equation 4.5 because, the phases having been separated, there is no I_L parameter — or $I_{\mathrm{peptidoglycan}}$, if you prefer. The non-linear, least squares fit of the equation to the data is not perfect, but still remarkably good for a one-parameter regression.

The fit returned a D_v about one order of magnitude lower than the

K_p of the peptide binding to anionic vesicles. As the peptidoglycan in a Gram-positive has a proportionally larger volume than that of the membrane, a similar overall amount of peptide can be expected to bind the two bacterial constituents — this is a conclusion that will be important later on.

To me, however, the successful determination of D_v was rewarding in itself. It represented the design of a complete method — one of my first — from the theoretical conception to the practical implementation.

5. Saturation

The partition model accounts for fairly ideal systems where the peptide does not get close to saturation in the membrane. But a model is only as strong as its assumptions. As described in Part I, deviations were observed almost as soon as I started measuring partition curves.

The partition curves of omiganan with anionic vesicles, and later those of BP100, were "plagued" by spikes or humps (see Sections 2.1 and 3.2). Initially, Miguel and I put forward many explanatory hypotheses but most, like multiple partitions within the membrane or some sort of self-quenching occurring only at intermediate concentrations, were a bit far-fetched and difficult to test.

We then turned to what we were most certain of: the deviations occurred early in the partition curve — in most cases there were even enough remaining points to describe a hyperbolic-like variation (see Figure 2.2). This indicated the deviations occurred as high bound concentrations were reached (remember one of the implications from the definition of K_p: peptide concentrations in the membrane increase as the concentration of lipid decreases). Something was causing the peptides to either fluoresce more or bind more above a given concentration.

This way of visualizing the process of binding prompted for an experimental setup inverse of that of the partition curves, in which peptide is added to vesicles. Under normal partition circumstances such a titration should yield a linear increase of the fluorescence intensity: from Equation 4.3 we can see that I depends on the bound and unbound peptide fractions and on the magnitudes of I_L and I_W. Equation 4.2 tell us that, since $[L]$ is being kept constant, X_L (and, by definition, X_W) must remain constant. Because I_L and I_W, the fluorescence intensities of the

fully bound and unbound peptide, are proportional* to the total peptide concentration, *I* will also be so. I expected to see an upward deviation to linearity after a certain point in that line, corresponding to the hypothesized increase in binding or in fluorescence output — such an observation could be a starting point for the characterization of the phenomenon. It turned out that the titrations with peptide did put me on the right track but not at all with the results** I expected.

5.1 Saturation curves

Titration of vesicles with peptide (the one in question at the time of these experiments being omiganan) produced almost perfect straight lines. At best, a slight downward deflection could be observed after the midpoint of titration. It was ironic that the moment I wanted to observe a system misbehave it neatly yielded canonical results. But I did not give up. The system I was using (4 : 1 POPG : POPC — see Figure 2.2) induced relatively low humps: it could just be that the increase I was expecting to see was too inconspicuous to be detected using that experimental setup.

I insisted on the method, this time after soaking the whole system in acrylamide. Acrylamide is a good quencher of either tryptophan or tyrosine fluorescence, but interacts very poorly with membranes, quenching only exposed fluorophores — it is actually frequently used to gauge in-depth insertion of peptides. I expected that acrylamide might enhance the deviations to linearity by selectively affecting either the pre- or the post-deviation state of the peptide. At the time, inspired by interaction models in which peptide molecules internalize to form pores, I imagined omiganan would be driven inward, and away of acrylamide, at that post-deviation state. This should lead to an upward deviation to linearity, as illustrated in Figure 5.1A. I obtained the exact opposite result — Figure 5.1B.

*A linear relationship between emission intensity and fluorophore concentration is assumed. Loss of linearity may occur because of inner filter (the fluorophore absorption significantly dims the excitation light within the sample) or self-quenching effects, none of which occurs at the micromolar peptide concentrations that were used.

**Almost all the results mentioned in this chapter can be found in Articles III and IV.

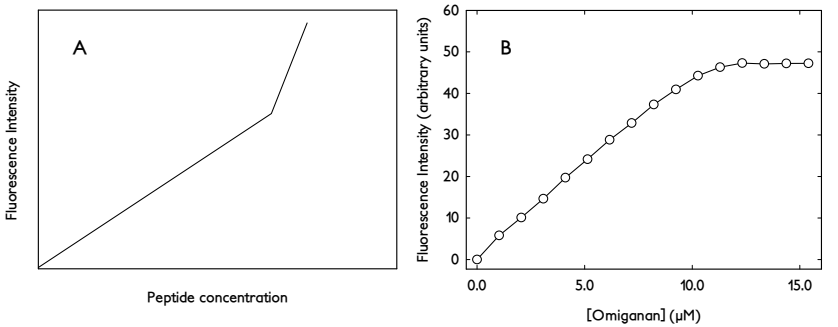

Figure 5.1 – A: Predicted results of a titration of anionic vesicles with omiganan in the presence of acrylamide. The peptide was assumed to burrow into the membrane above a threshold concentration. B: Results obtained with the setup described for A; vesicles composed of 4 : 1 POPG : POPC, at a concentration of 75 μM; acrylamide at 300 mM.

I was extremely surprised by the outcome, but at once realized what it meant: there is a point when the membrane becomes saturated and further added peptide remains in the aqueous phase, fully exposed to acrylamide. I would have never imagined, however, that this point could be reached with micromolar peptide concentrations.

Evoking saturation raised more questions than it solved. Was it really saturation that had occurred? Was there a correlation between saturation and the deviations? And if the membrane was saturated and some peptide molecules were being left out of the interaction, how come there was an overshoot above the partition curve instead of a depression? Also disguising as a question was the important hypothesis we would later stand by: could such an extreme event as the complete coverage of the membrane have physiological significance?

First things first, I needed to make sure the phenomenon was indeed saturation. It was possible, though unlikely, that we were simply looking at a different organization of the peptide in the membrane; one that completely exposed it to acrylamide, resulting in a flat post-break segment in the curve. This hypothesis was dismissed by a partition curve also taken in the presence of acrylamide: the hump persisted; were it to represent an

exposed state it should have been abolished by the quencher. (But why no increase correspondent to such hump had been observed in the titration of lipid with peptide I did not know). Measurement of more of these titrations provided further evidence of saturation. The phenomenon was shown to be related to a concentration-dependent threshold: titrations in the presence of little lipid arrived at a break sooner (in peptide amounts) than those with a large amount of it. Miguel and I decided it was legitimate to start calling the titrations 'saturation curves'.

5.2 Further characterization

Saturation invalidates the partition formalism: Equation 4.1 makes no allowance for a saturated phase because if only ideally dilute solutions are considered solute molecules are always free to enter any of them. Because of this, the K_p value that dictates binding at lower peptide concentrations is no longer valid at saturation — it made sense that this phenomenon was behind the deviations to hyperbolic partition curves. Indeed, I was able to neatly correlate the breaks in the saturation curves with the deviations in the partition curves. As stated earlier, the shape of partition curves that are normalized to I_W should not depend on the overall peptide concentration because the fraction of bound peptide (X_L) only depends on the lipid concentration. Yet, if the deviations resulted from membrane saturation they had to depend on the bound peptide concentration ($[P]_L$). Having a constant X_L implies that $[P]_L$ will change proportionally to the total peptide concentration, and this meant that I should be able to influence the occurrence of the deviations in partition curves simply by varying the initial peptide concentration. This time, as shown in Article III, the results did come out as I had predicted: the lower the peptide concentration in a partition curve, the sooner, in terms of lipid concentrations, were the spikes observed — and vice-versa.

At this point I had an important insight: given the linearity of the saturation curve up to the saturation point it seemed that the partition formalism was valid in that region. Above the saturation point peptide distribution between the two phases was taken over by whatever order

ruled that state. It was reasonable to assume that these two distinct partition behaviors were equivalent *at* the saturation point.

Finding the binding distribution under saturation was straightforward. It is easy to see that when the membrane is saturated the amount of bound peptide must be proportional to the total amount of lipid — double the lipid available for interaction and the amount of bound peptide will also double (with the consequence that the local peptide concentration in the membrane will remain constant, which makes sense since the phase is at maximum capacity). From $n_{\mathrm{peptide},L} \propto n_L$ we can easily get to the value of the bound peptide fraction under saturation ($X_{L,s}$):

$$X_{L,s} = \frac{\sigma[L]}{[P]} \tag{5.1}$$

where σ is the proportionality constant between the lipid and the bound peptide molecules (we called it saturation proportion, hence the sigma).

Following the assumption that both distributions would be equivalent at the saturation point I equated $X_{L,s}$ from the equation above to X_L from Equation 4.2. As a result I obtained a relationship between lipid and peptide at the saturation point.

$$[P]_{\mathrm{sat}} = \frac{\sigma}{K_p \gamma_L} + \sigma[L]_{\mathrm{sat}} \tag{5.2}$$

The sat subscripts were added to $[P]$ and $[L]$ because this equation is only applicable at the saturation point.

According to Equation 5.2 there is a linear relationship between the global amounts of lipid and peptide at the saturation point. Furthermore, the relationship allows the extraction of the values of both K_p and σ from saturation data. And data would not be a problem because by the time I arrived at this equation I had already taken several saturation curves. I immediately attempted to fit Equation 5.2 to the saturation points of those curves and the results were very exciting: the points aligned very well and the extracted parameters were in good agreement with saturation (a lipid-to-peptide-ratio of 5.9). The value of K_p, however, was one order of

magnitude higher than previous estimates. I could blame the very small intercept for the inaccuracy, as its inverse was required for calculating K_p; still, I was a bit skeptical. Miguel, on the other hand, was optimistic. I recall he remarked something like: "You designed a model, almost from scratch, that could return K_p and σ values anywhere from minus infinity to plus infinity. The fact that they landed on reasonable numbers, very much so in the case of σ, is more than could be asked for."

Indeed, in spite of early skepticism I became very proud of Equation 5.2, a successful attempt at model customization. However I soon found out this was not a pioneering achievement. A few months after I derived Equation 5.2, I came across a paper,[63] published years earlier by Tanja Pott and coworkers, where a similar relationship was used with the peptide melittin. There was no mention to saturation in that paper: the used points were critical disruptive thresholds that occurred at given concentrations of melittin in the membrane. Also, K_p was not explicitly included in the equation — but the authors did describe how to obtain it. Lastly, the authors had derived their equation from assumptions distinct from mine. Still, it was basically the same equation. I was a bit upset but managed to find some value in having been able to arrive at my own equation and from a different starting point. And I did learn that such linear equations are valid for any event that occurs at a specific local concentration of peptide; one just has to replace sat with the appropriate subscript.

To compensate for the mild disappointment, Equation 5.2 provided the ultimate evidence linking the deviations in partition curves to saturation. As mentioned before, I had taken several partition curves at different concentrations of peptide. I plotted the $([P], [L])$ pairs corresponding to the deviation maxima of those curves, and compared the result with the plot of the saturation points (Article III – Figure 6). There was an almost perfect alignment: both events corresponded to the same phenomenon.

5.3 Extended models

My next challenge would be to devise a way to fit whole partition curves, including the deviations. Up until then I had only been able to extract

information by fitting the non-saturated segment of the curve or by using the deviation maxima.

My first attempt involved the description of X_L by a piecewise function. One of the pieces would be given the definition in Equation 5.1 and the other by the definition in Equation 4.2. Both should be equivalent at the saturation point (for the remainder of this chapter the fraction of bound peptide under and outside of saturation conditions will be denoted $X_{L,s}$ and $X_{L,ns}$, respectively; X_L will be used to generally denote the bound fraction irrespectively of its saturation state). The implementation of the idea amounted to take X_L as the minimum of $X_{L,s}$ and $X_{L,ns}$. Application of Equation 4.3 to obtain the global fluorescence intensity as a function of $[L]$ resulted in a curve equation determined by three parameters: K_p, σ and I_L (Article III – Figure 7A). This approach, however, emphasized a so far unaddressed issue: because saturation limits the amount of peptide that can bind, an overshoot can never be accounted for without additional assumptions. The following step was to hypothesize some sort of reorganization of the peptide upon saturation that led to an increase in the bound fluorescence. This required the introduction of a second fluorescence contribution to the model, which was termed I_S (for the fluorescence intensity all the peptide would display if it was bound and in the saturated state). The bound peptide would emit with an intensity proportional to I_S when under saturation, and to I_L otherwise. By using a value for I_S greater than I_L I was able to generate partition curves with an overshoot at saturation (Article III – Figure 7B). Still, this was not a satisfactory solution: there would be a discontinuity at the saturation point that, besides being unnatural, did not fit the observed data. I had to make the model more complex so that it would account for some sort of transition between the saturated and non-saturated states.

So far I had assumed in the curve models that the humps occurred due to saturation and that they represented an alternative conformation with higher quantum yield (and by alternative conformation I meant anything from a structural rearrangement to movement within the bilayer — I did not want to commit to a particular view). It then came to me that it was

unlikely that the transition of the bound peptide to that conformation happened all at once. Rather, a gradual progression to the saturated state was more plausible and could explain the softness of the deviations in the partition curves, as opposed to the sharp transition of the two-piece model. Because we were dealing with saturation I hypothesized that the conformation change that took place involved a reduction of the bilayer space occupied by each peptide. This meant that there would be a point above which the two conformations of bound peptide coexisted; any added peptide would push more of the bound molecules into the saturated conformation. The membrane would be able to take up peptide as long as the available space wasn't completely occupied by molecules in the saturation conformation. The mathematical description of this intermediate situation between excess lipid and full saturation — a bit more complex than the previous cases — is carried out in the appendix of Article III. In the end I arrived at a three-piece, five-parameter equation that could do a relatively good job at fitting whole partition curves (Article III – Figure 7C). In addition to the already introduced K_p, σ, I_L, and I_S I had also to include the parameter S: the bound concentration above which the saturation conformation was induced.

The fit results were in very good agreement with previous determinations of either K_p and of σ. Furthermore, σ could now be determined from a single titration, no longer requiring multiple saturation curves. I, however, felt that a five-parameter equation was a somewhat dirty way to fit just about anything and was not confident in its application. I had looked at the whole enterprise mainly as a challenge to find a plausible model for the data and just because in the end the model did fit it did not mean it was valid. Manuel Prieto, Miguel's PhD supervisor (which makes him akin to a scientific grandfather) and a close collaborator of our group, disagreed of my position — I must thank Manuel for having always been enthusiastic about my work, in these and in other occasions. He pointed out the fit-worthiness of the equation: the saturated and the non-saturated segments of the curve were only dependent on two parameters each; only the very short intermediate state and its boundaries depended on all five parameters. This realization gave me confidence to

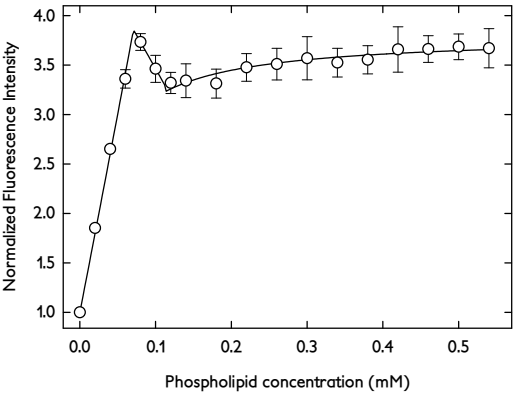

Figure 5.2 – Fitting of the three-state model to the entire partition curve of 10 µM BP100 with 2:1 POPG:POPC vesicles (unpublished). Extracted parameters were: $K_p = (46 \pm 14) \times 10^3$, $I_L/I_W = 3.80 \pm 0.09$, $I_{L,s}/I_W = 4.55 \pm 0.29$ $\sigma = 0.11 \pm 0.01$, and $S = 88 \pm 11$mM.

describe the model in Article III but not enough to later apply it to BP100.* I now regret not having used it to fit the partition curves of BP100 *before* Article IV was published — the results also agreed with measured K_p and σ (Figure 5.2) and their inclusion would have added value to both the article and the model. It serves me well for my skepticism. To compensate for this less positive note I may add that recent developments, described ahead, have presented the opportunity to put this method to a use far more interesting than mere parameter determination. The 'three-state model' will certainly be mentioned in upcoming publications.

5.4 Unpublished results

Recent observations have shed more light on the events surrounding the occurrence of saturation. One of those was made when Rafael, who

*Back then I was fitting this model using a makeshift least-squares approach coupled to Microsoft Excel's solver — I was not totally confident on the output. I have since adapted the model to be non-linearly fitted as a piecewise function by Systat's SigmaPlot; despite its more advanced solution-searching algorithms the results are practically the same.

re-visited Lisbon for a short spell, and I were looking for alternative ways to measure saturation curves — the reason why will be given in Section 6.2. Of the biophysical parameters that changed upon saturation the one most closely linked to the phenomenon was the optical density of the vesicle suspensions. Indeed, saturation curves of BP100 could be obtained from the optical density of the sample, and Equation 5.2 successfully applied (Figure 5.3). The data presented in Figure 5.3 result from fluorescence intensity and OD measurements of the same sample, which means that acrylamide had to be used. OD-only saturation curves have also been obtained; in this case not only is acrylamide unnecessary, but the measurement can also be carried out in an absorbance plate reader, which significantly simplifies data acquisition.

Intriguingly, two breaking points are visible in the OD saturation curves. At first we assumed the saturation point to lie midway between the two; after comparison with the fluorescence intensity curves, however, it became clear that it is the second breaking point that corresponds to saturation. What, then, was the meaning of the first point? I now believe it is the equivalent, in the OD curves, of the beginning of the intermediate state hypothesized in the previous section. Corroborating this interpretation is the fact that an ever-so-slight upward deviation in the fluorescence curves occurs alongside the first breaks in the OD curves. In fact, this is the very deviation I was expecting to see the first time I measured a saturation curve! Such faint breaks are likely caused by a small increase in quantum yield upon saturation. From the results of the application of the three-state model to BP100 (Figure 5.2) that increase is indeed expected to be only of ~20%. It is interesting that titrations of peptide with lipid (partition curves) allow the observation of deviations by fluorescence while the inverse setup (saturation curves) does not. On the other hand, saturation is only clearly visible in the latter. The bottom line is that in this kind of binding studies it matters which variable — lipid or peptide — is scanned, and that complementary information can be obtained from both approaches.

Another unpublished advance to a better understanding of saturation explores that same concept. It involves the results of CD experiments

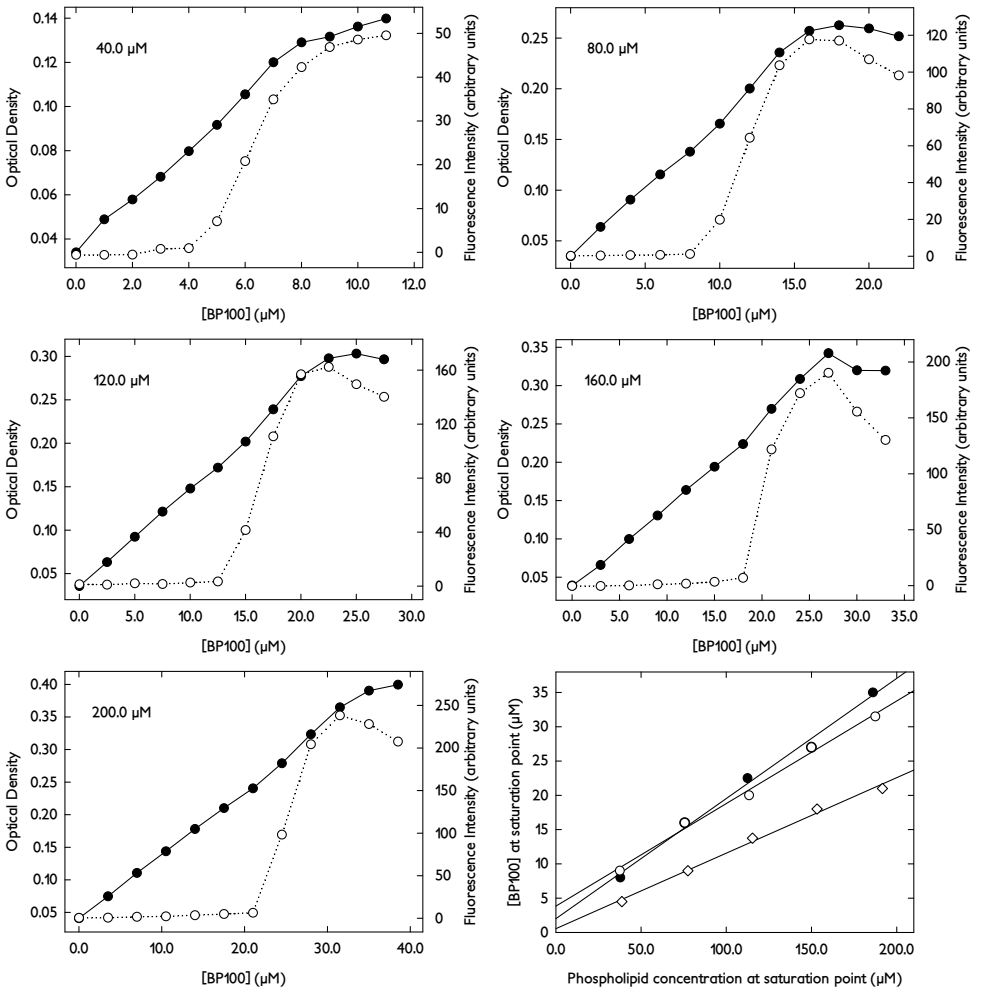

Figure 5.3 –Saturation curves of BP100 with 2 : 1 POPG : POPC vesicles, obtained from fluorescence intensity and optical density measurements (full and empty symbols, respectively; unpublished). The lipid concentration at the beginning of the titration is indicated in each panel. The breaking points of each curve are plotted in the lower-right panel and fit by Equation 5.2; empty squares: first breaking point of the OD curves; empty circles: second breaking point of the OD curves; full circles: breaking point of the fluorescence curves. The extracted fit parameters are, respectively, $\sigma = 0.110 \pm 0.005$, K_p not determined (too large associated error); $\sigma = 0.136 \pm 0.007$, $K_p = (39.4 \pm 9.2) \times 10^3$; and $\sigma = 0.175 \pm 0.009$, $K_p = (166 \pm 100) \times 10^3$. In some of the fluorescence saturation curves an upward deviation is visible alongside the first breaking point of the OD curves. It can also be seen that this method is not well suited to the determination of K_p values.

carried out in Karlsruhe, which have been partly described in Section 3.4. Most of the NMR and CD protocols implemented in Karlsruhe relied on varying only the peptide concentration. CD has a narrow dynamic range and data quality heavily depends on peptide concentration*; titrations with peptide, frequently covering more than one order of magnitude of concentrations, meant that some of the spectra had to be taken at suboptimal conditions. A second problem arose from the fact that high lipid concentrations would be used, within the limits imposed by the technique; the objective of such high concentrations was to promote maximum peptide interaction in order for the bound structure to be easily detected; however, under such circumstances crossing the saturation threshold would require very high peptide concentrations. This was often unfeasible both because of the inability of the technique to withstand the resulting high absorptions and of the sheer amount of required peptide. Still, some of the measurements under that setup did hint at the possibility of a structural change at high bound concentrations. Such observations were mostly inconclusive: usually only at the highest peptide concentration would a structural change be visible, and, given the above technique limitations, the spectrum would inevitably be of poor quality.

After becoming acquainted with the practical details of CD spectroscopy I was able to adapt the partition curve protocol (peptide titration with lipid) to that technique. The differences relative to the conditions used with fluorescence amounted to the use of KF instead of NaCl to maintain the system's ionic strength (chloride ions absorb at low wavelengths, preventing a proper CD measurement) and the use of an optical pathlength suited to the overall sample absorption (for the data presented in Figure 3.3, taken with 20 µM BP100, a 2 mm pathlength was used; lower peptide concentrations could require up to 10 mm pathlengths to generate acceptable signal-to-noise ratios). With this setup all the bound

*CD spectroscopy relies on the measurement of the difference in sample absorption of right- and left circularly polarized light. Some practical limitations arise from that difference usually being minute compared to total sample absorption. When a sample is intensely absorptive there are very few transmitted photons to accurately measure an absorbance. When the chromophore is too diluted, there will not be a detectable difference in the transmitted light.

states of the peptide could be clearly observed — from the initial random-coil structure in water, through saturation, to the α-helical structure when in excess lipid. Furthermore, the spectra obtained by this type of titration had the advantage over the reverse setup that the chromophore concentration was kept approximately constant along the titration. Signal-to-noise ratios were therefore also fairly constant, decreasing only slightly due to light scattering at saturation and at the highest lipid concentrations.

I was able to identify, from the CD measurements, a transition upon saturation to a second bound structure or organization of BP100. The relevance of such a concentration-dependent event to the mechanism of the peptide has been discussed in Part I. In this part, that transition is an important observation that supports two assumptions central to the proposed interaction models: it justifies an increase in fluorescence quantum yield at saturation and supports the existence of the intermediate state postulated in the formulation of the three-state model. Curiously, however, no significant change upon saturation was observed in the measured fluorescence lifetime of BP100. As with the faint breaks in the fluorescence saturation curves in Figure 5.3, I believe this to be a consequence of the actual increase in lifetime also being relatively small.

6. Saturation and the MIC

Ever since we suspected that the spikes, or humps, could reflect some sort of threshold we have wondered at the possibility of a link to the macroscopic event of bacterial death (the observant reader will have noticed that of all questions/hypotheses raised by saturation in Section 5.1 this is the only one that has not yet been addressed). The notion that saturation brought more than just a high membrane-bound peptide concentration grew stronger with the observation that many biophysical parameters changed when that threshold was crossed. With omiganan, saturation was shown to induce a deepening of the peptide position. As for BP100, vesicle aggregation and turbidity, ζ-potential, leakage, and CD measurements all indicated a distinct and potentially disruptive behavior upon saturation.

The ideas described ahead were first included in Articles III and IV and then fully developed in Articles V and VI at the end of this chapter. They represent theoretical research carried out in parallel with experimental work along practically all my PhD. Most importantly, the following notions inspired hypotheses that aim at being applicable to the generality of AMPs, and not exclusively to our peptides.

6.1 Theoretical correlation

My first approach to test the physiological possibility of high membrane bound peptide concentrations was a theoretical one. It was initially spurred by a review[64] by Alessandro Tossi, who is most famous for having compiled a database of AMP sequences.[65] In his review Tossi makes an estimation of the bacterial membrane lipid concentration available under

MIC assay conditions and remarks that it is about forty times lower than a typical AMP MIC. If all the peptide would bind the membrane there would be a very large oversaturation. Tossi concludes that the only way to make sense of this is to admit that other elements besides the membrane are able to significantly bind and sequester the peptide. What first drew my attention in this estimate was that no notion of water-membrane partition was included. Conversely, it was assumed that in absence of sequestering elements all the peptide would bind the membrane. Having been raised to the concept of partition (scientifically speaking) I redid the estimate, this time introducing a K_p of 50×10^3, a typical magnitude for AMPs. The result was quite different from the estimate in the review: I obtained about 26 lipid molecules per bound peptide and no need to evoke peptide sequestering. (I later found a paper by Jack Blazyk and coworkers[66] where essentially the same approximation as Tossi's is carried out, but less dire conclusions are made. The authors even allow for the possibility that the peptide remains in solution and recognize that binding will depend on an affinity constant.) But what was exciting about the result I had obtained was not the dismissal of the hypothesis in Tossi's review. I found it much more interesting that the resulting lipid-to-peptide (L:P) ratio represented a relatively high concentration of the peptide in the membrane. A concentration which, depending on the peptide size, could be very close to saturation.

Those were very stimulating results: at once I had established a theoretical basis that predicted that saturation was physiologically possible and also that it might correspond to the MIC (recall that in the estimate a typical AMP MIC was taken for the global peptide concentration). This became even more exciting when I used in the model the K_p values I had obtained for omiganan and BP100, and the respective MICs: the expected bound peptide-to-lipid (P:L) ratio was very close to the saturation proportion (σ) I had determined for the peptides! (Articles III and IV.)

There was another important conclusion to be taken from the calculation I made: Tossi estimated the overall lipid concentration to be of 25 nM, which is a very low concentration. Applying a K_p value of 50×10^3 Equation 4.2 returns an expected fraction of bound peptide of merely

0.09%. There is so little lipid that practically all the peptide remains in the aqueous phase, though still being able to reach a high concentration in the membrane. This setup is the *in vivo* equivalent of the $[L] \to 0$ limit discussed earlier: the concentration in each phase is maximal. Such conditions allow an important approximation to be made: because the peptide concentration in the bulk phase is virtually unchanged by the presence of the lipid, one can assume that $[P]_W \approx [P]_{\text{total}}$. At the MIC $[P]_W$ becomes the MIC itself. Combination with Equation 4.1 allows the membrane-bound peptide concentration to be calculated from the MIC and the partition constant:

$$[P]_{L,\text{MIC}} = K_p \cdot [P]_{W,\text{MIC}} \approx K_p \cdot \text{MIC} \tag{6.1}$$

where the MIC subscripts were added to denote MIC conditions. Multiplication of $[P]_{L,\text{MIC}}$ by the lipid molar volume yields the bound peptide-to-lipid ratio at the MIC:

$$P{:}L_{\text{MIC}} = K_p \cdot \gamma_L \cdot \text{MIC} \tag{6.2}$$

With Equation 6.2 I could now easily estimate how concentrated an AMP would get in a membrane at its MIC, provided a K_p or a related constant were available. Furthermore, as remarked earlier, the saturation proportion, σ, is also a P:L ratio. This means that if saturation is assumed to occur at the MIC Equation 6.2 can be used to calculate σ.

Equation 6.2 was arrived at following some severe approximations, the validity of which I have to address: in Tossi's and Blazyk's papers the amount of available lipid was geometrically estimated from the bacterial surface area and the area per phospholipid. In my published results I have adapted that approach (essentially, by assuming a different bacterial shape) with only slightly different results. The reduction of the bacterial shape to a geometric surface representing an average bacterium will certainly introduce an error into the estimate of available lipid concentration in a MIC assay. However, that level of precision in this estimate is not important for the above conclusions: the lipid concentration needs only be low enough to maintain valid the approximation $[P]_W \approx [P]_{\text{total}}$. I

show in the Supplementary Material of Article VI that, for typical K_p values of AMPs, that approximation holds if the lipid concentration is lower or equal to the MIC. Because AMP MICs are in the micromolar range there is wide margin for error in the nanomolar estimates of the lipid concentration. Still, to make sure, I estimated the lipid concentration by another approach. I took published results on the fraction of phospholipids per bacterial dry weight[67] and on the weight of a single bacterium[68] (Article VI) and obtained a value of 58 nM. The value is very close to the geometrical estimates, which is quite remarkable given the coarseness of the geometrical calculation and the drastically different approaches to the two estimations.

Other system components that may be able to sequester the peptide are the anionic peptidoglycan and the nucleic acids. Should significant binding occur the approximation $[P]_W \approx [P]_{\text{total}}$ could be invalidated. It is here that the peptidoglycan interaction studies from Section 4.3 come in handy: the amount of peptide that binds the peptidoglycan is, at most, of the same order of magnitude of that which binds the membrane. It would be as if twice the lipid were present, which is well within the allowable error. The same consideration stands for Gram negatives, which have twice as much membrane (but only a very small peptidoglycan layer). As to the nucleic acids a quick estimate (see Article VI) tells us that under the aforementioned MIC assay conditions, about 8 nM of a peptide with 6+ charge would be enough to neutralize all the anionic DNA, mRNA and tRNA bases in an *E. coli* suspension. As the MICs are in the micromolar range, most of the peptide (~99% of it) would still remain unbound.

* * *

With the issue of the validity of the approximation out of the way I started looking for AMPs for which threshold events at the molecular level had been observed. I was trying to validate the use of Equation 6.2 by showing that from the MIC and the partition constant one would be able to infer the conditions at which such thresholds occurred. I looked especially for peptides that underwent behavior changes at, or close to, saturation.

Many authors, however, refrain from using high bound concentrations, under claims that it is not physiologically relevant. This was the posture of Robert Hancock, a central figure in AMP studies, when we met at the Workshop of Membrane-Active Peptides and I told him I had convincing evidence that pointed otherwise — I admit that much of my resolve to tell the world about my findings was spurred by the challenge to contest such preconceptions.

Despite the taboo on using high bound concentrations I did find such reports on some AMPs; it was not easy, though: to validate Equation 6.2 I needed to find peptides whose MICs were known (trivial), for which K_p values with relevant systems had been measured (not so trivial but still easy to find), and with reported molecular-level threshold events at high P:L ratios (very rare!). For many of the AMPs for which all that information was available, the critical molecular-level P:L ratio — always measured in model membranes — could be reasonably well predicted by Equation 6.2. And I could still make use of the cases for which only the MIC and K_p were available: using those two elements with Equation 6.2 I estimated for each peptide what would be its critical ratio in the membrane at the MIC. In agreement with our predictions, most P:L ratios were high enough to be considered saturation. It all comes together in Article V, which describes this theoretical approach to the action of AMPs (unfortunately, tacit editorial rules prevented most of the mathematics to be formally included, hence the need for Article VI). I hoped that publication of this work would contribute to the recognition of the relevance of high membrane-bound concentrations of AMPs; indeed, I have since received very positive informal feedback from several AMP researchers who had used our article to justify their replies to overly conservative referees.

6.2 Prediction

Equation 6.2 plays an important role in the mathematical validation of the occurrence of saturation. Still that is not all there is to that simple expression. Some months after I had arrived at Equation 6.2 Rafael, then

working at our lab, pointed out a trivial algebraic manipulation (I was ashamed for not having thought of it myself!) that gave the equation a whole new meaning:

$$\mathrm{MIC} = \frac{P{:}L_{\mathrm{MIC}}}{K_p \cdot \gamma_L} \tag{6.3}$$

This formulation emphasizes the possibility to estimate the activity of a peptide from two biophysical parameters of the interaction with model membranes, the K_p and the critical P:L ratio. It is a simple relationship, but one that is able to bridge the far-apart fields of Biophysics and Microbiology.

We applied the equation to omiganan and BP100, using the saturation proportion as the critical P:L ratio. Because of that we knew that the results of MIC prediction had to be good: Equation 6.2 had predicted from the MIC a P:L ratio close to the observed values of σ; the opposite process should be coherent. Indeed, the yielded MICs are very close to the actual values (actually, right on target in the case of omiganan — see Article VI).

One of the weaknesses of Equation 6.3 is that it is seldom known *a priori* which is the threshold event that is related to the MIC. Given that a peptide can display many such thresholds[63] this can be a limitation to the application of the equation. Still, Miguel, Rafael and I put efforts into devising a simple and robust method for the biophysical estimation of MIC values (we also aimed at patenting such methods, but because their innovativeness relied mostly on an equation, which is not a patentable find in Europe or Japan, we let go of that idea). It was then that we started looking into alternative methods to measure saturation curves — that one experiment at once yielded a K_p and a P:L ratio (σ), enough to calculate a MIC.

The use of optical density proved to be a very good substitute for fluorescence: it was readily adaptable to microplate measurements and it obviated the need of acrylamide and of a more complex fluorescence measuring apparatus. As mentioned in Section 5.4 the use of OD was powerful enough to reveal a second breaking point, and thus expose the

limitation stated above. One other method that is able to provide the elements necessary to estimate a MIC is the fitting of whole partition curves using the three-state model: it allows the extraction of a value of K_p and of two thresholds (S and σ) from a single titration. The involved analysis, however, is definitely more complex than that of saturation curves and we ended up focusing mainly on the simpler methodology.

The next breakthrough would be made by Miguel. He remarked another obvious property of the prediction model and of saturation curves: if we assume saturation to be the critical P:L ratio, then the MIC, as defined by Equation 6.3, is the intercept of the linear fit of the saturation points (see Section 5.2). Again, an extremely simple observation! And one that significantly simplifies the analysis of saturation curves: if all that is wanted is the MIC, taking the value of the intercept will be sufficient; there is no need to specifically calculate K_p and σ values. It is also a parameter of the linear fit subject to a much smaller error than K_p.

The ease-of-use of the MIC estimation method can be seen by looking at any $[P]_{\mathrm{sat}}$ *vs* $[L]_{\mathrm{sat}}$ plot of saturation points (in Articles III, IV and VI, or in Figure 5.3). The predicted MIC can simply be read from the y-axis. Again, this is so because the low amount of lipid available under *in vivo* conditions mimics the biophysical limit of $[L] \to 0$. Furthermore, as stated in Section 5.2, the linear $[P]$ *vs* $[L]$ relationship is not restricted to the representation of saturation points — it is applicable to any concentration-dependent critical point in the membrane. A broader range of AMP-induced membrane disruptions can thus be used for MIC prediction.

A last improvement to the method was made when I noticed that the estimated MIC, being the intercept of the curve, did not change with the slope. In other words, if the lipid concentration scale were to be stretched or compressed, the same MIC would be calculated; all that is needed is that the relative lipid concentrations among the data points are correct. Independence of lipid concentration confers a great robustness to this method, as only the peptide must be accurately quantified, but it also allows a significant experimental simplification to be made: when using model membranes vesicle unilamellarity is needed to ensure a proper control over the lipid concentration available for interaction; this is so

because when vesicles are multilamellar an undetermined portion of the lipid becomes inaccessible. For MIC estimation, however, unilamellarity is an irrelevant issue as long as all the saturation points are determined using the same batch of multilamellar vesicles (MLVs) — obviating the need for time-consuming procedures required to obtain unilamellarity. This proved to be a successful strategy as results with MLVs, though noisier, produce a MIC estimate very close to observed values.

The estimate with MLVs was also very close to the one obtained with LUVs (Figures 1 and 2 of Article VI), both only slightly below the observed MICs. The fact that both procedures agree in an underestimation of the MIC possibly reflects the use of an excessively anionic membrane model, as discussed in Chapter 'My work and the AMPs'. I must, however, point out that the method is robust even in this aspect: a more anionic system leads to a higher neutralization P:L ratio; at the same time, the K_p of the peptide towards this system will be larger because of a greater electrostatic contribution. It can be seen in Equation 6.3 that a simultaneous increase of these two parameters will partly cancel out, allowing a good MIC estimate even with a suboptimal membrane model.

On a practical aspect, what started out as a theoretical exploration evolved into an idea with potential to be implemented as a kit for MIC estimation without the need for bacteria: microplates covered by films of phospholipid to which the user need only add water and peptide, and that could be measured in any OD plate reader. But perhaps a more valuable use of our conclusions would be the integration of the critical-ratio–K_p–MIC relationship into drug design algorithms: K_p-predicting models exist[69]; if methods are devised to also estimate critical ratios in the membrane then a powerful *in silico* approach to AMP design can be envisioned.

Article V

OPINION

Antimicrobial peptides: linking partition, activity and high membrane-bound concentrations

Manuel N. Melo, Rafael Ferre and Miguel A. R. B. Castanho

Abstract | An increasing amount of information on the action of antimicrobial peptides (AMPs) at the molecular level has not yet been translated into a comprehensive understanding of effects in bacteria. Although some biophysical attributes of AMPs have been correlated with macroscopic features, the physiological relevance of other properties has not yet been addressed. Pertinent and surprising conclusions have therefore been left unstated. Strong membrane-binding and micromolar therapeutic concentrations of AMPs indicate that membrane-bound concentrations may be reached that are higher than intuitively expected, triggering disruptive effects on bacteria.

Antimicrobial peptides (AMPs) represent a wide range of short, cationic, gene-encoded peptide antibiotics that can be found in virtually every organism[1]. Different AMPs display different properties, and many peptides in this class are being intensively researched not only as antibiotics, but also as antivirals[2,3], templates for cell-penetrating peptides[4], immunomodulators[5] and antitumoural drugs[6].

Despite sharing a few common features (for example, cationicity, amphipathicity and short size), AMP sequences vary greatly, and at least four structural groups (α-helical, β-sheet, extended and looped) have been proposed to accommodate the diversity of the observed AMP conformations[7,8]. Likewise, several modes of action as antibiotics have been proposed, and there is debate about whether the primary target of many of these peptides is the cell membrane or whether the primary target is cytoplasmic invasion and disruption of core metabolic functions[9].

Several bilayer interaction and disruption models have been proposed for those AMPs that depend on membrane interference for their antimicrobial activity[10–12] (FIG. 1). However, it is now becoming obvious that such models might be too rigid to account fully for the many interactions that these small molecules can establish in a complex environment, such as the cell membrane. The limitations of the previously proposed models have been exposed in molecular dynamics simulations of AMPs interacting with phospholipid bilayers. Observations from these studies included multiple coexistent structures (frequently unrelated to clean α-helices or β-sheets), nonspecific peptide–peptide interactions and membrane perturbation dictated by stochastic events[13–15] (FIG. 1). The advantage of this indefinite behaviour is that bacteria seem to find it hard to circumvent AMP action, which is certainly a reason behind the multistep mutations usually required for resistance to evolve[16].

Independently of the chosen membrane perturbation model, an implicit concentration threshold is always required for disruption (FIG. 1). This is supported by several observations, in model systems, of phenomena related to such threshold crossings[13,17–19]. Nevertheless, AMP concentrations that are close to full membrane coverage, which are often considered unphysiological conditions, are a frequent requisite for such observations (TABLE 1).

In this Opinion, we survey reports of threshold events of AMPs and propose a correlation between these events and properties such as bactericidal concentration and membrane binding. We use this relationship to support our view, which reconciles existing interaction models with

> “Independently of the chosen membrane perturbation model, an implicit concentration threshold is always required for disruption.”

© 2009 Macmillan Publishers Limited. All rights reserved

Table 1 | **Antimicrobial peptides that display interaction thresholds at high membrane-bound concentrations***

Peptide	Sequence‡	Threshold L:P§	Phospholipid system	Observed effect‖	Refs
Omiganan	ILRWPWWPWRRK-NH_2	6:1	POPC:POPG = 1:4	Internalization; bilayer saturation¶	18
Cecropin–melittin hybrids	KWKLFKKIGAVLKVL-NH_2; KKLFKKILKYL-NH_2	8.4:1; 13:1; 25:1	POPE:POPG: cardiolipin (–2 charge) = 14:5:1; DMPC:DMPG = 3:1	Internalization; pore formation; membrane charge neutralization; bilayer saturation and aggregation	19,26, 38
Melittin	GIGAVLKVLTTGLPALISWIKRKRQQ-NH_2	12:1; 20:1; 23:1	Sphingomyelin; DPPC	Membrane solubilization	23
Tritrpticin (and analogues)	VRRFPWWWPFLRR	25:1	POPE:POPG = 7:3; *Escherichia coli* polar lipids	Increase of membrane leakage¶	33
PGLa	GMASKAGAIAGKIAKVALKAL-NH_2	18:1	DMPC	Complete peptide realignment	39
Tachyplesin I	KWCFRVCYRGLCYRRCR-NH_2	7:1	Egg yolk phosphatidylglycerol	Membrane charge neutralization; vesicle micellization	34
Aurein 2.2	GLFDIVKKVVGALGSL-NH_2	15:1	DMPC	Internalization	40

*In the context of this article, high membrane coverage is used to describe bound antimicrobial peptide (AMP) concentrations that yield 25 phospholipid molecules, or less, per peptide. As a guideline, if it is assumed that an α-helical structure is adsorbed parallel to the bilayer (using 12 Å as the average helix diameter, including side chains, and 0.7 nm^2 as the area per phospholipid[41]), the upper bound 25:1 value results in a relative membrane coverage of between one-fifth and one-third for a peptide that is 20– 30 amino acids long. ‡NH_2 denotes carboxy-terminal amidation. §If information was unavailable, it was assumed that either the reported ratio at the thresholds was relative to the membrane-bound peptide concentration or that the lipid concentration allowed the global L:P to be approximately the same as the local ratio. ‖Only the most structurally relevant effects, which occur at an L:P below 25:1, are listed. ¶Membrane charge neutralization can also be expected at the reported threshold ratios by taking into account the peptide charge and lipid composition of the system. DMPC, dimyristoylphosphatidylcholine; DMPG, dimyristoylphosphatidylglycerol; DPPC, dipalmitoylphosphatidylcholine; POPC, palmitoyloleoylphosphatidylcholine; POPE, palmitoyloleoylphosphatidylethanolamine; POPG, palmitoyloleoylphosphatidylglycerol.

requirements of high membrane-bound peptide concentrations.

Microscopic and macroscopic studies

Since their discovery, AMPs have been the subject of both biological and biophysical studies. Biological studies are required to characterize the activity of the peptides at a macroscopic level; for example, by profiling efficiency against a number of relevant strains[20] or toxicity towards mammalian cells[21]. Biophysical studies attempt to find the molecular bases for macroscopic characteristics, usually with the ultimate goal of rational improvement of AMPs or design of related drugs[4]. However, integration of data from these two fields has not been straightforward. For example, molecular-level information on the membrane interaction and activity of AMPs obtained *in vitro* or *in silico* using model phospholipid bilayers has not been clearly correlated with observations of cell death[22].

AMPs as antibiotics: the threshold

As for all antibiotics, AMPs require a minimum concentration to be effective against a particular strain of bacteria. This concentration, often expressed as the minimum inhibitory concentration (MIC), is used as a parameter to compare antibiotic efficiencies and as a guideline for antibiotic dosage. Although the macroscopic effects of crossing the MIC are easily observed (for example, lysis, loss of viability or bacteriostasis[20]), identification of the molecular events that cause inhibition to occur only after this threshold is another area where the macroscopic and microscopic characterizations of AMPs still do not overlap.

At the molecular level, the threshold that divides a thriving bacterium from a dying one can have several causes. Antibiotic-induced cell death may occur, for example, owing to inhibition of an enzyme, leading to a block in bacterial metabolism. Alternatively, antibiotic molecules may become concentrated enough to exhibit cooperative activity despite the absence of specific target binding; for example, by forming a pore in the membrane, as is the case for most AMPs[13,17]. Indeed, several independent studies have described the changes in the membrane interactions of different AMPs when certain threshold concentrations were reached (for an overview of this behaviour in the widely studied AMPs alamethicin, melittin, magainin and protegrin, see REF. 17). These changes include alterations in conformation[17], in-depth membrane localization[18,19] or association state[13], as well as indirect changes in bilayer topology, such as pore formation or disintegration[11,23–27]. As these are all potentially disruptive events, such transitions have been suggested to be the molecular processes that trigger antibiotic activity and lead to cell death. However, these phenomena have only been observed in model phospholipid bilayers, and in some cases, AMP concentrations in the membrane that were as high as one peptide molecule per six phospholipid molecules[18] were required for these events to occur. These concentrations are close to, if not at, full membrane saturation (see TABLE 1 for a list of peptides that display transitions at high concentrations in the membrane). As the MICs for AMPs are typically in the low micromolar range, scepticism has understandably arisen regarding the relevance of these thresholds and their importance *in vivo*[28,29].

How much peptide in a membrane?

Because important aspects of peptide–membrane interactions are neglected, the general notion that close-to-saturation peptide concentrations in the membrane are impossible *in vivo* could stem more from intuition than accurate interpretation of facts.

Setting the rules: partitioning to the membrane. A common biophysical approach for the study of AMP–membrane interactions involves determination of the extent of peptide partitioning or binding to model membranes, which is commonly translated into partition constants (BOX 1). The fact that these partition constants are usually significantly higher for bacterial model membranes than mammalian ones explains, in part, AMP selectivity and safety, and is considered when rationally designing new

© 2009 Macmillan Publishers Limited. All rights reserved

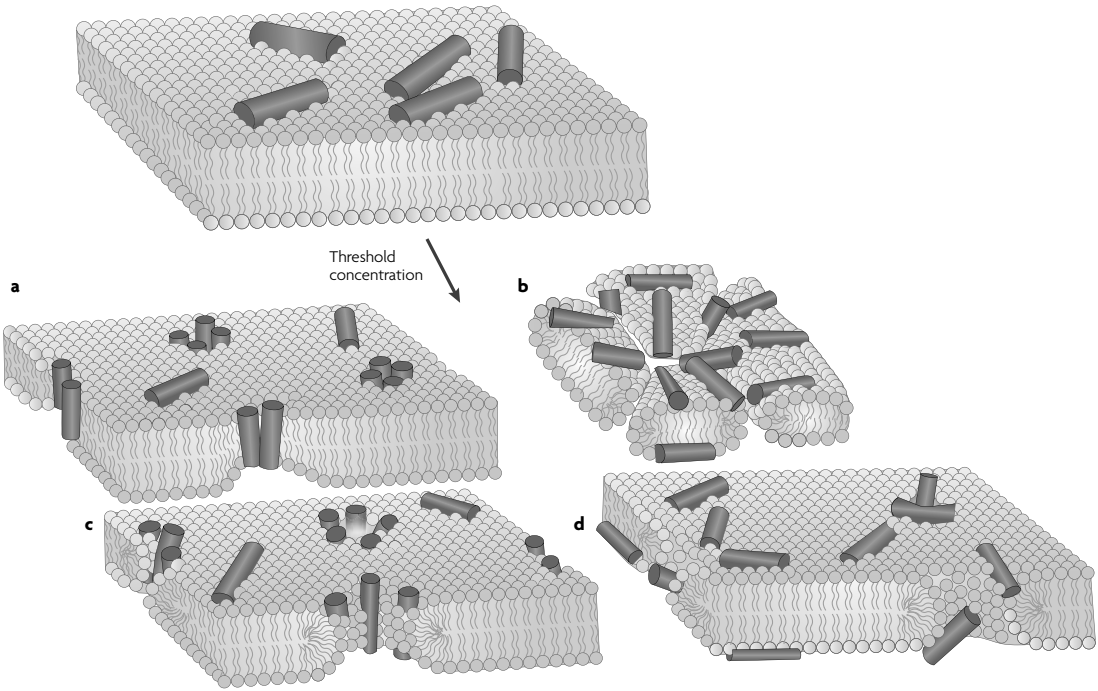

Figure 1 | **Proposed mechanisms of antimicrobial peptide-mediated membrane disruption.** Antimicrobial peptides (AMPs) have been proposed to disrupt the membrane bilayer during binding by different processes. All these models require, either explicitly or implicitly, that a threshold concentration in the membrane be crossed for disruption to occur. **a** | Barrel-stave pore[10]. Peptides insert perpendicularly in the bilayer, associate and form a pore. The peptides line the pore lumen in a parallel direction relative to the phospholipid chains, which remain perpendicular to the bilayer plane. **b** | Carpet mechanism[11]. Peptides adsorb parallel to the bilayer and, after reaching sufficient coverage, produce a detergent-like effect that disintegrates the membrane. Specific peptide–peptide interactions are not required. **c** | Toroidal pore[12]. As for the barrel-stave pore, peptides insert perpendicularly in the bilayer, but instead of packing parallel to the phospholipid chains, induce a local membrane curvature in such a way that the pore lumen is lined partly by peptides and partly by phospholipid head groups. A continuity between inner and outer leaflets is established. **d** | Disordered toroidal pore[13]. A recent modification to the toroidal pore proposes that less-rigid peptide conformations and orientations are formed; the pore lumen is lined by the phospholipid head groups.

peptides[8] (BOX 2). Although this is a good example of correlation between molecular-level information and macroscopic AMP characteristics, the analysis of partition constants has typically been restricted to this biophysical approach. Partition constants are seldom considered in an absolute sense, but rather they are normally used to compare different systems. For example, partition constants in the order of 10^4 are common for the interaction of AMPs with bacterial membrane models (TABLE 2). This value does not only indicate that there is a stronger interaction with bacterial membranes than mammalian ones[8,18,30], but also means that the local peptide concentration in a model bacterial membrane is approximately 10,000 times higher than its concentration in the aqueous phase.

By taking into consideration absolute values of partition constants and their physical indications, it can be shown that AMPs with MIC values that are usually in the micromolar range can reach millimolar concentrations in a membrane environment. For a typical MIC of 2 μM and a partition constant of 40×10^3, a high membrane-bound peptide concentration of 80 mM would be expected, which corresponds to approximately 16 phospholipid molecules per bound peptide (assuming typical values for the phospholipidic molar volume[31]). Actual values have been used to estimate the concentration of the peptide omiganan, also resulting in a high concentration[18]. TABLE 2 provides this result, as well as predictions for widely studied AMPs, using a similar approach. The fact that all these peptides are expected to have a low lipid to peptide ratio (L:P) in the membrane at the MIC shows that high levels of membrane coverage are, indeed, plausible.

> “…the local peptide concentration in a model bacterial membrane is approximately 10,000 times higher than its concentration in the aqueous phase.”

The work described above focuses on peptides that exert their action primarily at the membrane level; only at this level is there a strong link between cell death and threshold concentrations in the

© 2009 Macmillan Publishers Limited. All rights reserved

Box 1 | **The partition constant**

The extent of the solute–membrane interaction is usually expressed, in thermodynamic terms, by means of binding or partition constants. Antimicrobial peptides (AMPs) have been observed to partition strongly towards anionic bacterial membrane models and such constants have been determined for many bacterial systems (for examples, see TABLE 2).

Under a commonly accepted framework — fully developed elsewhere[26,35,36] — the partition constant (denoted K_p) is defined as the concentration ratio of the peptide in the lipidic and aqueous phases ($[P]_L$ and $[P]_W$, respectively), in which the lipidic phase corresponds to the membrane volume (Equation 1).

$$K_p = \frac{[P]_L}{[P]_W} \quad (1)$$

Although K_p is constant, the values of $[P]_L$ and $[P]_W$ depend on the relative amounts of lipidic and aqueous phases available for peptide interaction. However, when the amount of membrane is small — as estimated to be the case for bacterial membranes under physiological conditions, in which only nanomolar phospholipidic concentrations are expected[18,37] — both $[P]_W$ and $[P]_L$ approach their respective maximal values of $[P]_{TOTAL}$ and $K_p \cdot [P]_{TOTAL}$; $[P]_{TOTAL}$ being the total peptide concentration[36]. This means that, for the small quantities of phospholipid at physiological bacterial densities[18,37], the membrane-bound concentration of an AMP can be calculated by multiplying the global AMP concentration by the partition constant.

A related and also commonly used binding constant, usually denoted K_b and expressed in reciprocal molar units per mole, can be converted into K_p after division by the lipidic molar volume[26,31] (0.763 litres per mole for fluid phase systems).

membrane. In the case of peptides that target intracellular components[4], the relationship between the partition constant, aqueous phase and membrane-bound peptide concentrations is still valid. However, these parameters do not directly correlate with the disruptive threshold events that take place in the cytoplasm. Adaptations of the previous assumptions must also be made if the antibiotic is immobilized in a solid matrix or linked to a larger carrier[32].

Saturation: unlikely, possible or essential? The values for L:P from the estimates in TABLE 2 correspond clearly to situations of high membrane coverage, showing that high peptide concentrations in the membrane can be expected. It should also be noted that these estimates took into account published parameters that mimicked an *in vivo* environment, rather than unphysiologically high peptide concentrations that are achievable only in the laboratory.

Therefore, available data on the interaction properties of AMPs with membranes, as well as their efficiency profiles against bacteria, validate the plausibility of the occurrence *in vivo* of membrane-bound AMP concentrations at, or close to, bilayer saturation. In addition, another important aspect must be pointed out: the high predicted membrane conentrations were calculated using peptide concentrations that were equal to the MIC and not any other concentration. Because the MIC represents the macroscopically observable threshold for the onset of AMP activity, the obtained relationship between a low L:P and the MIC strongly suggests that high membrane coverage may be an actual requirement for AMP activity. This is supported by the biophysical observations discussed above of membrane-disrupting events that occur at such low L:P values (TABLE 1).

It should be noted that this hypothesis accommodates observations of low L:P disruptive thresholds from current membrane-perturbation models (FIG. 1), and as such, does not encompass AMPs, such as alamethicin, that display activity thresholds at higher L:P values[17].

Saturation and surface charge neutralization. Because AMPs are highly cationic and bind strongly to the membrane, neutralization of bacterial surface charge would be likely for L:P ratios that are similar to those in TABLE 2. This phenomenon would be expected to severely affect membrane function as well as integrity. For example, the intrinsic surface potential generated by the asymmetry of charged membrane phospholipids would be perturbed and, if not a lethal event as such, would be likely to stimulate the onset of antibacterial action[8]. Indeed, taking into account the peptide and membrane charges, an analysis of published data reveals that neutralization does occur along threshold events displayed by several AMPs[18,26,33,34] (TABLE 1). As such, membrane charge neutralization coupled to saturation of the bacterial membrane is a likely killing mechanism, at least for some peptides.

Table 2 | **MIC ranges, partition constants and predicted L:P values for AMPs**

Peptide	MIC range (μM)*	$K_p/10^3$ ‡	Expected L:P in the membrane§	Refs
Melittin	9–18	60	2.5:1	42,43
Magainin-2-amide	40–50	7	5:1	25,44,45
Omiganan	4–8	23	14:1	18,46
Indolicidin	2–16	39	17:1	20,47
Dermaseptin S1	1.4–25	37	26:1	11,48
Cecropin P1	0.3–17	157	28:1	20,30

*Average minimum inhibitory concentration (MIC) range against susceptible *Escherichia coli* and *Staphylococcus aureus* strains. ‡The published partition constant from the system that best mimicked bacterial membranes was chosen for each peptide. §The lipid to peptide ratio (L:P) = 1/($K_p \cdot$ MIC $\cdot$ 0.763); 0.763 being the phospholipidic molar volume, in litres per mole[31]. The L:P provided is the largest obtained from the range of MICs, thus reflecting the lowest expected membrane concentration. AMP, antimicrobial peptide.

Reasoning or intuition

Because of the different magnitudes of AMP partition constants, MICs and physiological phospholipid concentrations, it is hard to assess the actual amount of interacting peptide without resorting to calculation. This may be the reason behind the intuitive idea that it is impossible for a peptide that is present only in micromolar concentrations in the aqueous phase to saturate the cell membranes of bacteria in suspension. We have reviewed and presented published observations that support our view that high peptide concentrations can be expected *in vivo*.

In addition, the reviewed literature clearly suggests that there is a simple correlation between AMP MICs, partition constants and threshold concentrations in the membrane, which can ultimately be used to predict activity ranges *in vivo* from simple biophysical parameters (see the relationship in the footnote of TABLE 2) and thus better design new antibiotics.

© 2009 Macmillan Publishers Limited. All rights reserved

Box 2 | **Antimicrobial peptide affinity for bacteria**

The mechanisms of antimicrobial peptide (AMP) action are not always precisely defined; nevertheless, the main factors that lead to high levels of binding and selectivity towards bacteria have been identified[8].

Peptide characteristics

Charge. High levels of cationic residues in AMPs result in stronger interaction with, and preference for, the anionic bacterial membranes.

Hydrophobicity. Together with cationic residues, AMPs are frequently enriched in hydrophobic amino acids. The presence of such amino acids correlates not only with stronger partitioning to membranes, but also with higher levels of haemolytic activity.

Conformation and amphipathicity. During membrane interaction, AMPs adopt preferred conformations that frequently involve segregation of polar and apolar residues to opposite regions of the structure. The resulting amphipathicity leads to higher levels of peptide internalization and membrane perturbation.

Bacterial characteristics

Hydrophobicity and charge. Bacterial membranes are composed of a large proportion of anionic phospholipids. Mammalian phospholipids are essentially neutral and enriched in sterols. The anionic and more fluid bacterial bilayers are more susceptible to binding and probable disruption by the cationic AMPs.

Transmembrane potential. The usually higher, negative-inside, transmembrane potential found in bacteria promotes AMP interaction while acting as a potential driving force for peptide insertion and translocation.

Bilayer asymmetry. Differences in inner and outer leaflet compositions provide a basis for further discrimination, despite occurring in both bacterial and mammalian membranes. Different densities of charged phospholipids also contribute to the transmembrane potential.

AMP ligands. Besides electrostatic and hydrophobic interactions, some AMPs display specific structural affinity for bacterial membrane constituents, such as phospholipid head groups.

Cell wall. The anionic lipopolysaccharide and peptidoglycan further enhance peptide binding. Peptidoglycan, however, has been shown to compete only weakly with the membrane for the AMP interaction[18].

These characteristics ensure a strong affinity of AMPs for bacteria, not only relative to the weaker interactions established in mammalian cell membranes, which result in selectivity, but also in an absolute sense; high bound-peptide concentrations are produced.

Manuel N. Melo and Miguel A. R. B. Castanho are at the Instituto de Medicina Molecular, Faculdade de Medicina de Lisboa, Av. Professor Egas Moniz, 1649-028 Lisboa, Portugal.

Rafael Ferre is at the Laboratori d'Innovació en Processos i Productes de Síntesi Orgànica (LIPPSO), Departament de Química, Universitat de Girona, Campus Montilivi, 17071 Girona, Spain.

Correspondence to M.A.R.B.C.
e-mail: macastanho@fm.ul.pt

1. Zasloff, M. Antimicrobial peptides of multicellular organisms. *Nature* **415**, 389–395 (2002).
2. Robinson, W. E. Jr, McDougall, B., Tran, D. & Selsted, M. E. Anti-HIV-1 activity of indolicidin, an antimicrobial peptide from neutrophils. *J. Leukoc. Biol.* **63**, 94–100 (1998).
3. Albiol Matanic, V. C. & Castilla, V. Antiviral activity of antimicrobial cationic peptides against Junin virus and herpes simplex virus. *Int. J. Antimicrob. Agents* **23**, 382–389 (2004).
4. Henriques, S. T., Melo, M. N. & Castanho, M. A. Cell-penetrating peptides and antimicrobial peptides: how different are they? *Biochem. J.* **399**, 1–7 (2006).
5. Bowdish, D. M., Davidson, D. J. & Hancock, R. E. A re-evaluation of the role of host defence peptides in mammalian immunity. *Curr. Protein Pept. Sci.* **6**, 35–51 (2005).
6. Hoskin, D. W. & Ramamoorthy, A. Studies on anticancer activities of antimicrobial peptides. *Biochim. Biophys. Acta* **1778**, 357–375 (2008).
7. Hancock, R. E. Peptide antibiotics. *Lancet* **349**, 418–422 (1997).
8. Yeaman, M. R. & Yount, N. Y. Mechanisms of antimicrobial peptide action and resistance. *Pharmacol. Rev.* **55**, 27–55 (2003).
9. Brogden, K. A. Antimicrobial peptides: pore formers or metabolic inhibitors in bacteria? *Nature Rev. Microbiol.* **3**, 238–250 (2005).
10. Baumann, G. & Mueller, P. A molecular model of membrane excitability. *J. Supramol. Struct.* **2**, 538–557 (1974).
11. Pouny, Y., Rapaport, D., Mor, A., Nicolas, P. & Shai, Y. Interaction of antimicrobial dermaseptin and its fluorescently labeled analogues with phospholipid membranes. *Biochemistry* **31**, 12416–12423 (1992).
12. Ludtke, S. J. *et al.* Membrane pores induced by magainin. *Biochemistry* **35**, 13723–13728 (1996).
13. Leontiadou, H., Mark, A. E. & Marrink, S. J. Antimicrobial peptides in action. *J. Am. Chem. Soc.* **128**, 12156–12161 (2006).
14. Hsu, J. C. & Yip, C. M. Molecular dynamics simulations of indolicidin association with model lipid bilayers. *Biophys. J.* **92**, L100–L102 (2007).
15. Sengupta, D., Leontiadou, H., Mark, A. E. & Marrink, S. J. Toroidal pores formed by antimicrobial peptides show significant disorder. *Biochim. Biophys. Acta* **10**, 2308–2317 (2008).
16. Perron, G. G., Zasloff, M. & Bell, G. Experimental evolution of resistance to an antimicrobial peptide. *Proc. Biol. Sci.* **273**, 251–256 (2006).
17. Huang, H. W. Molecular mechanism of antimicrobial peptides: the origin of cooperativity. *Biochim. Biophys. Acta* **1758**, 1292–1302 (2006).
18. Melo, M. N. & Castanho, M. A. Omiganan interaction with bacterial membranes and cell wall models. Assigning a biological role to saturation. *Biochim. Biophys. Acta* **1768**, 1277–1290 (2007).
19. Pistolesi, S., Pogni, R. & Feix, J. B. Membrane insertion and bilayer perturbation by antimicrobial peptide CM15. *Biophys. J.* **93**, 1651–1660 (2007).
20. Giacometti, A. *et al. In vitro* susceptibility tests for cationic peptides: comparison of broth microdilution methods for bacteria that grow aerobically. *Antimicrob. Agents Chemother.* **44**, 1694–1696 (2000).
21. Staubitz, P. *et al.* Structure–function relationships in the tryptophan-rich, antimicrobial peptide indolicidin. *J. Pept. Sci.* **7**, 552–564 (2001).
22. Friedrich, C. L., Moyles, D., Beveridge, T. J. & Hancock, R. E. Antibacterial action of structurally diverse cationic peptides on gram-positive bacteria. *Antimicrob. Agents Chemother.* **44**, 2086–2092 (2000).
23. Pott, T., Paternostre, M. & Dufourc, E. J. A comparative study of the action of melittin on sphingomyelin and phosphatidylcholine bilayers. *Eur. Biophys. J.* **27**, 237–245 (1998).
24. Weiss, T. M. *et al.* Two states of cyclic antimicrobial peptide RTD-1 in lipid bilayers. *Biochemistry* **41**, 10070–10076 (2002).
25. Wenk, M. R. & Seelig, J. Magainin 2 amide interaction with lipid membranes: calorimetric detection of peptide binding and pore formation. *Biochemistry* **37**, 3909–3916 (1998).
26. Bastos, M. *et al.* Energetics and partition of two cecropin–melittin hybrid peptides to model membranes of different composition. *Biophys. J.* **94**, 2128–2141 (2008).
27. Papo, N. & Shai, Y. Can we predict biological activity of antimicrobial peptides from their interactions with model phospholipid membranes? *Peptides* **24**, 1693–1703 (2003).
28. Zhang, L., Rozek, A. & Hancock, R. E. Interaction of cationic antimicrobial peptides with model membranes. *J. Biol. Chem.* **276**, 35714–35722 (2001).
29. Giacometti, A., Cirioni, O., Greganti, G., Quarta, M. & Scalise, G. *In vitro* activities of membrane-active peptides against gram-positive and gram-negative aerobic bacteria. *Antimicrob. Agents Chemother.* **42**, 3320–3324 (1998).
30. Gazit, E., Boman, A., Boman, H. G. & Shai, Y. Interaction of the mammalian antibacterial peptide cecropin P1 with phospholipid vesicles. *Biochemistry* **34**, 11479–11488 (1995).
31. Chiu, S. W., Jakobsson, E., Subramaniam, S. & Scott, H. L. Combined monte carlo and molecular dynamics simulation of fully hydrated dioleyl and palmitoyl-oleyl phosphatidylcholine lipid bilayers. *Biophys. J.* **77**, 2462–2469 (1999).
32. Haynie, S. L., Crum, G. A. & Doele, B. A. Antimicrobial activities of amphiphilic peptides covalently bonded to a water-insoluble resin. *Antimicrob. Agents Chemother.* **39**, 301–307 (1995).
33. Andrushchenko, V. V., Aarabi, M. H., Nguyen, L. T., Prenner, E. J. & Vogel, H. J. Thermodynamics of the interactions of tryptophan-rich cathelicidin antimicrobial peptides with model and natural membranes. *Biochim. Biophys. Acta* **1778**, 1004–1014 (2008).
34. Matsuzaki, K., Fukui, M., Fujii, N. & Miyajima, K. Permeabilization and morphological changes in phosphatidylglycerol bilayers induced by an antimicrobial peptide, tachyplesin I. *Colloid Polym. Sci.* **271**, 901–908 (1993).
35. Nernst, W. Verteilung eines Stoffes zwischen zwei Lösungsmitteln und zwischen Lösungsmittel und Dampfraum. *Z. Phys. Chem.* **8**, 110–139 (1891).
36. Santos, N. C., Prieto, M. & Castanho, M. A. Quantifying molecular partition into model systems of biomembranes: an emphasis on optical spectroscopic methods. *Biochim. Biophys. Acta* **1612**, 123–135 (2003).
37. Tossi, A., Sandri, L. & Giangaspero, A. Amphipathic, α-helical antimicrobial peptides. *Biopolymers* **55**, 4–30 (2000).
38. Ferre, R. *et al.* Synergistic effects of the membrane actions of cecropin–melittin antimicrobial hybrid peptide BP100. *Biophys. J.* (in the press).
39. Burck, J. *et al.* Conformation and membrane orientation of amphiphilic helical peptides by OCD. *Biophys. J.* **95**, 3872–3881 (2008).
40. Pan, Y. L. *et al.* Characterization of the structure and membrane interaction of the antimicrobial peptides

© 2009 Macmillan Publishers Limited. All rights reserved

aurein 2.2 and 2.3 from Australian southern bell frogs. *Biophys. J.* **92**, 2854–2864 (2007).
41. White, S. H. & King, G. I. Molecular packing and area compressibility of lipid bilayers. *Proc. Natl Acad. Sci. USA* **82**, 6532–6536 (1985).
42. Beschiaschvili, G. & Seelig, J. Melittin binding to mixed phosphatidylglycerol/phosphatidylcholine membranes. *Biochemistry* **29**, 52–58 (1990).
43. Blondelle, S. E. & Houghten, R. A. Hemolytic and antimicrobial activities of the twenty-four individual omission analogues of melittin. *Biochemistry* **30**, 4671–4678 (1991).
44. Dathe, M., Nikolenko, H., Meyer, J., Beyermann, M. & Bienert, M. Optimization of the antimicrobial activity of magainin peptides by modification of charge. *FEBS Lett.* **501**, 146–150 (2001).
45. Maloy, W. L. & Kari, U. P. Structure–activity studies on magainins and other host defense peptides. *Biopolymers* **37**, 105–122 (1995).
46. Sader, H. S., Fedler, K. A., Rennie, R. P., Stevens, S. & Jones, R. N. Omiganan pentahydrochloride (MBI 226), a topical 12-amino-acid cationic peptide: spectrum of antimicrobial activity and measurements of bactericidal activity. *Antimicrob. Agents Chemother.* **48**, 3112–3118 (2004).
47. Subbalakshmi, C., Krishnakumari, V., Sitaram, N. & Nagaraj, R. Interaction of indolicidin, a 13-residue peptide rich in tryptophan and proline and its analogues with model membranes. *J. Biosci.* **23**, 9–13 (1998).
48. Mor, A. & Nicolas, P. The NH_2-terminal α-helical domain 1–18 of dermaseptin is responsible for antimicrobial activity. *J. Biol. Chem.* **269**, 1934–1939 (1994).

Acknowledgements
Fundação para a Ciência e a Tecnologia (Portugal) is acknowledged for a grant to M.N. Melo (SFRH/BD/24,778/2005). M.M. Melo is thanked for critical revision of the manuscript.

FURTHER INFORMATION
Miguel A. R. B. Castanho's homepage:
http://www.biochemistry-imm.org/cat.php?catid=104

ALL LINKS ARE ACTIVE IN THE ONLINE PDF

© 2009 Macmillan Publishers Limited. All rights reserved

Article VI

Prediction of antibacterial activity from biophysical properties of antimicrobial peptides

Manuel N. Melo,[a] Rafael Ferre,[b] Lidia Feliu,[b] Eduard Bardají,[b] Marta Planas[b] and Miguel A. R. B. Castanho[a]

a) Instituto de Medicina Molecular, Faculdade de Medicina, Universidade de Lisboa, Lisbon, Portugal;
b) Laboratori d'Innovació en Processos i Productes de Síntesi Orgànica, Departament de Química, Universitat de Girona, Girona, Spain.

Consensus is gathering that antimicrobial peptides (AMPs) that exert their antibacterial action at the membrane level must reach a local concentration threshold to become active. Studies of peptide interaction with model membranes do identify such disruptive thresholds but demonstrations of the possible correlation of these with the in vivo onset of activity have only recently been proposed. Here we fully develop an interaction model of AMPs with membranes, and explore the consequences of the underlying partition formalism. Disruptive thresholds in model membranes and the onset of antibacterial peptide activity are shown to occur over the same range of locally bound peptide concentrations (10 to 100 mM), supporting a correlation between the two types of observations. The interaction model further yields a relationship that provides AMP activity prediction from simple biophysical parameters. A straightforward and robust method to implement this relationship is presented, with potential application to high-throughput screening approaches.

Antimicrobial peptides (AMPs) are a broadly defined class of gene-encoded peptides produced by virtually all organisms. Members of this class are usually short, cationic, and able to adopt amphipathic structures, especially when in interaction with membranes. The most studied feature of AMPs, as the name indicates, has been their antibiotic potential, and since their discovery several microbiology methodologies have been developed and employed to characterize the in vivo action against their targets, usually prokaryotes.[1,2]

In turn, the relative simplicity in sequence and secondary structure of AMPs, together with mechanisms that depend largely on membrane interaction,[3] prompted the use of biophysical tools as the methodologies of choice for identifying the molecular level modes of action of AMPs. The distinct microbiological and biophysical approaches have, however, opened a gap in the information on AMPs: the macroscopic information on AMP activity from biological studies is seldom correlated to the findings on peptide behavior at the molecular level. This is not to say that the bases of all macroscopic phenomena displayed by AMPs are poorly understood – for instance, AMP selectivity has been successfully modeled and described by a preferred partitioning of the peptides towards bacterial versus mammalian membrane models.[3] Nonetheless, some very detailed molecular descriptions from biophysical models, such as pore formation in phospholipid bilayers, need to be more clearly connected to the events that, in vivo, lead to AMP-mediated bacterial death.

There is one point where observations from biological studies overlap with molecular models of AMP action: a given peptide concentration must be overcome to trigger peptide activity. From a biological, macroscopic perspective this threshold is expressed as the minimum inhibitory concentration (MIC); the molecular level parallel of this threshold is the membrane-bound peptide concentration above which a disrupting process (disintegration, pore formation, translocation, etc.) is initiated – in fact, several cases have been reported where peptides become disruptive against membrane models above a certain threshold.[4] It is tempting to assume a correlation between the macroscopic MICs and the molecular level disruptions, but the fact is that it is not yet known if the topology of membrane perturbation in vivo is at all related to what is observed in artificial phospholipid membranes.

Quantification of binding to model phospholipid membranes has been an important aspect of studies on drug interactions.[3,5,6] In the case of AMPs, information on the membrane-bound peptide concentration in bacterial and model membranes may explain more than just selectivity. It may corroborate the connection between the MIC and the molecular level observations of disruption in model membranes if both thresholds are shown to occur at the same local concentrations in the membrane. Indeed that correlation was recently shown to be expected for typical AMPs, even at seemingly high bound concentrations.[4,7,8]

Concentrations corresponding to disruption thresholds in model membranes can be directly extracted from published data as these are usually expressed as the peptide-to-lipid ratio (*P/L*) at which the threshold occurs – commonly falling in the 1:10 to 1:100 range[4,9] (see the Supplementary Material for possible approximations in the values taken from published data). Division by the phospholipid molar volume (γ_L) readily translates *P/L* values into concentrations, which range, in this case, from 13 to 130 mM.

A peptide-lipid interaction model was constructed to calculate the extent of AMP binding to real bacterial membranes (all equations derived in the Methods section). This model was based on a set of parameters that reflect a relevant scenario of peptide-bacteria interaction – a MIC assay – involving a generic AMP with typical characteristics. We then explored the consequences of the underlying chemical biology to arrive at theoretical and practical conclusions on the parallelism of peptide activity against model and bacterial membranes.

The peptide fraction bound to bacterial membranes at activity thresholds was calculated using Equation 2, which requires knowledge of the amount of membrane lipid available for peptide binding under MIC assay conditions. An estimate based on reported values for the dry weight per bacterium and phospholipid mass percentage of dry bacteria (for *E. coli*) yielded, under MIC assay conditions, a total membrane phospholipid concentration ($[L]_{MIC\ assay}$) of 58 nM. This value is in good agreement with, and corroborates, published results from distinct calculations based on bacterial surface area[10,11] (66 and 25 nM, respectively); the impact of the accuracy of the estimates on the results is discussed in the Supplementary Material. Application of Equation 2 also requires knowledge of the partition constant (K_p) of the peptide towards bacterial membranes. It was assumed that an AMP interacts with such membranes and their model counterparts with similar affinity and, so, that binding or partition constants determined for the latter are valid to predict behavior in real membranes. Equation 2 was solved using a typical[4] AMP-membrane partition constant of 5×10^4. With the given parameters only 0.22% of the total peptide was predicted to bind bacterial membranes in a MIC assay.

The very low fraction obtained indicates that almost all peptide remains in the aqueous phase but it does not mean that the local concentration in the membrane is low: indeed, for a typical MIC value of 2 μM a bound concentration of 100 mM is expected (see Equation 3). This is a high concentration – about 13 phospholipids per bound peptide – which matches some of the highest reported bound threshold concentrations in model membranes. Such a high bound concentration predicted from physiological parameters supports the notion that, as recently remarked,[4] high membrane-bound AMP concentrations, rather than unphysiological, are expectable events in vivo.

The observed agreement between concentrations at microscopic and macroscopic threshold events supports assumptions that phenomena that take place in the simpler membrane models parallel those occurring in vivo. The usefulness of the same relationship was extended, in a more quantitative sense, to predict antimicrobial activities from known threshold occurrences in model membranes (denoted here as a critical peptide-to-lipid ratio P/L^*). Equation 6 explicitly relates simple physical-chemical parameters of peptide-membrane interactions (K_p and P/L^*) with antibacterial activity. Prediction was tested with the published parameters and activities of the peptides omiganan[8,12] and BP100.[7,13,14] A remarkable agreement of the predicted activities with the observed antibacterial performance was obtained for both peptides, summarized in Table 1.

A linear relationship can be established (Equation 7) relating the global peptide and lipid concentrations when threshold events occur in the membrane. The remarkable feature of this linear correlation is that its intercept is the global peptide concentration required to reach P/L^* in the membrane when $[L] \rightarrow 0$, which is a condition that parallels the very low $[L]_{MIC\ assay}$. Indeed, the MIC estimate defined in Equation 6 is equivalent to the intercept of the straight line defined by Equation 7 (see equation 8). Thus, upon identification of the critical threshold event in model membranes, MIC values can be estimated from a single experiment consisting in the determination of peptide *vs.* lipid threshold curves. This method does not require explicit calculation of K_p or P/L^* values – although these can be recovered if needed.[8,15]

Table 1 – Estimated and observed activities for the AMPs BP100 and omiganan against Gram-negatives.

Peptide	*Membrane interaction parameters*		*MIC estimate (μM)*	*Observed MIC (μM)*
	$K_p/10^3$	P/L^*		
BP100[7,13]	17.8 – 90.1	1 : 8.4	1.7 – 8.8	2.5 – 7.5
Omiganan[8,12]	23.5 – 43.5	1 : 5.9	5.2 – 9.8	4.5 – 9.0

Furthermore, because the MIC estimate only depends on the intercept of the curve, the prediction is relatively independent of the actual stock lipid concentrations that are used, as long as the relative dilutions between data points are kept. Inaccurate concentrations of lipid stocks *will* generate incorrect P/L^* and K_p values, but the intercept – and thus the MIC estimate – will not be affected. This robustness not only avoids the need for accurate lipid quantification but also introduces the possibility of using liposomes that have not been subjected to any process to induce unilamellarity[16,17] (such as freeze-thaw, extrusion, or sonication), obviating a time- and resource-consuming step usually associated to the use of model membranes.

Application of the approach to published threshold data for the peptides omiganan and BP100 was successful, with good approximations of the actual MICs (Figure 1). The method was further tested using threshold points of BP100 interaction with multilamellar vesicles, determined from the optical density of the system. The results are in good agreement with the other predictions and with the actual MICs (Figure 2). In this case two threshold points were detected, only one of which corresponds to the P/L^* determined elsewhere.[7] The prediction is consistent with that from Figure 1 and the observed range of activities of the peptide, not being affected by the use of multilamellar vesicles.

The relevant biophysical parameters for MIC estimation can be alternatively obtained by methods[8] that involve the explicit calculation of P/L^* and K_p. Some of these approaches may have the advantage of providing parameter estimation from a single data curve, unlike the application of Equation 8 (see Figure 2). However, these methods require complex and time-consuming analyses of peptide binding, not suitable for routine implementation.

The method based on Equations 6 – 8 may also be used to estimate other relevant thresholds, such as the minimum hemolytic concentration (MHC) of a peptide. The concentration of erythrocyte membrane phospholipid in an MHC assay ($[L]_{\text{MHC assay}}$) was estimated to be of 89 μM (see Methods). This is a much higher concentration than that in MIC assays, and of the same order of magnitude, or higher, as MHC values of hemolytic peptides.[18,19] This is a borderline situation regarding the validity of Equation 6, and the method is more likely to estimate a lower bound of an MHC than a central value. Published threshold data on the interaction of the AMP melittin with different erythrocyte membrane models is available.[15,20] These verify the linearity expected from Equation 7 and predict MHC values from 0.02 to 15.3 μM. Notwithstanding the high $[L]_{\text{MHC assay}}$ and the wide prediction interval, the values do overlap with the observed MHC range,[18,21] between 0.9 and 2.5 μM.

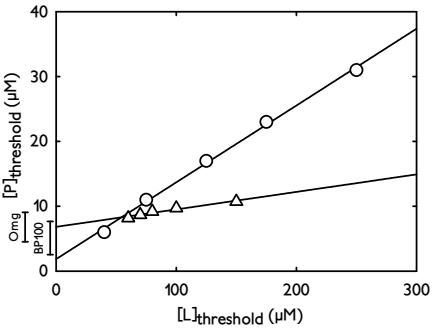

Figure 1 – Application of the MIC prediction method to published threshold data on the interaction of the AMPs BP100 and omiganan with model membranes. Data adapted from refs. [7,8] for the interaction of BP100 (circles) and omiganan (Omg, triangles) with POPC:POPG 1:2 unilamellar vesicles. Data were fit with Equation 8, yielding intercepts of 1.8 ± 0.5 μM and 6.8 ± 0.3 μM, respectively. Intervals drawn next to the $[P]_{\text{threshold}}$ axis indicate the range of MIC values determined in vivo against different Gram negatives, for each peptide[12,13] (Table 1); the regression intercepts, predictive of the MIC (see text), lie within, or very close to, these ranges.

It can be seen that, within a simple binding formalism, the average local peptide concentrations predicted at the MIC and those observed for thresholds in model membranes occur over the same magnitude of concentrations. This concurrence strongly supports a correlation between both observations and validates the use of model systems to study these phenomena. Indeed, a recent study has shown that the energetics of membrane disruption become largely favorable when surface-wide coverage is attained,[22] this being a possible origin of threshold behavior.

In addition to its simplicity and robustness, the prediction method is relatively independent of the chosen technique to detect threshold points: data in Figure 1 were obtained from the peptides' fluorescence, those in Figure 2 and reference 15 from the turbidity of liposome suspensions, and those from reference 20 by detection of liposomal leakage. It should be noted that, because biophysical parameters are usually obtained from model systems, only an approximate rendition of a biological behavior can be expected from our inter-

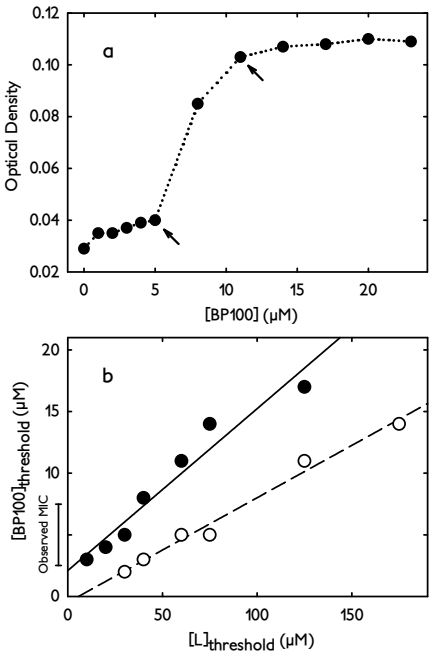

Figure 2 – Application of the MIC prediction method to thresholds in BP100 interaction with multilamellar vesicles. (**a**) Optical density of a suspension of multilamellar vesicles (60 μM POPC:POPG 1:2) at different concentrations of added BP100. Critical threshold points are indicated by arrows. (**b**) Plot and linear fit, according to Equation 8, of critical points in **a**) and in similar curves obtained with different lipid concentrations; empty and full symbols denote the first and second critical points, respectively, of each curve. The intercept of the line fitted to the second critical points yields a MIC estimate of 2.1 ± 0.9 μM, according to Equations 6 – 8. The value is both close to the estimate in Figure 1 and to the observed activity range of BP100, indicated next to the $[BP100]_{threshold}$ axis.

action model; furthermore, the offset of some of the predictions relative to observed values stresses the importance of using relevant model membrane systems. However, since MICs and MHCs are seldom determined in vivo with great precision, Equation 6 still allows for useful, educated guesses of activity ranges to be made relying solely on biophysical data.

This work demonstrates that it is possible to use a purely physical-chemical reasoning to understand, model, and predict the mechanisms of complex biological interactions such as AMP-mediated bacterial death. The resulting methodology is a fast, cost-effective way to screen libraries of AMP drug leads by means of high throughput techniques. Moreover, the predictive relationships can be coupled with drug design algorithms, further improving the process. More than bridging the fields of chemistry and biology, these findings have important practical applications that may ultimately lead to a faster, more efficient antibiotic drug development.

METHODS

Peptide partition to the membrane

The developed interaction model follows a commonly used simplification in which the membrane is considered a lipidic phase in coexistence with the bulk aqueous phase; the distribution of the peptide in both phases then obeys a simple Nernst equilibrium.[23] Under this framework, fully developed elsewhere,[5] the partition constant K_p is defined as the concentration ratio of the peptide in the lipidic and aqueous phases:

$$K_p = \frac{[P]_L}{[P]_W} \qquad \text{Eq. 1}$$

where $[P]_L$ and $[P]_W$ are the peptide concentration in the lipidic and aqueous phases, respectively – the Supplementary Material details some simplifications implicit in this definition, as well as the conversion from other types of binding constants.[6]

From Equation 1, the fraction of peptide molecules in the lipidic phase (X_L) can be obtained as

$$X_L = \frac{K_p \gamma_L [L]}{1 + K_p \gamma_L [L]} \qquad \text{Eq. 2}$$

where $[L]$ is the total lipid concentration and γ_L is the molar volume of the lipid phase.

Finally, the local peptide concentration in a membrane at a lipid concentration $[L]$ will be given by

$$[P]_L = \frac{X_L \cdot [P]_{TOTAL}}{[L] \cdot \gamma_L} \qquad \text{Eq. 3}$$

where $[P]_{TOTAL}$ is the peptide concentration over the global volume.

In addition to this process, if the bound peptide-to-lipid ratio (P/L) is known, $[P]_L$ can be obtained easily after division of P/L by γ_L.

Membrane-bound concentrations

Membrane-bound peptide concentrations were calculated according to Equation 3. A K_p value of 5×10^4 was used together with a global peptide concentration,

$[P]_{TOTAL}$, of 2 μM. A γ_L value of 0.76 M,[1] reported for fluid phospholipid systems,[24] was used. Lastly, the amount of membrane lipid available for interaction was calculated at the bacterial densities of a MIC assay (thus termed $[L]_{MIC\ assay}$): a bacterium dry mass of 489 fg was assumed,[25] 8.2% of which are phospholipids[26] (data for *E. coli*); admitting a maximum bacterial titre[27] of 10^6 cfu/mL this yields an $[L]_{MIC\ assay}$ of 4 μg/L. A molar value can be obtained by approximating all phospholipids to have the molecular weight of dipalmitoylphosphatidylethanolamine (691.96 $g.mol^{-1}$).

A surface area approach was taken to estimate the concentration of membrane phospholipid in an MHC assay ($[L]_{MHC\ assay}$). The $[L]_{MHC\ assay}$ was obtained from the concentration of erythrocytes in the human blood[28] (5×10^6 cells/μL) their average surface area[29] (150 μm^2), the area per phospholipid headgroup[30] (0.7 nm^2), and a commonly used dilution in MHC determination[14,18] (final 5% vol/vol of blood).

MIC prediction

Equations 2 and 3 were combined to define *P/L* as a function of $[P]_{TOTAL}$, K_p and $[L]$ (because thresholds are often reported as the bound *P/L* ratio rather than a local concentration the former was preferred):

$$P/L = \left(\frac{1}{[P]_{TOTAL} K_p \gamma_L} + \frac{[L]}{[P]_{TOTAL}} \right)^{-1} \quad \text{Eq. 4}$$

Under the conditions where activity is triggered in vivo $[P]_{TOTAL}$ is the MIC, *P/L* is the disruption threshold in the membrane (here termed *P/L**) and $[L]$ is of the magnitude of $[L]_{MIC\ assay}$. Equation 4 can be rewritten as

$$P/L^* = \left(\frac{1}{MIC \cdot K_p \gamma_L} + \frac{[L]_{MIC\ assay}}{MIC} \right)^{-1} \approx MIC \cdot K_p \gamma_L \quad \text{Eq. 5}$$

The approximation in the expression is possible because the nanomolar values of $[L]_{MIC\ assay}$ are two to three orders of magnitude smaller than the typical micromolar MICs,[1] and, given average values for AMP partition constants,[4] $[L]_{MIC\ assay}$/MIC becomes negligible for the result. Finally, a clear relationship between the activity (MIC) of an AMP and its disruptive behavior on a model membrane (*P/L**) can be obtained from a simple rearrangement of Equation 5:

$$MIC = \frac{P/L^*}{K_p \gamma_L} \quad \text{Eq. 6}$$

A method to apply Equation 6 values from biophysical data implements a relationship, deduced elsewhere,[8,15] between the global peptide and lipid concentrations at a critical threshold:

$$[P]_{threshold} = \frac{P/L^*}{K_p \gamma_L} + P/L^* \cdot [L]_{threshold} \quad \text{Eq. 7}$$

According to Equation 6 the MIC is given by the intercept of this straight line:

$$[P]_{threshold} = MIC + P/L^* \cdot [L]_{threshold} \quad \text{Eq. 8}$$

Method implementation

The prediction method was implemented using the AMP BP100 (H-KKLFKKILKYL-NH_2; synthesized as described elsewhere[7]) and multilamellar vesicles of a 1:2 proportion of the phospholipids POPC and POPG (1-palmitoyl-2-oleoyl-sn-glycero-3-phosphocholine and 1-palmitoyl-2-oleoyl-sn-glycero-3-phospho-rac-1-glycerol, from Avanti Polar Lipids, Inc., Alabaster, Alabama). Multilamellar vesicles were prepared as described elsewhere.[7] Optical densities of the vesicle suspension were measured for several lipid-peptide concentration pairs; breaking points putatively corresponding to disruption were fittted according to Equation 7. An MTX Labsystems, Inc. (Vienna, Virginia) Multiskan EX plate reader and BD Falcon (San Jose, California) UV-transparent 96-well plates were used for measurement.

REFERENCES

1. Giacometti, A., Cirioni, O., Greganti, G., Quarta, M. & Scalise, G. In vitro activities of membrane-active peptides against gram-positive and gram-negative aerobic bacteria. *Antimicrob Agents Chemother* **42**, 3320-3324 (1998).
2. Friedrich, C.L., Moyles, D., Beveridge, T.J. & Hancock, R.E.W. Antibacterial action of structurally diverse cationic peptides on gram-positive bacteria. *Antimicrob Agents Chemother* **44**, 2086-2092 (2000).
3. Yeaman, M.R. & Yount, N.Y. Mechanisms of antimicrobial peptide action and resistance. *Pharmacol Rev* **55**, 27-55 (2003).
4. Melo, M.N., Ferre, R. & Castanho, M.A. Antimicrobial peptides: linking partition, activity and high membrane-bound concentrations. *Nat Rev Microbiol* **7**, 245-250 (2009).
5. Santos, N.C., Prieto, M. & Castanho, M.A. Quantifying molecular partition into model systems of biomembranes: an emphasis on optical spectroscopic methods. *Biochim Biophys Acta* **1612**, 123-135 (2003).
6. Matos, C., Lima, J.L., Reis, S., Lopes, A. & Bastos, M. Interaction of antiinflammatory drugs with EPC liposomes: calorimetric study in a broad concentration range. *Biophys J* **86**, 946-954 (2004).
7. Ferre, R. et al. Synergistic effects of the membrane actions of cecropin-melittin antimicrobial hybrid peptide BP100. *Biophys J* **96**, 1815-1827 (2009).
8. Melo, M.N. & Castanho, M.A. Omiganan interaction with bacterial membranes and cell wall models. Assigning a biological role to saturation. *Biochim Biophys Acta* **1768**, 1277-1290 (2007).

9. Huang, H.W. Molecular mechanism of antimicrobial peptides: the origin of cooperativity. *Biochim Biophys Acta* **1758**, 1292-1302 (2006).
10. Blazyk, J. et al. A novel linear amphipathic beta-sheet cationic antimicrobial peptide with enhanced selectivity for bacterial lipids. *J Biol Chem* **276**, 27899-27906 (2001).
11. Tossi, A., Sandri, L. & Giangaspero, A. Amphipathic, alpha-helical antimicrobial peptides. *Biopolymers* **55**, 4-30 (2000).
12. Sader, H.S., Fedler, K.A., Rennie, R.P., Stevens, S. & Jones, R.N. Omiganan pentahydrochloride (MBI 226), a topical 12-amino-acid cationic peptide: spectrum of antimicrobial activity and measurements of bactericidal activity. *Antimicrob Agents Chemother* **48**, 3112-3118 (2004).
13. Badosa, E. et al. A library of linear undecapeptides with bactericidal activity against phytopathogenic bacteria. *Peptides* **28**, 2276-2285 (2007).
14. Ferre, R. et al. Inhibition of plant-pathogenic bacteria by short synthetic cecropin A-melittin hybrid peptides. *Appl Environ Microbiol* **72**, 3302-3308 (2006).
15. Pott, T., Paternostre, M. & Dufourc, E.J. A comparative study of the action of melittin on sphingomyelin and phosphatidylcholine bilayers. *Eur Biophys J* **27**, 237-245 (1998).
16. Szoka, F., Jr. & Papahadjopoulos, D. Comparative properties and methods of preparation of lipid vesicles (liposomes). *Annu Rev Biophys Bioeng* **9**, 467-508 (1980).
17. Mayer, L.D., Hope, M.J. & Cullis, P.R. Vesicles of variable sizes produced by a rapid extrusion procedure. *Biochim Biophys Acta* **858**, 161-168 (1986).
18. Blondelle, S.E. & Houghten, R.A. Hemolytic and antimicrobial activities of the twenty-four individual omission analogues of melittin. *Biochemistry* **30**, 4671-4678 (1991).
19. Subbalakshmi, C., Krishnakumari, V., Nagaraj, R. & Sitaram, N. Requirements for antibacterial and hemolytic activities in the bovine neutrophil derived 13-residue peptide indolicidin. *FEBS Lett* **395**, 48-52 (1996).
20. van den Bogaart, G., Guzman, J.V., Mika, J.T. & Poolman, B. On the mechanism of pore formation by melittin. *J Biol Chem* **283**, 33854-33857 (2008).
21. Sessa, G., Freer, J.H., Colacicco, G. & Weissmann, G. Interaction of a lytic polypeptide, melittin, with lipid membrane systems. *J Biol Chem* **244**, 3575-3582 (1969).
22. Huang, H.W. Free energies of molecular bound states in lipid bilayers: lethal concentrations of antimicrobial peptides. *Biophys J* **96**, 3263-3272 (2009).
23. Nernst, W. Verteilung eines Stoffes zwischen zwei Lôsungsmitteln und zwischen Lôsungsmittel und Dampfraum. *Z Phys Chem* **8**, 110-139 (1891).
24. Chiu, S.W., Jakobsson, E., Subramaniam, S. & Scott, H.L. Combined monte carlo and molecular dynamics simulation of fully hydrated dioleyl and palmitoyl-oleyl phosphatidylcholine lipid bilayers. *Biophys J* **77**, 2462-2469 (1999).
25. Loferer-Krossbacher, M., Klima, J. & Psenner, R. Determination of bacterial cell dry mass by transmission electron microscopy and densitometric image analysis. *Appl Environ Microbiol* **64**, 688-694 (1998).
26. Kaneshiro, T. & Marr, A.G. Phospholipids of Azotobacter Agilis, Agrobacterium Tumefaciens, and Escherichia Coli. *J Lipid Res* **3**, 184-189 (1962).
27. Giacometti, A. et al. In vitro susceptibility tests for cationic peptides: comparison of broth microdilution methods for bacteria that grow aerobically. *Antimicrob Agents Chemother* **44**, 1694-1696 (2000).
28. Rosen, R. Optimality principles in biology. (London: Butterworths, 1967).
29. Bray, D. Cell movements : from molecules to motility, Edn. 2nd ed. (Garland, New York ; [Great Britain]; 2001).
30. White, S.H. & King, G.I. Molecular Packing and Area Compressibility of Lipid Bilayers. *Proc Natl Acad Sci U S A* **82**, 6532-6536 (1985).

The BioNumbers database (http://bionumbers.hms.harvard.edu) maintained by R. Milo, P. Jorgensen and M. Springer was an important starting point to finding many of the values, and respective references, used in the estimates.

ACKNOWLEDGEMENTS

The authors thank Uris Ros for the valuable insights on the extension of some of the conclusions to hemolysis assays. Fundação para a Ciência e Tecnologia (Portugal) is acknowledged for a grant to M.N.M. (SFRH/BD/24778/2005) and the project PTDC/QUI/69937/2006.

AUTHOR CONTRIBUTIONS

M.N.M. developed the binding model, applied MIC predictions to published data, and contributed to the design of the practical implementation of the prediction method, its experimental testing, and the writing of the manuscript. R.F. designed and synthesized BP100, adapted the binding model to allow MIC prediction, and contributed to the design of the practical implementation of the prediction method and its testing. L.F., M.P. and E.B. contributed to the design and synthesis of BP100 and with critical discussions. M.A.R.B.C. planned the project and contributed to the writing of the manuscript and the design of the practical implementation of the prediction method.

Supplementary Discussion 1 – Analyzing published data

Published data regarding thresholds in the membrane is not always clearly presented as the bound *P/L* ratio. Instead, the global *P/L* ratio is often found. This ratio is not as accurate as the local ratio as no information is provided on the amount of peptide that is actually bound to the membrane. If K_p and the sample volume are known, a global ratio can be corrected, but if no binding information is available approximations must be made: a shortcut to obtaining the local ratio without exact knowledge of K_p is to consider X_L very close to 1, in which case the global *P/L* ratio will tend to the value of the local ratio. From Equation 2 in the main article it can be seen that this is valid if $[L]$ is large enough so that $K_p \cdot \gamma_L \cdot [L]$ is much greater than 1. For a K_p of 5×10^5 more than 90% of bound peptide will be attained for $[L]$ greater than 0.3 mM. Because many studies with AMPs are in such conditions, one can usually approximate the global P/L ratio as the local one, if no better alternatives are available.

Supplementary Discussion 2 – Robustness of the in vivo binding model

In the calculations carried out in this work an in vivo scenario was severely simplified in several aspects. It is thus important to assess the extent to which approximations affect the obtained practical and theoretical conclusions.

– Estimation of $[L]_{MIC\ assay}$

The estimation of $[L]_{MIC\ assay}$ from a bacterium's weight is prone to error and implicitly assumes an average value. Likewise, the geometric estimates approximate the bacterium membrane as a spherical shell, which may not be entirely accurate, especially if rod- or spiral-shaped bacteria are considered; the same stands for the number of leaflets – which may double if a Gram-negative outer membrane is added – and for the area per phospholipid – which will surely vary under physiological conditions. However, the precise value of $[L]_{MIC\ assay}$ is unimportant because the term containing $[L]_{MIC\ assay}$ in Equation 5 (in the main article) is negligible when $[L]_{MIC\ assay} << MIC$, and, since $(MIC \cdot K_p \cdot \gamma_L)^{-1}$ is in the order of 1×10^{-1}, even $[L]_{MIC\ assay}$ equal to the MIC will only add around 10% error to the result. As such, any errors in the approximation of $[L]_{MIC\ assay}$ will only be of significance if they impose a correction larger than the two to three orders of magnitude by which typical MICs are greater than the estimated nanomolar lipidic concentrations.

– Presence of other system components

This model does not take into account possible interactions of the peptide with other system components besides the cell membrane. However, for such interac-

tions to influence the bound concentrations – namely by significantly reducing the unbound amount of peptide – they would have to be extremely strong or the interacting components would have to be in a very high concentration. The only other cellular constituent present in enough quantity to potentially sequester a significant amount of peptide is the anionic Gram-positive peptidoglycan wall. Even so, this structure has at most only 20 times the volume of the membrane[1] and, despite not being the subject of many studies, a proportionally lower affinity towards it was reported for the peptide omiganan,[2] meaning that the presence of peptidoglycan is roughly equivalent to having a second membrane for the peptide to interact with.

Likewise, bacterial DNA and RNA molecules, being markedly anionic, could bind a significant portion of the peptide and render the above conclusions invalid (irrespectively of the physiological relevance of such interactions[3]). This, however, should have little impact on the results: a total of about 3×10^7 nucleotide-associated anionic charges per bacterium can be obtained taking into account average amounts of DNA, mRNA and tRNA in an *E. coli* cell.[4,5] Under MIC assay conditions that number of anionic charges would bind 8 nM of a 6+ charged peptide, assuming a one-to-one charge interaction. This is 0.4% of a 2 μM MIC – low enough not to significantly affect the estimations.

However, while cellular components seem to be unable to prevent high peptide accumulation in the membrane, the same might not be true for bulk phase constituents,[6,7] which are often present in milimolar concentrations: one can expect high ionic strengths to reduce the degree of peptide interaction with the membrane by neutralizing the effective charge of both the peptide and the membrane surface, especially if the involved counterions are not easily displaced. This effect can be compensated for by using physiological ionic strengths when measuring partition constants.

Supplementary Discussion 3 - Approximations in the partition model

There are two simplifications implicit in the definition of the partition constant and partitioned peptide fraction (Equations 1 and 2 in the main article) where it is assumed that the amounts of peptide in the membrane ($n_{p,L}$) and in the aqueous phase ($n_{p,W}$) are small compared to the total amount of lipid (n_L) and water (n_W) molecules, respectively.[8] While $n_{p,W} << n_W$ is valid for practical peptide concentrations, $n_{p,L} << n_L$ may not always be true for some of the high concentrations considered. The bound peptide concentration can be corrected by using the full K_p definition,[8] as per Supplementary Equation 1:

$$K_p = \frac{\dfrac{n_{p,L}}{(n_L + n_{p,L})\gamma_L}}{\dfrac{n_{p,W}}{(n_W + n_{p,W})\gamma_W}} \approx \frac{\dfrac{[P]_L}{1+\gamma_L[P]_L}}{[P]_W} \Leftrightarrow [P]_L = \frac{K_p[P]_W}{1-\gamma_L K_p[P]_W} \qquad \text{SE.1}$$

where γ_L and γ_W are, respectively, the molar volumes of the lipid and water molecules; the approximation can made assuming $n_{p,W} << n_W$. Using Equations 1 and SE.1, the relative change in the $[P]_L$ value upon correction can be obtained (the '*c*' subscript stands for corrected parameters):

$$\frac{[P]_{L,c}}{[P]_L} = \frac{\dfrac{K_{p,c}[P]_{W,c}}{1-\gamma_L K_{p,c}[P]_{W,c}}}{K_p[P]_W} \qquad \text{SE.2}$$

One can assume that K_p values, being calculated away from excessively high peptide densities in the membrane, are equivalent to $K_{p,c}$. In addition, admitting that $[P]_W$ will not change significantly in vivo (see text), $[P]_{W,c}$ can be made approximately equal to $[P]_W$. Thus,

$$\frac{[P]_{L,c}}{[P]_L} = \frac{1}{1-\gamma_L K_p[P]_W} = \frac{1}{1-\gamma_L[P]_L} = \frac{1}{1-P/L} \qquad \text{SE.3}$$

This correction, even at $[P]_L$ = 130 mM (P/L = 1:10), amounts to a difference of only 11% in the corrected concentration. Furthermore, it is a correction in the direction of higher bound concentrations. Rather than invalidating any of the conclusions in the analysis this further approximates the results to membrane saturation.

It should be borne in mind that, besides the above correction, the entire partition formalism as presented here is based on the assumption of the two phases being ideally diluted solutions (i.e. the peptide molecules are dilute enough not to significantly interact with each other). As one approaches high extents of membrane coverage this assumption is inevitably invalidated. However, the fact that peptide *vs.* lipid fluorescence curves for BP100 and omiganan are essentially linear almost up to membrane saturation[2,9] suggests that there is little error introduced by having high bound concentrations, in that range of conditions.

Supplementary Discussion 4 – Conversion from other constants

A different binding constant, K_b (M^{-1}) – or its inverse, the dissociation constant K_d (M) – is also commonly used, where it is assumed that the peptide interacts with the membrane phospholipids to form a 1:1 complex[10] with reaction equilibrium constant K_b; the validity of this approach to interpret membrane partitioning is dis-

cussed elsewhere.[8,11] Because published data are sometimes analyzed in this alternative framework, a conversion between both K_p and K_b is presented. K_b is defined as:

$$K_b = \frac{[PL_{complex}]}{[P]_{free}[L]_{free}} \approx \frac{X_L[P]}{(1-X_L)[P][L]} = \frac{X_L}{(1-X_L)[L]} \qquad \text{SE.4}$$

where $[PL_{complex}]$ is the concentration of the 1:1 peptide:lipid complex, $[P]_{free}$, $[P]$, $[L]_{free}$ and $[L]$ are the unbound and the total concentrations of peptide and phospholipid, respectively, and X_L is the mole fraction of the bound peptide. The approximation of $[L]_{free}$ to $[L]$ significantly simplifies the calculations, but, in the case of high extents of binding, an error will be introduced. Because this approximation is roughly equivalent to the assumption of $n_{p,L} << n_L$ in Supplementary Discussion 3, the resulting correction of the bound concentrations will be subject to an error of similar magnitude.

Supplementary Equation 4 can be solved for X_L:

$$X_L = \frac{K_b[L]}{1+K_b[L]} \qquad \text{SE.5}$$

It then becomes obvious, by comparison with Equation 2 in the main article, that in the limit of weak interactions:

$$K_p = K_b / \gamma_L \qquad \text{SE.6}$$

Supplementary Material References

1. Jawetz, E., Melnick, J.L. & Adelberg, E.A. in, Edn. 16 197-201 (Lange Medical Publications, Los Altos, California; 1984).
2. Melo, M.N. & Castanho, M.A. Omiganan interaction with bacterial membranes and cell wall models. Assigning a biological role to saturation. *Biochim Biophys Acta* **1768**, 1277-1290 (2007).
3. Brogden, K.A. Antimicrobial peptides: pore formers or metabolic inhibitors in bacteria? *Nat Rev Microbiol* **3**, 238-250 (2005).
4. Blattner, F.R. et al. The complete genome sequence of Escherichia coli K-12. *Science* **277**, 1453-1462 (1997).
5. Sundararaj, S. et al. The CyberCell Database (CCDB): a comprehensive, self-updating, relational database to coordinate and facilitate in silico modeling of Escherichia coli. *Nucleic Acids Res* **32**, D293-295 (2004).
6. Tossi, A., Sandri, L. & Giangaspero, A. Amphipathic, alpha-helical antimicrobial peptides. *Biopolymers* **55**, 4-30 (2000).
7. Blazyk, J. et al. A novel linear amphipathic beta-sheet cationic antimicrobial peptide with enhanced selectivity for bacterial lipids. *J Biol Chem* **276**, 27899-27906 (2001).
8. Santos, N.C., Prieto, M. & Castanho, M.A. Quantifying molecular partition into model systems of biomembranes: an emphasis on optical spectroscopic methods. *Biochim Biophys Acta* **1612**, 123-135 (2003).
9. Ferre, R. et al. Synergistic effects of the membrane actions of cecropin-melittin antimicrobial hybrid peptide BP100. *Biophys J* **96**, 1815-1827 (2009).
10. Christiaens, B. et al. Tryptophan fluorescence study of the interaction of penetratin peptides with model membranes. *Eur J Biochem* **269**, 2918-2926 (2002).
11. Matos, C., Lima, J.L., Reis, S., Lopes, A. & Bastos, M. Interaction of antiinflammatory drugs with EPC liposomes: calorimetric study in a broad concentration range. *Biophys J* **86**, 946-954 (2004).

This concludes my account of the methodological side of my research — although the interested reader can find in the Appendix further experimental processes I developed during my PhD.

Looking back, I am amazed at the time it took to make all the relatively simple connections described in this part. The theoretical notions derived in this section can be explained to any biophysicist in less than an hour. Still, they took five years to mature! It is somewhat scary, and challenging, that a trivial breakthrough can be as elusive as a complex find. In the end I am glad that with this PhD I also got to learn such peculiarities of the construction of scientific knowledge.

End of Part II

Unfinished business

During this project there were, inevitably, several avenues of investigation that were only partly undertaken at one time or another, or that are still open at the time of writing. The reasons for not having carried them out to completion range from lack of motivation to lack of time. Nevertheless, I find it positive that my work consisted not only in addressing scientific questions but also in generating them – even if these remain unanswered for the time being.

The toxicity of BP100 to mammalian cells

The move to the Institute of Molecular Medicine drove my research towards more biological goals. Namely, the inclusion of Ana Correia in the group prompted us to try and tackle questions that could be addressed by her technical expertise in cell biology. In this section, all the experimental aspects of cell preparation were carried out by Ana, whereas I was mainly involved in fluorescence microscopy and data analysis (although I had little prior experience in fluorescence microscopy, by being familiar with its spectroscopic counterpart as well as having attended an IMM shortcourse on bioimaging, I was able to learn the basic practical aspects and become independent pretty quickly).

Ana started out by subjecting three types of cultured mammalian cells (V79 Chinese hamster lung fibroblast, Huh-7 human hepato cellular carcinoma, and HeLa — henceforward collectively abbreviated "cultured cells") to BP100, and the first observation was that these cells were about five-fold more susceptible to the peptide than what had been reported for erythrocytes[42] (the initial set of these results, with hamster fibroblasts,

was included in Article IV). Three different viability assays testing for membrane integrity, mitochondrial function, and adhesion, closely agreed on the IC_{50} value, the drug concentration required to kill half of the cells. In spite of this susceptibility, BP100 is still a good 10- to 20-fold more active against the Gram-negatives tested in Gerona[42] and by us (see Section 3.5) than against the cultured cells.

This observation indicated that the erythrocyte may be an overly simple model, at least concerning this peptide's toxicity, and the possibility that the same might be true for other AMPs is very interesting: the erythrocyte is a prevalent model in AMP toxicity assessment; if discredited, the safety of many AMPs would have to be reevaluated. Once again, we were aiming at hypotheses with far more impact than just the peptide at hand.

Differences in the composition of the plasma membranes of the erythrocyte and the cultured cells could account for a distinct lytic behavior but we preferred to focus on a much more interesting hypothesis based on the difference in organelles between the two cell types: admitting that BP100 is able to translocate across the plasma membrane, a very likely inner target in the cultured cells, given the peptide's affinity for bacteria, would be the mitochondria. And these happen to be conveniently absent from the mature erythrocyte.[70] Equipped with this hypothesis I started envisioning toxicity processes by which mitochondria would burst, leaving the cell to die of ATP deprivation, or, alternatively and more spectacularly, releasing mitochondrial effectors[71] that would trigger cascades ultimately culminating in apoptosis! This last hypothesis-from-a-hypothesis was particularly appealing, as there is something about "apoptosis-mediated toxicity" that distinctly sounds like "cancer therapy."[72]

At this point we had two hypotheses to test: are the mitochondria the primary targets in BP100 toxicity? And could other AMPs act similarly? We put our efforts into following, in real time under the microscope, the fate of the mitochondria in the hamster fibroblasts upon addition of BP100. To this end we relied on JC–1, a two-in-one fluorescent mitochondrial probe that fluoresces red if there is a transmembrane potential (i.e. mitochondrial respiration is active) and green if not. While JC–1 fluorescence

was observed, the shape of the cells was monitored, using transmitted light, to detect occurrence of lysis.

The first images we took, in the absence of peptide, were great. Bunches of green mitochondria filaments, not unlike noodles, spotted bright red here and there, could be clearly seen within the cells: it was very interesting to observe, though expected from other reports on mitochondrial staining,[73] that only a small segment of the mitochondrion is normally polarized while the rest sits idle, perhaps awaiting a sudden increase in the demand for ATP. The recorded images, captured in a confocal microscope, were not as cool as observed through the eyepiece in widefield mode* but were good enough to attempt quantification of the increase/decrease of either color upon addition of BP100 and, indeed, a clear reduction of the red fluorescence intensity was visible in the first few minutes after peptide addition. Because mitochondrial depolarization would strongly support our hypothesis we were very excited about this, only to learn shortly afterwards that the controls displayed the same intensity decrease due to a very fast and red-selective photobleaching. Disappointed, we carried on, trying to adjust observation parameters to get rid of the dreaded bleaching, hoping that some peptide effect would be visible underneath. These hopes were not completely unfounded: in the same experiment where the fast decrease of the JC–1 red fluorescence intensity was observed, a small increase of the green fluorescence, indicative of depolarization, was also detected; and this increase was visible even before any correction for photobleaching. In another occasion I made an interesting observation, albeit anecdotal like most in these experiments: we had left for a couple of hours a fibroblast culture incubating, under the microscope, with a BP100 concentration equal to its IC_{50}. When I returned I found that apart from the imaged region, which had become inevitably bleached, most adherent cells were bright red — quite unlike the situation at rest — but several others had detached (and presumably died), and these were mostly green.

*At the time we were using a confocal microscope not because we needed confocality — which actually was not ideal for whole cell observation — but because it was the microscope most accessible to us with temperature and CO_2 control, required to keep the cells alive during the observation time.

Many possible direct and indirect effects of BP100 may have elicited that cellular response in the survivors; in any case, had we been able to reproduce the observation, this would be a clear link between the mitochondria and the toxicity process.

To deal with the photobleaching issue, we started using a widefield microscope, but the change in system entailed further steps of optimization. Even after those, no matter what we tried, the probe seemed to be getting more and more susceptible to photobleaching. At this point, things took another turn for the worst: our cells started to mysteriously lose viability and JC–1 seemed to be the culprit — although it had behaved perfectly well in the initial runs! I was quickly losing motivation: what had begun as a challenging biophysics-meets-biology experiment had by then become a problem of optimization of several parameters, most of them related to cell culture techniques. Not only did I find this very unappealing, I also felt impotent to provide valuable input and, eventually, I stopped dedicating effort to this project. We never got to testing other AMPs.

Testing saturation in bacteria

After having found evidence linking the *in vivo* charge neutralization of *E. coli* with the MIC Carla Alves and I looked for a way to verify the MIC-saturation correlation hypothesis. The co-occurrence of saturation and neutralization in model membranes had been observed, which indirectly supported the hypothesis, but we needed stronger evidence.

We decided to employ with BP100 a method similar to the approach I describe in Section 4.3 to measure the magnitude of omiganan interaction with peptidoglycan: BP100 was incubated with bacteria, the suspension was then centrifuged and the fluorescence emission of the unbound peptide measure from the supernatant. As we were looking for saturation, and contrary to the work with peptidoglycan, it was the peptide concentration to be scanned instead of the amount of bacteria. Carla carried out the majority of the practical part of the work and I did most of the data analysis.

I was aware that the main obstacle to this, and probably most approaches, is that the recommended bacterial densities for MIC assays[74] (between 2 and 7×10^5 cfu/mL — 'cfu' standing for 'colony-forming unit') are likely to be too low for even a strong binding to be detected, much less for a distinction between saturation and non-saturation to be observed — recall the conclusion from the application of Equation 4.2 to an *in vivo* setting, in Section 6.1. Our workaround was to use higher bacterial densities: at 10^9 cfu/mL Equation 4.2 predicts 43% of bound peptide (under the assumptions detailed in Section 6.1), which should already be measurable.

In practice, we took a bacterial suspension in exponential growth phase, washed it thrice in buffer (in the process concentrating it to the target 10^9 cfu/mL), incubated with different amounts of peptide (10 minutes), centrifuged one last time, discarded the pellet and collected the supernatant for measuring. Using such high densities, however, departed from ideal conditions and if saturation was observed any relation to the MIC would have to be extrapolated. Furthermore, the *E. coli* strain we were using reached at most 10^8 cfu/mL on its stationary phase: forcing a density ten times higher than that value, even for the short preparation period, could have unexpected results. I hoped, nevertheless, that the putative saturation would be observed and that, consistently, the saturating peptide concentration would be proportional to the bacterial density — in that case the extrapolation back to MIC assay bacterial concentrations would be straightforward.

I expected saturation points to be identifiable from a curve of bound fraction vs BP100 concentration: if anything similar to a K_p or a D_v partition was valid then the bound fraction should be constant before saturation, whereas afterwards it should decrease with every addition of the peptide. However, when we tried to obtain those points Carla and I came across a serious obstacle: strong contaminating fluorescence was visible in the samples' emissions. The responsible compounds were either being released by bacteria into the supernatant (as the peptidoglycan had in the omiganan–cell wall interaction studies) or they were unwashed growth medium leftovers. These contaminants had a high protein content, judging by the characteristic tryptophan and tyrosine emission spectrum,

and their fluorescence overwhelmed the peptide's tyrosine emission at all but the highest BP100 concentrations. Correction using controls without peptide was error-prone because of a high variability in the degree of contamination and of the difference in magnitudes between the peptide and contaminant fluorescent intensities — not to mention the possibility that release of cellular contents depended on peptide concentration.

Instead of attempting the subtraction of a given control I tried instead to fit the observed emission spectra with a linear combination of the spectra of BP100 and of the contaminants (obtained from a control). I hoped to reach good fits because the contaminants' spectrum was dominated by tryptophan emission, with only a small relative contribution of tyrosine (as expected for any biological sample with average amounts of tryptophan and tyrosine, given the latter's lower absorptivity and quantum yield). Any tryptophan-like emission in our samples could then be used to gauge the relative contribution of the contaminants' spectrum; the remaining fluorescence would be due to BP100 emission. At this point we became aware of an additional, and significant, fluorescence contamination that prevented the spectral decomposition of the emission spectra of our samples. This time the offending compound was polypropylene. Polypropylene is a ubiquitous material in sample preparation and has an emission spectrum that significantly overlaps with tryptophan. We were able to narrow down the main source of polypropylene to the filters we were using to sterilize the stock peptide solutions; by skipping this step, which was unnecessary since we were not interesting in observing bacterial growth, we were able to drastically reduce contamination. Still, centrifugation in plastic tubes and the use of plastic pipette tips was enough to introduce some polypropylene into the samples. To be able to achieve good spectral decompositions despite of this fluorescence background I opted to take excitation–emission maps of samples and controls (Figure A.1). The three-dimensional fluorescence spectra did allow a better separation of the emissions of BP100 and contaminants but spectral decompositions was not of good quality (Figure A.1F). I suspect that the spectrum of the biological contamination was not constant, probably due to variable contributions of tyrosine and tryptophan emission. The

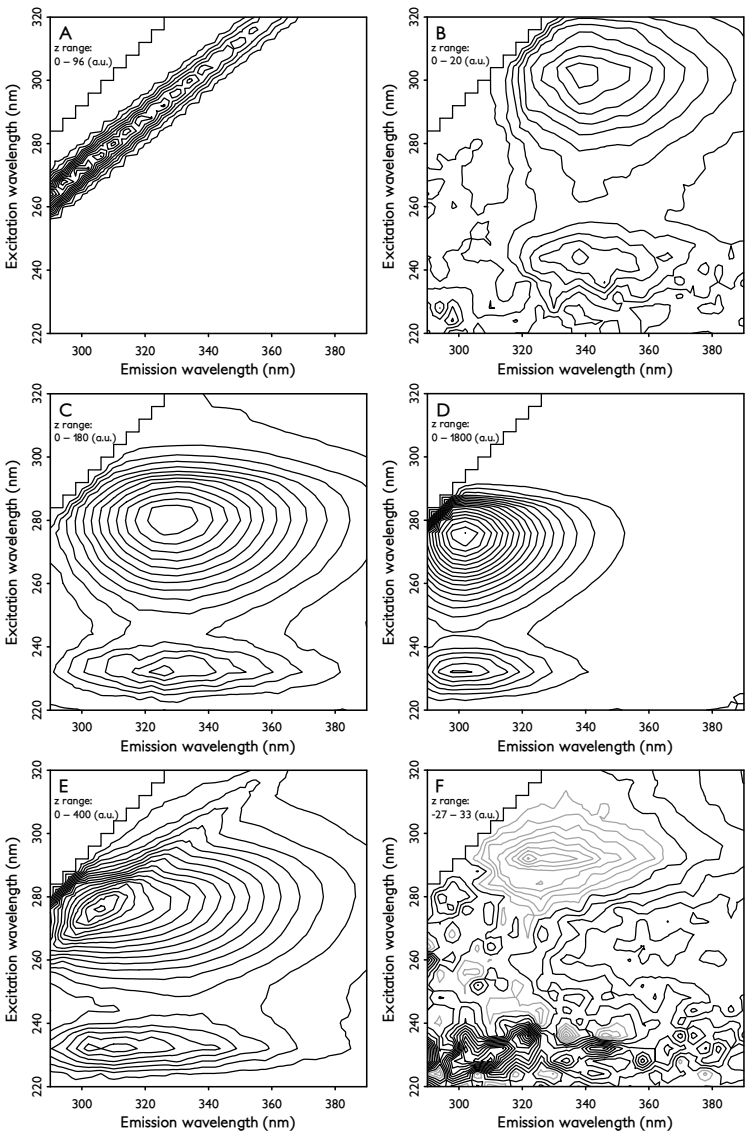

Figure A.1 –Excitation–emission maps (unpublished) of (A) buffer, (B) polypropylene, (C) proteic contaminant from bacteria or growth medium, and (D) 50 µM BP100; intensities in arbitrary units (a.u.). Map A was previously subtracted from maps B through D. These four spectra were used to decompose the excitation–emission map of the supernatants from peptide-bacteria incubations. Spectrum E is one such map, at 10 µM BP100; residuals from the best decomposition fit are plotted in F (lighter traces indicating negative values) and are clearly not random, especially in the 340 nm, 290 nm region; combination factors were 1.86, 1.16, and 0.14 for maps B, C, and D, respectively; the factor of map A was always 1.

results obtained this way did not exhibit any sign of saturation. On the contrary, the more peptide was added to bacteria the more it seemed to bind. Many inferences would be possible from this observation, such as cooperative peptide-bacterium interaction, or permeabilization of bacteria followed by binding to internal components. I preferred, however, not to waste clean thoughts on dirty data, especially since the error in the decomposition (expressed as the sum-of-squares of the residual spectra) increased with peptide concentration.

Carla's departure and my starting to write this book put an end to our efforts to observe saturation *in vivo*. Alternatives to our method may include peptide labeling with a fluorophore, although I always feel uncomfortable at the idea of appending anything to such a short sequence. Another option may be to synthesize ^{13}C or ^{15}N labeled BP100 and proceed to its detection by liquid NMR (or even to use the already synthesized fluorinated analogs). This approach would, in principle, allow the detection of binding without the need for phase separation: the molecules that are bound to bacteria will have a very slow correlation time, which causes their signal to vanish (very slow correlation times entail very fast spin-spin relaxations and a consequent broadening and flattening of the corresponding peaks); the measured signal would then be proportional to the unbound peptide fraction.

Other work

The work I carried out during my PhD was mainly related to AMPs. There were, however, some exceptions that fell outside the scope defined by the title of this thesis — sometimes even unrelated to the field of peptide studies altogether. For that reason publications resulting from this work were not included in this book and are only referred to instead.

Work with non-AMPs stemmed mostly from a partnership Miguel established with the group of Andrea da Poian at the Federal University of Rio de Janeiro. This collaboration focused on the study of dengue virus and, as usual, we provided biophysical expertise on the characterization of peptide-membrane interactions. The Rio group expressed and purified relevant peptides (from the capsid and envelope proteins), and performed a wide range of biochemical and biological studies with both peptides and whole viruses. Fausto Stauffer, then finishing his PhD under Andrea's supervision, was the first exchange student under this collaboration. He visited our group to apply our methodologies to study segments of the dengue virus envelope protein, namely, peptides putatively responsible for fusion of the viral envelope with the host's membrane.

At the time Miguel and I were reaching the first conclusions on saturation and it was interesting to observe that Fausto's peptides also displayed changes in interaction behavior upon the crossing of some sort of bound concentration threshold. I helped Fausto apply my recent conclusions to his case and design some relevant experiments. I also analyzed data he had obtained on the in-depth bilayer localization of the peptide, using the algorithm I had been working on (see Section 'Differential quenching' in the Appendix). Lastly, I wrote a small part of the resulting paper,[75] of which I am co-author.

* * *

Shortly after I began my studies with BP100 I was given the opportunity to go to Rio for a six months' stay to learn NMR techniques. Work was carried out in the groups of Ronaldo Borges and Fábio Almeida, both close collaborators of Andrea's. The objective was to better understand the fusion process of the dengue virus, using NMR to structurally characterize the binding to membranes of the viral fusion peptide.

While in Rio, I learnt the basics of NMR spectroscopy, from spectrometer operation to data analysis. I also became familiar with some of the technique's idiosyncrasies, namely, the complex and lengthy data acquisition process and the highly disputed operation time. Indeed, during those six months I only used an NMR spectrometer in about ten occasions — too little equipment time for me to become an independent user. Also because of the limitations on equipment time measurements were restricted to the fusion peptide, although I had initially hoped to also be able to study my AMPs by NMR. I did, however, get a first-author publication on the findings with that peptide.[76] In addition, after I learned the basics of spectral analysis, and also as part of my training, I collaborated with the group of José and Lúcia Previato in a study on glycolipids, which also resulted in a publication.[77]

Besides NMR, I also did some molecular biology work while in Brazil: the cloning of *E. coli* bacteria with a gene encoding for the fusion peptide. The objective was to mass express the peptide while being able to incorporate ^{13}C or ^{15}N isotopes into it, thus widening the range of applicable NMR methodologies. Although the peptide expression would turn out to be too low for purification, practice in the handling of bacteria came in very handy later, when Carla and I were planning and carrying out *in vivo* validation of hypotheses.

My training in Rio was not sufficient for me to be able to independently perform NMR measurements upon returning to Lisbon, especially since no high-field spectrometers were readily available to our group. To use NMR we would have to either buy equipment time or partner with an NMR group, which was what we later did with the Ulrich lab.

NMR is a very powerful technique and my training made me aware of its possibilities — namely, those of liquid NMR, the variety I worked with in Rio. As the reader will have noticed, I always seek to expand upon the methods I use and there are many ways NMR can be customized and potentially improved. I was a bit disappointed, though, that given the scarcity and cost of equipment time there is usually little chance for trial-and-error experiments with measurement conditions. Still, and despite being mostly unrelated to AMP studies, my trip to Brazil was of great importance to the construction of my scientific background.

Postface

In this book I frequently departed quite a lot from a formal scientific writing. More than a matter of style this was a way to convey the true dimension of my first years as a researcher and the contribution of each advance and failure to my learning.

I also wanted to transmit my view on the different facets of research, which is something I found very important to become aware of. I now have a much better idea of which kind of work I prefer and am more productive at. Taking that into account, I recently chose to direct my future training and research towards computational simulation techniques, namely those involving molecular dynamic simulations of peptide-membrane interactions. Working in this field will allow me to test some of the hypotheses raised during my PhD, and, very importantly, to do so using methodologies where experiments and mathematical models come together. In addition, I will very likely be addressing some of the ends that were currently left loose.

Future directions are, by no means, restricted to the incomplete work described in the 'Unfinished business' chapter: in this book many conclusions were taken on the mechanism of "typical" AMPs and on the applicability of methods to peptides in a general sense. While the performance of some of the predictions against peptides other than omiganan and BP100 was assessed in Articles V and VI, most other hypotheses and methods remain only weakly tested. There is plenty of room for improving upon the research presented here.

Lastly, I must say I have looked upon the writing of this book hardly as an obligation but as an opportunity to use my creativity to honor my many collaborators and the good scientific work they helped me achieve. And,

irrespectively of the actual impact (if any) on the field of peptide studies, it seems — judging from the selected news clippings in the opposite page — that I am already leaving a legacy!

2008

FEBS Congress Events

View from the FEBS Booth

By Louise

This year I have decided to give out two special FEBS News awards. The winners are:

Bravery Award

Last year FEBS News reported that fearless Secretary-General Israel Pecht, was the only man to attend the Women in Science Career lunch. This year the honour went to this chap, whose name I don't know, but I do know he was from Portugal. The WISE lunch is open to all, yet this fool hardy man was the only one strong enough to take on the might of 76 women participants. I hear on the rumour mill that he enjoyed it and found it interesting. So hats off to you!

The thing I want to know is why more men don't attend. Come on chaps! 75 intelligent, articulate, scientists with varied and interesting opinions from all over the world all together in one room!! Yes dreams can come true!

For our 2008 Bravery Award winner, If you are reading get in touch, we would really like to hear your opinions.

in FEBS News, Sep 2008

2009

FEBS NEWS

Prague Congress News

View from the FEBS Booth

By Louise McSeveny

I also have to make a special mention to participant Henri Franquelim from Portugal. Last year I reported that only one brave Portuguese man had what it took to attend the Women in Science lunch and enjoy the company of room full of intelligent women. Well this unnamed chap went back home told Henri he should attend, which he did and here he is:

Obviously Portuguese men are made of sterner stuff.

I should point out that the WISE career lunch is about discussing careers of women, but can the careers of women be discussed in a vacuum without the participation of men? Shouldn't we work together to resolve issues of family, glass ceilings and career development? I lay down the challenge to all young men reading this for more active participation in the WISE event in Gothenburg next year. You too can have your photo on these pages!

in FEBS News, Sep/Oct 2009

Appendix — Other methods

The methods I have developed, though always involving peptide-membrane interaction, are not limited to the scope of partition and saturation. In this chapter I present other contributes I made: on the assessment of peptide translocation across membranes, on the detection of peptide-induced vesicle leakage, and on the measurement of in-depth peptide positioning in a bilayer.

I sought a method to detect translocation for about three years; in the meantime Miguel, Sónia (who had also carried out work involving translocation) and I even got to write a review on available alternatives, classifying them and detailing their pros and cons. I start out by presenting this review, the writing of which inspired subsequent ideas.

Article VII

Molecular Membrane Biology, May–June 2007; 24(3): 173–184

informa
healthcare

How to address CPP and AMP translocation? Methods to detect and quantify peptide internalization *in vitro* and *in vivo* (Review)

SÓNIA TROEIRA HENRIQUES, MANUEL NUNO MELO, & MIGUEL A. R. B. CASTANHO

Centro de Química e Bioquímica, Faculdade de Ciências da Universidade de Lisboa, Lisbon, Portugal

(Received 22 June 2006 and in revised form 13 October 2006)

Abstract

Membrane translocation is a crucial issue when addressing the activity of both cell-penetrating and antimicrobial peptides. Translocation is responsible for the therapeutic potential of cell-penetrating peptides as drug carriers and can dictate the killing mechanisms, selectivity and efficiency of antimicrobial peptides. It is essential to evaluate if the internalization of cell-penetrating peptides is mediated by endocytosis and if it is able to internalize attached cargoes. The mode of action of an antimicrobial peptide cannot be fully understood if it is not known whether the peptide acts exclusively at the membrane level or also at the cytoplasm. Therefore, experimental methods to evaluate and quantify translocation processes are of first importance. In this work, over 20 methods described in the literature for the assessment of peptide translocation *in vivo* and *in vitro*, with and without attached macromolecular cargoes, are discussed and their applicability, advantages and disadvantages reviewed. In addition, a classification of these methods is proposed, based on common approaches to detect translocation.

Keywords: *Cell-penetrating peptides, antimicrobial peptides, membrane translocation, peptide uptake, evaluation of peptide internalization*

Introduction

The introduction of hydrophilic molecules into mammalian cells has become a key strategy for the investigation of intracellular processes and drug therapy. Several methods have been devised to achieve this goal, but they all have limitations [1]. Some peptides are able to translocate across cell membranes with low toxicity [2–5] and to mediate cellular uptake of proteins [3] and other macromolecules [6,7]. These peptides are known as cell-penetrating peptides (CPPs) but the CPP designation is now generalized for all the peptides with the ability to translocate across membranes even when cargo uptake properties are unknown. They include natural, newly synthesized and chimeric peptides [8]. Beside the ability to translocate through cell membrane, these peptides are normally characterized as short, cationic, water-soluble peptides with high efficiency and low cytotoxicity [9]. The mechanism used by CPPs to pass the membrane is not well understood and is a controversial topic in the literature. At the beginning the internalization mechanism of CPPs was generalized and considered to be endocytosis-independent [2,5]. Nowadays there is experimental evidence for both endocytic and non-endocytic routes (for further information see [9,10]). Considering the information available in the literature a unique mechanism for all the peptides does not seem reasonable and more than one mechanism can operate for a single peptide [10].

Ribosomal antimicrobial peptides, or AMPs, are efficient antibiotics against a variety of microbial pathogens [11–14]. These peptides are usually short and cationic [15] such as CPPs, but they are also characterized by a strong interaction with cellular membranes, and by the ability to selectively attack pathogens without disturbing host cell integrity [16,17]. AMPs are potential candidates of a new antibiotic generation against multiresistant bacterial strains [16].

Despite the fact that most AMPs exert their principal activity at the membrane level [15,17], translocation processes have been shown to occur for many of them [18,19]. Considering this, AMPs are natural templates for designing cell-penetrating

Correspondence: Miguel A. R. B. Castanho, Centro de Química e Bioquímica, Faculdade de Ciências da Universidade de Lisboa, Ed. C8, Campo Grande, 1749-016 Lisbon, Portugal. Tel: +35 1217500931; Fax: +35 1217500088. E-mail: castanho@fc.ul.pt

ISSN 0968-7688 print/ISSN 1464-5203 online © 2007 Informa UK Ltd
DOI: 10.1080/09687860601102476

molecules, which can be developed into carriers [9,20]. AMPs and their derivatives are thus very promising molecules to use both as antibiotics and as drug transporters.

To guarantee that a specific peptide works as a CPP, its ability to cross the membrane and the capacity to transport attached cargoes is of first importance. Regarding AMPs, internalization is not a prerequisite and the biological efficiency of AMPs can be evaluated without translocation assessment. However the characterization of such membrane processes is of great value both in the development of new antibiotics and in the design of templates for CPPs [10].

In this paper we will review methods that are available to evaluate peptide uptake into cells or vesicular model membranes.

Methods used to evaluate peptide uptake

Assessment of peptide translocation without attached cargo or labelled with a fluorescent probe

In vivo *methods.* The CPPs internalization mechanism is a matter of vibrant discussion in the literature. To evaluate if CPPs are internalized by endocytosis the dependence of translocation on temperature, or in the presence of specific endocytic inhibitors must be assessed *in vivo*. The intrinsic fluorescence of Trp or Tyr residues cannot be used to investigate peptide internalization *in vivo*, due to the relatively large cellular background fluorescence in the near-UV. Therefore, CPPs are normally derivatized with fluorophores such as Rhodamine B (Rh) [21–24], Fluorescein [5,25–32] and Nitrobenzoxadiazole (NBD) [24,33]. Alternatively, the properties of macromolecular cargoes can be used. In most of the methods described in this section, peptide fluorescence is the experimentally measured signal. However the need to derivatize a peptide can be a limitation not only due to experimental and costly requirements but also because the presence of a dye may alter its properties [34].

Available methods for the *in vivo* detection of peptide internalization can be divided into three categories: quantification of cytosolic concentration, direct visualization of internalization and peptide activity analysis.

Quantification of cytoplasmic concentration. Quantification of cytoplasmic concentration is usually carried out by means of direct measurement of fluorescence emission of peptides. In these methods, elimination of the non-internalized and cell-adsorbed peptide fractions is required to avoid an overestimation of peptide internalization; consequently, extensive washing procedures, including trypsinization and centrifugation, are required [21,22,29,30,35,36]. Quenching of peptide fluorescence is an alternative to annihilate non-internalized peptide signal [24,33,37].

A cell lysate should be prepared and the fluorescence intensity of labelled-CPP in supernatant measured [29,32]. The washing procedures can be responsible for a signal reduction, due to sample loss and fluorescence bleaching. An additional limitation is the necessity to distinguish the peptide fluorescence from the cell background fluorescence; to assure a good signal/noise ratio the fluorophore should be chosen carefully to avoid overlap with intrinsic cellular fluorescence emissions and to circumvent a fast fading of fluorescence. For instance, Trp fluorescence of peptide can hardly be used due to the intrinsic fluorescence of cellular proteins. The fluorescence of cellular NAD(P)H (~460 nm) and FAD (~530 nm) is an additional concern. A high amount of cellular sample should be used to provide a good emission signal and controls without fluorophore in the same conditions (e.g., cell number and washing procedures) must also be used; a calibration curve should be prepared to allow quantification of internalization. In this case, absolute quantification of the internal peptide concentration may also require information on the total cellular volume.

Oehlke et al. developed a method to discriminate membrane surface-bound, membrane-inserted and internalized peptide fractions [38]. To obtain quantitative information on the peptide fraction associated with plasma membrane and the peptide fraction actually internalized, the exposed peptide was treated with diazotized 2-nitroaniline. This procedure modifies the peptide fraction bounded to the surface, without damaging the cell [39]. Bound and internalized fractions were detected by HPLC analysis of cell lysates and quantified by spectrofluorimetry (5(6)-carboxyfluorescein-N-hydroxysuccinilmide ester–labelled peptide detected with excitation at 445 nm and emission at 520 nm). The fraction of surface bound peptide is strongly modified by the diazo reagent which renders the peptide completely undetectable in HPLC chromatogram (there is a strong retention of highly hydrophobic modified products on the stationary phase of the HPLC column). The fraction of peptide inserted into plasma membrane is slightly protected from the attack of the diazo reagent, so this fraction is only partially modified. The fraction of peptide inaccessible to the diazo reagent is the internalized fraction [38].

Flow cytometry analysis by fluorescence activated Cell Sorter (FACS) is a tool to quantify cellular

association of a fluorophore-labelled peptide. A large number of cells are analysed and dead cells are identified by propidium iodide staining [21,22,30, 32,33,35,40]. The cell subpopulation displaying significant fluorescence emission is identified and quantified, and the CPP uptake is measured as the cell-associated fluorescence intensity. An absolute quantification of the internalized amount of peptide requires either a comparison with a standard [41] or the use of additional methods, such as the ones described above. The need to wash/quench the membrane-bound peptide fraction, also applies for flow cytometry analysis.

A kinetic evaluation of the translocation process has been obtained by testing the inaccessibility of externally added trypan blue to fluorescein-labelled peptides [42]; the rationale behind this approach is shared by many methods described for *in vitro* translocation studies (see below).

Matrix-assisted laser desorption ionization-time-of-flight mass spectroscopy (MALDI-TOF MS) has been used to evaluate the exit of internalized peptides from cells into the culture medium [32,43], to detect peptide internalization and to investigate intracellular degradation [32,36,43–45]. This method allows the direct detection of the peptide and uptake quantification [44]. The sample (extracellular or intracellular supernatant) has to be concentrated to improve the signal. Elmquist and Langel proposed a procedure where samples are zip-tipped, analysed by MALDI-TOF MS and compared with synthetic peptides for a quantitative analysis [32,43]. Instead of synthetic peptides the quantification of the internalized CPP can be achieved with an internal standard with the same sequence but labelled with deuterium. Peptides are biotinylated and, after cell lysis, they are captured by streptavidin-coated magnetic beads. Finally, beads are washed and analyzed by MALDI-TOF MS and the absolute amount of internalized peptide is determined. This procedure is also adequate to know if the peptide has been degraded during sample preparation or inside the cell [44]. Inherent disadvantages in this method are the necessity for specialized and expensive procedures, and equipment to obtain peptide quantification. Moreover, it is rather time-consuming.

Direct visualization of internalization. In early studies, CPP internalization into cells was studied by fluorescence microscopy or in fixed cells where the fluorescence emission of a peptide-derivatized probe was directly visualized [5,26,33,46]. Internalization of some AMPs has also been identified by a fluorescent label and visualized under the confocal microscope. For instance, biotin-labelled polyphemusin I [47] and FITC-labelled buforin II [48] were detected in the cytoplasm of *E. coli* without damaging the membrane; FITC-labelled magainin 2 was detected on the *E. coli* cell wall [48]. Internalization in mammalian cells was also observed with biotin-labelled LL-37 and localization in the perinuclear region was detected [49]. Alternatively, the presence of peptides in cells can be detected by immunofluorescence; for example, the localization of LL-37 was visualized with a specific antibody [49].

Fixation procedures can bias the location of peptides in cells as the illusionary presence of peptides inside cells can arise from the high affinity of cationic peptides to cell surface [50]. Therefore, peptide internalization in cells has to be compared in fixed and non-fixed conditions [27,30]. Cell treatment with trypsin to digest the peptide at cell surface [27,30,32], or quenching of peptide fluorescence has to be performed to remove the interference of the membrane-bound fraction. In these conditions it is possible to distinguish a deep localization inside the cell from membrane adsorption [24]. With confocal microscopy different cellular plans can be used to confirm, or refute, peptide internalization.

Peptide activity analysis. In this class of methodologies, the effect of the peptides in the cytosol or in the membrane is evaluated. AMP translocation *in vivo* has been inferred from observations of intracellular damage (e.g., [51]) or morphological alterations of bacteria [52–54].

In other reports, the peptide interaction with membranes was evaluated by electrophysiological transmembrane current measurements in oocytes [55,56]. With this setup it is possible to have access to both sides of lipidic membranes and it is not necessary to derivatize the peptide with a fluorophore. However, this detection can be ambiguous because transbilayer current can arise from the activation of endogenous channels in oocyte membranes. In order to rule out this possibility these experiments should be repeated on artificial lipid membranes [57]. In addition, only qualitative information about translocation can be obtained unless a quantitative relationship between transmembrane current and internalization is assumed. Lastly, the occurrence of membrane destabilizations induced by peptides is not a proof of their ability to translocate across the membrane and reach the cytoplasm.

In vitro *methods*. Various biophysical approaches have been used to study peptide-lipid interaction in model bilayers. When CPPs are internalized by a physically-driven translocation mechanism, peptide-lipid interactions are truly important. Application of

in vitro methods to evaluate the internalization of CPP is, however, scarce; on the other hand, AMP translocation has been essentially studied using model membranes. Nevertheless, *in vitro* studies face some difficulties and limitations. Large unilamellar vesicles (LUV), or small unilamellar vesicles (SUV), are the most used membrane models for the *in vitro* study of peptide-bilayer interactions. But, detection of peptide entry into the vesicular lumen is not easy. Theoretically, in a simple setup, it is possible to encapsulate an aqueous phase entity that could report peptide proximity or interaction (a quencher, or a fluorescence resonance energy transfer (FRET) acceptor for Trp fluorescence for example) and use it to probe the translocation event. However, the feasibility of this task can be hampered by several factors (see worked examples in part 1 of the Supplementary material in the online version). Several methods have been proposed to overcome these limitations, for instance peptide-lipid FRET (e.g., between Trp-labelled peptide and Dansyl-PE-labelled lipidic vesicles) and/or permanent alteration of the peptide either in or out of the vesicles (e.g., peptide digestion by trypsin) [18,19]. A classification of methods can be devised regarding the peptide location with respect to the bilayer: (i) detection of entrapped peptide lack of accessibility from the outer phase, (ii) detection of inward peptide positioning within the membrane, (iii) direct detection of peptide in the inner phase, and (iv) detection of encapsulated peptide escape. Because of the many possible combinations of techniques and experimental setups some reported methods do not fall within the given categories, therefore, a fifth group of 'unclassified methods' is also presented. This classification differs from the one used for the *in vivo* methods mostly because for *in vitro* a wider range of approaches to the assessment of translocation have been described.

A schematic representation of *in vitro* methods from all the classes, with focus on the fluorescence methodologies, is depicted in Figure 1.

Detection of entrapped peptide lack of accessibility from the outer phase. A semi-quantitative determination of translocation can be performed by detection of peptide inaccessibility to a non-translocating entity [19,24,58–60] after incubation with the model membranes (see Figure 1, panel A). For example, translocation of AMP magainin 2 was identified by the observation that the percentage of inaccessible peptide increases with peptide-lipid incubation time [19]. To perform this experiment trypsin was used to digest peptide after interaction with acceptor-labelled lipid vesicles. It was shown that proteolysis-dependent FRET reduction decreases with incubation time before trypsin addition. It was thus concluded that the peptide becomes inaccessible to trypsin with time. This is consistent with peptide translocation.

This concept can be used with different external components, for instance non-labelled vesicles to desorb the peptide from the labelled vesicles [19,60]. An inverted setup has also been reported where the peptide (in this case, labelled with NBD or bimane fluorophores) was incubated with the non-labelled vesicles and desorption was induced by addition of acceptor-labelled anionic vesicles [59] (a FRET increase, rather than a decrease, was detected in this case). The use of NBD-labelled peptides and addition of dithionite ion as the non-translocating entity is another possibility; in this case, the NBD fluorescence intensity was measured without the need to label the vesicles [24,59]; dithionite acts in a way similar to digestion by trypsin in that the NBD reduction/quenching is permanent. In all these approaches, an estimation of the translocation kinetics can be obtained by adding the non-translocating component at different incubation times [24,59].

It should be noted that in all these methods a time-dependent measurement is required to determine the degree of peptide inaccessibility (as explained in detail in section 2 in the Supplementary material online).

These methods have a number of disadvantages: first, they are unable to discriminate membrane-bound and internalized peptide; second, in the case of lysis, which can occur for AMPs, peptide populations in inner and outer layers could be accounted as accessible, resulting in a low extent of apparent translocation; finally, not all of these methods are compatible with all peptides: for instance some AMPs are resistant to trypsin proteolysis (e.g., Polymixin B and Gramicidin S) [18]. In addition, when using trypsin, extents of translocation may be overestimated if the peptide fragments also interact with the membrane.

Detection of inward peptide positioning within the membrane. In this category, the passage of the peptide to the inner leaflet of the bilayer is monitored. In all the reports where this method is used [19,61,62], internalization is evaluated by the use of vesicles with asymmetric labelling. The fluorophore in membranes is a FRET acceptor for Trp-containing peptides (see Figure 1, panel B).

Wimley and White developed a methylcoumarin derivatized lysophospholipid (LysoMC). This lipid is easily incorporated into bilayers (into both bilayers or only into the outer one) and is able to act as an efficient Trp-fluorescence acceptor/quencher [63].

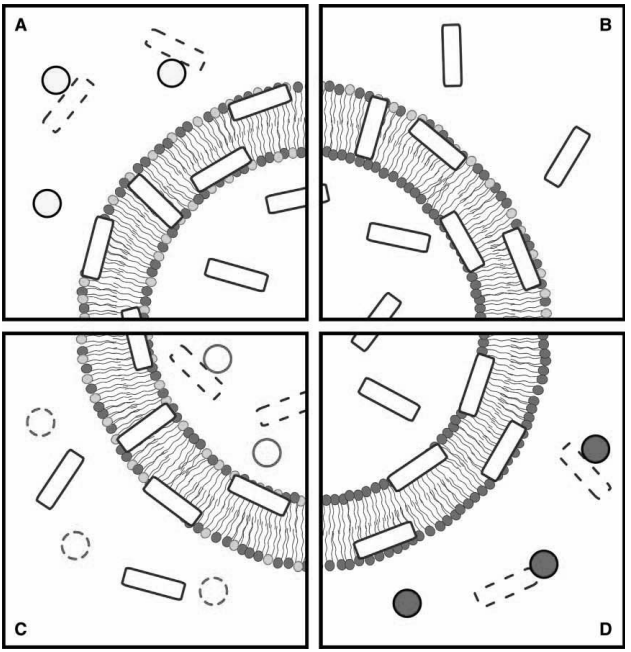

Figure 1. *In vitro* methods for translocation assessment, using FRET and quenching methodologies. Peptide molecules are represented by empty rectangles and additional non-translocating compounds by circles; peptide molecules that have interacted with those compounds are dashed; phospholipids labelled with an acceptor for the peptide's fluorescence are indicated by light grey headgroups. (A) Measurement of the inaccessibility of the peptide to a non-translocating entity with the ability to digest, sequester or permanently quench it; the interaction between the two prevents the peptide from acting as a FRET donor to the labelled phospholipids; small FRET reductions will indicate that the peptide was protected from that interaction; this indicates that the peptide is buried in the membrane or is located in lumen. (B) Detection of inward peptide movement; after the initial adsorption interaction of the peptide with asymmetrically acceptor-labelled vesicles (despite the representation, both inner-leaflet and outer-leaflet labelling can be used), translocation or membrane penetration processes causes the mean distance between peptide and labelled phospholipids to increase (assuming an outer-leaflet labelling) and a concomitant reduction of FRET. If the peptide has quenching capabilities, a quenchable probe can be used to symmetrically label the vesicles; translocation can then be identified by full probe quenching, which is only possible if the peptide reaches the inner bilayer surface. (C) Detection of peptide in the inner phase; in the case of translocation, digestion by encapsulated trypsin (solid circles) reduces the overall amount of peptide available for membrane interaction and, consequently, FRET between peptide and labelled-membrane; trypsin inhibition (dashed circles) is required in the outer phase, prior to peptide addition. (D) Detection of encapsulated peptide escape; in the event of translocation, the peptide fluorescence decreases as it becomes accessible to an externally added, non-translocating quencher; the quencher can, alternatively, be co-encapsulated with the peptide, and the quenching reduction monitored instead. The figure is reproduced in colour in *Molecular Membrane Biology* online.

This probe was initially used to characterize the in-depth membrane distribution of Trp-containing peptides [63], but more recently, Norden and co-workers have developed a method in which LysoMC is used to specifically test translocation; in addition, they described a procedure where is possible to use LysoMC to selectively label the inner layers [61,62]. Experimentally, translocation information is obtained by comparison of emission spectra of inner leaflet LysoMC-labelled vesicles in the presence and absence of the peptide. The Trp residues are donors for FRET. An increase in FRET efficiency in the presence of the peptide means internalization; however, because some outer-to-inner bilayer FRET may occur, it becomes necessary to compare the obtained results with controls where translocating (tryptophan octyl esther [63]) or non-translocating (Ac-18A-NH_2: Ac-DWLKAFYDKVAEKLKEAF-NH_2 [63]) Trp-containing molecules are used [61,62].

Matsuzaki and co-workers had already described a similar method to assess peptide translocation in which vesicles are labelled only on the outer leaflet, with the tryptophan FRET acceptor DNS-PE [19]. With this method it is possible to follow the FRET change during time with a single sample and an end-point approach for each incubation time is not required. Experimentally, after peptide addition, there is an initial increase in FRET efficiency (this corresponds to a peptide partitioning to the outer

leaflet); with time, a decrease in FRET efficiency is observed (which corresponds to translocation where peptide is no longer close to the FRET acceptor in the outer leaflet). With this method, a kinetic analysis of the translocation event can be carried out. Quantitative information may be obtained if additional methods are used to quantitatively relate FRET intensity to luminal peptide concentration.

With these methodologies, peptides do not need to be derivatized and small peptide and lipid concentrations can be used (0.7μM and 100μM respectively [61]). With these methods, in-depth location of peptide can be erroneously measured as translocation; inaddition, they cannot be used with peptides that induce lipid flip flop (FRET acceptor bilayer asymmetry is lost). So far this methodology has been applied only to Trp-containing peptides, although the use of others donor/acceptor pairs is also possible.

Direct detection of peptide in the inner aqueous phase. Methods based on this principle are able to detect the presence of peptides in the inner luminal aqueous phase. With this approach actual translocation, rather than just membrane internalization, is measured (see Figure 1, panel C).

Three different approaches fit in this class of methods. In the first, described by Matsuzaki and co-workers [19], encapsulated trypsin and a peptide-lipid FRET system (Trp-containing peptide and Dansyl chromophore incorporated in vesicles) is used: trypsin is added at the hydration stage of the preparation of symmetrically labelled vesicles; after extrusion, non-encapsulated trypsin is inhibited by a trypsin inhibitor. Upon addition of the peptide to this system, an increase in acceptor fluorescence through FRET is expected as the peptide enters the bilayer; if the peptide is not internalized afterwards, the fluorescence intensity is expected to remain constant after the initial increase. However, if the peptide translocates into the vesicle lumen, it becomes accessible to the uninhibited trypsin and is digested; assuming that the resulting fragments do not interact with the membrane, this degradation of the peptide will lead to a decrease of the amount of peptide in the bilayer and consequent reduction of FRET. A quantitative analysis of the extent of translocation can be easily carried out considering that 100% translocation implies the digestion of all the peptide molecules and absence of FRET; the fluorescence intensity of the system should be the same as in the absence of the peptide. Conversely, 0% translocation will correspond to the maximum fluorescence intensity right after the peptide addition [18,19]. This method cannot be applied to proteolysis-resistent peptide and/or without Trp residues (e.g., Polymixin B and Gramicidin S) [18]. At high translocation efficiency, membrane perturbation caused by peptide fragment accumulation inside vesicles can cause difficulties in internalization quantification. In addition, there is the possibility of digested fragments re-entering the membrane, which can lead to a translocation underestimation.

A second method that detects the presence of the peptide in the inner aqueous phase was recently developed by Bárány-Wallje et al. In this method the experiment is performed with planar lipid membranes (PLMs) and the distribution of fluorescently-labelled peptides, between the two compartments and partitioned in PLM, is followed by confocal fluorescence spectroscopy [64]. This powerful method allows the direct scanning of fluorescence intensity and quantification of peptide in each compartment. Another advantage is the possibility to easily generate asymmetric aqueous phase conditions: a transmembrane potential can be set without the need for ionophores [64]. Besides the need to label the studied peptides (and care must be taken to choose a photostable label), this method has the disadvantage of requiring an uncommon setup with a custom PLM trough.

Another possible method to evaluate peptide translocation with model membranes is to follow peptide interaction with giant vesicles (GVs). With this method direct visualization of peptide interaction with membranes is possible by confocal microscopy. The translocation of peptide across these vesicles can be confirmed by the presence of the fluorophore inside the vesicles [64,65]; in this case, just as with the methodology described for fluorescence imaging of *in vivo* internalization, the use of confocal analysis is crucial to distinguish whether the peptide is inside the vesicle or only adsorbed at the membrane surface. As with the PLM method described above, the peptide has to be derivatized with a fluorophore, which should be carefully chosen to avoid photobleaching.

With GVs it is possible not only to directly visualize the peptide inside the vesicles but also to evaluate its effect on membrane properties: membrane integrity can be followed with a labelled lipid such as N-Rh-PE (the fluorochrome has to be different from the one used to label the peptide), and the possibility of pore formation can be evaluated in GVs loaded with two similar dyes attached to other molecules of very different sizes (for instance Alexa^{488}-Dextran (MW 10000) and Alexa^{546}-maleimide (MW ~1300)). This experimental setup enables direct observation of changes in the membrane permeability during the course of observations and in the case of pore formation to

have information on pore size due to sequential escape of the dyes from the GVs [66,67].

Detection of encapsulated peptide escape. Using a fluorescence quenching assay, Magzoub et al. had developed methodologies in which the escape of a CPP from liposomes is determined in the presence and absence of a pH gradient [68] (see Figure 1, Panel D). To track the peptide escape two assays based on encapsulation were carried out: (i) vesicles were prepared with the peptide inside and the Trp quencher acrylamide was added to the outer phase (the escape of peptide from liposomes was followed by fluorescence quenching of peptide Trp residues caused by acrylamide); (ii) fluorescein-labelled peptides were encapsulated with a quencher (iodide) and, in the case of translocation, a de-quenching of the fluorescein label was observed. The fluorescence intensity corresponding to 100% peptide escape was determined by vesicle lyses with Triton X-100 and the fraction of peptide escape was calculated at different incubation times [68].

Both these approaches allow the quantification of translocation as well as the determination of membrane crossing kinetics. Under certain situations, however, both methods can lead to misleading conclusions: in method (i) acrylamide is excluded from membranes, so only the fraction of peptide that reaches the outer aqueous environment is accounted for (if the peptide remains essentially partitioned in the outer leaflet after crossing the membrane, a lower translocation extent is measured); in method (ii) if the peptide does not translocate but has a deep location in the bilayer, it becomes inaccessible to the encapsulated quencher and is counted as having crossed the membrane.

In these methods if the peptide translocates very efficiently a significant amount of peptide can escape from the liposome during the gel filtration step (used to remove non-encapsulated peptide); therefore, these methods are only applicable to peptides that require special conditions to translocate (such as pH or potential membrane gradients), so that membrane crossing can be triggered only after the separation procedure.

Another peptide escape assay was described by Bárány-Wallje et al. in which vesicles uniformly preloaded with peptide both in the lumen and outer medium are dialysed so that any peptide outside of the liposomes is washed away [64]. If any peptide absorption/fluorescence remains after the dialysis, it can be concluded that translocation from the lumen/inner leaflet to the outer side did not occur; conversely, the occurrence of translocation can be inferred from the absence of any peptide signal. Due to the very simple setup and instrumentation requirements, this seems a good option to begin a translocation study with; however, there are a number of disadvantages that are addressed in section 3 of the Supplementary material online.

Other methods. A methodology based on a particular peptide property was developed in reference [69]. For this purpose, the specific fluorescence quenching of Rh by the CPP pep-1 was taken advantage of. Vesicles labelled symmetrically with N-Rh-PE were used to evaluate fluorescence emission quenching of Rh by pep-1 in the presence and absence of a transmembrane potential. After the peptide is added to LUVs, Rh fluorescence in the outer layer is quenched. If translocation occurs, it can be identified by a further reduction in Rh fluorescence due to contact of the peptide with Rh in the inner leaflet. The effect can be improved by using labelled multilamellas vesicles (MLVs): the fraction of Rh-PE available for peptide access is smaller than if LUVs are used, therefore a much larger relative increase in quenching is expected if the peptide translocates and accesses all the phospholipids [69]. Alternatively, soluble Rh can be encapsulated in vesicles and its fluorescence followed after peptide addition [69].

This method allows measurements to be taken during a time course, enabling the kinetic evaluation of the translocation process. Its main disadvantage is that it is only applicable to peptides that are able to quench a given fluorophore.

Another method using MLVs has been reported [60,70]: dithionite ion was externally added to NBD-PE-doped MLVs, resulting in quenching of the fluorophores in the outermost leaflet; upon the addition of a pore-forming peptide the dithionite ion will have access to the first intramembranar space of the MLVs, resulting in an increase in quenching; full NBD quenching, however, will only be attained if the peptide can translocate and form pores in the inner bilayers because only then will all the fluorophore become accessible to the dithionite ion.

This method does not require any peptide labelling or intrinsic fluorescence but, on the other hand, this can only be applied to peptides that perturb the membrane to an extent where dithionite can cross it (by a pore or otherwise). Kinetic information can be extracted but it is necessary to take into consideration the multiple membrane crossing steps.

Assessment of peptide translocation with attached cargo

The translocation process of CPPs may vary if the peptide is in free form or attached to a cargo. Differences in peptide kinetics and cell localization can occur [71–73]. In the above described methodologies the only attached 'cargoes' were

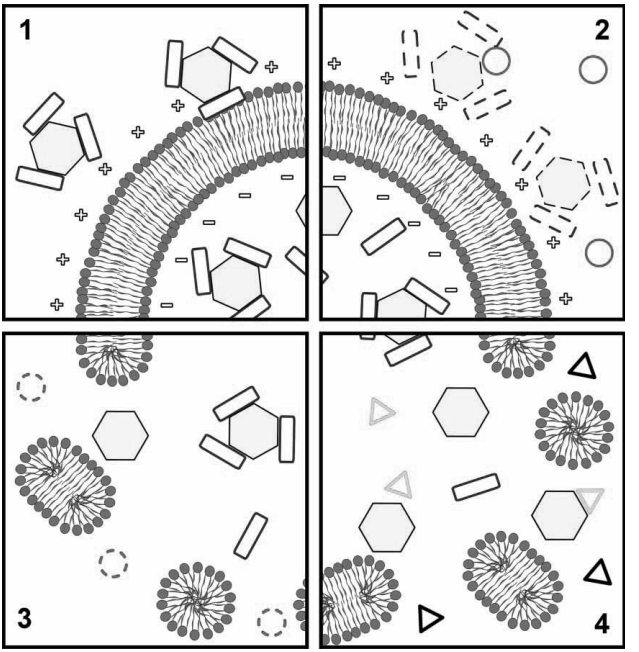

Figure 2. To evaluate the translocation of β-Gal/pep-1 (hexagons/rectangles) complexes across model membranes the following steps were reported [81]: (1) valinomycin was added to K^+-loaded vesicles in Na^+-buffer to create a negative transmembrane potential; the complex was added to the solution and translocated across bilayer; (2) trypsin (circles) was added to digest non-incorporated complex and free pep-1 or β-Gal (dashed hexagons/rectangles); (3) after digestion, trypsin was inhibited (dashed circles) with phenylmethylsulfonyl fluoride and TX-100 was then added to facilitate the release of internalized β-Gal and allow its quantification (digestion debris were excluded from the last two panels, and inhibited trypsin from the last, to avoid image crowding); (4) β-Gal activity was assayed by MUG (black triangles) hydrolysis to a fluorescent product, 4-MU (lighter triangles). The figure is reproduced in colour in *Molecular Membrane Biology* online.

fluorophores. The nature and size of the cargoes and the nature of attachment to the peptide (whether covalent [3,74] or weaker [7,75]) can also be a determinant for the translocation mechanism. Given these differences, development of consistent methods to evaluate the capacity to translocate/deliver proteins across artificial/natural membranes would be fruitful to systematically confirm (or refute) vector properties of CPPs. Practically all methods described above for *in vivo* or *in vitro* testing can, in principle, be extended to assess the translocation of CPP-cargo complexes, although no reports on such usage were found; however, some properties of the macromolecule attached to the peptide are additional advantages to detect and quantify translocation, opening the possibility for more sensitive methodologies. Three methods that have been reported for the *in vivo* studies and one for the *in vitro* studies of the internalization of CPP-cargo complexes are discussed here; while these can easily fit into the above classification, they are presented separately to underscore their importance in confirming the vector properties of a CPP.

Morris et al. had observed the efficiency of pep-1 to deliver GFP [75] and a similar approach demonstrated the ability of the AMP buforin 2 to translocate across bilayers with a macromolecular cargo [76]. Recombinant proteins with CPP and GFP domains have also been produced [77–79]. Instead of GFP, Wadia et al. labelled TAT-Cre recombinase by coupling it to Alexa 488 or Alexa 546 fluorophores [80]. GFP or Cre recombinase translocation is followed by its intrinsic fluorescence; this is in all aspects identical to what was previously described for the *in vivo* direct visualization of internalization. Another possibility to measure Cre recombinase translocation mediated by TAT is by recombination reporter assay, where the expression of enhanced GFP (EGFP) is dependent on TAT-Cre transduction into cells, followed by nuclear import. The signal of EGFP is followed and measured as a consequence of TAT-Cre import [80].

Detection of β-Gal delivery into cells was also reported. Translocation was assessed by monitoring the X-Gal staining enzymatic activity of β-Gal [75]. The detection of the enzymatic activity of the cargo not only allows a sensitive detection of the

Table I. Classification of available methods for *in vivo* and *in vitro* translocation assessment, and respective advantages and disadvantages.

		Refs	Advantages			Disadvantages			
			Can provide kinetic information	Can use intrinsic peptide fluorescence	Can quantify the internalized peptide	Cannot identify translocation with certainty	Peptide derivatization is an absolute requirement	Complex/lengthy experimental setup	Not applicable to all peptides
in vivo methods	*Quantification of cytoplasmic concentration*								
	Fluorescence spectroscopy	[29,32,33,37]			●		●	●	
	Mass spectrometry	[32,36,43–45]			●		●	●	
	Flow cytometry	[30,41,42]	●		●		●	●	
	Direct visualization of internalization								
	Confocal microscopy	[5,27,30,50]	●				●	●	
	Peptide activity analysis								
	Visualization of cytoplasmic damage	[51–54]				●			●
	Channel detection	[55,56]				●			●
	Methods used for peptides with attached cargo								
	Visualization of attached GFP	[75–77]	●						
	Measurement of cargo enzymatic activity	[37,75,81]			●				
	Immunofluorescence visualization (antibodies raised against cargo)	[81]							
in vitro methods	*Measurement of peptide inaccessibility from the outer phase*								
	FRET within the membrane; trypsin addition	[19]	●	●		●			●
	FRET within the membrane; vesicle addition	[19,59,60]	●	●		●			
	Quenching of NBD-derivatized peptides by added dithionite	[24,59]	●			●	●		
	Detection of inward peptide positioning within the membrane								
	Asymmetrical labeling of vesicles with LysoMC or DNS-PE	[19,61,62]	●	●		●	●		●
	Detection of peptide in the inner phase								
	Trypsin digestion in the vesicular lumen	[19]	●	●	●				●
	PLM assembly visualized by confocal microscopy	[64]	●		●		●	●	
	Detection of encapsulated peptide escape								
	External quencher addition to encapsulated peptide	[68]	●	●				●	●
	Co-encapsulation of quencher and peptide	[68]	●	●				●	●
	Dialysis of peptide-LUV mixtures	[64]		●				●	●
	Other methods								
	Rh quenching by the peptide	[69]	●		●				●
	Peptide-promoted NBD-PE quenching by dithionite in MLVs	[60,70]	●						●
in vitro methods	*Methods used for peptides with attached cargo*								
	Measurement of cargo enzymatic activity	[80,81]			●				

internalized CPP-cargo complex, but also tests whether CPP-mediated translocation can occur without cargo damage/denaturation. A quantification of β-Gal internalization was developed by means of its enzymatic activity on the substrate 4-methylumbelliferone β-D-galactopyranoside (MUG), a non fluorescent substrate that is converted to 4-methylumbelliferone (4-MU), which is a fluorescent product. 4-MU production enables quantification of protein internalization from its activity [37,81].

Another possibility to evaluate protein delivery efficiency is by immunofluorescence, using a primary antibody raised against the carried protein and a fluorescently labelled secondary antibody, as was preformed with β-Gal [81]. This method is independent of particular cargo properties; therefore, it is suited to study the transport of cargoes that do not have intrinsic fluorescence or detectable enzymatic activity. With these methodologies it is possible to obtain cell transfection efficiency, but not the quantification of peptide/protein internalization.

Protein uptake was also evaluated *in vitro* with pep-1/β-Gal, by taking advantage of the β-Gal enzymatic activity and 4-MU fluorescent properties (see Figure 2). Briefly, after peptide/protein incubation with LUVs, trypsin was added externally to digest the non-incorporated peptide and β-Gal; afterwards, phenylmethanesulfonyl fluoride (PMSF) was added to inhibit trypsin. To induce LUV permeabilization and leakage of the incorporated β-Gal, Triton X-100 was added, and enzymatic activity of β-Gal was determined by MUG hydrolysis [81]. Intrinsic cargo fluorescence and/or enzymatic activity are specific properties that can be used for application of a similar methodology to other peptides/proteins complexes.

The classification and the general advantages and disadvantages of the application of each reviewed method are summarized in Table I.

For all the methods presented here, it is possible to conclude about the ability of peptides to translocate. When further information is sought, quantitative analysis should always be carefully carried out; for this, several different complementing methodologies should be conjugated, regarding not only the actual evaluation of translocation but also to quantify the peptide distribution between the membrane and aqueous environments and to characterize the membrane topology upon peptide interaction (occurrence of membrane thinning, pore formation, lysis, etc.).

Concluding remarks

Because most methods for the assessment of membrane translocation have only been reported during the last decade, it is understandable that this field is regarded as being underdeveloped, methodology-wise [18]. In addition, the description of new methods has not always been given the due emphasis by their authors, which further contributed to the lack of visibility of these procedures. Yet, over 20 methods that address the assessment of membrane translocation have been found. The authors of this work hope that the gathering of this knowledge will help others find and use the most appropriate methods for their studies. On the other hand, this compilation should by no means be regarded as an ultimate source for information on translocation assessment methodologies in a way that the development of new methods, or the improvement of already described ones, is discouraged. Rather, by exposing the strengths and weaknesses of several methodologies, it is hoped that the development of newer and better methods is encouraged and facilitated.

References

[1] Wadia JS, Becker-Hapak M, Dowdy SF. 2002. Protein transport. In: Langel Ü, editor. Cell-penetrating peptides, processes and applications. 1st ed. New York: CRC Press. p. 365–375.

[2] Derossi D, Joliot AH, Chassaing G, Prochiantz A. 1994. The third helix of the Antennapedia homeodomain translocates through biological membranes. J Biol Chem 269:10444–10450.

[3] Fawell S, Seery J, Daikh Y, Moore C, Chen LL, Pepinsky B, Barsoum J. 1994. Tat-mediated delivery of heterologous proteins into cells. Proc Natl Acad Sci USA 91:664–668.

[4] Schwarze SR, Ho A, Vocero-Akbani A, Dowdy SF. 1999. In vivo protein transduction: delivery of a biologically active protein into the mouse. Science 285:1569–1572.

[5] Vives E, Brodin P, Lebleu B. 1997. A truncated HIV-1 Tat protein basic domain rapidly translocates through the plasma membrane and accumulates in the cell nucleus. J Biol Chem 272:16010–16017.

[6] Allinquant B, Hantraye P, Mailleux P, Moya K, Bouillot C, Prochiantz A. 1995. Downregulation of amyloid precursor protein inhibits neurite outgrowth in vitro. J Cell Biol 128:919–927.

[7] Morris MC, Vidal P, Chaloin L, Heitz F, Divita G. 1997. A new peptide vector for efficient delivery of oligonucleotides into mammalian cells. Nucleic Acids Res 25:2730–2736.

[8] Lindgren M, Hallbrink M, Prochiantz A, Langel U. 2000. Cell-penetrating peptides. Trends Pharmacol Sci 21:99–103.

[9] Magzoub M, Graslund A. 2004. Cell-penetrating peptides: from inception to application. Q Rev Biophys 37:147–195.

[10] Henriques ST, Melo MN, Castanho MA. 2006. Cell-penetrating peptides and antimicrobial peptides: how different are they? Biochem J 399:1–7.

[11] Koczulla AR, Bals R. 2003. Antimicrobial peptides: current status and therapeutic potential. Drugs 63:389–406.

[12] Tossi A, Mitaritonna N, Tarantino C, Giangaspero A, Sandri L, Winterstein KA. 2003. Antimicrobial Sequences Database.

[13] Powers JP, Hancock RE. 2003. The relationship between peptide structure and antibacterial activity. Peptides 24: 1681–1691.
[14] Hancock RE. 2001. Cationic peptides: effectors in innate immunity and novel antimicrobials. Lancet Infect Dis 1:156–164.
[15] Hancock RE. 1997. Peptide antibiotics. Lancet 349:418–422.
[16] Zasloff M. 2002. Antimicrobial peptides of multicellular organisms. Nature 415:389–395.
[17] Yeaman MR, Yount NY. 2003. Mechanisms of antimicrobial peptide action and resistance. Pharmacol Rev 55:27–55.
[18] Zhang L, Rozek A, Hancock RE. 2001. Interaction of cationic antimicrobial peptides with model membranes. J Biol Chem 276:35714–35722.
[19] Matsuzaki K, Murase O, Fujii N, Miyajima K. 1995. Translocation of a channel-forming antimicrobial peptide, magainin 2, across lipid bilayers by forming a pore. Biochemistry 34:6521–6526.
[20] Fischer R, Fotin-Mleczek M, Hufnagel H, Brock R. 2005. Break on through to the other side-biophysics and cell biology shed light on cell-penetrating peptides. Chembiochem 6:2126–2142.
[21] Mano M, Teodosio C, Paiva A, Simoes S, Pedroso de Lima MC. 2005. On the mechanisms of the internalization of S4(13)-PV cell-penetrating peptide. Biochem J 390:603–612.
[22] Jones SW, Christison R, Bundell K, Voyce CJ, Brockbank SM, Newham P, Lindsay MA. 2005. Characterisation of cell-penetrating peptide-mediated peptide delivery. Br J Pharmacol 145:1093–1102.
[23] Fuchs SM, Raines RT. 2004. Pathway for polyarginine entry into mammalian cells. Biochemistry 43:2438–2444.
[24] Drin G, Cottin S, Blanc E, Rees AR, Temsamani J. 2003. Studies on the internalization mechanism of cationic cell-penetrating peptides. J Biol Chem 278:31192–31201.
[25] Wender PA, Mitchell DJ, Pattabiraman K, Pelkey ET, Steinman L, Rothbard JB. 2000. The design, synthesis, and evaluation of molecules that enable or enhance cellular uptake: peptoid molecular transporters. Proc Natl Acad Sci USA 97:13003–13008.
[26] Vives E, Granier C, Prevot P, Lebleu B. 1997. Structure-activity relationship study of the plasma membrane translocating potential of a short peptide from HIV-1 Tat protein. Lett Pept Sci 4:429–436.
[27] Thoren PE, Persson D, Isakson P, Goksor M, Onfelt A, Norden B. 2003. Uptake of analogs of penetratin, Tat(48-60) and oligoarginine in live cells. Biochem Biophys Res Commun 307:100–107.
[28] Suzuki T, Futaki S, Niwa M, Tanaka S, Ueda K, Sugiura Y. 2002. Possible existence of common internalization mechanisms among arginine-rich peptides. J Biol Chem 277:2437–2443.
[29] Saalik P, Elmquist A, Hansen M, Padari K, Saar K, Viht K, Langel U, Pooga M. 2004. Protein cargo delivery properties of cell-penetrating peptides. A comparative study. Bioconjug Chem 15:1246–1253.
[30] Richard JP, Melikov K, Vives E, Ramos C, Verbeure B, Gait MJ, Chernomordik LV, Lebleu B. 2003. Cell-penetrating peptides. A reevaluation of the mechanism of cellular uptake. J Biol Chem 278:585–590.
[31] Potocky TB, Menon AK, Gellman SH. 2003. Cytoplasmic and nuclear delivery of a TAT-derived peptide and a beta-peptide after endocytic uptake into HeLa cells. J Biol Chem 278:50188–50194.
[32] Fischer R, Kohler K, Fotin-Mleczek M, Brock R. 2004. A stepwise dissection of the intracellular fate of cationic cell-penetrating peptides. J Biol Chem 279:12625–12635.
[33] Drin G, Mazel M, Clair P, Mathieu D, Kaczorek M, Temsamani J. 2001. Physico-chemical requirements for cellular uptake of pAntp peptide. Role of lipid-binding affinity. Eur J Biochem 268:1304–1314.
[34] Szeto HH, Schiller PW, Zhao K, Luo G. 2005. Fluorescent dyes alter intracellular targeting and function of cell-penetrating tetrapeptides. Faseb J 19:118–120.
[35] Boisseau S, Mabrouk K, Ram N, Garmy N, Collin V, Tadmouri A, Mikati M, Sabatier JM, Ronjat M, Fantini J, De Waard M. 2006. Cell penetration properties of maurocalcine, a natural venom peptide active on the intracellular ryanodine receptor. Biochim Biophys Acta 1758:308–319.
[36] Balayssac S, Burlina F, Convert O, Bolbach G, Chassaing G, Lequin O. 2006. Comparison of penetratin and other homeodomain-derived cell-penetrating peptides: interaction in a membrane-mimicking environment and cellular uptake efficiency. Biochemistry 45:1408–1420.
[37] Henriques ST, Costa J, Castanho MA. 2005. Re-evaluating the role of strongly charged sequences in amphipathic cell-penetrating peptides: a fluorescence study using Pep-1. FEBS Lett 579:4498–4502.
[38] Oehlke J, Scheller A, Wiesner B, Krause E, Beyermann M, Klauschenz E, Melzig M, Bienert M. 1998. Cellular uptake of an alpha-helical amphipathic model peptide with the potential to deliver polar compounds into the cell interior non-endocytically. Biochim Biophys Acta 1414:127–139.
[39] Oehlke J, Brudel M, Blasig IE. 1994. Benzoylation of sugars, polyols and amino acids in biological fluids for high-performance liquid chromatographic analysis. J Chromatogr B Biomed Appl 655:105–111.
[40] Richard JP, Melikov K, Brooks H, Prevot P, Lebleu B, Chernomordik LV. 2005. Cellular uptake of unconjugated TAT peptide involves clathrin-dependent endocytosis and heparan sulfate receptors. J Biol Chem 280:15300–15306.
[41] Raucher D, Chilkoti A. 2001. Enhanced uptake of a thermally responsive polypeptide by tumor cells in response to its hyperthermia-mediated phase transition. Cancer Res 61:7163–7170.
[42] Massodi I, Bidwell GL, 3rd, Raucher D. 2005. Evaluation of cell penetrating peptides fused to elastin-like polypeptide for drug delivery. J Control Release 108:396–408.
[43] Elmquist A, Langel U. 2003. In vitro uptake and stability study of pVEC and its all-D analog. Biol Chem 384:387–393.
[44] Burlina F, Sagan S, Bolbach G, Chassaing G. 2005. Quantification of the cellular uptake of cell-penetrating peptides by MALDI-TOF mass spectrometry. Angew Chem Int Ed Engl 44:4244–4247.
[45] Aussedat B, Sagan S, Chassaing G, Bolbach G, Burlina F. 2006. Quantification of the efficiency of cargo delivery by peptidic and pseudo-peptidic Trojan carriers using MALDI-TOF mass spectrometry. Biochim Biophys Acta 1758:375–383.
[46] Futaki S, Suzuki T, Ohashi W, Yagami T, Tanaka S, Ueda K, Sugiura Y. 2001. Arginine-rich peptides. An abundant source of membrane-permeable peptides having potential as carriers for intracellular protein delivery. J Biol Chem 276: 5836–5840.
[47] Powers JP, Martin MM, Goosney DL, Hancock RE. 2006. The antimicrobial peptide polyphemusin localizes to the cytoplasm of *Escherichia coli* following treatment. Antimicrob Agents Chemother 50:1522–1524.

[48] Park CB, Kim HS, Kim SC. 1998. Mechanism of action of the antimicrobial peptide buforin II: buforin II kills microorganisms by penetrating the cell membrane and inhibiting cellular functions. Biochem Biophys Res Commun 244: 253–257.

[49] Lau YE, Rozek A, Scott MG, Goosney DL, Davidson DJ, Hancock RE. 2005. Interaction and cellular localization of the human host defense peptide LL-37 with lung epithelial cells. Infect Immun 73:583–591.

[50] Lundberg M, Johansson M. 2001. Is VP22 nuclear homing an artifact? Nat Biotechnol 19:713–714.

[51] Friedrich CL, Moyles D, Beveridge TJ, Hancock RE. 2000. Antibacterial action of structurally diverse cationic peptides on gram-positive bacteria. Antimicrob Agents Chemother 44:2086–2092.

[52] Boman HG, Agerberth B, Boman A. 1993. Mechanisms of action on Escherichia coli of cecropin P1 and PR-39, two antibacterial peptides from pig intestine. Infect Immun 61:2978–2984.

[53] Shi J, Ross CR, Chengappa MM, Sylte MJ, McVey DS, Blecha F. 1996. Antibacterial activity of a synthetic peptide (PR-26) derived from PR-39, a proline-arginine-rich neutrophil antimicrobial peptide. Antimicrob Agents Chemother 40:115–121.

[54] Subbalakshmi C, Sitaram N. 1998. Mechanism of antimicrobial action of indolicidin. FEMS Microbiol Lett 160:91–96.

[55] Deshayes S, Heitz A, Morris MC, Charnet P, Divita G, Heitz F. 2004. Insight into the mechanism of internalization of the cell-penetrating carrier peptide Pep-1 through conformational analysis. Biochemistry 43:1449–1457.

[56] Deshayes S, Gerbal-Chaloin S, Morris MC, Aldrian-Herrada G, Charnet P, Divita G, Heitz F. 2004. On the mechanism of non-endosomial peptide-mediated cellular delivery of nucleic acids. Biochim Biophys Acta 1667:141–147.

[57] Chaloin L, De E, Charnet P, Molle G, Heitz F. 1998. Ionic channels formed by a primary amphipathic peptide containing a signal peptide and a nuclear localization sequence. Biochim Biophys Acta 1375:52–60.

[58] Pouny Y, Rapaport D, Mor A, Nicolas P, Shai Y. 1992. Interaction of antimicrobial dermaseptin and its fluorescently labeled analogues with phospholipid membranes. Biochemistry 31:12416–12423.

[59] Terrone D, Sang SL, Roudaia L, Silvius JR. 2003. Penetratin and related cell-penetrating cationic peptides can translocate across lipid bilayers in the presence of a transbilayer potential. Biochemistry 42:13787–13799.

[60] Drin G, Demene H, Temsamani J, Brasseur R. 2001. Translocation of the pAntp peptide and its amphipathic analogue AP-2AL. Biochemistry 40:1824–1834.

[61] Persson D, Thoren PE, Esbjorner EK, Goksor M, Lincoln P, Norden B. 2004. Vesicle size-dependent translocation of penetratin analogs across lipid membranes. Biochim Biophys Acta 1665:142–155.

[62] Thoren PE, Persson D, Esbjorner EK, Goksor M, Lincoln P, Norden B. 2004. Membrane binding and translocation of cell-penetrating peptides. Biochemistry 43:3471–3489.

[63] Wimley WC, White SH. 2000. Determining the membrane topology of peptides by fluorescence quenching. Biochemistry 39:161–170.

[64] Barany-Wallje E, Keller S, Serowy S, Geibel S, Pohl P, Bienert M, Dathe M. 2005. A critical reassessment of penetratin translocation across lipid membranes. Biophys J 89:2513–2521.

[65] Thoren PE, Persson D, Karlsson M, Norden B. 2000. The antennapedia peptide penetratin translocates across lipid bilayers – the first direct observation. FEBS Lett 482:265–268.

[66] Ambroggio EE, Kim DH, Separovic F, Barrow CJ, Barnham KJ, Bagatolli LA, Fidelio GD. 2005. Surface behavior and lipid interaction of Alzheimer beta-amyloid peptide 1-42: a membrane-disrupting peptide. Biophys J 88:2706–2713.

[67] Ambroggio EE, Separovic F, Bowie JH, Fidelio GD, Bagatolli LA. 2005. Direct visualization of membrane leakage induced by the antibiotic peptides: maculatin, citropin, and aurein. Biophys J 89:1874–1881.

[68] Magzoub M, Pramanik A, Graslund A. 2005. Modeling the endosomal escape of cell-penetrating peptides: transmembrane pH gradient driven translocation across phospholipid bilayers. Biochemistry 44:14890–14897.

[69] Henriques ST, Castanho MA. 2004. Consequences of nonlytic membrane perturbation to the translocation of the cell penetrating peptide pep-1 in lipidic vesicles. Biochemistry 43:9716–9724.

[70] Matsuzaki K, Yoneyama S, Murase O, Miyajima K. 1996. Transbilayer transport of ions and lipids coupled with mastoparan X translocation. Biochemistry 35:8450–8456.

[71] Rejman J, Oberle V, Zuhorn IS, Hoekstra D. 2004. Size-dependent internalization of particles via the pathways of clathrin- and caveolae-mediated endocytosis. Biochem J 377:159–169.

[72] De Coupade C, Fittipaldi A, Chagnas V, Michel M, Carlier S, Tasciotti E, Darmon A, Ravel D, Kearsey J, Giacca M, Cailler F. 2005. Novel human-derived cell-penetrating peptides for specific subcellular delivery of therapeutic biomolecules. Biochem J 390:407–418.

[73] Silhol M, Tyagi M, Giacca M, Lebleu B, Vives E. 2002. Different mechanisms for cellular internalization of the HIV-1 Tat-derived cell penetrating peptide and recombinant proteins fused to Tat. Eur J Biochem 269:494–501.

[74] Pooga M, Soomets U, Hallbrink M, Valkna A, Saar K, Rezaei K, Kahl U, Hao JX, Xu XJ, Wiesenfeld-Hallin Z, Hokfelt T, Bartfai T, Langel U. 1998. Cell penetrating PNA constructs regulate galanin receptor levels and modify pain transmission in vivo. Nat Biotechnol 16:857–861.

[75] Morris MC, Depollier J, Mery J, Heitz F, Divita G. 2001. A peptide carrier for the delivery of biologically active proteins into mammalian cells. Nat Biotechnol 19:1173–1176.

[76] Takeshima K, Chikushi A, Lee KK, Yonehara S, Matsuzaki K. 2003. Translocation of analogues of the antimicrobial peptides magainin and buforin across human cell membranes. J Biol Chem 278:1310–1315.

[77] Tyagi M, Rusnati M, Presta M, Giacca M. 2001. Internalization of HIV-1 tat requires cell surface heparan sulfate proteoglycans. J Biol Chem 276:3254–3261.

[78] Fittipaldi A, Ferrari A, Zoppe M, Arcangeli C, Pellegrini V, Beltram F, Giacca M. 2003. Cell membrane lipid rafts mediate caveolar endocytosis of HIV-1 Tat fusion proteins. J Biol Chem 278:34141–34149.

[79] Ferrari A, Pellegrini V, Arcangeli C, Fittipaldi A, Giacca M, Beltram F. 2003. Caveolae-mediated internalization of extracellular HIV-1 tat fusion proteins visualized in real time. Mol Ther 8:284–294.

[80] Wadia JS, Stan RV, Dowdy SF. 2004. Transducible TAT-HA fusogenic peptide enhances escape of TAT-fusion proteins after lipid raft macropinocytosis. Nat Med 10:310–315.

[81] Henriques ST, Costa J, Castanho MA. 2005. Translocation of beta-galactosidase mediated by the cell-penetrating peptide pep-1 into lipid vesicles and human HeLa cells is driven by membrane electrostatic potential. Biochemistry 44:10189–10198.

Supplementary Material

Problems associated with the detection of entry of peptide into vesicles

At usual lipid concentrations, used to perform *in vitro* studies, the volume occupied by the vesicles is very small when compared to the bulk aqueous phase: for 100 nm diameter LUVs, produced at a total lipid concentration of 1 mM, and assuming a mean membrane surface area of 0.7 nm^2 per phospholipid [1], the ratio of luminal volume over the total volume will be about $r = 0.003$ v/v. Another problem arises from the fact that these peptides usually have large molar ratio partition constants towards lipidic membranes (about 10^3 to 10^4, e.g., [2,3]). This means that only a small concentration of peptide will be in the aqueous phase unless relatively low lipid concentrations are used. Given the above-mentioned obstacles, it is clear that methods based on the detection of the concentration of internalized peptide will have to deal with very low signal intensities that will likely lie below instrumental detection limit.

Comments on time-dependent measurements

It should be noted that in all the methods presented in the section *Measurement of peptide inaccessibility from the outer phase* a time-dependent measurement is required to determine the degree of peptide inaccessibility: because the amount of free peptide in the outer phase will decrease – as it is digested, sequestered or permanently quenched – the internalized peptide will equilibrate back to the outer phase. Consequently, two stages are expected: in the first, signal magnitude increases (here 'signal', in a very broad sense, can be FRET reduction, FRET increase or fluorescence reduction, depending on the particular method used), detecting the adsorbed/non-internalized peptide fraction; then a second stage ensues with a usually slower signal increase [4,5], which corresponds to the detection of the internalized peptide molecules that are returning to the outer phase. At equilibrium, the signal magnitude should be approximately the same whether translocation has occurred or not. The percentage of accessible peptide is usually obtained by comparing the end of the first stage with a control where peptide, membrane and the non-translocating entity are added simultaneously [4, 5]. From this, it can be seen that, in a hypothetical situation where the translocation kinetics were of the same magnitude of the desorption kinetics, this method would be very difficult to apply as both stages would have the same approximate slopes and the end of the first stage would be hard to detect. On the other hand, information about translocation kinetics could, in principle, be obtained from the rate at which the peptide molecules return to the outer phase, in the second stage.

Advantages and disadvantages associated with the dialysis method

Due to the very simple setup and instrumentation requirements for this experiment (see the section *Detection of encapsulated peptide escape*) this seems a good option to begin a translocation study with, because membrane crossing may be ruled out immediately avoiding the need to use more complex and costly methodologies. However, in order for this method to provide a measurable absorbance/fluorescence peptide signal in the absence of translocation it is required that the amount of internalized peptide be relatively large, to compensate for the effect of the small encapsulation volume. This is only possible to attain if the peptide partitions strongly towards the bilayer and the lipid concentration is high enough: under these conditions, upon vesicle preparation, the peptide molecules can be expected to be equally distributed by the inner and outer leaflets and very few to be left in the aqueous phase; in the absence of translocation, roughly one half of the peptide signal will remain, correspondent to the peptide molecules partitioned in the inner leaflet. Should the peptide partition weakly to the membrane or there be a small lipid concentration, the inner leaflet peptide fraction could be undetected in the absence of translocation, which would generate a false positive. This limitation has to be accounted for by quantifying the extent of membrane interaction. Other disadvantages include the lengthy dialysis process and the lack of any kind of translocation characterization, which makes this method more suited to rule out, rather than ascertain, peptide translocation.

References

[1] Marsh D. 1990. CRC handbook of lipid bilayers. Boca Raton: CRC Press.
[2] Heerklotz H, Seelig J. 2001. Detergent-like action of the antibiotic peptide surfactin on lipid membranes. Biophys J 81:1547–1554.
[3] Strahilevitz J, Mor A, Nicolas P, Shai Y. 1994. Spectrum of antimicrobial activity and assembly of dermaseptin-b and its precursor form in phospholipid membranes. Biochemistry 33:10951–1060.
[4] Terrone D, Sang SL, Roudaia L, Silvius JR. 2003. Penetratin and related cell-penetrating cationic peptides can translocate across lipid bilayers in the presence of a transbilayer potential. Biochemistry 42:13787–13799.
[5] Matsuzaki K, Murase O, Fujii N, Miyajima K. 1995. Translocation of a channel-forming antimicrobial peptide, magainin 2, across lipid bilayers by forming a pore. Biochemistry 34:6521–6526.

Translocation

The concept of peptide translocation detection seems, at first, to be easy to implement. When using vesicles, the membranes effectively divide the aqueous phase into two compartments and it would suffice to detect the peptide in the lumen to ascertain translocation. As noted in Article VII, however, practical aspects prevent such a straightforward approach: at millimolar lipidic concentrations the fraction of luminal over the total volume is very small, which means that only a negligible fraction of the peptide will actually enter the lumina; this is worsened by the fact that, given typical AMP partition constants, most of the peptide will leave the aqueous phase and bind the membranes at typical 0.1 to 1 millimolar lipid concentrations. Indeed, most of the methods described in Article VII indirectly detect translocation into vesicles from its consequences to the peptide-membrane interaction.

Sónia had had the fortune of working with a peptide that was able to quench rhodamine: she would measure the quenching of rhodamine-labeled phospholipid vesicles and determine if the quencher (peptide) had access to all of the fluorophore — translocation — or only to the outer fraction — no translocation.[78] I was not so lucky as to have a quenching peptide and had to work out another solution. I did so mostly because I found the methods in Article VII unsatisfactory: either they were too complex, involving techniques we didn't have ready access to, or required the labeling of the peptide,* or didn't unequivocally identify translocation.

Miguel and I tried to find some compound that we could encapsulate, that would bind the few peptide molecules that reached the lumen, and that would then produce a strong signal in such a way that the above-mentioned limitations were overcome. I spent quite a lot of time trying to measure fluorescence transfer in the lumen between omiganan and ANTS, a fluorophore with suitable spectral properties to accept trypto-

*Peptide labeling was something I really wanted to avoid. For such short sequences as the AMPs', addition of fluorophores — usually hydrophobic in nature — may cause drastic changes in membrane interaction behavior. Sónia observed precisely that with her carboxyfluorescein-labeled cell-penetrating peptide.[79]

phan emission. I did not succeed: fluorescence transfer strongly depends on acceptor concentration and millimolars of ANTS would have to be encapsulated in order for a signal to be measured. Even if such high concentrations of ANTS would be used and if the vesicles did not burst because of the resulting osmotic difference, there would be too little signal and too much excitation light sharing* for any conclusion to be drawn.

After writing Article VII, and inspired by the methods that involved MLVs,[80,81] it dawned on me and Miguel that the reporter entity that we were looking for could be the very phospholipid bilayer: peptides that translocate have access to all the lipid in MLVs, whereas peptides that don't can only bind the outer fraction. And this was something very simple to test by a simple adaptation of the fluorescence methodologies we already used for measuring peptide-membrane binding. I implemented the approach by following the binding of peptide, using fluorescence, with time: AMP interactions with LUVs — at least of the peptides I studied — reached equilibrium very quickly (far more quickly than the time it took me to pipette the sample and place the cuvette in the fluorometer). When MLVs were used, however, the membrane crossing steps took extra time. Fluorescence intensity now took minutes instead of milliseconds to reach equilibrium. Using this time-based measurement I was able to extract two parameters to relate with translocation: the overall binding of the peptide and the time to reach equilibrium. Figure 1 in Article IV outlines the expected behavior of translocating and non-translocating peptides.

Some further steps were needed for a consistent application of the method. The first was the realization that the overall lipid concentration strongly influences how different the interaction kinetics with LUVs and MLVs will be. If too much lipid is used it may happen that the exposed lipid of MLVs is enough for almost total peptide binding. In this case the binding kinetics should be fast in both cases. If too little lipid is used there may not be a measurable binding. Of course, 'too much' and 'too

*Excitation light sharing refers to the process of acceptor fluorescence by direct absorption of excitation light — thus 'sharing' it with the donor. Fluorescence transfer pairs are usually chosen so that the acceptor absorbs very little light at the wavelength of donor excitation; however, high concentrations of acceptor may still significantly fluoresce due to this effect.

little' depend on how strongly the peptide binds the membrane (K_p) and how brighter it fluoresces when bound (I_L/I_W): it is thus very useful to obtain a partition curve prior to the application of the method. Another modification that enhanced the time-based detection of peptide binding was the use of acrylamide. By quenching the water fraction of the peptide I was able to increase I_L/I_W from 3.6 to close to 20, which gave me a wider range of useful lipid concentrations to work with.

I successfully applied the method to BP100 (Article IV) and omiganan and both did translocate across bacterial membrane models. By the time of publication of Article IV, however, I had not yet tested the protocol with a negative control. This gap would be bridged a few months later when Joana Matos, a postgraduate researcher at the group, applied my method to two of her peptides (segments of the dengue virus capsid protein). One of them clearly translocated, the other clearly did not.

The method is very simple in concept and in experimental setup — it may even be applied to molecules other than peptides. But it does have its shortcomings. According to the advantage/disadvantage list we used in Article VII to qualify other methods, this one has the pro of being able to use intrinsic peptide fluorescence but the con of being limited to peptides with appropriate partition and kinetic properties. It is also unable to quantify translocation rates or the amount of internalized peptide.

Margarida Rodrigues contributed to the extension of the method to microscopy: her peptide did not have a suitable I_L/I_W — even after addition of acrylamide — but it was rhodamine-labeled and its binding to giant unilamellar vesicles (GUVs) could be observed by fluorescence microscopy. We came up with the idea of trying to confocally image multilamellar GUVs (they sometimes show up in GUV suspensions) to see if the peptide also bound the inner membranes. Indeed, that was precisely what was observed. Whether this is another method altogether or just a variation on the same theme is left up to the reader. In the end I am very glad I was able to tackle several theoretical and practical problems of the detection of translocation. The fact that the method has been successfully applied by others, and to peptides that are not necessarily AMPs, is rewarding in itself.

Leakage

Detection of peptide-induced leakage is a frequent way to assess membrane perturbation. The standard, widespread method to this end consists in encapsulating very high concentrations of the fluorescent probe carboxyfluorescein — so high that it quenches itself. After the washing of the leftover fluorophore on the outside of vesicles, and the addition of the agent of interest, leakage can be monitored as an increase in carboxyfluorescein emission; this occurs as a consequence of probe molecules escaping the self-quenching environment of the lumen. 100% leakage can be obtained by lysing the vesicles, usually with a detergent.

A major disadvantage of this method is that the separation of vesicles from unencapsulated probe molecules requires a filtration step (in other methodologies where encapsulation is needed it is sometimes sufficient to dilute the vesicle-probe suspension several-fold; in this case, however, that shortcut is not possible as it would lead to the de-quenching of the outer phase molecules). Besides time-consuming, the filtration process produces a vesicle suspension of unknown lipid concentration. This may be acceptable in some situations, but I wanted to test pre- and post-saturation conditions (Article IV), and thus needed to accurately know lipid concentration.

To overcome the limitation of the carboxyfluorescein method I tried to use ANTS (described in the previous section) as the encapsulated probe, and externally added iodide ions as a quencher. Upon membrane leakage the quencher would come into contact with the probe and an overall reduction in emitted intensity would be observed. Using this method I could prepare a concentrated suspension (about one-hundred-fold) of vesicles with ANTS and then dilute it to the required — and relatively accurate — lipid concentration. The outer fraction of ANTS would then become equally diluted while the inner fraction was kept at the initial concentration. External addition of iodide further reduced the contribution of the external ANTS molecules to global fluorescence.

I successfully applied the method to omiganan (Article III) but was not satisfied with its low sensitivity (again, the issue of there being too

little luminal volume in a vesicle suspension). I then decided to adopt a method used by Sónia,[78,82] which involves the preparation of vesicles doped with a fluorescently labeled phospholipid — in this case, phosphatidylethanolamine labeled in its headgroup with a nitrobenzoxadiazole moiety. Similarly to the ANTS-iodide procedure, a quencher (Co^{2+}) is externally added to the suspension. If the membrane is intact the quencher will only affect the fluorophores labeling the outer headgroups, whereas if it leaks all the headgroups become accessible.

My small contribution to the method consisted in deducing a relationship between total fluorescence and percent leakage (incidentally, after a referee prompted us to correct an overly simple initial approach). The relationship was necessary in order to properly plot time-dependent leakage observations. Both the deduced equation and the application of the method can be found in Article IV. In the article a correlation between a change in leakage-inducing behavior and saturation is identified; this was only possible by knowing the correct lipid concentration in the leakage assays.

Differential quenching

One of the biophysical methods routinely carried out at the lab is the already frequently mentioned measurement of in-depth peptide insertion in membranes. This is a type of information not usually sought in studies of peptide-membrane interaction but one that is valuable to the understanding of peptide action. Regarding the studies with omiganan, for example, the peptide was shown to move within the bilayer upon saturation, which is important evidence supporting a saturation-triggered mechanism.

Methods to obtaining depth information from fluorescence measurements usually involve doping membranes with at least two quencher-labeled lipids.[83, 84] In one of those the quencher is usually placed near the carboxyl group while in the other it is closer to the end of the acyl chain. The depth of the peptide (more accurately, of the reporting fluorophore moiety within the peptide) is then inferred from the quenching performances of each quencher: the peptide is closer to the one which quenches it the most — hence the term 'differential quenching'.

A quantitative measurement of the depth of peptide insertion can be obtained if some assumptions are made on the quencher-fluorophore interaction. A model of static[83, 84] or collisional[85] quenching* (or even a mixed one) can be used to analyze each of the quenching profiles and calculate the difference in depth between fluorophore and quencher. This is where the use of a pair of quenchers comes in: a given fluorophore-quencher distance translates into two possible depths in the membrane, with the quencher position midway between the two; by using two quenchers at different depths four possible locations are calculated, two of which should overlap and correspond to the actual peptide position. The general method has been appropriately termed parallax measurement.

*Static quenching is characterized by the fluorophore being in contact with the quencher at the moment light is absorbed; there is a resonant fluorophore-quencher effect that prevents the fluorophore from reaching the excited state; fluorescence emission lifetime is maintained, but the number of emitting molecules decreases. In collisional quenching the fluorophores are free to reach the excited state upon absorption but decay without emission if then hit by a quencher molecule; this leads to a decrease in emission lifetime.

Earlier work by Miguel involved the adaptation of the parallax method to deal with fluorophore and quencher distributions. Previous implementations considered that fluorophore and quencher molecules lie exactly at a given depth,[83] or at least that the quencher molecules do.[84] This is an unrealistic approach as fluctuations in the depth of the system constituents are very likely to occur, especially so in the case of the quenchers — usually charged or very polar and not expected to sit unperturbed amidst the apolar acyl chains. Miguel's (and his coworkers') approach was to find the in-depth distributions of the quencher molecules and then to infer the fluorophore's from quenching information.

Quencher distributions were obtained by simulations of Brownian motion within the bilayer — see the full work in reference 85. The quenchers in question were stearic acid molecules labeled with nitroxide doxyl groups, which are free radicals, at the fifth and sixteenth carbons (5NS and 16NS; Figure A.2). The distributions were unimodal and could be fit by Lorentzian curves (similar to Gaussians but with slower descents to zero away from the mean).

Under a typical experimental setup the fluorescence lifetime of the peptide in a peptide-vesicle system is measured as quencher is gradually added; only one of the quenchers is used at a time. In measurements of fluorescence lifetimes instead of steady-state emission only the dynamic component of quenching is detected, which simplifies the quenching model. Bruno Castro, a PhD student working with Manuel Prieto and a long-time friend of mine, provided valuable input on the acquisition and analysis of lifetime data, especially on ways to circumvent the artifacts introduced by the intense light scattering of vesicle suspensions.

The fluorophore distribution is that which, under the assumptions of collisional quenching and given the quenchers' distributions, predicts an emitted intensity as close as possible to the observed. The algorithm developed by Miguel and coworkers for finding the best fitting fluorophore curve involves the generation of a large number of possible distributions. The central value of these distributions is swept along the depth of one bilayer leaflet and their width is scanned from very narrow curves to almost flat ones (for simplicity, the fluorophore distribution was assumed to

also be a Lorentzian). For each of the generated distributions an expected quenching behavior is computed (a numerical approach that integrates the expected fluorescence over small steps in the membrane[85]) and the difference relative to the observed value is calculated. A solution surface is thus generated for each quencher, corresponding to the difference to the observed data as a function of the mean and width of the fluorophore distribution; the fluorophore distribution will be that at which both surfaces and the plane $z = 0$ intersect. The method was nicknamed SIMEXDA, for SImulated EXperimental Data Analysis.

It was from this point that I contributed to the analysis process of differential quenching. I first translated into Visual Basic the FORTRAN

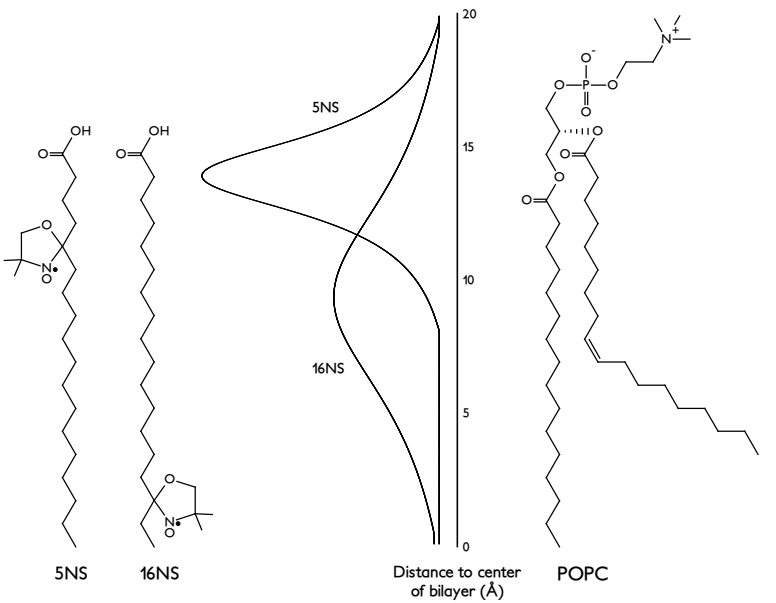

Figure A.2 – Chemical formulas of 5NS and 16NS and the in-depth distribution of the free-radical doxyl moiety in bilayers (from reference 85); a POPC phospholipid is included for comparison. It can be seen that the distributions are shifted towards the bilayer surface relative to the doxyl position in the acyl chain. This is likely due to the instability of the radical moiety in the apolar region of the bilayer and to the short size of the stearic acid next to neighboring phospholipids.

code used to generate the solution surfaces. Visual Basic code can be readily integrated into Microsoft Excel or OpenOffice.org Calc spreadsheets, which simplifies data analysis by not requiring an external program to be run. I would later retranslate the code to C++ and compile it into a shared library loadable from Visual Basic (the commented source code files, as well as a working implementation in an Excel spreadsheet can be found in the digital supporting material of this thesis); this afforded a five-fold increase in computation speed — important since the algorithm may take several seconds to complete and is often invoked several times in a spreadsheet. Further gains in speed are achievable by creating an Excel specific library (termed XLL) in C++; this approach obviates the intervention of the slower Visual Basic code and allows a spreadsheet to make use of multiple processors by running several instances of the algorithm in parallel (useful when more than one cell uses the code). Not being a critical upgrade, I have not yet endeavored to create an XLL.

My second contribution was to modify the algorithm into a least-squares approach. As it stood, the method only used one data point per quencher. This did not include any tolerance for error, which, besides being a severe limitation by itself, often prevented the determination of the fluorophore's distribution because solution surfaces would not intersect in the $z = 0$ plane. Under the least-squares approach each of the generated fluorophore distributions is assigned a set of three scores: one sub-score for each quencher — the sum of the square of the differences between the predicted and the observed relative decrease in emission at each data point; and a global score — the sum of the two sub-scores. The selected distribution will be that which generates the smallest global score.

Users of this method — which so far have been most of the people that have arrived at the lab after me — must always carefully analyze the results for inconsistencies. The code also outputs the distribution parameters that generated the minimum for each sub-score; it is unlikely that the global solution lies very far from those. There is, however, an exception to this: when dealing with relatively narrow fluorophore distributions each sub-score will usually have two minima, corresponding to central values on each side of the quencher distribution. This results

from the approximately symmetric shape of the quenchers' profiles, which makes it hard to distinguish which side the fluorophore lies on — it is basically the same problem that has prompted the use of two quenchers in the parallax method: it may happen that the minimum that generates the least sub-score of a quencher points to the "wrong" side of its distribution. In this case the user should check if that sub-score is not much lower than the one that generated the minimal global score (all values are output by the code).

So far the score values and the above consistency checks are the only indicators of fit quality. The analysis would greatly benefit from the computation of confidence intervals of the returned parameters as well as of the dependence between them. In addition, the quality of results could be further improved by coupling one of several available minimum-finding algorithms to the code, which should also become much faster.

I made some further additions to the algorithm: I included the possibility to generate multimodal fluorophore distributions and to account for a static quenching contribution (for the cases where only steady-state fluorescence data is available). None of the approaches, however, is reliable. The consistency of multimodal distributions with the data is hard to verify and I suspect that the returned parameters are heavily dependent on each other. The inclusion of static quenching would considerably simplify data collection as steady-state fluorescence measurements are much easier to acquire and analyze than time-resolved ones. Unfortunately I came to the conclusion that most of the static quenching under this experimental setups is generated by peptide-quencher binding outside of the membrane (the 5NS and 16NS also partition between the aqueous phase and the bilayer — K_p values in the order of 10^4 —, meaning that there will always be some unbound quencher molecules). This fact, together with the addition of another parameter (the quencher-fluorophore distance under which static quenching occurs) prevents proper data analysis. The code in the digital supporting material does not contain these features.

Good fits have been obtained by employing the unimodal, least-squares, collisional-quenching SIMEXDA to fluorescence lifetime data. In-depth measurement of BP100 results was very reproducible and consistent with

a parallel burying of the helix as Rafael had predicted. Unfortunately — from a methodological perspective — the method was not duly emphasized in Article IV because the peptide depth was little affected by saturation. The differential quenching data of omiganan interacting with vesicles was presented in raw form in Article III: at the time I had not yet added the least-squares analysis to SIMEXDA and as it stood the method would return extreme results (very narrow distributions centered either at the surface or the middle of the bilayer). Inward movement upon saturation may still be qualitatively deduced from the data that were published.

In Miguel's work it was mentioned that the results would be fairly independent of the Stern-Volmer quenching constant (K_{SV}, in M^{-1} — the product of the bimolecular quenching kinetic constant and the fluorescence lifetime of the unquenched fluorophore). I found however, that results were sensitive to K_{SV} changes in the order of $0.1\,\text{M}^{-1}$, which possibly results from the adaptation of the method to a least-squares approach. In any case, that parameter is now also scanned when looking for the best fitting fluorophore distribution. The tyrosine-containing peptides with which the method has been applied consistently return K_{SV} values in the $1 - 2\,\text{M}^{-1}$ range.

There are some pitfalls in the interpretation of results from SIMEXDA. As the method returns a unimodal distribution one cannot expect to detect peptide insertion if most molecules remain adsorbed. Such may be the case of peptides that form disordered toroidal pores (recall Figure 1.1). Also regarding toroidal pores, if the quencher lipid is bent or rotated at the pore site the reported depth will be skewed. Lastly, peptides bearing more than one fluorophore will have a broadened distribution and may be poorly fit by a unimodal curve.

Overall, this is a method that is not straightforward to apply and whose solutions need careful user inspection. Still, it is a method able to produce good results if fed good data. And, besides the application aspect, I had a great time putting my amateur programming skills into practice while programming it.

Bibliography

1 Zasloff, M. Magainins, a class of antimicrobial peptides from *Xenopus* skin: isolation, characterization of two active forms, and partial cDNA sequence of a precursor. *Proc Natl Acad Sci U S A* **84**(15), 5449–5453 (1987).

2 Fennell, J. F., Shipman, W. H., and Cole, L. J. Antibacterial action of melittin, a polypeptide from bee venom. *Proc Soc Exp Biol Med* **127**(3), 707–710 (1968).

3 Steiner, H., Hultmark, D., Engstrom, A., Bennich, H., and Boman, H. G. Sequence and specificity of two antibacterial proteins involved in insect immunity. *Nature* **292**(5820), 246–248 (1981).

4 Hancock, R. E. Peptide antibiotics. *Lancet* **349**(9049), 418–422 (1997).

5 Yeaman, M. R. and Yount, N. Y. Mechanisms of antimicrobial peptide action and resistance. *Pharmacol Rev* **55**(1), 27–55 (2003).

6 Maloy, W. L. and Kari, U. P. Structure-activity studies on magainins and other host defense peptides. *Biopolymers* **37**(2), 105–122 (1995).

7 Yang, L., Harroun, T. A., Weiss, T. M., Ding, L., and Huang, H. W. Barrel-stave model or toroidal model? A case study on melittin pores. *Biophys J* **81**(3), 1475–1485 (2001).

8 Baumann, G. and Mueller, P. A molecular model of membrane excitability. *J Supramol Struct* **2**(5-6), 538–557 (1974).

9 Pouny, Y., Rapaport, D., Mor, A., Nicolas, P., and Shai, Y. Interaction of antimicrobial dermaseptin and its fluorescently labeled analogues with phospholipid membranes. *Biochemistry* **31**(49), 12416–12423 (1992).

10 Ludtke, S. J., He, K., Heller, W. T., Harroun, T. A., Yang, L., and Huang, H. W. Membrane pores induced by magainin. *Biochemistry* **35**(43), 13723–13728 (1996).

11 Leontiadou, H., Mark, A. E., and Marrink, S. J. Antimicrobial peptides in action. *J Am Chem Soc* **128**(37), 12156–12161 (2006).

12 Brogden, K. A., Ackermann, M., McCray, P. B., and Tack, B. F. Antimicrobial peptides in animals and their role in host defences. *Int J Antimicrob Agents* **22**(5), 465–478 (2003).

13 Zanetti, M., Gennaro, R., and Romeo, D. Cathelicidins: a novel protein family with a common proregion and a variable C-terminal antimicrobial domain. *FEBS Lett* **374**(1), 1–5 (1995).

14 Hancock, R. E. and Chapple, D. S. Peptide antibiotics. *Antimicrob Agents Chemother* **43**(6), 1317–1323 (1999).

15 Perron, G. G., Zasloff, M., and Bell, G. Experimental evolution of resistance to an antimicrobial peptide. *Proc Biol Sci* **273**(1583), 251–256 (2006).

16 Zasloff, M. Antimicrobial peptides of multicellular organisms. *Nature* 415(6870), 389–395 (2002).

17 Kuzin, A. P., Liu, H., Kelly, J. A., and Knox, J. R. Binding of cephalothin and cefotaxime to D-Ala-D-Ala-peptidase reveals a functional basis of a natural mutation in a low-affinity penicillin-binding protein and in extended-spectrum β-lactamases. *Biochemistry* 34(29), 9532–9540 (1995).

18 Robinson, W. E., J., McDougall, B., Tran, D., and Selsted, M. E. Anti-HIV-1 activity of indolicidin, an antimicrobial peptide from neutrophils. *J Leukoc Biol* 63(1), 94–100 (1998).

19 Albiol Matanic, V. C. and Castilla, V. Antiviral activity of antimicrobial cationic peptides against Junin virus and herpes simplex virus. *Int J Antimicrob Agents* 23(4), 382–389 (2004).

20 Hoskin, D. W. and Ramamoorthy, A. Studies on anticancer activities of antimicrobial peptides. *Biochim Biophys Acta* 1778(2), 357–375 (2008).

21 Bowdish, D. M., Davidson, D. J., and Hancock, R. E. A re-evaluation of the role of host defence peptides in mammalian immunity. *Curr Protein Pept Sci* 6(1), 35–51 (2005).

22 Free Patents Online Database (accessed Jan 2010). http://www.freepatentsonline.com.

23 Staubitz, P., Peschel, A., Nieuwenhuizen, W. F., Otto, M., Gotz, F., Jung, G., and Jack, R. W. Structure-function relationships in the tryptophan-rich, antimicrobial peptide indolicidin. *J Pept Sci* 7(10), 552–564 (2001).

24 Selsted, M. E., Novotny, M. J., Morris, W. L., Tang, Y. Q., Smith, W., and Cullor, J. S. Indolicidin, a novel bactericidal tridecapeptide amide from neutrophils. *J Biol Chem* 267(7), 4292–4295 (1992).

25 News Release: MIGENIX Announces OMIGARD™ Phase III clinical trial results. MIGENIX Inc. (March 2009). http://www.migenix.com/newsreleases/NR%20Mar%2012%202009%20Cadence%20Results%20final.pdf.

26 News Release: Micrologix Reports Phase III Trial Results of MBI 226. Micrologix Biotech Inc. (July 2003). http://www.migenix.com/newsreleases/072303.pdf.

27 Cadence Pharmaceuticals Reports Fourth Quarter and Full Year 2008 Financial Results and Provides Corporate and Clinical Updates. Cadence Pharmaceuticals, Inc. (March 2009). http://files.shareholder.com/downloads/CADX/862454458x0x279689/fc8ced2b-e816-4b3c-bc93-890a99c174fd/CADX_News_2009_3_12_General_Releases.pdf.

28 Mayer, L. D., Hope, M. J., and Cullis, P. R. Vesicles of variable sizes produced by a rapid extrusion procedure. *Biochim Biophys Acta* 858(1), 161–168 (1986).

29 Wilschut, J. and Hoekstra, D. Membrane fusion: lipid vesicles as a model system. *Chem Phys Lipids* 40(2-4), 145–166 (1986).

30 Franklin, J. C. and Cafiso, D. S. Internal electrostatic potentials in bilayers: measuring and controlling dipole potentials in lipid vesicles. *Biophys J* 65(1), 289–299 (1993).

31 Santos, N. C., Prieto, M., and Castanho, M. A. Quantifying molecular partition into model systems of biomembranes: an emphasis on optical spectroscopic methods. *Biochim Biophys Acta* **1612**(2), 123–135 (2003).

32 Friedland, H. D., Sharp, D. D., Erfle, D. J., and Rubinchik, E. Omiganan (MBI 226) 1% Gel: a novel topical antimicrobial agent with a favorable safety profile. In *43rd Interscience Conference on Antimicrobial Agents and Chemotherapy*, F–1843 (Chicago, IL, 2003).

33 Sader, H. S., Fedler, K. A., Rennie, R. P., Stevens, S., and Jones, R. N. Omiganan pentahydrochloride (MBI 226), a topical 12-amino-acid cationic peptide: spectrum of antimicrobial activity and measurements of bactericidal activity. *Antimicrob Agents Chemother* **48**(8), 3112–3118 (2004).

34 Henriques, S. T. and Castanho, M. A. Environmental factors that enhance the action of the cell penetrating peptide pep-1: A spectroscopic study using lipidic vesicles. *Biochim Biophys Acta* **1669**(2), 75–86 (2005).

35 Dugourd, D., Pasetka, C., Erfle, D., Rubinchik, E., Lee, K., Friedland, H. D., and McNicol, P. J. MBI 226 antimicrobial peptide interacts with Gram-positive and Gram-negative cell membranes. In *ASM General meeting* (Salt Lake City, UT, 2002).

36 Andreu, D., Ubach, J., Boman, A., Wahlin, B., Wade, D., Merrifield, R. B., and Boman, H. G. Shortened cecropin A-melittin hybrids. Significant size reduction retains potent antibiotic activity. *FEBS Lett* **296**(2), 190–194 (1992).

37 Hancock, R. E. and Sahl, H. G. Antimicrobial and host-defense peptides as new anti-infective therapeutic strategies. *Nat Biotechnol* **24**(12), 1551–1557 (2006).

38 Cavallarin, L., Andreu, D., and San Segundo, B. Cecropin A-derived peptides are potent inhibitors of fungal plant pathogens. *Mol Plant Microbe Interact* **11**(3), 218–227 (1998).

39 Dathe, M. and Wieprecht, T. Structural features of helical antimicrobial peptides: their potential to modulate activity on model membranes and biological cells. *Biochim Biophys Acta* **1462**(1-2), 71–87 (1999).

40 Bardají, E., Montesinos, E., Badosa, E., Feliu, L., Planas, M., and Ferre, R. Antimicrobial linear peptides. Oficina Española de Patentes y Marcas, P200601098 (April 28th 2006).

41 Ferre, R., Badosa, E., Feliu, L., Planas, M., Montesinos, E., and Bardají, E. Inhibition of plant-pathogenic bacteria by short synthetic cecropin A-melittin hybrid peptides. *Appl Environ Microbiol* **72**(5), 3302–3308 (2006).

42 Badosa, E., Ferre, R., Planas, M., Feliu, L., Besalu, E., Cabrefiga, J., Bardají, E., and Montesinos, E. A library of linear undecapeptides with bactericidal activity against phytopathogenic bacteria. *Peptides* **28**(12), 2276–2285 (2007).

43 Matos, C., Lima, J. L., Reis, S., Lopes, A., and Bastos, M. Interaction of antiinflammatory drugs with EPC liposomes: calorimetric study in a broad concentration range. *Biophys J* **86**(2), 946–954 (2004).

44 Afonin, S., Mikhailiuk, P. K., Komarov, I. V., and Ulrich, A. S. Evaluating the amino acid CF_3-bicyclopentylglycine as a new label for solid-state ^{19}F-NMR structure analysis of membrane-bound peptides. *J Pept Sci* **13**(9), 614–623 (2007).

45 Ulrich, A. S. Solid state ^{19}F-NMR methods for studying biomembranes. *Progress in Nuclear Magnetic Resonance Spectroscopy* **46**(1), 1–21 (2005).

46 Bürck, J., Roth, S., Wadhwani, P., Afonin, S., Kanithasen, N., Strandberg, E., and Ulrich, A. S. Conformation and membrane orientation of amphiphilic helical peptides by oriented circular dichroism. *Biophys J* **95**(8), 3872–3881 (2008).

47 Manavalan, P. and Johnson, W. C. Variable selection method improves the prediction of protein secondary structure from circular dichroism spectra. *Anal Biochem* **167**(1), 76–85 (1987).

48 Whitmore, L. and Wallace, B. A. DICHROWEB, an online server for protein secondary structure analyses from circular dichroism spectroscopic data. *Nucleic Acids Res* **32**(Web Server issue), W668–W673 (2004).

49 Huang, H. W. Molecular mechanism of antimicrobial peptides: the origin of cooperativity. *Biochim Biophys Acta* **1758**(9), 1292–1302 (2006).

50 Huang, H. W. Free energies of molecular bound states in lipid bilayers: lethal concentrations of antimicrobial peptides. *Biophys J* **96**(8), 3263–3272 (2009).

51 Matsuzaki, K., Sugishita, K., Harada, M., Fujii, N., and Miyajima, K. Interactions of an antimicrobial peptide, magainin 2, with outer and inner membranes of Gram-negative bacteria. *Biochim Biophys Acta* **1327**(1), 119–130 (1997).

52 Wu, M. and Hancock, R. E. Interaction of the cyclic antimicrobial cationic peptide bactenecin with the outer and cytoplasmic membrane. *J Biol Chem* **274**(1), 29–35 (1999).

53 Drin, G. and Temsamani, J. Translocation of protegrin I through phospholipid membranes: role of peptide folding. *Biochim Biophys Acta* **1559**(2), 160–170 (2002).

54 Gupta, S. M., Aranha, C. C., Bellare, J. R., and Reddy, K. V. R. Interaction of contraceptive antimicrobial peptide nisin with target cell membranes: implications for use as vaginal microbicide. *Contraception* **80**(3), 299–307 (2009).

55 Berthelot, M. and Jungfleisch, E. Sur les lois qui président au partage d'un corps entre deux dissolvants (éxperiences). *Ann Chim Phys* **26**, 396–407 (1872).

56 Berthelot, M. Sur les lois qui président au partage d'un corps entre deux dissolvants (théorie). *Ann Chim Phys* **26**, 408–417 (1872).

57 Nernst, W. Verteilung eines Stoffes zwischen zwei Lösungsmitteln und zwischen Lösungsmittel und Dampfraum. *Z Phys Chem* **8**, 110–139 (1891).

58 Levine, I. N. *Physical Chemistry*, chapter 9, 224–256. McGraw-Hil, New York (1995).

59 Chiu, S. W., Jakobsson, E., Subramaniam, S., and Scott, H. L. Combined monte carlo and molecular dynamics simulation of fully hydrated dioleyl and palmitoyl-oleyl phosphatidylcholine lipid bilayers. *Biophys J* **77**(5), 2462–2469 (1999).

60 Sleytr, U. B. Regular arrays of macromolecules on bacterial cell walls: structure, chemistry, assembly, and function. *Int Rev Cytol* **53**, 1–62 (1978).

61 Gjerde, D. T. and Fritz, J. S. *Ion chromatography*. 2nd ed., Alfred Hüthig Verlag, Heidelberg (1987).

62 Ou, L. T. and Marquis, R. E. Electromechanical interactions in cell walls of Gram-positive cocci. *J Bacteriol* **101**(1), 92–101 (1970).

63 Pott, T., Paternostre, M., and Dufourc, E. J. A comparative study of the action of melittin on sphingomyelin and phosphatidylcholine bilayers. *Eur Biophys J* **27**(3), 237–245 (1998).

64 Tossi, A., Sandri, L., and Giangaspero, A. Amphipathic, alpha-helical antimicrobial peptides. *Biopolymers* **55**(1), 4–30 (2000).

65 Tossi, A., Mitaritonna, N., Tarantino, C., Giangaspero, A., Sandri, L., and Winterstein, K. A. Antimicrobial Sequences Database (accessed Jan 2010). http://www.bbcm.univ.trieste.it/~tossi/amsdb.html.

66 Blazyk, J., Wiegand, R., Klein, J., Hammer, J., Epand, R. M., Epand, R. F., Maloy, W. L., and Kari, U. P. A novel linear amphipathic β-sheet cationic antimicrobial peptide with enhanced selectivity for bacterial lipids. *J Biol Chem* **276**(30), 27899–27906 (2001).

67 Kaneshiro, T. and Marr, A. G. Phospholipids of *Azotobacter agilis*, *Agrobacterium tumefaciens*, and *Escherichia coli*. *J Lipid Res* **3**(2), 184–189 (1962).

68 Loferer-Krossbacher, M., Klima, J., and Psenner, R. Determination of bacterial cell dry mass by transmission electron microscopy and densitometric image analysis. *Appl Environ Microbiol* **64**(2), 688–694 (1998).

69 Klamt, A., Huniar, U., Spycher, S., and Keldenich, J. COSMOmic: a mechanistic approach to the calculation of membrane-water partition coefficients and internal distributions within membranes and micelles. *J Phys Chem B* **112**(38), 12148–12157 (2008).

70 Zhang, J., Kundu, M., and Ney, P. A. *Autophagy in Mammalian Systems*, *Part B*, chapter Mitophagy in mammalian cells: The reticulocyte model, 227–245. Academic Press, San Diego (2009).

71 Brenner, D. and Mak, T. W. Mitochondrial cell death effectors. *Curr Opin Cell Biol* **21**(6), 871–877 (2009).

72 Ghobrial, I. M., Witzig, T. E., and Adjei, A. A. Targeting apoptosis pathways in cancer therapy. *CA Cancer J Clin* **55**(3), 178–194 (2005).

73 Nicoletti, I. Mitochondrial staining with JC–1 (accessed Jan 2010). http://www.med.unipg.it/imagelab/mitoch.html.

74 Giacometti, A., Cirioni, O., Barchiesi, F., Del Prete, M. S., Fortuna, M., Caselli, F., and Scalise, G. In vitro susceptibility tests for cationic peptides: comparison of broth microdilution methods for bacteria that grow aerobically. *Antimicrob Agents Chemother* **44**(6), 1694–1696 (2000).

75 Stauffer, F., Melo, M. N., Carneiro, F. A., Sousa, F. J., Juliano, M. A., Juliano, L., Mohana-Borges, R., Da Poian, A. T., and Castanho, M. A. Interaction between dengue virus fusion peptide and lipid bilayers depends on peptide clustering. *Mol Membr Biol* **25**(2), 128–138 (2008).

76 Melo, M. N., Sousa, F. J. R., Carneiro, F. A., Castanho, M. A. R. B., Valente, A. P., Almeida, F. C. L., Poian, A. T. D., and Mohana-Borges, R. Interaction of the Dengue

virus fusion peptide with membranes assessed by NMR: The essential role of the envelope protein Trp101 for membrane fusion. *J Mol Biol* 392(3), 736–746 (2009).

77 Gutierrez, A. L., Farage, L., Melo, M. N., Mohana-Borges, R. S., Guerardel, Y., Coddeville, B., Wieruszeski, J. M., Mendonca-Previato, L., and Previato, J. O. Characterization of glycoinositolphosphoryl ceramide structure mutant strains of *Cryptococcus neoformans*. *Glycobiology* 17, 1C (2007).

78 Henriques, S. T. and Castanho, M. A. Consequences of nonlytic membrane perturbation to the translocation of the cell penetrating peptide pep-1 in lipidic vesicles. *Biochemistry* 43(30), 9716–9724 (2004).

79 Henriques, S. T., Costa, J., and Castanho, M. A. R. B. Re-evaluating the role of strongly charged sequences in amphipathic cell-penetrating peptides: a fluorescence study using Pep-1. *FEBS Lett* 579(20), 4498–4502 (2005).

80 Matsuzaki, K., Yoneyama, S., Murase, O., and Miyajima, K. Transbilayer transport of ions and lipids coupled with mastoparan X translocation. *Biochemistry* 35(25), 8450–8456 (1996).

81 Drin, G., Demene, H., Temsamani, J., and Brasseur, R. Translocation of the pAntp peptide and its amphipathic analogue AP-2AL. *Biochemistry* 40(6), 1824–1834 (2001).

82 Chattopadhyay, A. and London, E. Spectroscopic and ionization properties of N-(7-nitrobenz-2-oxa-1,3-diazol-4-yl)-labeled lipids in model membranes. *Biochim Biophys Acta* 938(1), 24–34 (1988).

83 Chattopadhyay, A. and London, E. Parallax method for direct measurement of membrane penetration depth utilizing fluorescence quenching by spin-labeled phospholipids. *Biochemistry* 26(1), 39–45 (1987).

84 Ladokhin, A. S. Analysis of protein and peptide penetration into membranes by depth-dependent fluorescence quenching: theoretical considerations. *Biophys J* 76(2), 946–955 (1999).

85 Fernandes, M. X., Garcia de la Torre, J., and Castanho, M. A. Joint determination by Brownian dynamics and fluorescence quenching of the in-depth location profile of biomolecules in membranes. *Anal Biochem* 307(1), 1–12 (2002).